HOMOGENEOUS CATALYSIS AND MASS TRANSFER IN BIPHASIC IONIC LIQUID SYSTEMS WITH COMPRESSED CO_2 AND ORGANIC COMPOUNDS

By

Azita Ahosseini

Submitted to the graduate degree program in Chemical and Petroleum Engineering and the Graduate Faculty of the University of Kansas School of Engineering in partial fulfillment of the requirements for the degree of Doctor of Philosophy

_____
Chairperson: Aaron M. Scurto

_____
Committee members * Laurence Weatherley

_____
Bala Subramaniam

_____
Jon Tunge

_____
Raghunath V.Chaudhari

Date defended: 01/15/2010

The Dissertation Committee for Azita Ahosseini certifies
that this is the approved version of the following dissertation:

HOMOGENEOUS CATALYSIS AND MASS TRANSFER IN BIPHASIC IONIC LIQUID SYSTEMS WITH COMPRESSED CO_2 AND ORGANIC COMPOUNDS

Committee:

_____
Chairperson* Aaron M. Scurto

_____
Laurence Weatherley

_____
Bala Subramaniam

_____
Jon Tunge

_____
Raghunath V.Chaudhari

Date approved_____

Homogeneous Catalysis and Mass Transfer in Biphasic Ionic Liquid Systems with Compressed CO_2 and Organic Compounds

ABSTRACT

Homogeneous catalysis in which the catalyst, solvents and reactants are all in the same phase can yield high activity and selectivity and efficiently produce chemical products. However, the main problem with these kinds of reactions is separating and reusing precious metal catalyst; therefore, it needs to be performed in a convenient platform. To figure out this problem, a biphasic system can be suggested in which one phase sequesters the solid catalyst and the other phase delivers reactants to and remove products from the reaction media. But, there are some problems using these methods such as thermodynamics and solubility issues, mass transfer limitations, cross-contamination problems, environmental concerns and possibility for a continuous process. Thus, a biphasic ionic liquid (IL) /CO_2 system is suggested, which may solve these problems.

In this research, special properties of ionic liquids that can make them be the next class of alternative solvents is introduced, and subsequently the main issues in using them is discussed. Then, to overcome the abovementioned problems, a combined biphasic ionic liquid / CO_2 system is managed to be used for homogeneous catalytic reactions.

The main purpose of this project is running homogeneous catalytic reactions in biphasic IL/CO_2 media and managing key parameters in kinetics, momentum and mass transfer, and phase behavior to control the reaction in an efficient zone. For this reason, two typical and large homogeneous catalytic reactions that are practiced in industry, hydroformylation and hydrogenation of 1-octene, have been selected.

In order to investigate the effect of CO_2 pressure on controlling the reaction over the mass transfer or kinetic zones, thorough studies have been arranged to determine the phase behavior and thermodynamic properties of compounds (reactants, products, and solvents) within the reaction conditions. It has also been revealed in this work that the momentum and mass transfer parameters (diffusivity and viscosity) of ionic liquids can be managed by either the structure of ionic liquids or the pressure of various compressed gases. Thus, the measured and correlated results of viscosities and diffusivities for pure

and saturated of different types of ionic liquids with compressed CO_2 and 1,1,1,2-tetrafluoroethane **(**R134a) are reported for further studies to choose the best media (ionic liquid/compressed gas) for reactions.

Due to significant impacts of mass transfer on the reaction because of the high viscosity of ionic liquids, it is quite necessary to find mass transfer parameters for the reaction in the biphasic IL/CO_2 system. At the first step in these studies, the phase equilibrium, volumetric, and interfacial properties of the catalytic media (ionic liquid phase) and the main substrate (1-octene) have been determined. Then, using the obtained information, the mass transfer coefficient is calculated. Finally, based on these experimental results, a robust, realistic, and efficient finite element method has been developed by Petera - Weatherley to model mass transfer between an ionic liquid droplet and 1-octene continuous system.

At the end, further studies are recommended to find mass transfer parameters under compressed CO_2 pressure and in presence of gas reactants on the reaction condition to superior understanding and managing the reaction characteristics.

DEDICATED TO

my lovely husband, Shahram

for all of his amazing support, patience, and assistance

during my PhD program,

AND

my mom, in the memory of her efforts to provide me with a successful life. She will be in my heart for ever and I will never forget her generosity and kindness.

ACKNOLEDGEMENT

I would like to thank:

My adviser, Professor Aaron M. Scurto, for all of his supports and efforts to lead this study with integrity and wealth of knowledge. I have learned a lot from him throughout the years and his recommendations have always been of great value to me. I admire his sharp-sighted, hardworking, and considerable interests in the scientific issues and I am proud to have him as a head of my PhD research program.

Professor Laurence Weatherley and Professor Jerzy Petera who have advised me within my mass transfer studies in this research. They led me systematically to figure out the helpful methods and parameters for modeling and further studies. I really appreciate their knowledgeable discussions to open a new world of study to me.

My honorable committee Professors, Professor Bala Subramaniam, Professor Jon A. Tunge, and Professor Chaudhari for all of their guidance, supports and very helpful advice.

Professor Shapour Vossoughi, the first individual I met from the University of Kansas. I am very grateful to him because he familiarized me with a remarkable and educational school and a pleasant place to learn and be trained. My appreciation goes for not only coming to achieve a higher degree, but also for opening a new window to a wonderful culture, its people and their ethics.

Entire faculty and staff of Chemical and Petroleum Engineering (CPE) department, and Center for Environmentally Beneficial Catalysis (CEBC), especially, Professor Trung van Nguyen for his impressive teaching of transport phenomena, Professor Mike Dudukovic whom I learned a lot about kinetics of environmental chemical reactions, Professor Daryl Fahey, Professor Javier Guzman, Professor Marylee Southard, Professor Cory Berkland, Prof. Jenn-Tie Liang, and Dr.Claudia Bode, for their consultative helps, Dr. W. Kirk Snavely for aiding me in the setup of the viscometer, Alan Walker, Jim Pilch, Ed Atchison, Nate Oborny, and Jim Busse for their remarkable technical assistance in the laboratory issues like instrumentation set up and computer matters, Cyndi Hurst, Carol Miner, Lori Ann Pearson, Gerri Wetzel, Deanna Bieberly, and Nancy Crisp for their helps and supports, Mike Beerbower and Scott Jeffress from CEBC facility

operations and maintenance for their permanent alerts to help us whenever we were in trouble.

My dear lab mates, Wei Ren, Jay Schleicher, Sylvia Nwosu, and Satya Gangu for their caring assistance during my PhD program. Valuable collaborations of Wei Ren in phase behavior studies ought to have additional appreciations.

Dr. David van derVelde from Nuclear Magnetic Resonance Laboratory, for his bright advising in NMR method and programming.

All of organizations and instructional services at the University of Kansas that have helped me to successfully complete my studies such as, International Student & Scholar Services (ISSS), Environment, Health, & Safety (EHS), Watkins Health Center, and Libraries.

Finally, Special thanks to my funding sources NSF-ERC Center of Environmentally Benign Catalysis (NSF EEC-0310689), National Science Foundation (NSF EEC-0649257), US National Science Foundation under Grants No. CBET-0626313 and CBET-0731244; and the Department of Transportation-KU Transportation Research Institute (TRI) (DOT No. DT0S59- 06-G-00047)

At the end, just as a personal note, I would like to thank my husband, Shahram Samandi, and my daughter, Gelareh Samandi, who have endured such a hard time throughout my PhD program. Without their patience and support I would not be able to terminate these challenging years.

TABLE OF CONTENTS

TABLES

FIGURES

Chapter 1 Introduction

1 Introduction

To keep the Earth clean for the present and next generation, scientists and especially chemists and chemical engineers are considerably responsible for finding new ways to decrease waste production and energy consumption. The chemical industry faces many demands for higher environmental performance in this century. They have to meet these challenges on parallel with maintaining global competitiveness and consumer satisfaction of product quality. So, technical solutions are needed to turn these problems into advantaged opportunities.

The main purpose of this research is substitution of hazardous and volatile organic solvents with environmentally benign compounds in homogeneous catalytic reactions. For this reason, a biphasic ionic liquid / carbon dioxide (CO_2) system is suggested as a green media for both reaction and separation in two common homogeneous catalytic reactions. In this work, the real effect of CO_2 pressure on hydroformylation and hydrogenation reactions of 1-octene are investigated in ionic liquid catalytic media. The phase behavior, thermodynamic and transport properties of solvent (ionic liquid), reactants (syngas, hydrogen, 1-octene), and products (linear and branched nonanal, octane) in abovementioned reactions can be affected by introducing CO_2 that eventually influenced kinetics of reaction. Thus, all of these effects have systematically quantified in the reaction conditions.

The current chapter presents an introduction about ionic liquids and problems in using them, and then explains how to overcome some of these challenges with compressed CO_2. The advantage of replacing volatile organic solvents with biphasic ionic liquids / CO_2 system in homogeneous catalysis is another important task that this chapter covers. All sections are supported with comprehensive literature survey and related studies that have recently been done by other research groups. At the end, objectives, outcome, and outline of this research are described.

1.1 Ionic liquids

Ionic liquids (ILs) are melted salts that are liquid at or near room temperature (T_m < 100°C). There are numbers of organic cation with inorganic anion combinations that can

yield melted salts. Several of the most common cation classes of ionic liquids are quaternary ammonium, imidazolium, pyridinium, and phosphonium. Ionic liquids can be molecularly engineered for specific physico-chemical properties through various "R-groups" and cation/anion selection such as viscosity, solubility properties, density, acidity/basicity, co-ordination properties, and stereochemistry. It has been estimated that ~10^{14} unique cation/anion combinations are possible.[1] Figure 1-1 shows different classes of cations and anions used with ionic liquids.

According to their strong electrostatic, culombic, and hydrogen bonds, ILs have unique characteristics. They have high flash points, no measurable vapor pressure, and, so, no air pollution potential. Thus, they have been considered as environmentally benign solvents and using ILs is continually being developed for extractions, reactions, and material processing. However, toxicity in soil and water eco-systems must be carefully understood.

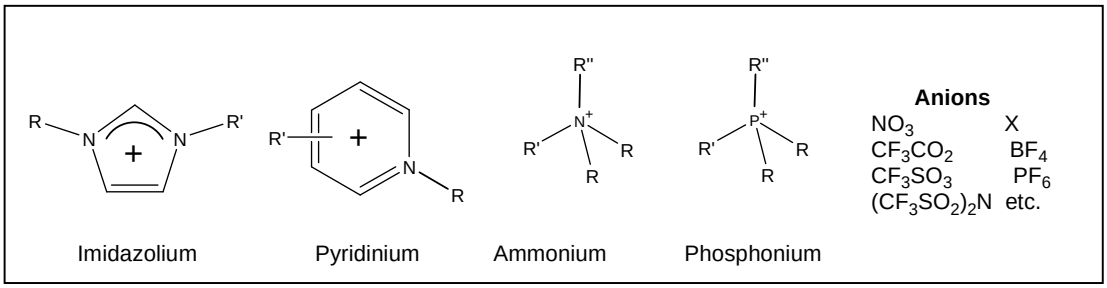

Figure 1-1 Common cation classes and anions used with ionic liquids.

1.2 Challenges with ionic liquids

Besides their advantages, ILs can present a number of challenges for their use in catalysis. ILs often have a lower solubility of reaction gases [2, 3] (H_2, CO, O_2, etc.) than organic solvents which can reduce reaction efficiency. Separating substances from ionic liquids can often be difficult, as common separation and fractionation techniques, such as distillation are no longer possible for the non-volatile IL solvent. While, the theoretical number of ionic liquids is amazing, the vast majority are actually *solids* with melting points above 100°C. Most ionic liquids are more viscous than organic-solvents [4, 5], which can lead to lower diffusivity and mass transfer (lower reaction rates, extraction efficiency, etc.). Several groups working in various fields have indicated the importance or

limitation of mass transfer for IL systems for gas solubility [2], based-catalyzed epoxidation [6], electrochemistry [7], three-phase heterogeneously catalyzed oxidations [8] enzyme catalysis [9], etc.

1.3 Compressed/supercritical CO_2

Compressed, dense-phase or supercritical (SC) carbon dioxide has also been shown as an environmentally-benign solvent with tunable physico-chemical properties for enhancing reactions and catalysis.[10] CO_2 can become miscible with liquids and reaction gases such as H_2, CO, O_2, etc., and eliminate gas-liquid phase limitations and their intrinsic mass transfer restrictions. Many researchers have demonstrated the improved catalytic performance in CO_2 systems; for recent reviews see Jessop[10] and Leitner.[11] However, often complicated ligand systems are required to make enough catalyst soluble in the supercritical CO_2 and obtain a high efficient reaction.

1.4 Biphasic ionic liquids/ CO_2 advantages

Coupling ionic liquids and CO_2 may overcome many of limitations with ionic liquids. A biphasic ionic liquid/CO_2 system utilizes the advantages of each of the respective technologies and helps overcome their challenges. IL/CO_2 systems are gas or CO_2 expanded liquids (GXLs/CXLs), which are melted salts with large amounts of dissolved CO_2 and have been used as a tunable media for reactions, extractions and materials processing.

Ionic liquids have unique phase behavior with CO_2. For instance, CO_2 is very soluble in the ionic liquid, but, the ionic liquid is immeasurably insoluble in the pure CO_2 phase and does not become miscible (critical) even at hyperbaric pressures.[12] This is unlike CO_2 with most organic solvents, which become critical (one phase) at moderate pressures (100-200bar).[13, 14] Few biphasic systems can achieve such lack of cross-contamination as with ILs and CO_2.

CO_2 can dramatically decrease the viscosity of ILs to that of common solvents and increases the diffusivity of compounds in IL. The groups of Leitner [15] and Brennecke [16] found that the presence of CO_2 can even increase the solubility of reaction gases (H_2 and O_2) into the IL-phase. Scurto *et al.* [17, 18] have demonstrated the ability to separate ILs

from organics or water using CO_2 pressure which can induce immiscibility and extraction. Scurto and Leitner [19] have demonstrated that CO_2 can dramatically decrease the melting point of many ionic solids, even inducing melting over 100 °C below their normal melting points. This new technique with CO_2 now allows much more of the ionic liquids/solids to be usable in a process as they have shown for a variety of catalytic reactions.

1.5 Homogeneously catalyzed reactions in biphasic IL/CO_2 systems

The combination of compressed CO_2 and ionic liquids offers a number of benefits for homogeneously catalyzed reactions, where the ionic liquid phase is employed to sequester the organometallic catalyst and the CO_2 phase becomes the mobile phase for reactants and products. A variety of reactions have been performed in biphasic IL/CO_2 systems. However, the effect of CO_2 on catalyzed reactions in ionic liquids is not consistent throughout the literature sources. Some indicate that CO_2 increases activity, while others demonstrate a decrease in activity with CO_2 pressure. However, most studies consistently find an increase in selectivity.

One of the first examples of an IL/CO_2 biphasic system was olefin hydrogenation by Tumas and coworkers.[20] They compared the results in a biphasic IL/CO_2 and IL/hexane system and found little difference in the reaction rate with pressurized CO_2 or hexane. Jessop, Eckert and co-workers [21] performed asymmetric Ru-catalyzed hydrogenations in an ionic liquid/CO_2 biphasic system with enantio-selectivity that was tunable with the pressure of CO_2. Leitner and coworkers [15] found for iridium catalyzed hydrogenation of aromatic imines an increase in reaction rate with the presence of CO_2 compared with H_2 pressure alone. From high-pressure NMR studies, the solubility of H_2 in the IL (as indicated by the size of the H_2 peak) increases with increasing CO_2 pressure while maintaining constant H_2 loading.

Hou *et al.*[22] investigated the Wacker oxidation of 1-olefins and found that increasing CO_2 pressure significantly improved the selectivity of the 2-ketone over 3-ketone. They hypothesize that the increase in pressure increases the solubility of the olefin into the CO_2 phase, thus creating lean conditions that prevented isomerisation. Zhao and Jiang [23] investigated the electro-oxidation of benzyl alcohol and found that a large amount of CO_2

dissolved in IL can increase the ionic conductivity and ion mobility of ionic liquids, which seems to improve the Faradic efficiency and selectivity over reactions without CO_2. However, the efficiency begins to decrease at higher pressure, which they attribute to the phase behaviour of products and reactants in CO_2 and IL media. Ballivet-Tkatchenko et al [24], used [BMIm][BF_4] and supercritical CO_2 for the biphasic palladium-catalysed dimerisation of methyl acrylate. The turn-over frequency (TOF) and selectivity was similar to the monophasic system.

To truly understand these biphasic systems, thermodynamic phase equilibria, kinetics and mass transfer are key aspects that are necessary to be considered. To illustrate these factors, model studies for the hydrogenation and hydroformylation of 1-octene in 1-hexyl-3-methyl-imidazolium bis(trifluoromethylsulfonyl)amide ([HMIm][Tf2N]) Figure 1-2 and CO_2 with a simple rhodium triphenyl phosphine (TPP) catalyst are presented in this project.

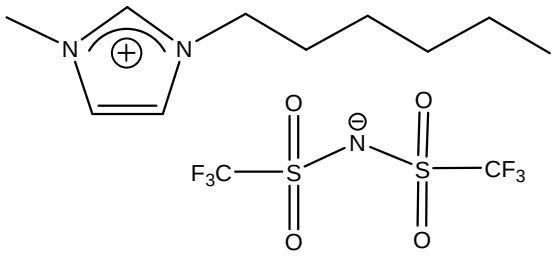

Figure 1-2 Structure of 1-hexyl-3-methyl-imidazolium bis(trifluoromethylsulfonyl) amide ([HMIm][Tf_2N])

1.6 Interfacial mass transport in the ionic liquid/1-octene system

A variety of applications of ionic liquids (ILs) often are based upon biphasic systems such as liquid-liquid (L-L), liquid-vapor (L-V), solid-liquid (S-L), etc.[25-27] These new applications are being developed for extractions, separations, reactions, and material processing.[28-33] However, there is a lack of information for systems involving ionic liquids in interfacial mass transfer area. So, in this work, liquid-liquid biphasic system with ionic liquids has been studied.

For this research, a system of 1-octene with a common ionic liquid ([HMIm][Tf_2N]) (Figure 1-2) has been selected, so the result of these studies can be helpful in better

understanding of kinetics in hydrogenation and hydroformylation reaction of 1- octene in the same solvent. In this study, the IL droplet interacts with 1-octene continuous phase. For fundamental studies in interfacial mass transfer, the concentration rate at each point should be known. Additionally, some thermodynamic and transport properties such as density, interfacial tension, viscosity, and diffusivity are essential properties that need to be measured. With this information and using a robust finite element method of professors Jerzy Petera and Laurence Weatherley, a model for mass transfer between a falling spherical, segregated droplet of [HMIm][Tf_2N] and 1-octene continuous phase has been developed.

To compare modeling results with real data, mass transfer experiments are done in a liquid-liquid contact column. Droplets fall through 1-octene in a column and mass transfer occurs between two phases. The falling of ionic liquid droplets is visualized by a high speed optical system in a transparent medium with a great precision. The velocity and droplet diameters are measured using the optical system. Finally, mass transfer coefficient is determined for different conditions and an empirical correlation is developed to relate it to dimensionless groups.

1.7 Research objectives

The main objective of this dissertation is to manage two types of homogeneous catalytic reactions, hydroformylation and hydrogenation of 1-octene, in environmentally benign biphasic ionic liquids / CO_2 media and study interfacial mass transport in the ionic liquid / 1-octene system. In general, thermodynamics and phase equilibria, momentum and mass transport phenomena, and kinetics issues can essentially control the reaction. Identification of the effect of the abovementioned fundamental aspects for a biphasic ionic liquids / CO_2 system is much more crucial than common organic solvents due to special properties of ionic liquids as well as compressed CO_2.

1.8 Research outcome

The outcome of these studies can be used to optimize the whole process of reaction and separation and direct it to a feasible condition for any further process intensifications.

Advanced modeling and investigations over other catalytic reactions in different platforms can be done using a know how package achieved from this research.

1.9 Research outline

The subjects of this dissertation will be clarified in the following chapters:

Chapter 2 covers all of the experimental methods for reactions and measurements, equipment set up, schematic and detailed description of apparatus modifications, and the result of calibrations that have been done in this research. It also includes the synthesis, purification, and analysis of ionic liquids that are used in this study.

Chapter 3 describes basic issues in biphasic ionic liquid/CO_2 systems for homogeneous catalysis focusing on hydroformylation and hydrogenation of 1-octene. In this chapter, thermodynamics, phase equilibria, and physical and interfacial properties that can affect the kinetics of reaction and change the reaction efficiency will be probed. The most important achievement of this chapter is understanding the real effect of CO_2 pressure on the apparent reaction rate in different conditions. It is shown that the CO_2 pressure enhances the mass transfer between reactants and affects the phase behavior and concentration of components inside the catalytic media. All of these parameters are very important in kinetics and can change the rate of reaction. Thus, the influences of CO_2 pressure on transport properties of ionic liquids with different structures are quantified in the following chapter.

Chapter 4 illustrates the results of viscosities and diffusivities of several pure imidazolium ionic liquids and their mixtures with compressed gases (CO_2 and R134a) at ambient and high pressures. The outcomes can be used as a basic for other studies in order to select the best media for catalytic reactions and control the mass transfer effects on the reaction efficiency.

Chapter 5 helps to understand thermodynamics, interfacial, and transport properties in biphasic 1-hexyl-3-methyl-Imidazolium bis (trifluoromethylsulfonyl) amide ([HMIm][Tf_2N]) and 1-octene. These studies are necessary to determine mass transfer effects on reactions under investigation in this work and will be a support for the next chapter to determine the overall mass transfer coefficient in this system.

Chapter 6 uses obtained results from Chapter 5 to determine the mass transfer phenomenon from a continuous phase (1-octene) to a droplet of IL ([HMIm][Tf_2N]) by measuring concentration over time under a variety of geometries and hydrodynamic conditions. Thorough studies on the liquid-liquid contact column and a high speed optical system are done and presented in this chapter to figure out this essential information. Based on the results of these investigations further studies for swarming droplets and with compressed gases can be accomplished. These conditions will be closer to the real multiphase reaction situation.

Chapter 7 includes conclusions of the whole thesis and recommendations for prospective investigations.

1.10 References

1. Holbrey, J. D.; Seddon, K. R., Ionic Liquids. *Clean Prod. Proc.* **1999,** 1, 4, 223-236.
2. Anthony, J. L.; Maginn, E. J.; Brennecke, J. F., Solubilities and Thermodynamic Properties of Gases in the Ionic Liquid 1-n-Butyl-3-methylimidazolium Hexafluorophosphate. *J. Phys. Chem. B* **2002,** 106, 29, 7315-7320.
3. Jacquemin, J.; Margarida F. Costa Gomes; Husson, P.; Majer, V., Solubility of carbon dioxide, ethane, methane, oxygen, nitrogen, hydrogen, argon, and carbon monoxide in 1-butyl-3-methylimidazolium tetrafluoroborate between temperatures 283 K and 343 K and at pressures close to atmospheric. *J. Chem. Thermodyn.* **2006**, 38, 490-502.
4. Brennecke, J. F.; Maginn, E. J., Ionic liquids: Innovative fluids for chemical processing. *AIChE J.* **2001,** 47, 11, 2384-2389.
5. Dzyuba, S. V.; Bartsch, R. A., Influence of structural variations in 1-alkyl (aralkyl)-3-methylimidazolium hexafluorophosphates and bis (trifluoromethylsulfonyl) imides on physical properties of the ionic liquids. *ChemPhysChem* **2002,** 3, 2, 160-166.
6. Wang, B.; Kang, Y. R.; Yang, L. M.; Suo, J. S., Epoxidation of a, ß-unsaturated carbonyl compounds in ionic liquid/water biphasic system under mild conditions. *J. Mol. Cat. A* **2003,** 203, 1-2, 29-36.
7. Zhang, J.; Bond, A. M., Comparison of Voltammetric Data Obtained for the trans-[Mn (CN)(CO) $_2$ {P (OPh) $_3$}($Ph_2PCH_2PPh_2$)] Process in BMIM. PF_6 Ionic Liquid under Microchemical and Conventional Conditions. *Anal. Chem* **2003,** 75, 24, 6938-6948.
8. Hardacre, C.; Mullan, E. A.; Rooney, D. W.; Thompson, J. M., Use of a rotating disc reactor to investigate the heterogeneously catalysed oxidation of cinnamyl alcohol in toluene and ionic liquids. *J.Catal.* **2005,** 232, 2, 355-365.
9. Guo, Z.; Xu, X., Lipase-catalyzed glycerolysis of fats and oils in ionic liquids: a further study on the reaction system. *Green Chem.* **2006,** 8, 1, 54-62.
10. Jessop, P. G.; Leitner, W., *Chemical Synthesis Using Supercritical Fluids*. Wiley-VCH: Weinheim, 1999.
11. Leitner, W., Supercritical Carbon Dioxide as a Green Reaction Medium for Catalysis. *Acc. Chem. Res.* **2002,** 35, 9, 746-756.
12. Blanchard, L.; Gu, Z.; Brennecke, J., High-pressure phase behavior of ionic liquid/CO_2 systems. *J. Phys. Chem. B* **2001,** 105, 12, 2437-2444.
13. Jessop, P. G.; Subramaniam, B., Gas-Expanded Liquids. *Chem. Rev.* **2007,** 107, 6, 2666-2694.
14. Brennecke, J. F.; Maginn, E. J., Ionic Liquids: Innovative Fluids for Chemical Processing. *AIChE J.* **2001,** 47, 11, 2384-2389.
15. Solinas, M.; Pfaltz, A.; Cozzi, P. G.; Leitner, W., Enantioselective Hydrogenation of Imines in Ionic Liquid / Carbon Dioxide Media. *J. Am. Chem. Soc.* **2004,** 126, 16142-16147.
16. Hert, D. G.; Anderson, J. L.; Aki, S. N. V. K.; Brennecke, J. F., Enhancement of oxygen and methane solubility in 1-hexyl-3-methylimidaxolium bis(trifluoromethylsulfonyl)imide using carbon dioxide. *Chem. Comm.* **2005**.
17. Scurto, A. M.; Aki, S.; Brennecke, J. F., CO_2 as a separation switch for ionic liquid/organic mixtures. *J. Am. Chem. Soc* **2002,** 124, 35, 10276-10277.

18. Scurto, A. M.; Aki, S.; Brennecke, J. F., Carbon dioxide induced separation of ionic liquids and water. *Chem. Comm.* **2003,** 2003, 5, 572-573.
19. Scurto, A. M.; Leitner, W., Expanding the useful range of ionic liquids: melting point depression of organic salts with carbon dioxide for biphasic catalytic reactions. *Chem. Comm.* **2006**, 35, 3681-3683.
20. Liu, F.; Abrams, M. B.; Baker, R. T.; Tumas, W., Phase-separable catalysis using room temperature ionic liquids and supercritical carbon dioxide. *Chem. Comm.* **2001**, 433-434.
21. Jessop, P. G.; Stanley, R. R.; Brown, R. A.; Eckert, C. A.; Liotta, C. L.; Ngo, T. T.; Pollet, P., Neoteric solvents for asymmetric hydrogenation: supercritical fluids, ionic liquids, and expanded ionic liquids. *Green Chem.* **2003,** 5, 2, 123-128.
22. Hou, Z.; Han, B.; Gao, L.; Jiang, T.; Liu, Z.; Chang, Y.; Zhang, X.; He, J., Wacker oxidation of 1-hexene in 1-n-butyl-3-methylimidazolium hexafluorophosphate ([bmim][PF_6]), supercritical (SC) CO_2, and SC CO_2/[bmim][PF_6] mixed solvent. *New J. Chem.* **2002,** 26, 1246-1248.
23. Zhao, G.; Jiang, T., Electro-oxidation of Benzyl Alcohol in a Biphasic System Consisting of Supercritical CO_2 and Ionic Liquids. *J.Phys.Chem.B* **2004,** 108, 13052-13057.
24. Ballivet-Tkatchenko, D.; Picquet, M.; Solinas, M.; Francin, G.; Wasserscheid, P.; Leitner, W., Acrylate dimerisation under ionic liquid–supercritical carbon dioxide conditions. *Green Chem.* **2003,** 5, 2, 232-235.
25. Zhao, H.; Xia, S.; Ma, P., Use of ionic liquids as 'green' solvents for extractions. *J. Chem. Technol. Biotechnol.* **2005,** 80, 10, 1089-1096.
26. Webb, P. B.; Sellin, M. F.; Kunene, T. E.; Williamson, S.; Slawin, A. M. Z.; Cole-Hamilton, D. J., Continuous flow hydroformylation of alkenes in supercritical fluid-ionic liquid biphasic systems. *J. Am. Chem. Soc.* **2003,** 125, 50, 15577-15588.
27. Scurto, A. M.; Aki, S. N. V. K.; Brennecke, J. F., CO_2 as a Separation Switch for Ionic Liquid/Organic Mixtures. *J. Am. Chem. Soc.* **2002,** 124, 10276-10277.
28. Roettger, D.; Nierlich, F.; Krissmann, J.; Wasserscheid, P.; Keim, W., Method for separation of substances by extraction or by washing them with ionic liquids. In US Patent 7,304,200: 2007.
29. Smith, R. S.; Herrera, P. S.; Reynolds, J. S.; Krzywicki, A., Use of ionic liquids to separate diolefins. In US Patent App. 10/308,307: 2002.
30. Pandey, S., Analytical applications of room-temperature ionic liquids: A review of recent efforts. *Anal. Chim. Acta* **2006,** 556, 1, 38-45.
31. Ahosseini, A.; Ren, W.; Scurto, A. M., Hydrogenation in biphasic ionic liquid-carbon dioxide systems. *ACS Symp. Ser. FIELD Full Journal Title:ACS Symposium Series* **2009,** 1006, Gas-Expanded Liquids and Near-Critical Media, 218-234.
32. Ahosseini, A.; Ren, W.; Scurto, A. M., Understanding Biphasic Ionic Liquid/CO_2 Systems for Homogeneous Catalysis: Hydroformylation. *Ind. Eng. Chem. Res.* **2009**, 95-101.
33. Ahosseini, A.; Ren, W.; Scurto, A. M., Homogeneous Catalysis in Biphasic Ionic Liquids/CO_2 Systems. *Chem. Today* **2007,** 25, 2, 40-42.

Chapter 2 Experimental methods

2 Experimental methods

Safety: most of the experiments described here were performed under elevated pressures and should be handled with care. All equipment should have the proper pressure ratings and standard operating procedures as determined by trained professionals. Some of the reactions can be highly exothermic and adequate solvent volumes and/or cooling must be provided during the reaction.

2.1 Reaction catalysis and product analysis

2.1.1 Biphasic IL/CO_2 hydroformylation of 1-octene

The biphasic IL/CO_2 hydroformylation reactions were carried out in a 10-cm^3 316 stainless steel high-pressure autoclave reactor similar to a design by Koch and Leitner and coworkers [1] and modified in our group (Figure 2-1). [2] The actual volume of this reactor considering lines and connections to the valves, which is measured accurately, is equal to 11.4 cm^3.

For the reaction experiments, catalyst pre-cursor (acetylacetonatodicarbonylrhodium, $Rh(CO)_2Acac$), and ligand (triphenylphosphine, TPP) were dissolved in ionic liquid and stirred for 30 minutes to allow dissolving and complexation of the ligand with the rhodium precursor (this time is in excess than required as observed by ^{31}P NMR studies and as described in subsection 2.2.1). The solution was then diluted with pure 1-hexyl-3-methyl-Imidazolium bis(trifluoromethylsulfonyl)amide ([HMIm][Tf_2N])) to obtain the low catalyst loadings used in these studies. The solution was added to the reactor under argon gas as an inert blanket. The argon was displaced with CO_2 and the reactant (1-octene) was injected into the reactor with a syringe. The reactor was heated to 70°C while stirring with a small stir bar. Stirring was temporarily halted and syngas was added to the reactor followed by CO_2 using a high-pressure syringe pump (Teledyne-Isco, Inc. 260D). Stirring was immediately resumed, and the reaction time started at a rate of 750 RPM with a 8mm (0.31 in) x 13mm (0.5 in) cylindrical stirrer. At the end of the reaction, the autoclave was placed in an ice-bath to quench the reaction and the gas phase vented into a

collection solution of n-hexane. This was necessary as significant quantities of 1-octene and n-nonanal are soluble in the CO_2 phase, especially at the higher pressures. The

Figure 2-1 Dismantled autoclave and reaction set up

ionic liquid phase was extracted by ~3mL of hexane three times, which is determined by GC calibration, for quantitative extraction. Both solutions are combined and analyzed by gas chromatography [3] (See section Gas chromatography analyses and calibration).

2.1.1.1 Hydrogenation

The biphasic IL/CO_2 hydrogenation reactions were carried out in a 10-cm^3 316 stainless steel high-pressure autoclave reactor similar to that is described in previous subsection. For the reaction experiments, catalyst (acetylacetonatodicarbonylrhodium, $Rh(CO)_2Acac$), and ligand (triphenylphosphine, TPP) were dissolved in dichloromethane. Dichloromethane solutions were used to obtain dilutions to achieve the small desired catalyst loading to high precision. The catalyst solution and ionic liquid were added to the reactor under argon gas as an inert blanket. The solution was stirred for 30 minutes at a rate of 750 RPM with an 8mm (0.31 in) x 13mm (0.5 in) cylindrical stirrer to allow complexation of the rhodium precursor with the ligand. This time allowed the complete dissolving and complexation of TPP with the Rh precursor in ionic liquid media as determined by ^{31}P NMR studies.

To remove the dichloromethane without entraining the catalyst or TPP the autoclave slowly heated under vacuum. Then, the reactant (1-octene) was injected to the above prepared catalyst mixture into the reactor. The reaction mixture was heated to 70°C, and then the desired amount of H_2 and CO_2 pressures were injected to the system, respectively. The gas phase is vented in hexane during depressurizing to trap the reactants and products, as significant quantities are soluble in the CO_2 phase at the higher pressures. The liquid phase is extracted by ~3mL of hexane three times (determined by GC calibration) for quantitative extraction. Both solutions are combined and analyzed by GC. [3]

2.2 Chemical analysis

Elemental analysis was performed by Desert Analytics Transwest Geochem. H-NMR and P-NMR spectra were recorded on a Bruker 400 NMR spectrometer using TMS as a reference for H chemical shifts. The water content was determined by a Mettler Toledo DL32 Karl Fischer Coulometer and the Br content was measured by a Cole-Parmer Bromide Electrode (27502-05) read with an Oakton Ion 510 series meter. Gas Chromatography analyses were carried out on a Varian CP-3800 Series gas chromatograph equipped with a Flame Ionization Detector (GC-FID for quantitative analyses) and a chrompack capillary column CP-Sil 5 CB (25m, .32mm, 1.2 μm).

2.2.1 ^{31}P NMR analyses

In order to find the time required for complexation of TPP ligands with the catalyst precursor (acetylacetonatodicarbonylrhodium, $Rh(CO)_2Acac$) in IL ([HMIm][Tf_2N]), a mixture with the ratio of TPP: precursor equal to 5 was dissolved in 10 mL IL. The time required for the sample preparation and ^{31}P NMR spectroscopy was totally 30 minutes. The ^{31}P NMR spectra for pure TPP, TPP oxide, and the final complex are shown in Figure 2-2. As can be seen, the doublet spectrum appears when the complexation occurs with the chemical shift of around 30 ppm. Due to use an excess amount of TPP, its spectrum can still be seen around the chemical shift of -6 ppm. The shorter spectrum besides the doublet represents existing of some phosphor oxides (P = O) formed in the solution during the sample preparation.

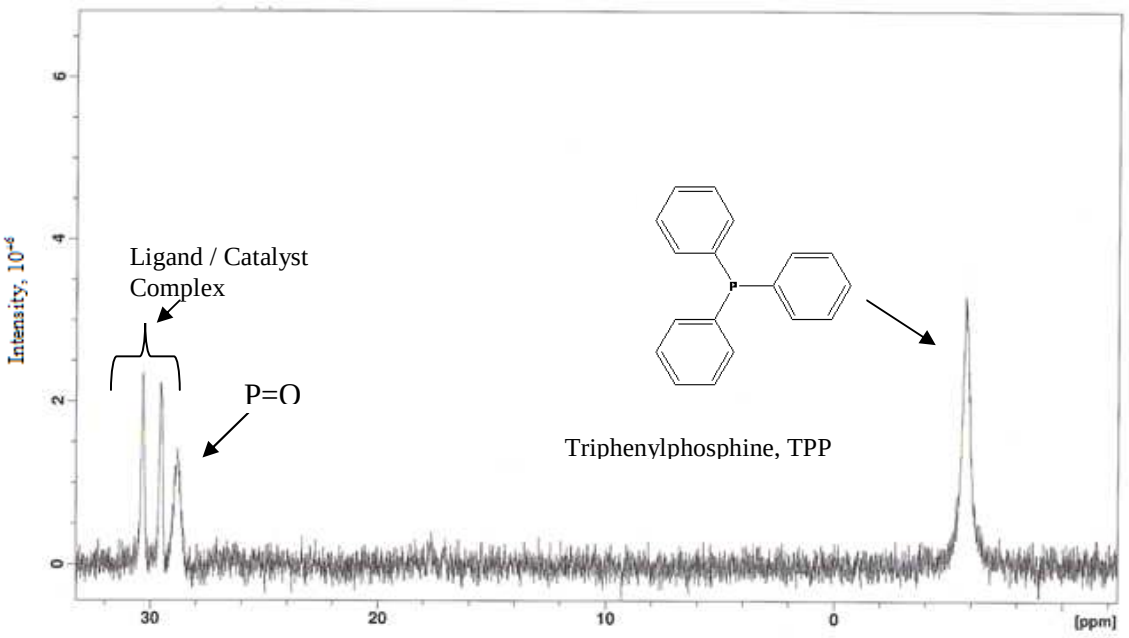

Figure 2-2 ^{31}P NMR spectra for the pure TPP, TPP Oxide, and ligand/catalyst complex

2.2.2 Gas chromatography analyses and calibration

2.2.2.1 Analyses

Gas Chromatography analyses of the product mixtures for hydroformylation and hydrogenation reactions in the present work were carried out on a Varian CP-3800 Series gas chromatograph equipped with a Flame Ionization Detector (GC-FID for quantitative analyses) and a chrompack capillary column CP-Sil 5 CB (25m, .32mm, 1.2 μm). GC oven program was developed as follows:

The capillary column was subjected 5 minutes to 30°C and with a program ramping of 10°C/min increased to 180°C then with a ramp of 20°C/min was increased to maximum 220°C and hold for about three minutes at this temperature. Injector type temperature was 250°C, constant column flow 2mL/min, pulse pressure 250 psi and pulse duration 1 minute. The FID detector temperature was 300 °C. The flow of hydrogen was 30 mL/min and of the air was 300 mL/min.

The product mixture detected includes aldehydes (linear and branched), residual octene and its isomers from 1-octene isomerization, and octanes from 1-octene hydrogenation. GC standards were used to classify the retention times for the chemical

components in the sample. The results of retention time for pure standards and their mixture solutions are shown in Table 2-1 and Table 2-2. As it is shown, the retention time can be affected by other compounds in the mixture. The amounts of components were calculated based on the integrated peak areas and the GC calibration. The regioselectivity in hydroformylation reaction is defined as the ratio of the linear to the branched aldehydes (*n*/*i*) in the product. The turnover frequency (TOF) is defined as the number of moles of product per moles of the catalyst per hour.

Table 2-1 Retention time for pure standards

Name	Retention time (min.)
2methyl heptane	10.25
4methyl heptane	10.30
3methyl heptane	10.44
trans 2 octene	10.85
trans 3 octene	11.01
1-octene	11.35
trans 4 octene	11.51
cis 4 octene	11.57
octane	11.64
octanal(b)	17.16
nonanal (l)	17.7
3-nonanol	18.1
2-nonanol	18.18
1-nonanol	19.1

Table 2-2 The retention time in the mixture		
NAME	RET.Time pure	RET.Time min.
hexane	4.81	4.93
1-octene	11.35	11.37
octane	11.64	11.66
octanal (b)	17.16	17.17
nonanal (l)	17.70	17.70
3-nonanol	18.10	17.74
2-nonanol	18.18	17.82
1-nonanol	19.10	18.74

2.2.2.2 Calibration

Firstly, standard solutions containing graded concentration of main products (nonanal for hydroformylation and octane for hydrogenation) in the extraction solvent (hexane) was prepared. The calibration curve was developed by plotting the peak area ratio versus molar concentration of products in solutions. The mole of product and TOF during the reaction was then calculated by considering the amount of hexane. The results of calibration for the correction factor of nonanal and octane was 0.9945 and 1.0071, respectively. (Table 2-3 and Figure 2-3)

For extraction of reactants and products from the ionic liquid mixture, care must be taken to quantitatively extract all of the materials. To determine the number of extraction steps that are needed to take most of nonanal and octene from the ionic liquid phase, the GC calibration was developed. In this method, graded amount of nonanal solutions in hexane were prepared.

Using the obtained chromatograms, a calibration curve was prepared by plotting peak areas vs. real concentration of nonanal. Then, a certain amount of nonanal was added to 2 mL ionic liquid and extracted 6 times by adding 3 mL hexane for ten minutes, by considering the amount of initial nonanal in ionic liquid, the mass of nonanal extracted in each step was calculated. The result showed in the following diagram indicates that after 5 steps all of nonanals can be extracted. (Figure 2-4, Figure 2-5)

Table 2-3 The results of calibration

Area ratio:(nonanal /(nonanal+octene)	Molar concentration: (Nonanal/Nonanal+Octene)
0.0104	0.1012
0.0283	0.1157
0.0771	0.1068
0.0983	0.1277
0.2899	0.3156
0.3318	0.3298
0.5016	0.5221
0.7648	0.7463
0.8560	0.8696
1.0000	1.0000

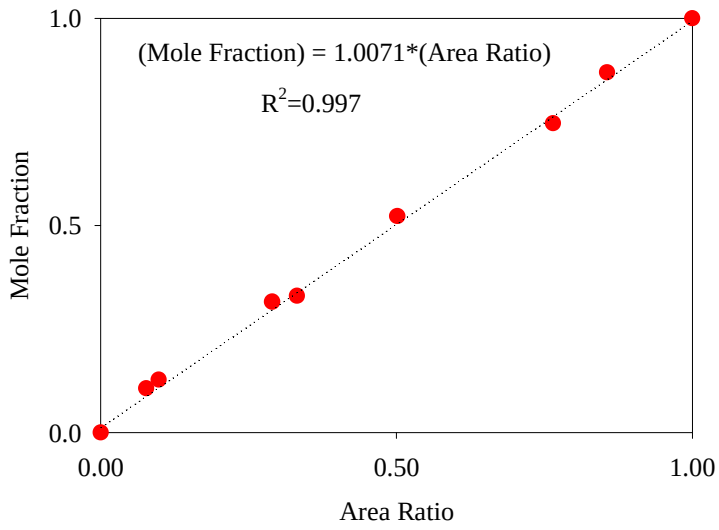

Figure 2-3 Calibration results

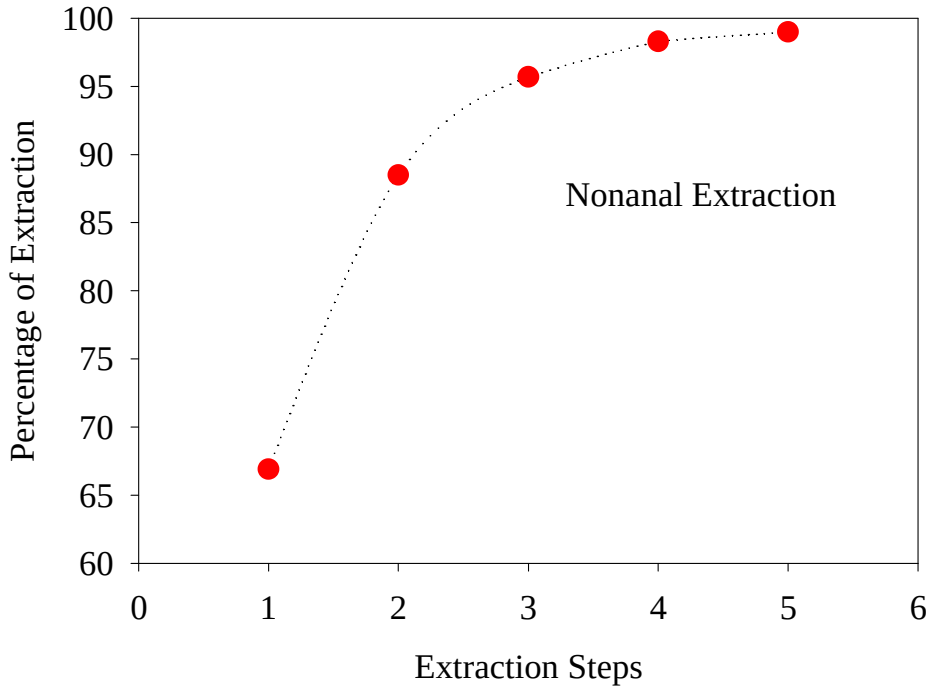

Figure 2-4 The number of steps for nonanal extraction using hexane

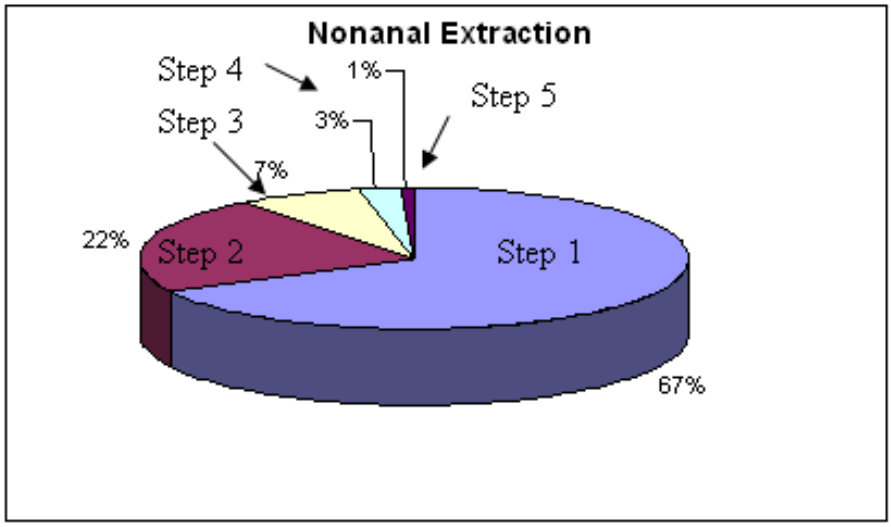

Figure 2-5 The percentage of nonanal separated from [HMIm][Tf_2N] / nonanal solution in consecutive sets of extraction with hexane

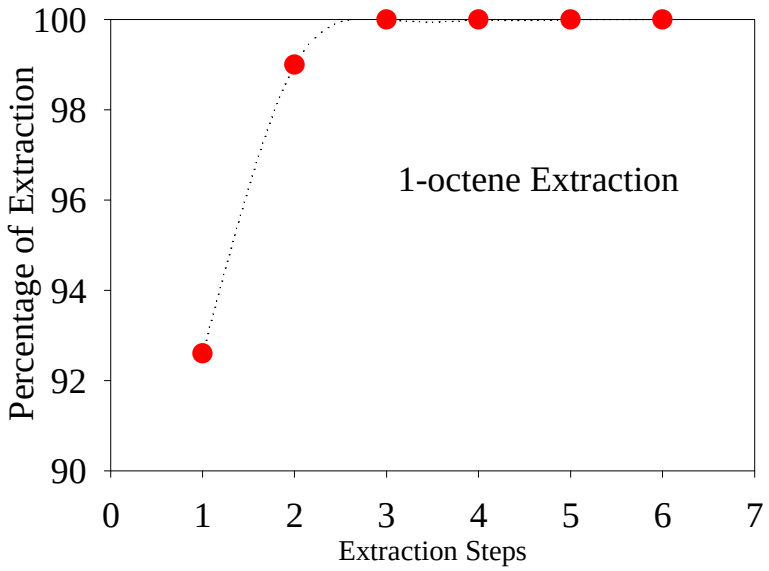

Figure 2-6 The number of steps for 1-octene extraction using hexane

The same procedure was used for 1-octene extraction and the result shows that after 3 times all of the reactant can be extracted by hexane at the described condition.
(Figure 2-7)

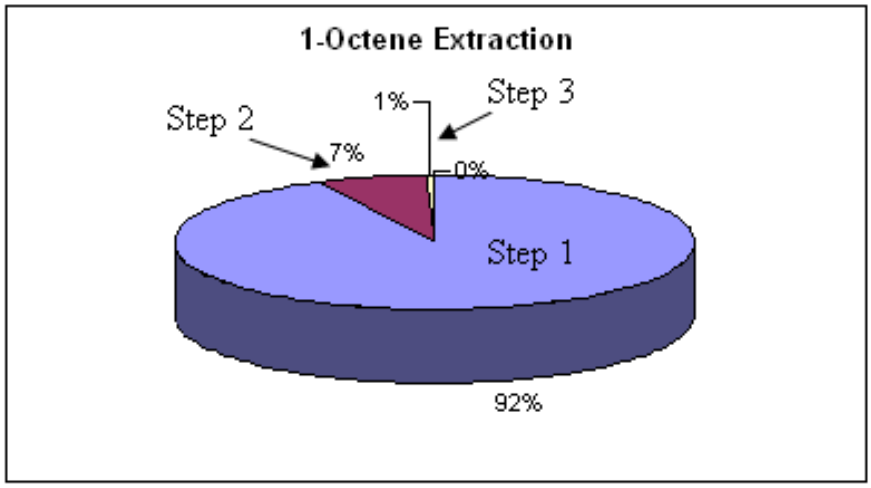

Figure 2-7 The percentage of 1-octene separated from [HMIm][Tf_2N] / 1-octene solution in consecutive sets of extraction with hexane, colors represent each step

2.3 Synthesis of ionic liquids

2.3.1 General method

Ionic liquids used in this study (Figure 2-8) were prepared by anion exchange from the corresponding bromide salts of the imidazolium cations with different n-alkyl substituents. [4, 5] The bromide salt of the imidazolium cation was prepared from a quaternization reaction of 1-methylimidazole with a slight excess amount of the corresponding alkyl bromide in acetonitrile at 313.15 K under an argon atmosphere with stirring for three days. *Caution: These reactions can be highly exothermic and adequate solvent volumes and/or cooling must be provided during the reaction.* The bromide salts of 1-alkyl-3-methyl-imidazolium were purified with activated charcoal (10%) stirring for 24 hours. Acetonitrile was added to reduce the viscosity of the ionic liquid, and the mixture was filtered. The mixture was then passed through a plug of celite (depth=7 cm, diameter=3 cm) and through a short column (height=20 cm, diameter=2.5 cm) of acidic alumina. The solvent was removed on a rotary evaporator under reduced pressure at 313.15 K and then connected to a high vacuum ($<10^{-4}$ torr) at 323.15 K for at least 48 hours. The ionic liquids were stored in Schlenk tubes under an atmosphere of dry argon.

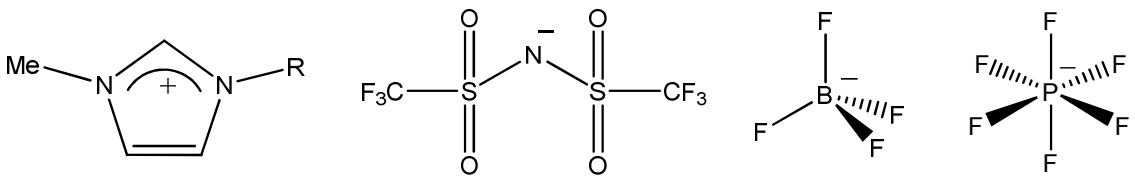

Figure 2-8 Structure of methyl imidazolium cations and anions investigated; for [R-MIm], R=ethyl- ([EMIm]), n-butyl- ([BMIm]), n-hexyl- ([HMIm]), and n-decyl- ([DMIm]).

2.3.1.1 1-Ethyl-3-Methylimidazolium Bis(Trifluoromethylsulfonyl)Imide ([EMIm][Tf_2N])

[EMIm][Tf_2N] was prepared from the anion exchange of [EMIm][Br] with Li[Tf_2N] in deionized water as described in the literature [6]. The denser hydrophobic IL phase is

decanted and washed with a volume of water approximately twice the volume of the IL for 6-8 times. The IL is then dried under vacuum. ^{1}H NMR chemical shifts (relative to TMS internal standard) and coupling constants: J/Hz: δ=8.59 (s, 1H), 7.42(t, 1H, J=1.59), 7.37(t, 1H, J=1.81), 4.24 (q, 2H, J=7.36), 3.93(s, 3H), 1.54 (t, 3H, J=7.4). Analysis calculated for $C_8H_{11}N_3F_6S_2O_4$: C, 24.55; H, 2.83; N, 10.74; S, 16.39. Found: C, 24.62; H, 2.84; N, 10.71; S, 15.88.

2.3.1.2 1-Hexyl-3-Methylimidazolium Bis(Trifluoromethylsulfonyl) Imide ([HMIm][Tf_2N])

[HMIm][Tf_2N] was prepared similarly to [EMIm][Tf_2N]. ^{1}H NMR chemical shifts (relative to TMS internal standard) and coupling constants J/Hz: δ=8.65 (s, 1H), 7.39(t, 1H, J=1.76), 7.37(t, 1H, J=1.48), 4.17 (t, 2H, J=7.4), 3.93(s, 3H), 1.87(m, 2H), 1.32(m, 6H) 0.87(t, 3H, J=6.53). Analysis calculated for $C_{12}H_{19}N_3F_6S_2O_4$: C, 32.2; H, 4.28; N, 9.39; S, 14.33. Found: C, 32.21; H, 4.27; N, 9.25; S, 14.19.

2.3.1.3 1-Decyl-3-Methylimidazolium Bis(Trifluoromethylsulfonyl)Imide ([DMIm][Tf_2N])

[DMIm][Tf_2N] was prepared similarly to [EMIm][Tf_2N]. ^{1}H NMR chemical shifts (relative to TMS internal standard) and coupling constants J/Hz: δ=8.66 (s, 1H), 7.36 (t, 1H, 1.58), 7.36 (t, 1H, 1.58), 4.15 (t, 2H, J=7.5), 3.92(s, 3H), 1.86(m, 2H), 1.26 (m, 14H), 0.87 (t, 3H, J=6.7). Analysis calculated for $C_{16}H_{27}N_3F_6S_2O_4$: C, 38.17; H, 5.4; N, 8.34; S, 12.73. Found: C, 38.55; H, 5.3; N, 8.15; S, 12.29.

2.3.1.4 1-Hexyl-3-Methylimidazolium Tetrafluoroborate ([HMIm][BF_4])

[HMIm][BF_4] was prepared from the anion exchange of [HMIm][Br] with ammonium tetrafluoroborate in deionized water. ^{1}H NMR chemical shifts (relative to TMS internal standard) and coupling constants J/Hz: δ=8.72 (s, 1H), 7.52(t, 1H, J=1.84), 7.5(t, 1H, J=1.38), 4.22 (t, 2H, J=7.23), 3.96(s, 3H), 1.89(m, 2H), 1.32(m, 6H), 0.86(t, 3H, J=6.54). Analysis calculated for $C_{10}H_{19}N_2BF_4$: C, 47.27; H, 7.54; N, 11.02; B, 4.25. Found: C, 46.99; H, 7.21; N, 10.88; B, 4.39.

2.3.1.5 1-Hexyl-3-Methylimidazolium Hexafluorophosphate ([HMIm][PF_6])

[HMIm][PF_6] was prepared from the anion exchange of [HMIm][Br] with ammonium hexafluorophosphate in deionized water [7, 8]. As the [PF_6] anion is known to decompose to HF over time, the compound was tested immediately after synthesis. ^{1}H NMR chemical shifts (relative to TMS internal standard) and coupling constants J/Hz: δ=8.43 (s, 1H), 7.33(t, 1H, J=1.84), 7.32(t, 1H, J=1.91), 4.12 (t, 2H, J=7.22), 3.87(s, 3H), 1.85(m, 2H), 1.28(m, 6H), 0.84 (t, 3H, J=6.96). Analysis calculated for $C_{10}H_{19}N_2BF_4$: C, 38.47; H, 6.134; N, 8.97; P, 9.92. Found: C, 38.64; H, 6.01; N, 9.01; P, 9.62.

2.3.1.6 1-Butyl-3-Methylimidazolium Hexafluorophosphate ([BMIm][PF_6])

[BMIm][PF_6] was prepared in a similar procedure as [HMIm][PF_6], but from the anion exchange of [BMIm][Br] with ammonium hexafluorophosphate in deionized water. As the [PF_6] anion is known to decompose over time, the compound was tested immediately after synthesis. ^{1}H NMR chemical shifts (relative to TMS internal standard) and coupling constants J/Hz: δ=8.35 (s, 1H), 7.31(t, 1H, J=1.79), 7.28(t, 1H, J=1.79), 4.09 (t, 2H, J=7.4), 3.83(s, 3H), 1.79(m, 2H), 1.29(m, 2H), 0.85 (t, 3H, J=7.4). Analysis calculated for $C_8H_{15}N_2PF_6$: C, 33.81; H, 5.32;N,9.86; P, 10.90; F,40.11. Found: C, 33.69; H, 5.21; N, 9.63; P, 10.40; F: 41.70.

2.4 Materials

1-Methyl-imidazole, (CAS# 616-47-7) 99+%, acetonitrile (CAS 75-05-8) ≥99.9%, toluene (CAS 108-88-3) ≥99.9 , acetone (CAS 67-64-1) HPLC grade ≥99.9, methanol (CAS 67-56-1) ≥ 99%, hexane (CAS 110-54-3) HPLC grade≥ 95%, 1-Octene (CAS 111-66-0) 98%, lithium bis(trifluoromethylsulfonyl)imide (CAS# 90076-65-6) 99.95%, ammonium hexafluorophosphate (CAS# 16941-11-0) 99.99%, ammonium tetrafluoroborate (CAS# 13826-83-0) 99.99%, acetylacetonato dicarbonylrhodium (CAS 14874-82-9) 98%, and triphenylphosphine (CAS 603-35-0) 99% were purchased from Sigma-Aldrich. Bromoethane (CAS# 74-96-4) 99+%, bromobutane (CAS# 109-65-9) 99%, bromohexane (CAS# 111-25-1) 99+%, bromodecane (112-29-8) 98%, and aluminium oxide (activated, acidic, for column chromatography; 100-500 micron) were obtained from Acros. Activated carbon 50-200 mesh was obtained from Fisher Scientific. Coleman Instrument grade CO_2, argon (extra dry grade 99.998%), H_2 (high purity grade

99.995%), syngas (H_2/CO: 0.98% purity, H_2: 99.999, CO:99.5%, certified standard) were obtained from Airgas, Inc. 1,1,1,2-Tetrafluoroethane (CAS# 811-97-2) (R134a) was purchased from INEOS Fluor Americas LLC. The $Rh(CO)_2Acac$ was placed in a Schlenk tube and stored under dry argon. The bromo-alkanes and 1-methylimidazole were vacuum distilled directly prior to use.

2.4.1 Bromide measurements

The amount of bromide in ionic liquids is very important to be determined especially when they are used as a solvent in homogeneous catalysis. In this type of catalysis, bromide can compete with reactants to coordinate with the catalyst and poison it and so affect the selectivity and activity of the reaction. In this work, the Br content was measured by a Cole-Parmer Bromide Electrode (27502-05) read with an Oakton Ion 510 series meter.

The bromide electrode must be calibrated each day for accurate readings, and must be done so at low and high level concentration of bromide. The solvent used to calibrate the electrode must contain some water, or the electrode cannot accurately measure the bromide concentration in the solution. Since the ionic liquids are not soluble in deionized water, bromide ions that have bonded to the ionic liquid in solution will not have dissociated when placed in deionized water, and thus would not be measured by the electrode. So, three different compounds were tested to determine the optimal solvent to use when testing bromide concentration in ionic liquids. The solvents tested were deionized water; equal parts deionized water and methanol; and equal parts deionized water, methanol, and acetonitirile. Acetonitrile and methanol were chosen because they are good solvents for imidazolium based ionic liquids. In addition, methanol can help to make a uniform organic and aqueous compound to dissolve ionic liquids.

2.4.1.1 Calibration

Standard solutions with known bromide concentrations were made to calibrate the electrode. From the 1000 ppm standard bromide solution, three standards of 1, 10, and 100 ppm were made by adding 100 mL of solvent to each of three 250 mL beakers and then adding 0.1, 1, and 10 mL of the 1000 ppm solution, respectively. To each of the standards, 2 mL of the 5 M bromide Ionic Strength Adjuster (ISA) should be added for

each 100 mL of solvent. These standard solutions should be saved and used for calibration of the instrument each day. To calibrate the electrode, begin with the lowest concentration solution (1 ppm) and mix gently using a magnetic stirring bar and stirring plate. Place the clean electrode in the solution and allow the electrode reading to stabilize. If the reading doesn't reach a constant amount after approximately 15 minutes, the electrode will have to be polished before further use. Record the millivolt reading for this concentration, clean the electrode, and then repeat with the other two concentrations. This high level calibration will have to be repeated every 2-4 hours.

To calibrate the instrument for lower bromide concentrations, the following procedure should be used. For low level concentrations, a lower molarity ISA (Ionic Strength Adjuster) must be prepared by diluting 20 mL of the standard 5 M ISA to 100 mL with deionized water. To calibrate the instrument begin with 100 mL of the solvent in a 250 mL beaker and add 1 mL of the low molarity ISA. A second solution of 10 ppm bromide standard will also have to be prepared as per the directions above, with the exception being that no ISA should be added to this standard. While stirring gently with the electrode in place add the following volumes of the 10 ppm bromide solution Table 2-4, allowing the instrument to stabilize between each step. The low level calibration should be completed each day.

Table 2-4 Stepwise Low Level Calibration

Volume Added (mL)	Concentration (ppm)
0.1	.01
0.1	.02
0.2	.04
0.2	.06
0.4	.99
2.0	2.9
2.0	4.8

The calibration data should be graphed on semi-logarithmic graph paper with the millivolt reading as the linear axis against the concentration (ppm) as the logarithmic axis.

2.4.1.2 Measuring procedure

To test the bromide concentration of a sample, add 100 mL of the solvent used for calibration and 1 mL of the sample to a 250 mL beaker with 2 mL of standard ISA. Gently stir the solution with the electrode immersed in the solution and allow the instrument reading to stabilize. Using the calibration curve, convert the millivolt reading to concentration. The concentration read from the calibration curve must be factored upwards by 100 since the solution tested diluted the ionic liquid sample by a factor of 100. The concentration of bromide in the ionic liquids tested in some cases varied widely depending on the solvent used. If the ionic liquid was not completely soluble in the solvent used, the measured bromide concentration was less accurate than when the ionic liquid was completely soluble in the solvent. Results from bromide concentration testing using three different solvents showed that some ionic liquids can not completely be soluble in the solvent used for testing. For instance, [DMIm][Tf_2N] and [BMIm][BF_4] can not completely be dissolved in methanol-water solvent but the combination of water, methanol, and acetonitrile was a good solvent for all of ionic liquids used in this project.

2.5 Phase behavior

The high-pressure phase equilibrium data were measured by a high pressure view cell and static vapor-liquid equilibrium (VLE) apparatus. The autoclave reactors were similar to those described above except with a high-precision pressure gauge, Omega DPG7000 with an error band of ± 0.05% of full scale (3000psi). The static VLE apparatus is described in detail by Ren and Scurto [9].

2.6 Viscosity measurement

2.6.1 Ambient pressure viscometer

The viscosity of liquids at ambient pressure (at different temperatures) was measured using a Wells-Brookfield Cone/Plate (DV-III ULTRA) Viscometer / Rheometer. The principle of operation of this instrument is to drive a rotating cone, which is immersed in the sample fluid between the cone and a stationary flat plate through a calibrated beryllium-copper spring. The viscose drag of the fluid against the cone is measured by the spring deflection. Spring deflection is measured with a rotary transducer.

The resistance to the rotation of the cone produces a torque that is proportional to the shear stress in the fluid. The amount of torque is indicated either on a dial or digital display, depending on model. This reading is easily converted to absolute centipoise units (mPa·s) from pre-calculated range charts. Alternatively, viscosity can be calculated from the known geometric constants of the cone, the rate of rotation, and the stress related torque. The stationary plate forms the bottom of a sample cup which can be removed, filled with .5 mL to 2.0 mL of sample fluid (depending on cone in use), and remounted without disturbing the calibration. The sample cup is jacketed and has tube fittings for connection to a constant temperature circulating bath. All wetted parts are stainless steel for corrosion resistance and ease of cleaning.

The system is accurate to within ±1.0% of the working range. Reproducibility is to within ±0.2%. Working temperature range is from 0°C to 100°C with the accuracy of ±0.1°C. The standard gravimetric method is used to make the solution of 1-octene in ionic liquid. The mixture prepared by weighing specific amount of each part into a 25 mL vial with an uncertainty of ±0.0002 gr.

2.6.2 High pressure viscometer

2.6.2.1 Principle of measurements

A Cambridge Applied Systems (currently Cambridge Viscosity, Inc., www.cambridgeviscosity.com) high pressure viscometer was utilized for these measurements (ViscoPro 2000 System 4- SPL-440 with Viscolab software). A picture of the viscometer is shown in Figure 2-9. The apparatus consists of a temperature-controlled oven which houses the high pressure viscometer sensor. The sensor is connected to a precision pressure transducer (PT) and a resistance temperature detector (RTD).

The viscometer utilizes the principles of annular flow around an axially oscillating piston [10]. A diagram of the testing chamber is found in Figure 2-9 and consists of the chamber, piston, electromagnetic coils, and RTD for temperature measurement. Two magnetic coils inside the sensor body oscillate the piston (one coil at a time) over a fixed distance, forcing the fluid to flow through the annular space between the rod and chamber. One magnetic coil applies a constant force on the piston while the other

determines the position of the piston. The roles of the coils reverse when the piston reaches the end of the cycle and changes direction. The time required for the rod to complete a cycle is directly related to the dynamic viscosity of the fluid.

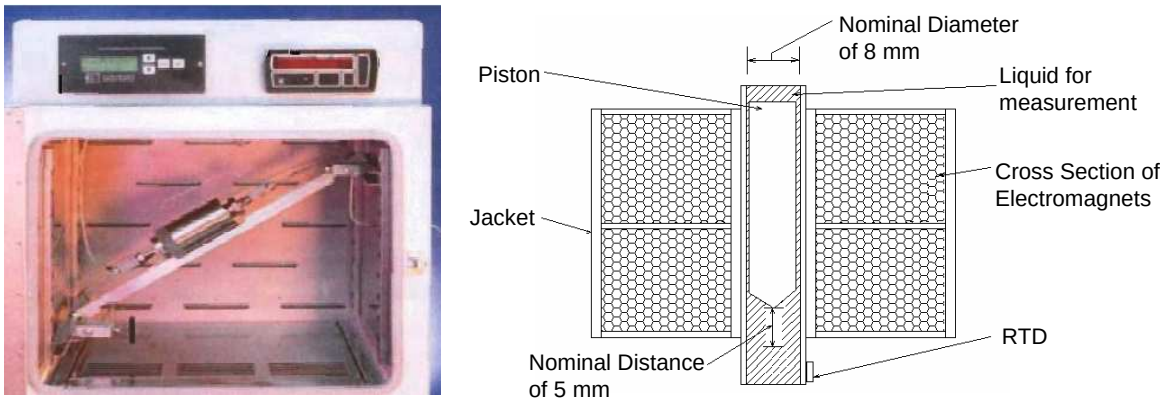

Figure 2-9 a) The Initial Set up From Cambrige Viscosity, inc. b) Features of the Cambridge Viscosity Viscometer Measurement Chamber

The sensor is capable of measurements from 0.2 to 10,000 cP (mPa·s), at a maximum pressure of 137.9 MPa and in a temperature range of 233.15 K to 463.15 K. Various piston sizes lead to more accurate results under different ranges of viscosity and are changed according to their factory-suggested conditions. As the diameter inside the Inconel 718 chamber slightly increases with pressure, these changes are corrected by a factory-provided conversion equation. The viscosity reading is the average of 20 viscosity measurements and is reported with the standard deviation of those measurements. The nominal uncertainty of the pressure gauge is 0.07% full-scale (FS=206.8 MPa); but the NIST-traceable calibration was accurate to 0.0084% full-scale. The maximum deviation of temperature from the set-point temperature for all data was 0.1 K, with the average deviation being ±0.07K.

2.6.2.2 Viscosity measurement of pure ionic liquids at elevated pressures

2.6.2.2.2 Set up

A schematic diagram of the set up is shown in Figure 2-10. [3] The apparatus consists of a temperature controlled oven (1) (±0.1K) which houses the high-pressure viscometer sensor (2). The testing chamber is connected to a rupture disk (RD) (up to 20000 psi) (3),

a precision pressure transducer (PT) (4), and a resistance temperature detector (RTD) (5). The viscometer was connected to a manual high-pressure syringe pump (6) purchased from High Pressure Equipment Company (HIP) (Model No. 50-575-30; 30,000 psi, capacity of 10cm^3 with PolyPak).

2.6.2.2.3 Measuring Procedure

A volume of approximately 30-40 mL of the dried compound was transferred into the high-pressure manual syringe pump from a Schlenk flask under the argon pressure using a stainless steel high pressure metering pump (Eldex Laboratories, Inc., Model 1020 BBB-4). The water content before and after measurement has been determined and the maximum amount (after measurement) is reported. The highest deviation of the before and after was 70 ppm. The liquid was forced through the lines to displace any argon pockets.

The viscometer has a "purge" feature which rapidly oscillates the rod in the measurement chamber to dislodge any potential bubbles. The outlet valve was closed, and the pressure was sequentially increased from 0.1 MPa to 126 MPa. To prevent damage to the viscometer, this pressure was applied at a rate of less than 7 MPa·min^{-1}. The temperatures of interest in this experiment were 298.15 K, 323.15 K, and 343.15 K.

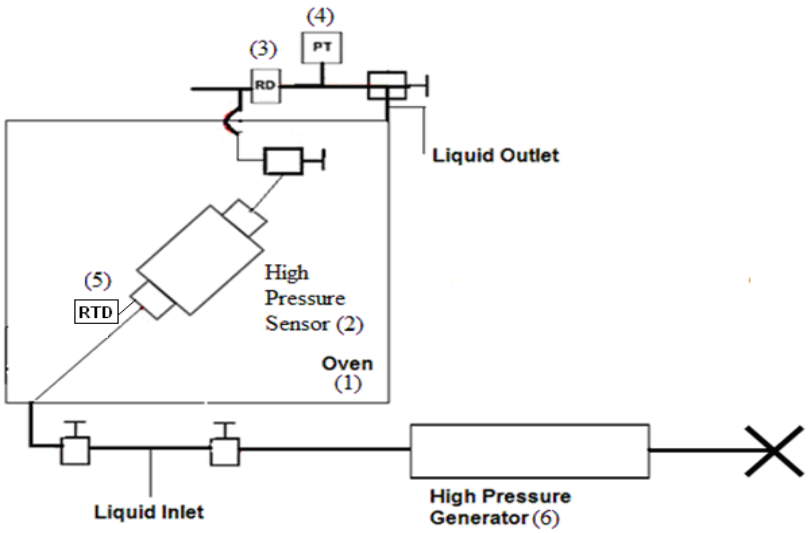

Figure 2-10 Schematic of the viscometer apparatus for pure liquid viscosity measurements (1) oven, (2) high pressure sensor, (3) rupture disc, (4) pressure transducer, (5) RTD temperature probe, and (6) high pressure generator

2.6.2.3 Viscosity measurement of ionic liquids with compressed gases

2.6.2.3.2 Set up

The set up used for the measuring viscosity of pure ionic liquids was modified to include a high pressure equilibrium Jerguson view cell (7), high pressure Teledyne-Isco, Inc. Syringe pump (model 260D) (8) and a Micropump Inc. (model 415A) recirculation system (9). The testing chamber is connected to a rupture disk (RD) (up to 5000 psi) (3). Figure 2-11 illustrates the modified system and components that are used to measure the viscosity of ionic liquids with compressed gases. [11]

2.6.2.3.3 Measuring procedure

A volume of approximately 25 mL of the dried compound was transferred into the high –pressure view-cell (7) from a schlenk flask under argon using a stainless steel high-pressure metering pump (Eldex Laboratories, Inc., Model 1020 BBB-4). A ~ 30cm^3 Jerguson view-cell is utilized as an equilibrium cell which holds the ionic liquid and the gas. A Teledyne- Isco, Inc. syringe pump (model 260D) (8) is used to administer and maintain gas pressure. A Micropump, Inc. (model 415A) recirculation pump (9) is used to draw ionic liquid from the viewcell, transport it through the viscometer sensor (2) and then back to the top of the view-cell where the material falls through the gas phase back to the liquid layer. This recirculation allows for a rapid approach to equilibrium, while being able to monitor the change in viscosity over time. Equilibrium is usually achieved in approximately 30 minutes at each pressure. However, at low temperatures and pressures (highest viscosity), up to 60 minutes or more is allowed. The error in viscosity is reported at each point based upon the sampling average of 20 measurements.

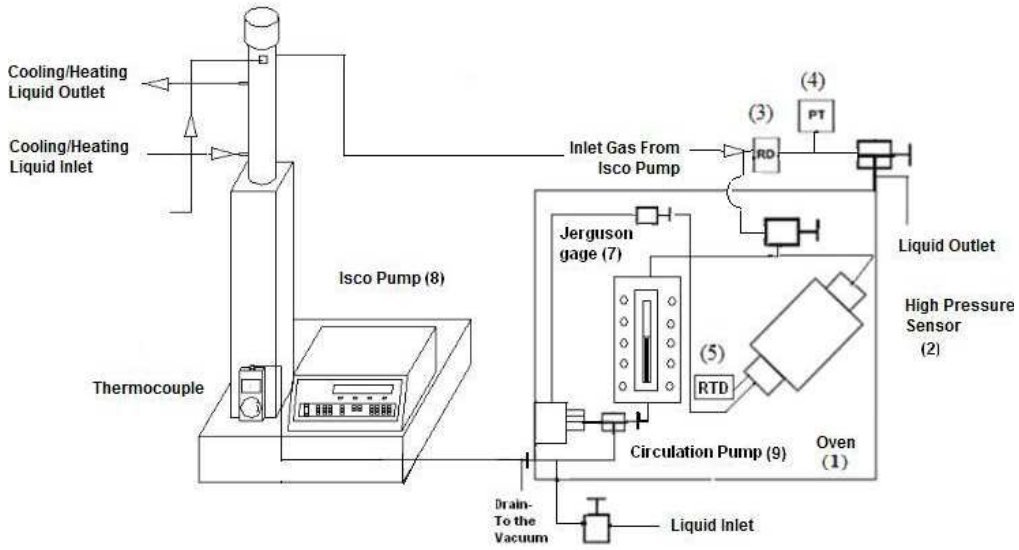

Figure 2-11 Schematic of the viscometer apparatus for viscosity measurement of liquids with compressed gases (1) oven, (2) high pressure sensor, (3) rupture disc, (4) pressure transducer, (5) RTD temperature probe, (6) high pressure generator (is not shown here) , (7) Jerguson view cell, (8) Syringe pump, (9) Micropump recirculation system

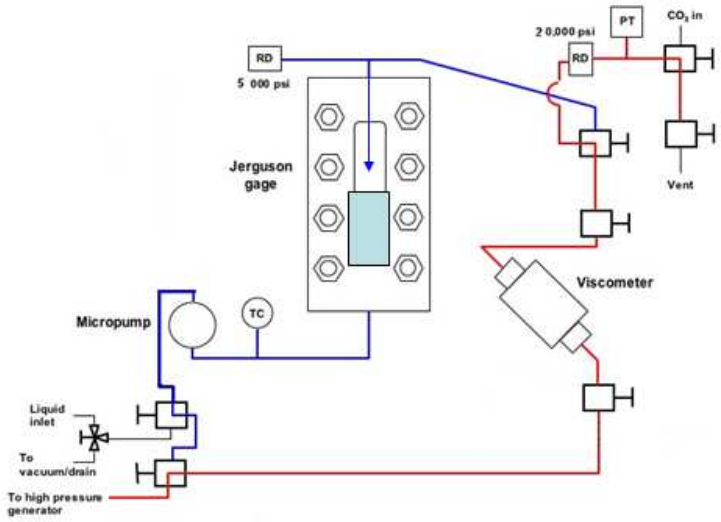

Figure 2-12 Schematic of two different paths in high pressure viscosity measurements

The whole system for measuring pure and saturated gas-liquid viscosity at elevated pressures is shown in Figure 2-12. Figure 2-13 shows the real set up.

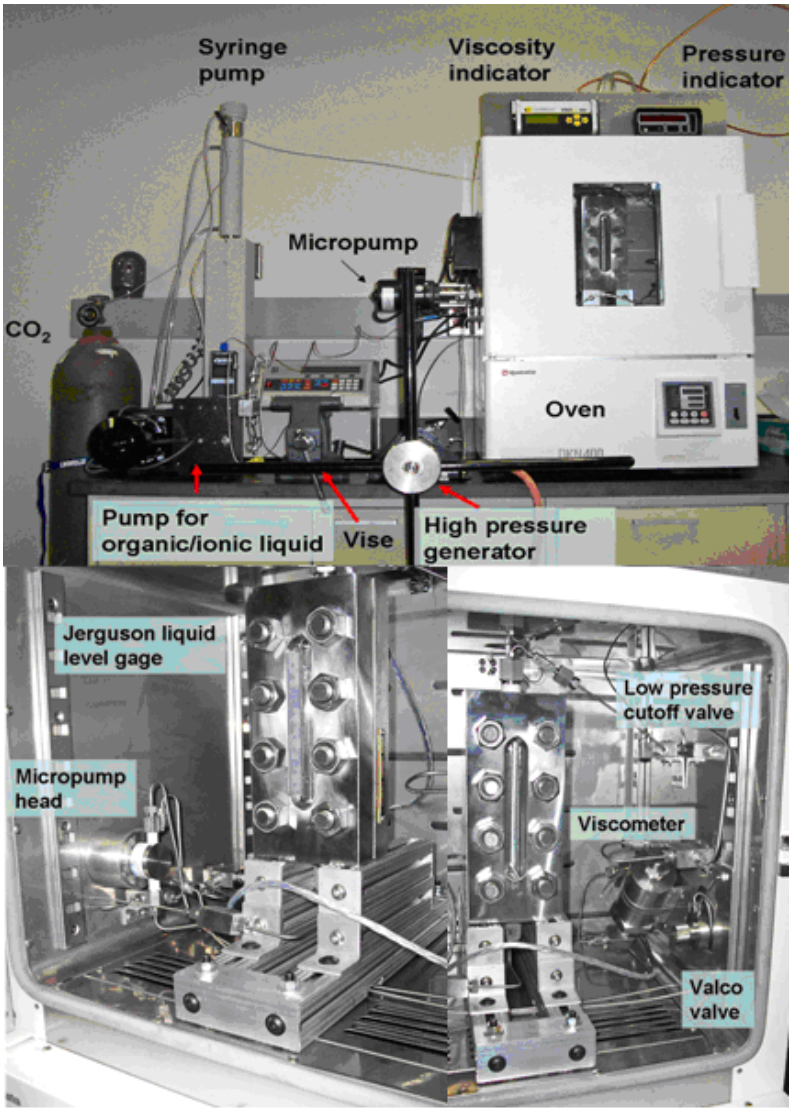

Figure 2-13 high pressure viscosity measurement set up

2.7 Diffusion coefficient measurements

2.7.1 Overview

Self diffusion, which is different from spin diffusion or rotational diffusion is defined as the random translational movement of molecules motivated by internal energy. [12] Translational diffusion is the most important form of transport in reactions that causes collision and interactions between reactants before they can react.

A Bruker 400 MHz ^{1}H NMR was used to measure the translational diffusion with a pulsed-field gradient (PFG) method. The software used to analyze the data was Topspin version 1.3.

The aim of this section is to introduce the PFG experiments and some theoretical basis to determine the diffusion coefficient of components. For a broader review of the literature, a number of relevant references have been mentioned in the text that may be consulted for more detailed understanding of some aspects. As analysis of PFG in NMR experiments is essentially mathematical, special effort is placed to create a physical feeling for how diffusion can be related to the reduction of the echo signal in this method. For this reason, the effects of a magnetic gradient on nuclear spins are discussed.

2.7.2 Fundamental aspects

The most important parts of an NMR spectrometer are the magnet, the radio frequency (rf) transmitter and detector (Figure 2-14). The NMR tube containing the sample is located in the external magnetic field. A radio frequency coil creates the radiation and the excited signal is detected, amplified, and finally recorded. Considering the number of atoms in a sample, an overall net momentum lies along the z-axis. [12-14]

In a pulsed-field gradient (PFG), the reduction of a signal intensity resulting from the combination of molecular diffusion and magnetic force gradient pulses on nuclear spins can be measured. The mechanism and the physics of this experiment can also be described referring to the diagrams shown in Figure 2-15 and Figure 2-16. [12, 14] Case (a) shows an overall net momentum M lies along the z-axis under the static magnetic force (B_0). An rf pulse in the x-direction leads to deviate the vector to y-axis (b). As a result of a pulse gradient of duration δ and magnitude g and the lack of homogeneity of main (B_0) field at time t_1, nuclear spins begin to spread out and the magnitude of magnetization decreases (c).

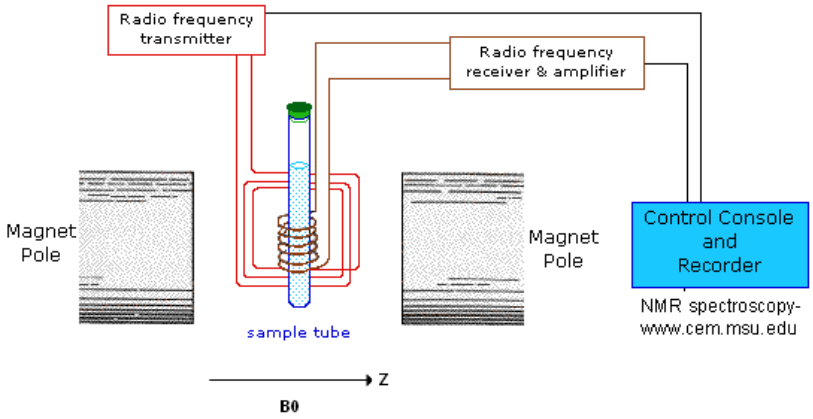

Figure 2-14 Schematic of the NMR spectrometer

After a certain time τ a π rf pulse is applied that has the effect of reversing the sign of the precession into the negative y-direction (d). At time $t_{1+\Delta}$, a second gradient pulse of equal magnitude and duration is applied and the vectors become focus in a negative y-direction in the lack of translational diffusivity. However, if there is a diffusion movement of molecules and spins with respect to the z-axis, the starting and finishing of an ensemble of nuclei will have different spatial position. The degree of this deviation is proportional to the displacement in the direction of the gradient and can be measured by the signal intensity, which will be decreased based on the diffusion time as well as the gradient parameters: gradient strength and length of gradient.

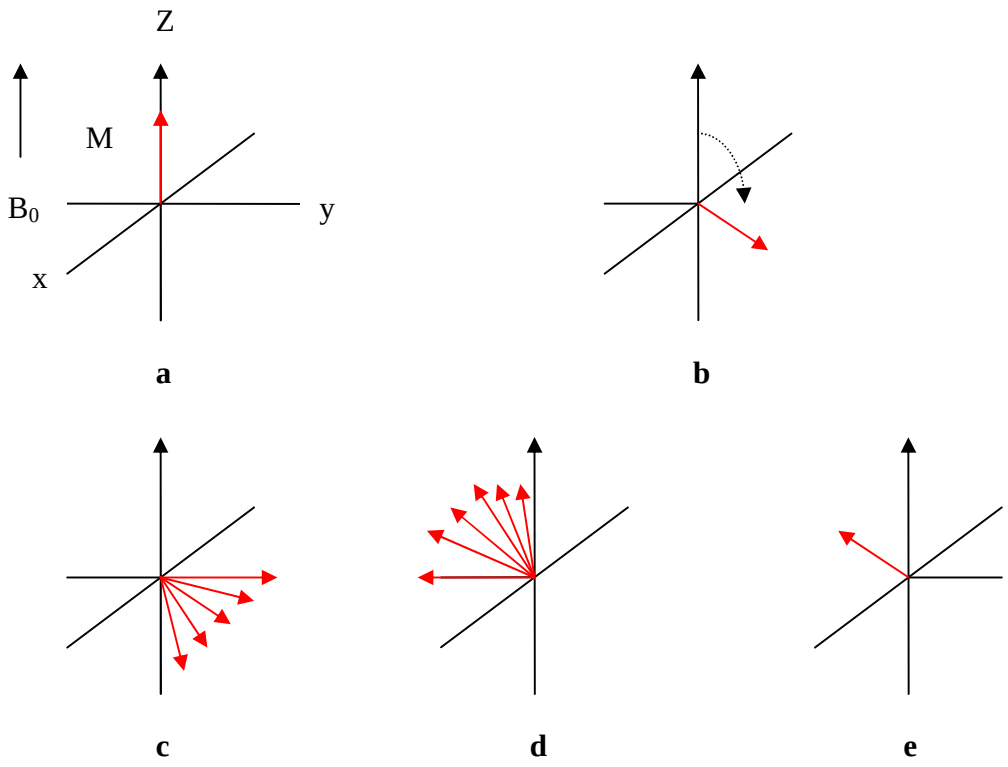

Figure 2-15 The physics of spin echo experiment [14]

The intensities for the sample are driven by Price and through the following equation: [12]

$$I = I^{o} e^{-(\gamma \delta g)^2 D\left(\Delta - \frac{\delta}{3} - \frac{\tau}{2}\right)} \qquad (2.1)$$

where I=Intensity of the NMR Peak; I^{o}=Intesnsity of NMR Peak initial; γ=gyromagnetic ratio that is equal to 26750 $Gauss^{-1}sec^{-1}$ for ^{1}H NMR; g= gradient strength [related to gpz6 using g=g*(gpz6/100)] where *g** is the total gradient strength; δ= length of gradient (p30=δ**0.5*); Δ= Diffusion time (d20); τ= the time between rf gradients (p31); and D= Diffusion coefficient.

Note: items in parenthesis are the parameters used for each symbol in the pulse sequence. For a more detailed analysis of the NMR method used for diffusion see Bruker's Manual under DOSY and other related references. [2, 12, 13, 15-20]

2.7.3 Calibration

All diffusion experiments at ambient pressure were conducted in standard 5 millimeter NMR tubes. To measure diffusion coefficients, the NMR need to be calibrated and the applied gradient strength (*g*) has to be determined by knowing all other parameters in equation 2.1. On average, the value for the diffusion time is milliseconds to seconds, length of gradient is 0-10 milliseconds, and the time between rf gradients is two to three milliseconds [13]. By calibrating the NMR, the value for *g* was obtained using known diffusion coefficient of two standards at 25°C, hexane (D= 4.15×10^{-9} m2/sec) [21] and water (D= 2.3×10^{-9} m2/sec) [22]. These standards were chosen because their diffusion coefficients in a pure condition have been measured before and reported in literature. Choosing pure compounds is preferred to avoid entering extra errors by making binary compounds. All of these measurements are done without using deuterated solvents.

For the calibrations, all the time parameters, Δ, δ, and τ remained constant, while the applied gradient strength was altered. To protect the gradient coil from burning the maximum gradient strength used was $g=70\%\times g_{max}$. [20] The applied gradient strength alteration was between $g=5\%$ to $g=70\%$ of the total applied gradient strength using [13, 20] equal increments.

From the two calibrations, the total applied gradient strength, which was experimentally determined, is 49.5 Gauss per meter (G/m). To validate the gradient strength obtained from experiments the diffusion coefficient for [HMIm][Tf_2N] was analyzed and compared with the literature. It has been reported that the diffusion coefficient for [HMIm][Tf_2N] at 25°C is 1.75×10^{-11} m^2/sec [23], which is close to the experimentally determined value of 1.79×10^{-11} m^2/sec. The standard deviation of the diffusion coefficients measurements out of five different experiments are less than 3%.

Similar procedure is followed for diffusion experiments. The only difference is instead of total gradient strength (g) in calibration the diffusion coefficient (D) has been measured. The value of diffusion coefficient was determined by the slope of the line obtained by graphing natural log of (I/I_0) vs. the amount of power without D in equation

2.1. The measuring procedure, which is a modified version of the previous report [2], is used for the calibration. In this method, an automatic optimization technique is developed to find an accurate 90 degree pulse (which is perpendicular to the magnetic field, z axis). This modification helps to have more precise results at the considerably shorter time. Detail procedure is described stepwise in the appendix (A).

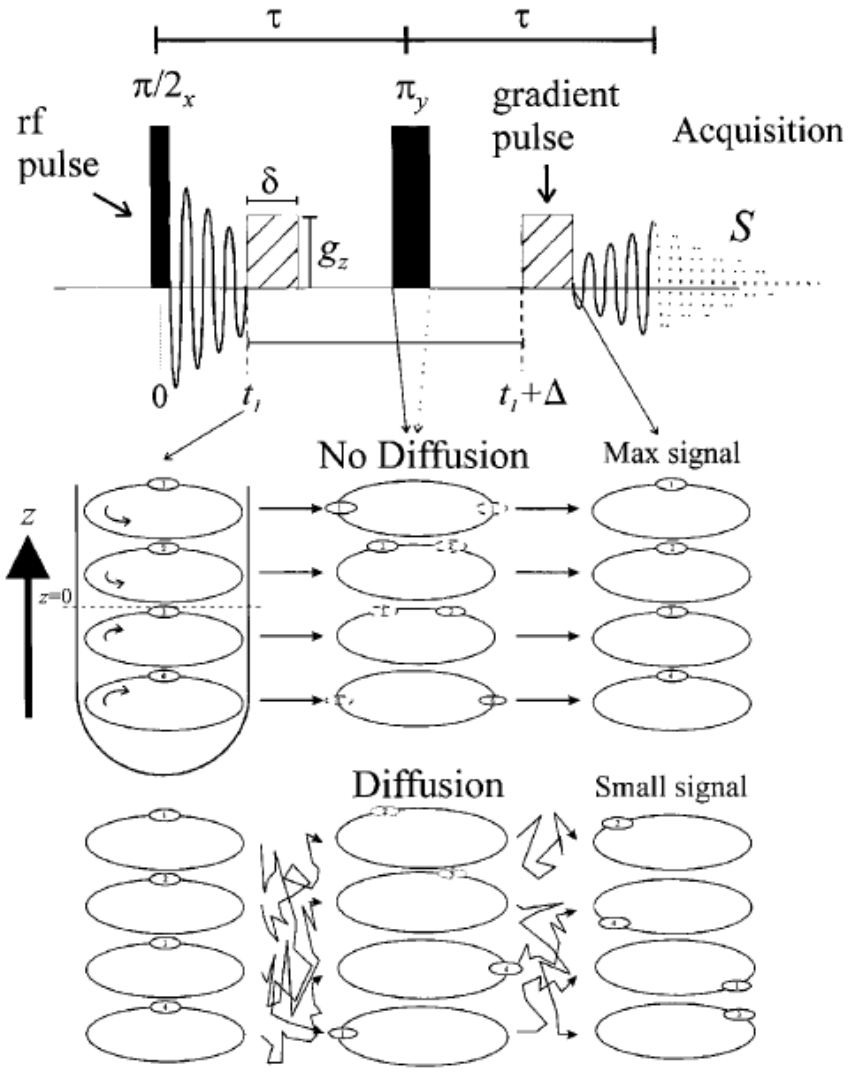

Figure 2-16 The Mechanism of Pulse Field Gradient (PFG) Method, [Price, 1997]

2.7.4 Moderate pressure diffusivity

To measure the diffusion coefficient of molecules of a liquid mixing with a compressed gas, the same procedure can be followed as the method for ambient pressure. A special NMR tube made of glass was utilized from Wilmad Lab Glass, Inc. (Model PV-ANV Pressure/Vacuum NMR Valve) in order to provide a moderate pressure condition (up to 13 bar) (Figure 2-17). To prepare a sample, ionic liquid is injected to the tube to the height of 3 cm. Then connect a 1/8 inch OD PEEK tube to

the Swagelok nut on the valve with a back ferrule and a front ferrule. This connection is used for injecting the gas into the tube. After introducing the gas by an Isco syringe pump, the valve is tightened. In the case of monitoring the pressure inside of the tube a valve with a hole is built to connect the inside of the tube to a pressure gauge. This pressure gauge was attached with one valve to the syringe pump and another valve to the NMR tube to control the gas injection. To accelerate reaching equilibrium condition the tube is shaken frequently. When the pressure gauge shows the desire pressure persistently the sample is ready for further measurements.

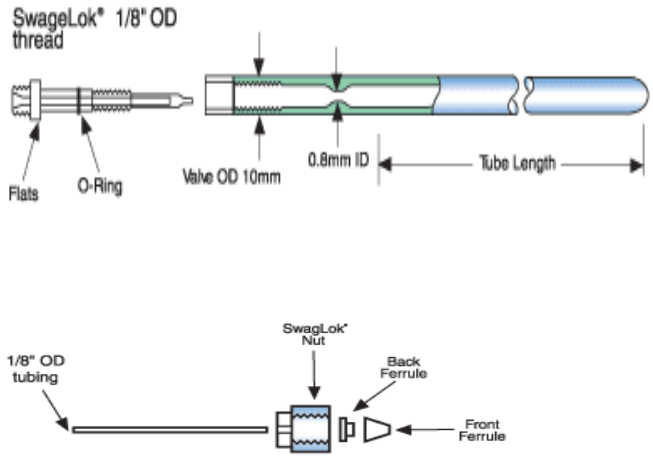

Figure 2-17 Medium pressure NMR tube – courtesy of Wilmad Lab Glass, Inc.website

2.8 Surface and interfacial tension

The Tensiometer EasyDyne from KRÜSS is used in this work to measure surface and interfacial tension of liquids. Measurements with EasyDyne above or below room temperature performed with the KRÜSS thermoset jacket TJ1020 being connected to a laboratory circulating pump. The instrument can tolerate temperature range between -10 °C and 100° C with the resolution ± 0.1°C. Measuring range for surface and interfacial tensions is between 1 to 999 mN/M with the resolution of ± 0.1 mN/M. The ring method is used for both measurements.

2.8.1 Ring method

There are two methods to measure surface and interfacial tension of liquids, Ring method and plate method. However, many values for interfacial and surface tension given in the literature are results of the ring method, because the ring method was first being developed. In the ring method, the liquid surface is raised as soon as getting contact with the ring. The sample is then moved so that the liquid film under the ring is stretched. At this time a maximum force is experienced and recorded in measurement. The maximum force vector is exactly parallel to the direction of movement; at this moment the force correlates to the surface or interfacial tension. The contact angle Θ (Figure 2-18) is 0 for an optimal wettability of the ring material as Pt/Ir.

The calculation is made according to the following equation:

$$\sigma = \frac{F\max - Fv}{L.\cos\theta} \qquad (2.2)$$

Where σ = surface or interfacial tension, Fmax=maximum force; F_V =weight of volume of liquid lifted; L=wetted length, and Θ= contact angle.

In each measurement the mean value of the individual measuring points and their standard deviation are calculated automatically. The result at the end of the measurement is an arithmetic average value calculated from a certain number of single measurements. Ten measurements are usually sufficient. In case of higher variations this number can be increased. For more information see Tensiometer EasyDyne from KRÜSS manual.

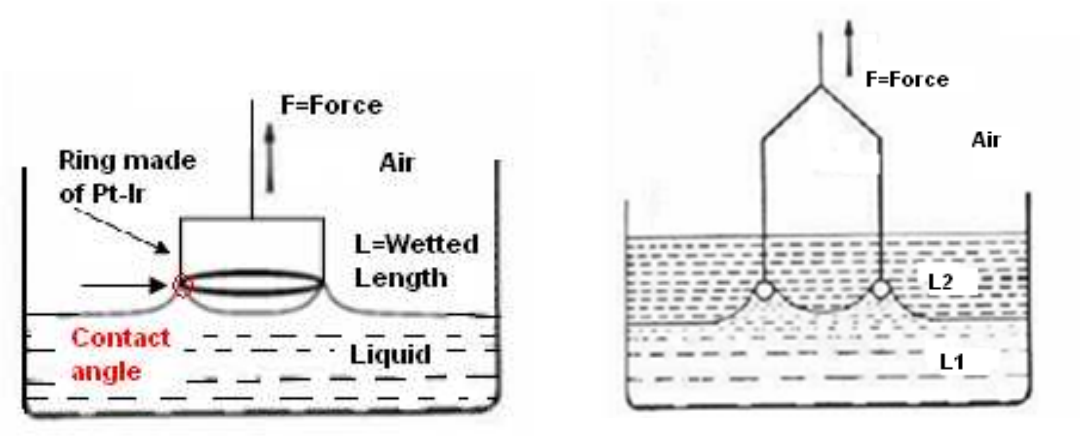

Figure 2-18 Measuring surface and interfacial tension using Ring Method

2.8.2 Procedure for Measuring Surface Tension

To measure the surface tension the procedure recommended by KRÜSS EasyDyne Tensiometer has been followed in this work. Before starting measurements the density of the liquid has to be entered to determine the weight of volume of liquid lifted (F_V). For interfacial tension measurements three milliliters of each liquid is used. The heavier phase [HMIm][Tf_2N] was added to the sample vessel (SV20) first and then the ring put on the surface of the liquid. The lighter phase was added slowly and after attaining a stable condition the tare button was pressed in order to tare the weight of the ring in the light phase. The ionic liquid phase was saturated with 1-octene before adding into the sample vessel. Entering the density difference between the two phases before starting interfacial tension measurements is particularly important. Table 2-5 shows the result of measurements in this work compared to the literature.

Table 2-5 Interfacial tension measurements comparing to the literature

Parameter	Temperature,°C	IFT($mN \cdot M^{-1}$) n-dodecane-water	IFT($mN \cdot M^{-1}$) octane-water
This work	25	52.5	51
Zeppieri et al.[24]	25	52.55	51.16
Zeppieri et al.[24]	22	52.67	51.38
Goebel et al.[25]	22	53.7	52.5

2.9 Density measurements

Density was measured using an Anton Parr densitometer (DMA 4500) which is a U-tube oscillating type. In the 1960s, Anton Paar introduced a new method of density measurement based on the law of harmonic oscillation. The accuracy and versatility of this oscillating U-tube principle has made it the standard method of density measurement. Repeatability is within ±0.00001 gr/cm^3.

2.10 The liquid- liquid contact experiments

To study mass transfer and related phenomena for systems involving ionic liquids, understanding and obtaining interfacial mass transfer data is necessary. However, despite of numerous applications, there is a lack of mass transfer studies in literature and no physical properties with concentration dependence are currently available for any system involving ionic liquids. Therefore, this research will attempt to establish a foundational methodology for process development using a model ionic liquid-solute system. In this work, mass transfer studies are performed through liquid-liquid extraction experiments for a common imidazolium based ionic liquid [HMIm][Tf_2N] and 1-octene system. In these experiments [HMIm][Tf_2N] droplets with diameter D are falling discretely through 1-octene continuous phase in a long column and creating the streamlines for flow around and within the droplets as can be seen in . 1-octene moves upward relative to each falling ionic liquid and circulating happens inside of the droplets because of relative velocities. (Figure 2-19)

Droplets of ionic liquid are introduced into the column by means of a syringe pump from World Precision Instruments- model AL-2000. A 20 mL luer lock syringe with the body diameter of 21mm is used to inject the ionic liquid. Tubes with different diameters are used to prepare various droplet sizes. The size of inner diameter of these tubes is 0.6, 1.59, and 1.8 mm. The tube is connected to the syringe using convenient connections to avoid the leakage at high pressures up to 5000 psi especially in the case of using tubes with smaller diameters. The droplets interact with 1-octene as they fall into the column and at the end mass transfer is stopped by a layer of water. Some glass beads which were held by a strainer make the contact of ionic liquid droplets with water faster. The strainer is connected to the top of the column with two thin wires and can vibrate the droplets trapped within the glass beads as needed. Water is selected because the solubility of IL in water is ~96 ppm (mole) [26] ; 1-Octene in water is ~2ppm [27]; and 1-octene in IL is 180000 ppm (mole, from our experiments) . So the solubility of 1-octene in IL is much higher than for the water solubilities. The ionic liquid is collected from the bottom of the column that has a slight slope to the sampling line and the outlet valve. In each batch 3 mL of ionic liquid are collected and separated from water by decanting. The amount of 1-octene

transferred to the ionic liquid phase has been quantified by the NMR method as will describe in the following section. See the detail of column structure in appendix D.

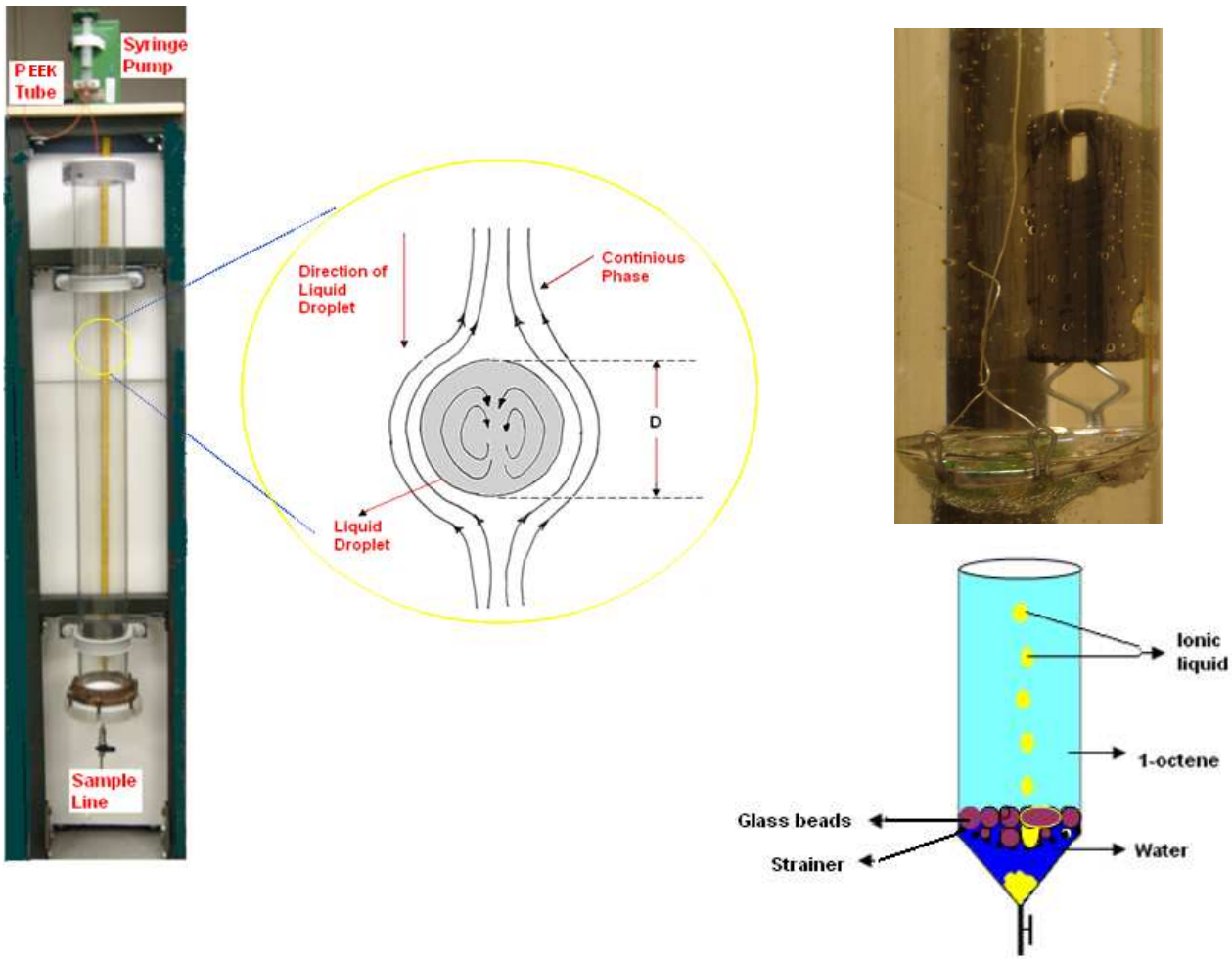

Figure 2-19 liquid – liquid extraction set up

2.10.1 Mutual solubility measurements of 1-octene and [HMIm][Tf_2N]

The liquid-liquid equilibrium envelope at ambient pressure of 1-octene and ionic liquid was determined in this study. The amount of 1-octene in [HMIm][Tf_2N] was measured by a cloud-point method where one component is continuously yet slowly added to the other component until the mixture becomes cloudy. The amount of each pure component was measured with a Mettler Toledo XS205 Dual Range Balance, with an accuracy of 0.01 mg for the range as maximum of 81 g and 0.1 mg for the range as

maximum of 220g. A Branson Model 2510 ultrasonic bath was used to mix the solutions. Temperature control at 10 °C and 25 °C was provided by a Fisher Scientific Isotemp 3016 circulating chiller with a resolution of ± 0.1 °C. For higher temperatures, samples were heated and stirred on an aluminum vial holder on an IKA RET basic C hotplate with ETS-D4 fuzzy logic controller and resolution of ±0.1 °C. To prevent the loss of 1-octene because of evaporation a septum cap was used.

The amount of [HMIm][Tf_2N] in the octene phase was measured by ICP-OES (Jobin-Yvon-Horiba JY2000). The ICP-OES is very sensitive to sulfur concentration as found in the anion even in non-aqueous solvents as configured here. Ionic liquid and 1-octene were mixed and stirred for one day (24 hours) at the four different isotherms (10 °C, 25 °C, 50 °C, 75 °C) using an oil bath with the temperature controller above. Four samples were taken from the 1-octene phase and mixed with ethanol to maintain a single phase at ambient temperature. Volumetric pipettes and flasks were used for all measurements. The samples were analyzed using the ICP-OES for the sulfur concentration which is in the anion.

The ICP parameters were: power = 1350 W; argon pressure =90 psi for plasma and nebulizer; plasma flow: 18 L/min; sheath flow; 0.8 L/min; auxiliary flow = 0.3 L/min; nebulizer type = concentric glass nebulizer; nebulizer flow = 1.63 L/min; nebulizer pressure 1.19 bar; and sample pump flow = 0.3 mL/min.

2.10.2 Quantifying 1-octene concentration in [HMIM][Tf_2N] using proton NMR

The concentration of 1-octene in [HMIM][Tf_2N] can be measured by using the NMR spectroscopy. Each substance gives an especial set of peaks in H NMR. Firstly, one of the signals from solvent ([HMIM][Tf_2N]) that has no interfere with the peaks of solute (1-octene) is chosen. In this study the hydrogen seated on the imidazolium ring (position No.2 in Figure 2-20) with the chemical shift of 9 ppm is selected for the solvent (Figure 2-21). For 1-octene, the peak of the proton which is located on the ß position in the double bond (Figure 2-20) and the chemical shift around 6 is followed (Figure 2-21). Integration is used to measure the relative intensity of the two peaks. If the concentration of 1-octene changes, as might occur in an extraction column, the intensity of the 1-octene peak will change but the intensity of the solvent peak should remain constant. The

solvent itself can be used as an internal standard for measuring the amount of 1-octene present.

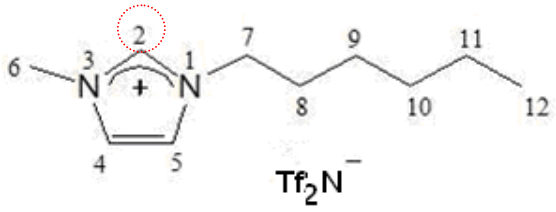

[HMIM][Tf_2N]

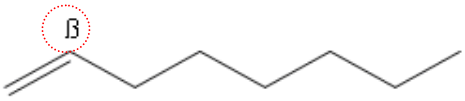

1-Octene

Figure 2-20 The structure of [HMIM][Tf_2N] and 1-octene

2.10.3 Measuring the size and velocity of a discrete falling drop of ionic liquid into the 1-octene continuous phase

In order to measure the size of droplets, having a very apparent and clear image is needed. Because of the large difference between the density of ionic liquid droplets and the Newtonian continuous 1-octene phase, the falling rate of drops is very fast. Also the drops are transparent and have no color contrasts with the continuous phase. So, using just ordinary cameras cannot help to distinguish the phase differences that have no color disparity. Also, using any dye is not suggested to make droplets colored because of the probable interferes on the mass transfer studies. Thus, a special technique is needed as well as a fast camera to take an obvious picture of transparent falling drops. In this work a high speed optical system with a FireWire Camera is used to prepare desired images. Besides, the ImageJ program developed at the National Institutes of Health is used to process and measure the area and diameter of drops.

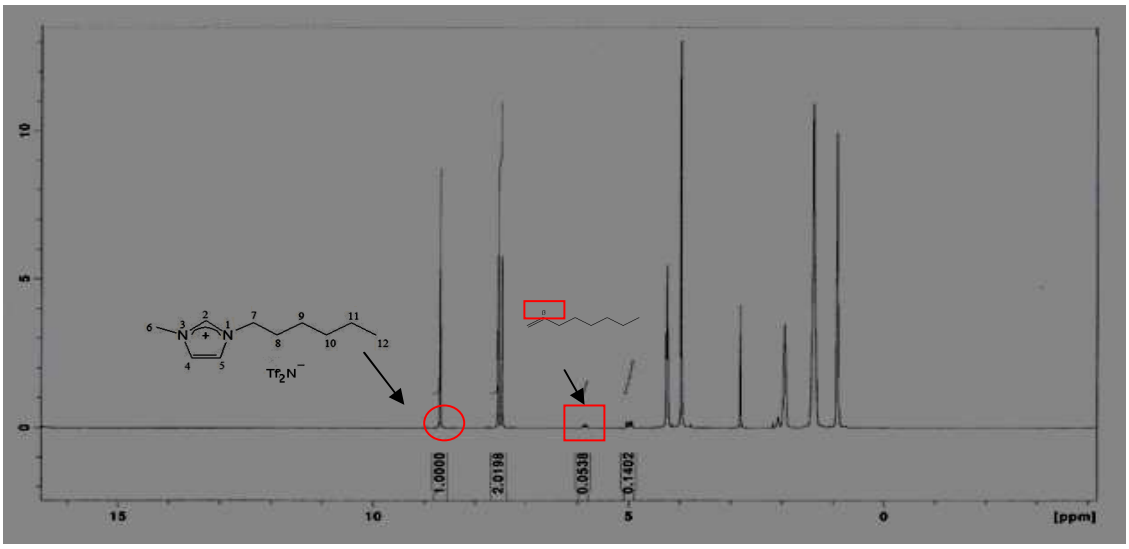

Figure 2-21 The NMR spectra of [HMIM][Tf_2N] / 1-octene solution

2.10.3.1 The high speed optical system

This technique is able to visualize the falling of ionic liquid droplets in a transparent medium with a great precision. As shown on Figure 2-22 the basic set up for this optical system contains a telecentric lens connected to a FireWire CCD color camera (Edmund optics – AVT PIKE F-100B MONO 2/3IN) and a light source (Table 2-6). The light source goes through the testing container (L*W*H=10*10*15 cm) and the lens transfers the light beam paralelly to the camera. This camera is able to take up to 60 images per second with the resolution of 1000 * 1000 pixels.

Table 2-6 the specification of camera	
Imaging device	2/3” progressive scan CCD
Sensing Area	7.4”*7.4”
Pixels (H*V)	1000*1000
Pixel size (µm)	7.4*7.4
Frame rate	60
Electronic shutter	43µs – 67 sec
Cable	IEEE-1394.B Cable 9 to 6 Pin

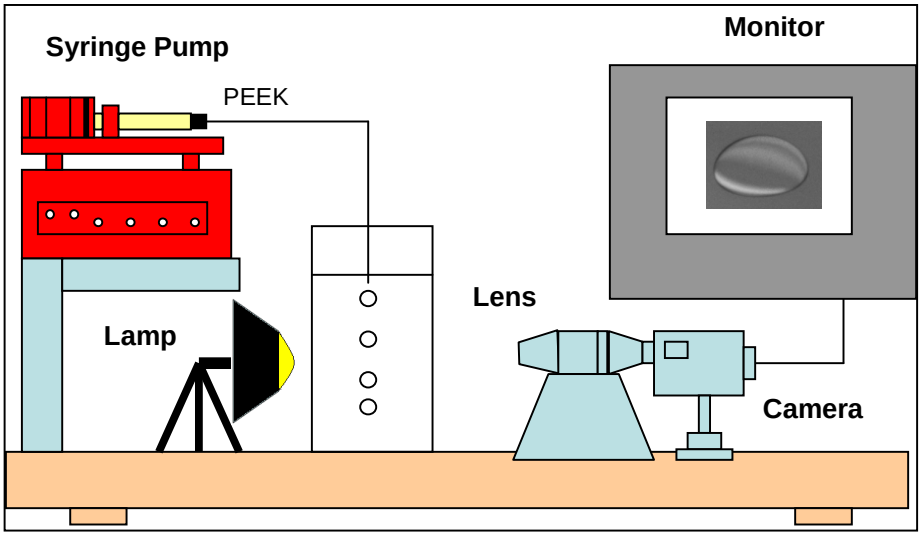

Figure 2-22 The high speed optical system

2.10.3.2 Calibration

The main objective of using the high speed optical system is measuring the diameter of droplets and the velocity of them at the end of the column. So an accurate calibration is necessary to trust the consistency of results. For this reason a precise “dot and square standard target” provided from “Edmond Optics” has been used (Figure 2-23, Figure 2-24, Table 2-7). It is a high contrast target for imaging elements from 0.5 to 10 mm. This target gives a highly accurate reference for feature sizes of circles and squares. The precision pattern is formed in Low Reflection Chromium on a stable Soda Lime Glass substrate in standard microscope slide format. The low reflection pattern surface provides high contrast against a light background, ideal for diffuse or coaxial illumination applications. The pattern is applied to the first surface and features both circles and squares in 0.5mm and whole number sized increments from 1mm to 10mm. The Positive Target that features an opaque pattern on a clear background was used.

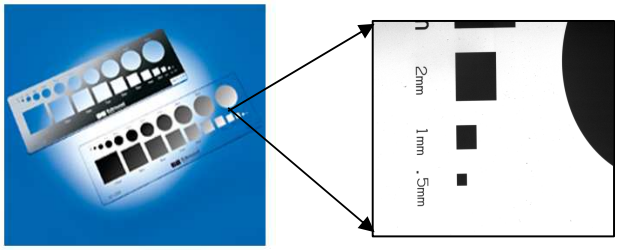

Figure 2-23 Dot and squared calibration target
Figure 2-24 Hanging target into the 1-octene phase

It is very important to hang the target exactly vertical otherwise the dimensions of the squares and the shape of the circles will not look real. (Figure 2-24)

Table 2-7 the specification of calibration target	
Substrate	Float Glass
Plate Dimensions	1” x 3” ± .02”
Thickness	0.060” ± .001”
Flatness	<4λ
Surface Quality	20-10
Parallelism	0.0005”
Element Size	2.5 µm

2.10.3.3 ImageJ Program

To measure the area and distances of images “ImageJ 1.41o program” is used in this work. This program is developed at the National Institutes of Health, USA, http://rsb.info.nih.gov/ij Java 1.6.0_10. It can display, edit, analyze, process, save, and print 8-bit, 16-bit and 32-bit images. This program is able to read many image formats including TIFF, PNG, GIF, JPEG, BMP, DICOM, FITS, as well as raw formats. ImageJ is capable of calculating area and pixel value statistics of user-defined selections. It can measure distances and angles. It supports standard image processing functions as well as

geometric transformations such as scaling, rotation and flips. The program supports any number of images simultaneously, limited only by available memory.

2.11 References

1. Koch, D.; Leitner, W., Rhodium-Catalyzed Hydroformylation in Supercritical Carbon Dioxide. *J. Am. Chem. Soc.* **1998,** 120, 13398-13404.
2. Schleicher, J. C., Kinetics and Solvent Effects in the Synthesis of Ionic Liquids. **2007**.
3. Ahosseini, A.; Scurto, A. M., Viscosity of Imidazolium-Based Ionic Liquids at Elevated Pressures: Cation and Anion Effects. *Int. J. Thermophys.* **2008,** 29, 4, 1222-1243.
4. Bonhote, P.; Dias, A. P.; Papageorgiou, N.; Kalyanasundaram, K.; Gratzel, M., Hydrophobic, highly conductive ambient-temperature molten salts. *Inorg. Chem* **1996,** 35, 5, 1168-1178.
5. Burrell, A. K.; Sesto, R. E. D.; Baker, S. N.; McCleskey, T. M.; Baker, G. A., The large scale synthesis of pure imidazolium and pyrrolidinium ionic liquids. *Green Chem.* **2007,** 9, 5, 449-454.
6. Nockemann, P.; Binnemans, K.; Driesen, K., Purification of imidazolium ionic liquids for spectroscopic applications. *Chem. Phys. Lett.* **2005,** 415, 1-3, 131-136.
7. Maruyama, T.; Nagasawa, S.; Goto, M., Poly (ethylene glycol)-lipase complex that is catalytically active for alcoholysis reactions in ionic liquids. *Biotech. Lett*.**2002,** 24, 16, 1341-1345.
8. Wang, B.; Kang, Y. R.; Yang, L. M.; Suo, J. S., Epoxidation of a, ß-unsaturated carbonyl compounds in ionic liquid/water biphasic system under mild conditions. *J. Mol. Cat. A* **2003,** 203, 1-2, 29-36.
9. Ren, W.; Scurto, A. M., High-pressure phase equilibria with compressed gases. *Rev. Sci. Instrum.***2007,** 78, 125104.
10. Bird, R. B.; Stewart, W. E.; Lightfoot, E. N., *Transport Phenomena*. Wiley: New York, 1960.
11. Ahosseini, A.; Ortega, E.; Sensenich, B.; Scurto, A. M., Viscosity of n-alkyl-3-methyl-imidazolium bis (trifluoromethylsulfonyl) amide ionic liquids saturated with compressed CO_2. *Fluid Phase Equil.* **2009,** 286, 1, 62-68.
12. Price, W., Pulse-Field Gradient Nuclear Magnetic Resonance as a Tool for Studying Translational Diffusion: Part 1. *Basic Theory, Conepts Magn. Reson* **1997,** 9, 299-336.
13. Price, W. S., Pulse-field gradient nuclear magnetic resonance as a tool for studying translational diffusion. II. Experimental aspects. *Concepts Magn. Reson* **1998,** 10, 197-237.
14. Gunther, H., *NMR Spectroscopy*. Wiley New York: 1994.
15. Wakai, C.; Nakahara, M., Attractive potential effect on the self-diffusion coefficients of a solitary water molecule in organic solvents. *J. Chem. Phys.***1997,** 106, 7512.
16. Becker, C. R.; Schad, L. R.; Lorenz, W. J., Measurement of diffusion coefficients using a quick echo split NMR imaging technique. *Magn. Reson. Imaging* **1994,** 12, 8, 1167-74.
17. Hayamizu, K.; Price, W. S., A new type of sample tube for reducing convection effects in PGSE-NMR measurements of self-diffusion coefficients of liquid samples. *J. Magn. Reson.* **2004,** 167, 2, 328-333.

18. Nakahara, M.; Wakai, C.; Yoshimoto, Y.; Matubayasi, N., Dynamics of Hydrophobic Hydration of Benzene. *J. Phys. Chem.* **1996,** 100, 1345-1349.
19. Annat, G.; MacFarlane, D. R.; Forsyth, M., Transport Properties in Ionic Liquids and Ionic Liquid Mixtures: The Challenges of NMR Pulsed Field Gradient Diffusion Measurements. *J. Phys. Chem. B* **2007,** 111, 30, 9018.
20. Kerssebaum, R., DOSY and diffusion by NMR. *Bruker BioSpin, Rheinstetten, Germany* **2002**, 3-23.
21. Harris, K. R., Temperature and density dependence of the self-diffusion coefficient of n-hexane from 223 to 333 K and up to 400 MPa. *Journal of the Chemical Society, Faraday Transactions 1* **1982,** 78, 7, 2265-2274.
22. Krynicki, K.; Green, C. D.; Sawyer, D. W., Pressure and temperature dependence of self-diffusion in water. *Faraday Discussions of the Chemical Society* **1978,** 66, 199-208.
23. Tokuda, H.; Ishii, K.; Susan, M.; Tsuzuki, S.; Hayamizu, K.; Watanabe, M., Physicochemical Properties and Structures of Room-Temperature Ionic Liquids. 3. Variation of Cationic Structures. *J. Phys. Chem. B* **2006,** 110, 6, 2833-2839.
24. Zeppieri, S.; Rodriguez, J.; de Ramos, A. L. L., Interfacial Tension of Alkane+ Water Systems. *J. Chem. Eng. Data* **2001,** 46, 5, 1086-1088.
25. Goebel, A.; Lunkenheimer, K., Interfacial Tension of the Water/n-Alkane Interface. *Langmuir* **1997,** 13, 369-372.
26. Freire, M. G.; Carvalho, P. J.; Gardas, R. L.; Marrucho, I. M.; Santos, L.; Coutinho, J. A. P., Mutual Solubilities of Water and the [C~ nmim][Tf~ 2N] Hydrophobic Ionic Liquids. *J. Phys. Chem. B* **2008,** 112, 6, 1604.
27. Rogers, R. D.; Seddon, K. R.; Volkov, S., *Green Industrial Applications of Ionic Liquids*. Kluwer Academic Pub: 2002.

Chapter 3 Understanding Biphasic Ionic Liquid/CO_2 Systems for Homogeneous Catalysis

3 Understanding Biphasic Ionic Liquid/CO_2 Systems for Homogeneous Catalysis

Homogeneous catalysis with organometallic complexes has been used for efficient chemical reactions with high selectivity, activity, and the ability of the catalyst separation. [1, 2] The recycle of the expensive catalyst and ligands in chemical processes is a key issue that would change their conditions from a non- feasible to an economically viable process. To find a scheme to figure out this issue, some scenarios have been developed. For instance, reactions in a single fluid phase followed by separation were arranged, or multiple fluid media have been found to sequester the catalyst, deliver the reactant and remove the product into and from the reaction zone. In multiphase systems, one phase maintains the catalyst and the other phase acts as a mobile phase to bring reactants and to take out products.

The best biphasic system would have complete immiscibility between phases (no cross-contamination) and no catalyst partitioning (leaching). Solid-support of metal complexes would be another alternative to facile separations of the catalyst from the products. However, the solid support can decrease the activity and importantly, selectivity of the catalyst. In addition, catalyst processing and final recovery of these materials would be a big issue and requires complete shut-down of a reactor.

One of the largest examples of biphasic homogeneous catalysis is the Ruhrchemie/Rhône-Poulenc process for short-chain olefin hydroformylation, which uses water to sequester and recycle a rhodium catalyst with sulfonate-modified triphenylphosphine ligands.[2] However, its application to higher olefins is limited by the solubility of the olefin ($<C_5$). Multiphase methods may suffer from thermodynamic (solubility) issues, mass transfer limitations, catalyst separation, and cross-contamination problems.

Developmment of methodologies for catalyst immobilization for continuous reactions is another fundamental concern for process development. Any new process should also be based around the principles of modern “green”/sustainable chemistry and engineering.[3, 4] A biphasic ionic liquid and compressed carbon dioxide system may solve

these important issues. As will be demonstrated in this chapter, phase equilibrium, mass transport and kinetic parameters are needed to entirely take advantage of this tunable system. These main concepts will be explained through two important homogeneous catalytic reactions, hydroformylation and hydrogenation, in this chapter.

3.1 Hydroformylation in IL/CO_2 Systems

As the first exemplar reaction to explain advantages of biphasic ionic liquid (IL) and compressed carbon dioxide system for efficient homogeneous catalysis, the hydroformylation of 1-octene to nonanal catalyzed by a rhodium-triphenylphosphine complex is studied.**(** Figure 3-1)

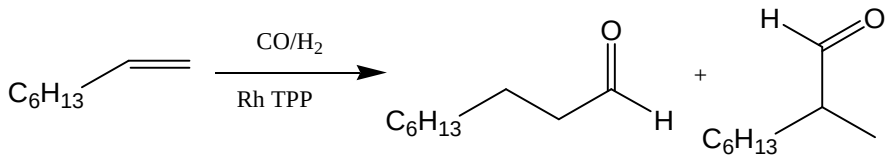

Figure 3-1 Hydroformylation of 1-octene with syngas (H_2:CO= 1:1 by mole) with rhodium and triphenylphosphine as a ligand to n-nonanal (preferred) and the branched 1-methyl-octanal.

The IL, 1-hexyl-3-methyl-imidazolium bis(trifluoromethylsulfonyl)amide ([HMIm][Tf_2N]) has been chosen by IUPAC (Committee on the Thermodynamics of Ionic Liquids, Ionic Liquid Mixtures, and the Development of Standardized Systems) to be a reference IL for worldwide study. [5] [HMIm][Tf_2N] will be used in this work for studies in catalysis, phase equilibrium, and mass transport. Detailed phase equilibrium studies were conducted to determine volume expansion of the IL phase and the phase behavior and mixture critical points between the reactant, product, and IL with CO_2 and syngas (CO/H_2). These phenomena eventually affect the concentration of the reactant and, thus, the apparent reaction rate. The viscosity of the IL with CO_2 pressure was measured and demonstrates the dramatic decrease with increasing CO_2 pressure. The self-diffusion coefficient of the ionic liquid and 1-octene were measured and indicate a large increase with CO_2 pressure (solubility). With an understanding of the kinetics,

phase behavior and mass transport, biphasic IL/CO_2 reaction systems may be properly understood and designed.

3.1.1 Background

Several studies exist in the literature which perform hydroformylation reactions in ionic liquid systems [6-8]; for a recent review, see Haumann and Riisagers.[9] Olivier-Bourbigou and coworkers [7] found that the reaction rate (TOF) in ILs was similar to organic solvents and directly correlated with the solubility of the olefin in different ionic liquids. Mehnert *et al.*[8] studied hydroformylation of 1-hexene with catalysts dissolved in ionic liquids on solid supports. Wasserscheid and coworkers[6] employed ionic phosphine ligands for the rhodium catalyzed hydroformylation of 1-octene and found high catalyst activity, high selectivity to the linear product, and no detectable catalyst leaching. Several groups have investigated various ligands for hydroformylation focusing their effect on catalyst leaching; for example Jin *et al.*[10]

Cole-Hamilton and coworkers [11, 12] investigated the hydroformylation reaction of long chain alkenes in a biphasic CO_2 /Imidazolium IL system with rhodium catalysts with modified phosphine ligands. The conversion rate was slightly lower than those obtained in toluene or ILs alone, but they exhibited similar or enhanced selectivity (linear to branched ratio). These systems were carried out in a continuous flow system where the CO_2 delivered the olefin and removed the aldehyde product at high turnover frequencies. Scurto and Leitner [13] illustrated the Rh-catalyzed hydroformylation of vinyl-naphthalene in a biphasic IL/CO_2 system, where CO_2 was used to induce melting of a quaternary ammonium salt, tetra-n-butyl-ammonium tetrafluoroborate, at a temperature over 100°C below its normal melting point. This platform was also used for hydrogenation and hydroboration.

In this work reaction rates, phase equilibrium thermodynamics, and mass transport properties will be studied to understand these tunable biphasic systems and to engineer efficient reactions and separations. These data will help to explain the different trends reported in the literature for the contribution of CO_2.

3.1.2 Results and Discussion

The Rh-catalyzed hydroformylation of 1-octene with triphenylphosphine ligands was chosen as a model reaction in the biphasic ionic liquid [HMIm][Tf_2N] and CO_2 system. Focus was placed on the effect of phase equilibria on the reaction rate. Elements of mass transport properties are also measured and discussed in relation to their effect on biphasic catalyzed reactions.

3.1.2.1 Effect of Pressure on Reaction Rates

From the literature, the effect of pressure on reaction rates in biphasic IL/CO_2 reaction systems is somewhat inconsistent: some report that CO_2 pressure increases the reaction rate others say that it decreases the rate. The hydroformylation of 1-octene with Rh-TPP catalytic system was conducted at constant loading of IL, 1-octene, 1:1 CO/H_2, and catalyst with pressure of CO_2 varied. As shown in Figure 3-2, the apparent reaction rate seems to decrease with increasing CO_2 pressure. Table 3-1 illustrates that the selectivity to the linear aldehyde, which is most often the industrially desired product, increases slightly with increasing pressure. These results are in spite of the apparent increase in mass-transport properties in the presence of CO_2 and several reports of increased reaction rate with CO_2 pressure. To find the main reason of CO_2 effects on the reaction rate, deeply studies around thermodynamic properties, phase behavior, volume expansion, and concentrations of compounds are necessary to be arranged.

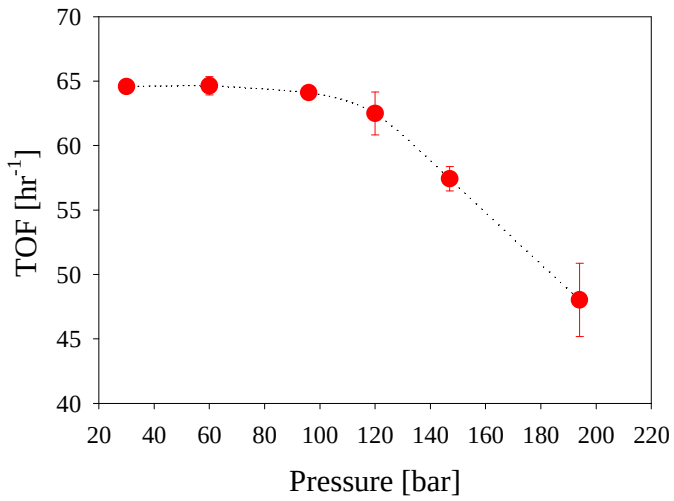

Figure 3-2 Reaction of the hydroformylation of 1-octene with total pressure CO_2. Line is of smoothed data.[14]

Table 3-1 The effect of CO_2 pressure on the apparent reaction rate for the hydroformylation[a] of 1-octene in [HMIm][Tf_2N].[14]

P [bar]	*TOF(SD)*	*Regio-Selectivity* (linear/branch)
30	64.6 (0.1)	2.7
60	64.6 (0.8)	2.7
96	64.1 (0.4)	2.7
120	62.5 (1.7)	2.7
147	57.4 (0.9)	2.8
194	48.0 (2.8)	2.8

[a] Reaction conditions: P_{sg}= 30 bar, 70**°C**; 1 hour catalyzed by Rh-TPP (1:4). [a] standard deviation with n ≥ 3.

From the literature, one of the most common generalized rate equations for olefin hydroformylation with rhodium/phosphine catalysts [15-20] is:

$$-r_{rxn} = k\left(\frac{[Olefin][H_2][CO][Rh]}{\left(1+K_{H_2}[H_2]\right)^a\left(1+K_{CO}[CO]\right)^b}\right) \quad (3.\ 1)$$

where a and b ($b > a$) are adjusted for the olefin (ethylene, 1-hexene, 1-dodecene, etc.) and solvent of the reaction. For a more recent review of hydroformylation kinetics, see Chaudhari *et al.*[20] From Purwanto and Delmas[19], the Rh-catalyzed hydroformylation of 1-octene in toluene, the parameters for the rate expression are a =1 and b = 2. This implies that the rate should be 1st order with 1-octene and have an overall negative order in CO at certain ranges of K_{H2}. From this general expression, there are two main ways that an inert component such as CO_2 can affect the reaction rate: modifying the concentrations and/or changing the intrinsic kinetic constant (k). Alternatively, if the reaction is diffusion controlled then the mass transport properties will also affect the apparent rate. The issues of mass transport (section 3.2.2.2) and phase equilibrium (Section 3.2.2.3) will be systematically addressed. Section (3.2.2.3.5) will then use these data to clarify the phenomena and explain clearly if there is any contradiction between experimental results and something that have been illustrated in the literature.

3.1.2.2 Mass Transfer Effects Biphasic IL/CO_2 Systems: Viscosity & Diffusivity

The hydroformylation reaction is a slow reaction and can be under kinetically-limited regime. However, mass transport phenomenon may occur and have significant impacts on the reaction rate and efficiency. Thus, it is necessary to quantify the mass transport effects under the reaction conditions of interest.

3.1.2.2.2 Viscosity

The mixture viscosity of the IL-phase with CO_2 was measured at 70°C with a high-pressure viscometer. The results are presented in Table 3-2 and Figure 3-3. As shown, the viscosity significantly decreases with increasing CO_2 pressure. More precisely, the viscosity decreases as the mole fraction of CO_2 dissolved in the IL phase increases**.** The mole fraction was determined by interpolating the phase equilibrium data. The viscosity of pure [HMIm][Tf_2N] with hydrostatic pressure has recently been measured in our laboratory.[21] These data have been used to determine the percentage of viscosity reduction with CO_2 pressure using pure IL viscosity at the corresponding pressure and are listed in Table 3-2. At 70 bar, the viscosity reduction approaches 43+%. After approximately 100 bar, the viscosity decrease with pressure becomes more marginal. Han and coworkers[22] investigated the viscosity of IL/methanol/CO_2 systems and report the viscosity of [BMIm][PF_6] with CO_2 pressure for three isotherms at elevated pressures . Eckert and coworkers[23] utilized a spectroscopic method to estimate the "micro-viscosity" of a probe molecule the IL/CO_2 mixture. Tomida *et al.* [24] measured the viscosities of 1-butyl-3-methylimidazolium tetrafluoroborate ([BMIm][BF_4])/CO_2 mixtures using a rolling ball viscometer from 293.15 to 353.15K and pressures of up to 200 bar.

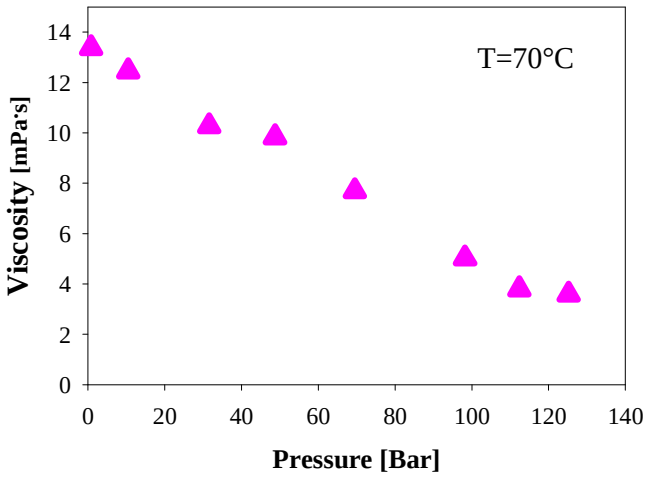

Figure 3-3 Viscosity of [HMIm][Tf_2N] at 70°C with pressure of CO_2.[14]

3.1.2.2.3 Diffusivity

Dissolved CO_2 reduces viscosity which also increases diffusivity. The self-diffusivity of 1-octene, [HMIm][Tf_2N], and mixtures of 1-octene in [HMIm][Tf_2N] at ambient pressure and 70° C have been measured using an NMR method as shown in Table 3-3**.** For the IL, the method can follow the diffusivity of the cation and anion independently. From Table 3-3**,** [HMIm][Tf_2N] has over one order of magnitude slower diffusion coefficient than 1-octene, and consequently reduces the diffusivity of 1-octene in the 0.2 M solution in [HMIm][Tf_2N] by approximately an order of magnitude over pure 1-octene. Thus, any improvement in the IL viscosity, will ultimately improved the diffusivity of the reactant, 1-octene, in the mixture.

Table 3-2 Viscosity of [HMIm]]Tf_2N] with CO_2 pressure/ concentration at 70°C.[14]			
P [bar]	***Viscosity, $\eta_{mixture}$*** *[mPa·s]*	***Viscosity, η_{IL}*** [a] *[mPa·s]*	***%Δ η*** [b]
1	-	13.37[b]	0
10	12.45	13.62	-9
32	10.27	13.90	-26
49	9.83	14.11	-30
69	7.69	14.37	-46
98	5.03	14.75	-66
112	3.79	14.93	-75
125	3.58	15.11	-76
[a] viscosity of pure IL at the pressure of the saturated mixture interpolated from data of Ahosseini and Scurto, 2008; [b] $\%\Delta\eta = (\eta_{mixture} - \eta_{IL}(P))/\ \eta_{IL}(P) \times 100$			

Table 3-3 Diffusivity of 1-octene and [HMIm][Tf_2N] at 70°C.[14]				
T = 70°C	**[HMIm]**	**[Tf_2N]**	**1-Octene**	**1-Octene in [HMIm][Tf_2N](0.2M)**
***D* [10^{-6} cm^2/s]**	**0.86**	**0.82**	**59.4**	**5.59**

The self-diffusivity of pure components and mixtures are often correlated with the Stokes – Einstein[25] equation for the diffusivity, *D*:

$$D = \frac{k_B T}{n\pi a \eta} \qquad (3.2)$$

where *n* is often 4 for smooth spherical objects (slip- boundary condition) and 6 for a rough one; *a*: is the hydrodynamic radius characteristic of the diffusing object; *T*, temperature; η, the viscosity; and k_B, Boltzmann constant. If a diffusion coefficient is known at a given temperature and viscosity of the solvent, then the diffusivity can be approximated at other viscosities by:

$$D = \frac{D_0}{\eta / \eta_0} \qquad (3.3)$$

where the subscript 0 indicates the diffusivity and viscosity of the pure IL at ambient conditions. This equation is used to predict the diffusivity of the IL in mixtures with CO_2

by knowing the IL/CO_2 viscosity. As shown in Figure 3-4, the predicted diffusivity increases by approximately 290% from ambient conditions to 125 bar. Of course, actual diffusivities are not just a function of the viscosity, but also the chemical composition which is changing throughout the pressure range. Regardless, this approximation does allude to the large increase with the presence of CO_2. High-pressure diffusivity measurements at these conditions are planned for the future. There are several reports of the diffusion of CO_2 into the IL at low pressures (infinitely dilute conditions) in the literature[26-30], but would be quite different at these larger pressures/compositions of CO_2.

For the hydroformylation reaction under study, these results indicate that 1-octene and syngas will diffuse more rapidly with increasing CO_2 pressure/composition and thus allow the reaction to proceed more easily into the kinetically-controlled regime. The lower viscosity and higher diffusivity may help to explain the increase in apparent reaction rate with CO_2 pressure as seen in our previous studies of hydrogenation in a mass-transport limited regime[31] and several reports in the literature.

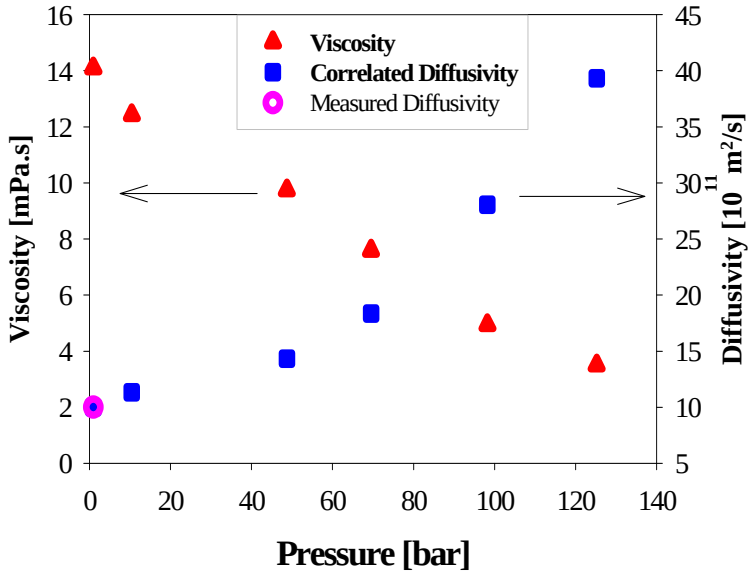

Figure 3-4 Viscosity and experimental and predicted diffusivity (cation) of [HMIm][Tf_2N] with pressure of CO_2.[14]

3.1.2.3 Phase Equilibria of IL, CO_2 and Reactants/Products

This section will present the phase behavior of the reactants, product, CO_2, and the ionic liquid that was investigated by Ren and Scurto[32] in order to connect to the apparent reaction studies.

3.1.2.3.2 Volume Expansion of the Ionic Liquid

CO_2 is highly soluble in ionic liquids as discussed before, and so it can increase the volume of the ionic liquid. This volume expansion would have large effects on reactions in biphasic IL/CO_2 systems as will be discussed below. The volume expansion of the [HMIm][Tf_2N] with CO_2 and with a mixture of CO_2 and syngas (H_2:CO =1:1 by mole) have been measured at 70°C and shown in Figure 3-5. The IL phase expands by approximately 25.0% at 119.8 bar with pure CO_2. The volume expansion of IL was also measured under similar reaction conditions with different pressures of syngas (CO/H_2). As the solubility of syngas is much lower than CO_2, the larger amount of the loaded syngas will stay in the gas (CO_2) phase and the change of volume expansion with the mixed gases (CO_2, CO/H_2) should be small. [33-36] However, at higher pressures the effect of syngas on the volume expansion will become greater. (Figure 3-5)

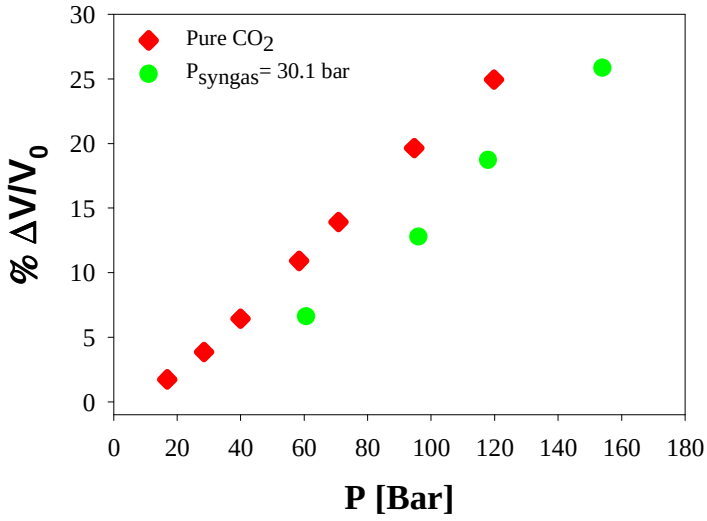

Figure 3-5 Volume expansion ($\%\Delta V/V_0 = (V-V_0)/V_0 \times 100$; pure IL volume, V_0) of [HMIm][Tf_2N] with CO_2 pressure with/without CO/H_2 at 70°C; molar ratio of syngas:IL in the system is 0.3 at P_{syngas} = 6 bar and at 30 bar, 0.8.[14]

3.1.2.3.3 Phase Behavior of the Reactants/Product and CO_2

The effect of pressure on the biphasic IL/CO_2 reaction system can be studied more deeply by learning the phase behavior of the reactants and products with CO_2 (without the IL). Organic liquids, such as 1-octene and n-nonanal, can immigrate to the CO_2 phase at conditions (temperature, pressure, and composition) above the bubble point (solubility of the CO_2 in the liquid phase) or at conditions beyond the mixture critical point. The mixture critical point is the highest pressure and composition at a given temperature in which a vapor and liquid phase can coexist. For liquid mixtures with two or more components, the mixture critical points can change with composition. The mixture critical points of the reactant and/or product with CO_2 will have direct effects on the biphasic IL/CO_2 system. As the ionic liquid is almost insoluble in the CO_2 phase under the conditions studied here, the fluid phase is directly related to the phase behavior of the reactants, product and CO_2**.** Figure 3-6 illustrates the mixture critical pressure at 70°C as the proportion of 1-octene to n-nonanal is varied between pure 1-octene and pure n-nonanal (on a CO_2-free basis). As seen in the Figure 3-6, the mixture critical pressure increases with concentration of nonanal from pure 1-octene (0% conversion), to pure n-nonanal (100% conversion). Thus in order to maintain a single phase throughout the reaction, the phase behavior throughout the entire composition (conversion) range must be known.

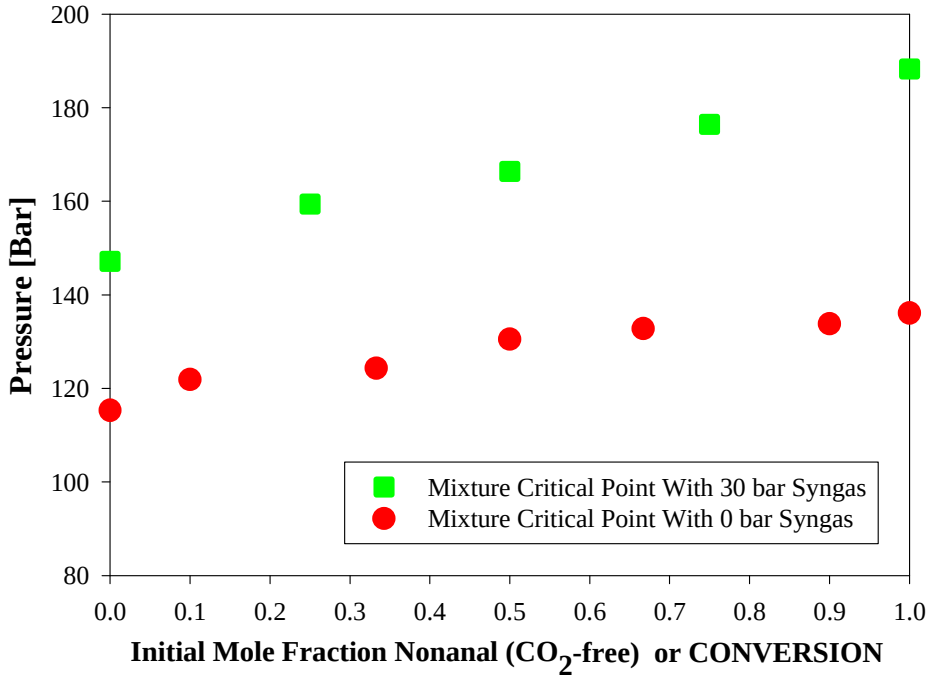

Figure 3-6 Phase behavior of 1-octene and n-nonanal and CO_2 as percent of initial amount of nonanal (CO_2-free basis); or can be read as phase behavior as a function of the conversion. (Ren-Scurto)[14, 32]

3.1.2.3.4 Phase Behavior of the H_2/CO in IL with CO_2

It has been indicated in the literature that the presence of CO_2 may enhance the solubility of permanent gases, such as CO, H_2, O_2, CH_4, in ionic liquids over the pure gases as similar pressures. Brennecke and coworkers[37] indicate moderate to no enhancement for O_2 and CH_4. However, Solinas *et al.* [38, 39] indicate significant enhancement of H_2 in ionic liquids as observed from proton NMR. This phenomenon has been well-established for the CO_2-enhanced solubility of gases in organic solvents (CXLs). [40-42]

3.1.2.3.5 Phase Behavior of the Reactant/Product, IL, and CO_2

The phase behavior of the ionic liquid, reactant, product and CO_2 have significant impacts not only on the reaction phenomena but on developing potential techniques for separation of reactants and products from the catalytic phase and ionic liquid media. Scurto *et al.*[43, 44] and other researchers [45-49] have indicated that CO_2 at certain conditions

can be used to split phases and separate them into an IL-rich phase and an organic-rich phase.

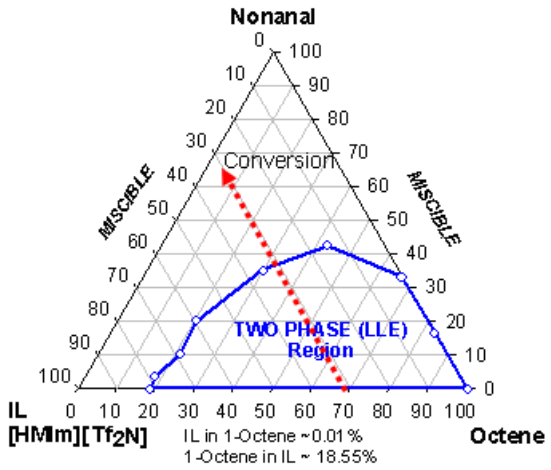

Figure 3-7 Ambient pressure phase behavior of 1-octene, n-nonanal, and [HMIm][Tf_2N] at 22°C.[14]

The ambient pressure phase behavior of 1-octene, n-nonanal and [HMIm][Tf_2N] is illustrated in Figure 3-7. As shown, the product is miscible with the IL phase, but the reactant, 1-octene, is only partially miscible. Thus, as conversion increases, the reaction could proceed from a two-phase region to a single miscible phase depending on the initial concentration of 1-octene. From a separations point of view, products would be preferred to be miscible and be naturally separated. However, with CO_2 there are other possibilities and regions of behavior that can be helpful in separations of the products and reactants at the end of reactions. With CO_2 pressure the organic liquids (reactant and product) may be forced to partition away from the IL mixture.

Figure 3-8 illustrates the qualitative phase behavior of loading of <30% of [HMIm][Tf_2N] with the product n-nonanal or mixtures with 1-octene. As shown, the mixture is homogeneous at ambient conditions. When CO_2 pressure is applied, the transition from VLE to vapor-liquid-liquid equilibrium (VLLE) (V-L → V-L_1-L_2) is encountered. As pressure is increased, the relative volume of the organic-rich phase increases until it reaches the "K-point" where the organic-rich phase and CO_2 phase become critical and miscible to each other leaving an IL-rich phase. Above the "K-

point" pressure, more of the remaining amount of organic in the IL phases partitions to the upper fluid phase, similar to supercritical fluid extraction from ionic liquids.[50] It has been seen that the presence of the IL has no effects on the K-point pressures of the mixture critical points of the binary organic and CO_2 system due to the lack of IL vapor phase in the CO_2.

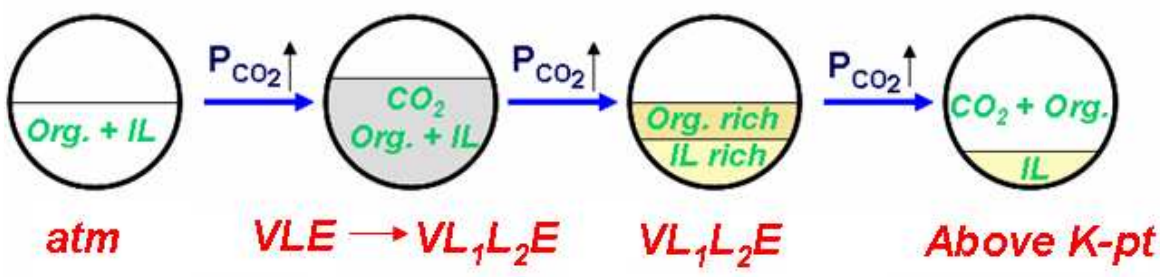

Figure 3-8 Diagram of the phase behavior in the autoclaves with increasing temperature and pressure for mixtures of the organic reactants/products with the IL and CO_2 pressure. (Ren-Scurto)[14, 32]

The pressure of the transition to VLLE (V-L→V-L_1-L_2) and back to VLE behavior (above K-point) for mixtures of the IL with the product n-nonanal with CO_2 are illustrated in Table 3-4. As shown, the mixture splits into two liquid phases at approximately 117 bar of pressure with an initial concentration of IL of 10% mole and 124 bar at 25% mole of the IL. The K-point of these two mixtures was nearly identical at 136 bar.

Table 3-4 Phase transition of n-nonanal, [HMIm][Tf_2N], with CO_2 at 70°C. (Ren-Scurto)[14, 32]

Initial loading IL[a] [mole %]	**Pressure VLE to VLLE (V-L→V-L_1-L_2) [Bar]**	**K-point (L-L=V) [Bar]**
0	--	136.1
10	117.3	136.2
25	124.2	136.3
31	No Split	--
50	No Split	--

[a] CO_2-free basis

For the case of incomplete conversion, mixtures of 1-octene and n-nonanal will co-exist and this will change the condition of the transition (V-L→V-L_1-L_2) and K-point. The VLE to VLLE transition and K-points are compared for various ratios of 1-octene to n-nonanal mixed with 10% mole of the IL in Table 3-4. As large loadings of 1-octene are only partially miscible with the IL, two phases occur at ambient pressures to the K-point. The mixture critical point without the ionic liquid (in parentheses in Table 3-5**)** is within experimental accuracy of the case with the IL. The mixtures of equal portions of 1-octene and n-nonanal (45%:45%) with 10% IL are initially miscible and separates to two liquid phase at relatively low pressure (32 bar). With higher proportion of n-nonanal, the VLE to VLLE transition pressure increases because of high miscibility of nonanal in the IL phase.

These results would help significantly in the design of efficient reactions in biphasic IL/CO_2 systems. The catalytic reactions presented in this contribution are performed below the concentrations where phase splitting occurs. However, for higher loadings and practical applications, the LLV and K-points must be known for proper engineering.

Table 3-5 Phase behavior of mixtures of 1-octene and n-nonanal with 10% mole [HMIm][Tf_2N] with CO_2 at 70°C. (Ren-Scurto)[14, 32]

Initial loading of 1-Octene [mole %][a]	**VLE to VLLE (**V-L→V-L_1-L_2**) [Bar]**	**K-point (L-L=V) [Bar]** [b]
Octene (90%)	LLE @ 1 bar	115.5 (115.3)
Nonanal(30%)+Octene(60%)	LLE @ 1 bar	124.1 (124.3)
Nonanal(45%)+Octene(45%)	32.0	131.0 (130.5)
Nonanal(60%)+Octene(30%)	87.4	132.5 (132.8)
Nonanal (90%)	117.3	136.2 (136.1)

[a] with 10% IL; [b] critical pressure without IL in parentheses.

3.1.2.3.6 Effects of Phase Equilibrium on the Catalytic Reaction Rate

The pressure/composition effect on the phase behavior of this system has dramatic effects on the reaction rates. From the reaction results, the apparent reaction rate

becomes lower at higher pressures (Figure 3-2), while the volume expansion increases with increasing pressure or CO_2 composition (Figure 3-5). If one assumes that the 1-octene is found exclusively in the IL phase at all pressures, then the moles of 1-octene will be constant, but the volume of the liquid phase will continually increase with increasing the pressure. This volume increase with constant moles of 1-octene will decrease the molarity of the reactant as shown in Figure 3-9 using the actual concentration loaded for the reaction results. For instance, if the concentration of 1-octene in the IL without CO_2 is approximately 45 mM, then at 160 bar of total pressure (30 bar syngas and CO_2), the concentration decreases to approximately 34mM; a decrease of ~25%. This dilution is before the reaction occurs and the overall reaction rate should decrease according to its rate law/order; for instance see equation 3.1. Using the volume expansion data from Figure 3-5 to compute the molarity at each pressure, Figure 3-2 is transformed from TOF versus pressure to TOF vs. molarity and is shown in Figure 3-10. The apparent reaction rate increases with increasing molarity as one would expect as shown by the dotted line. In this case, the highest molarity occurs at the lower pressures. However, as the volume expansion is relatively small and linear with pressure, the dilution effect on reaction rate would also be relatively small and linear as seen by the shallow slope of the higher molarity (lowest pressure) points. However, after approximately 120 bar a dramatic decrease is observed.

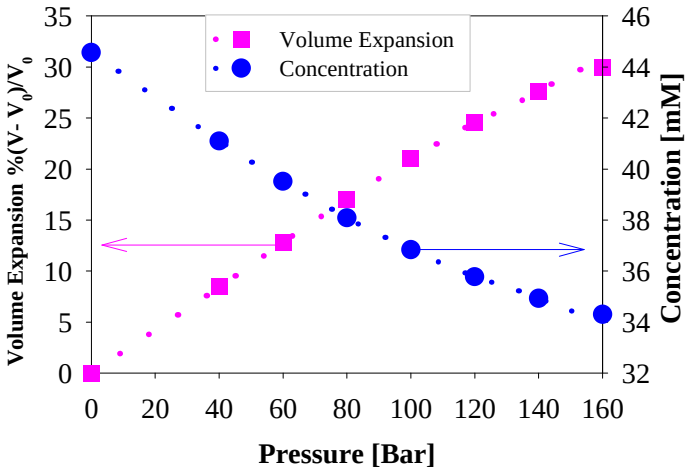

Figure 3-9 Volume expansion and nominal molar concentration of 1-octene in the IL phase as a function of CO_2 Pressure.[14]

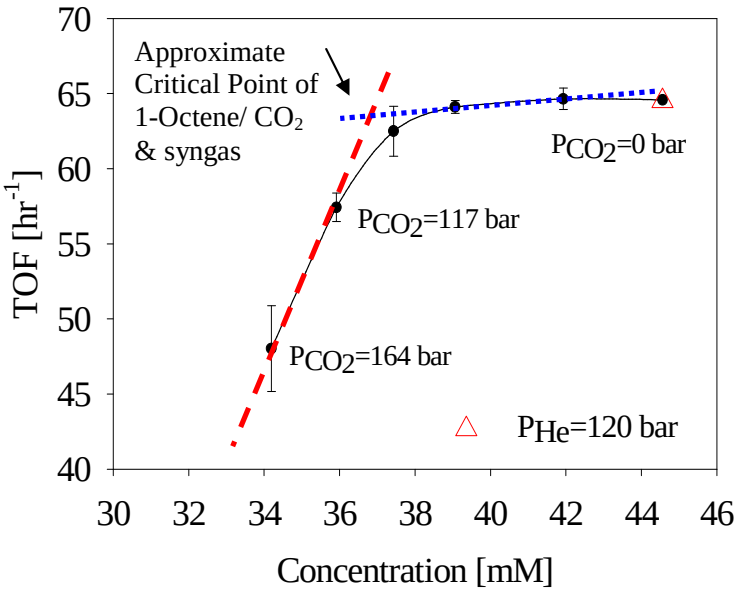

Figure 3-10 Hydroformylation results plotted versus nominal concentration [molarity]. Solid line is smoothed data. Dotted line is approximate linear behavior where volume expansion dominates. Dashed line is approximate point where the reactant and product are critical with respect to CO_2.[14]

The concentration plotted in Figure 3-10 assumes that all of the 1-octene is in the catalytic IL phase. However, the reactant, 1-octene, will partition between the two phases depending on the pressure. The pressure of the mixture critical point of the reactant and CO_2 indicates a region of complete solubility/miscible. This point of miscibility with CO_2 is the exact point (temperature and pressure) for the mixture of the reactant and product with the IL present. This point is drawn approximately in Figure 3-10 (dashed lines intersection). While the organic rich phase and the CO_2 phase become critical to each other, the organic compounds may still partition to some extent between the resultant CO_2 and IL phases. However, the majority of the organic compounds will be in the CO_2-rich phase [45] and the driving force for partitioning of the 1-octene from the catalytic IL-phase to the CO_2 phase increases as the CO_2 pressure increases. Thus, the low apparent reaction rate at the higher pressures (low molarity) can be ascribed to the

lower solubility and concentration of the 1-octene reactant. However, at lower pressures of CO_2, dilution rather than reactant partitioning will be the dominant factor.

To confirm this analysis, the reaction was performed at 120 bar total pressure with helium not CO_2. The solubility of helium in the ionic liquid is estimated to be very small and orders of magnitude lower than CO_2. The data indicates that hydrostatic pressure has little effect on the reaction. Zhao and Jiang [51] observed a decreased rate of electro-oxidation of benzyl alcohol at high pressures and also hypothesized, that this was due to reactants partitioning into the CO_2 phase.

The large decrease at the higher pressure may be hypothesized to be due to the partitioning of the Rh-TPP complex or the excess TPP into the CO_2 phase. Shimoyama *et al.*[52] have recently measured the solubility of both TPP and the Rh-complex, [carbonylhydridotris(triphenylphosphine)-rhodium], in supercritical CO_2. They found that the solubility of each at 60°C and approximately 15 bar to be a mole fraction of 8.7×10^{-4} for TPP and 5.8×10^{-7} for the Rh-complex. This low solubility of the complex in CO_2 indicates that little catalyst will partition out of the IL phase during the reactions. Wagner *et al.*[53] found similar solubilities for TPP in supercritical CO_2. Thus, the ligands will have 3 orders of magnitude more solubility in the CO_2 phase than the Rh-complex. For the biphasic IL/CO_2 system, selective partitioning may be an issue at the higher pressures, but selective extraction of the excess ligands (here Rh:TPP = 1:4) would actually increase the turnover frequency not decrease it. In addition, the conditions that would induce catalyst partitioning would simultaneously partition the 1-octene into the CO_2 phase. Therefore, catalyst partitioning is not believed to have much an effect in the observed reaction trends.

Thus, two major regions of behavior exist for the reaction rates with an increase in pressure: dilution of the reactant (from ~0 bar CO_2 to 100 bar total pressure); and partitioning (extraction) of the reactant from the IL phase. As shown for constant loading of the reactant, 1-octene, CO_2 pressure would appear to have a negative effect on the reaction, despite the improvements in mass transfer discussed above. However, this result is only at constant mass/moles loading of the reactant. With thorough characterization of the phase equilibrium, the actual concentrations of the reactants, including H_2 and CO can be determined. The actual concentrations will allow intrinsic

kinetic constants for a given rate mechanism to be determined. Once the phase behavior is known, then the full intrinsic kinetic rate can be achieved.

The effect of CO_2 concentration on the intrinsic kinetic constant (*k* from Eqn.3.1) in this ionic liquid is unknown. Brennecke and coworkers [54] have found that the polarity of the IL changes little with even large amounts (>50%mole) of CO_2 dissolved. Thus, one may assume as a first approximation that the intrinsic kinetics may change very little with the presence of CO_2. However, this proposed phenomenon is currently under investigation. Ultimately, both phase equilibrium and kinetics will allow reaction systems to be properly designed for reactant/catalyst loading, pressure, reactor configuration, etc. to achieve high throughput from a biphasic IL/CO_2 system.

3.1.3 Conclusion

Biphasic IL/CO_2 systems represent an efficient platform for homogeneously-catalyzed reactions. The present study based around the hydroformylation of 1-octene with a rhodium-triphenylphosphine catalyst system illustrates the potential to finely tune the reaction and separation. However, detailed phase equilibrium and mass transfer concepts are necessary to be understood for a fairly judge of CO_2 effects on the kinetic reaction. Without a clear understanding of the phase equilibrium (solubility and volume expansion), one may incorrectly recognize CO_2 to be unfavorable to the reaction system, despite the improvements of mass transfer parameters with CO_2.

3.2 Hydrogenation

The second model reaction for the biphasic ionic liquid (IL) and compressed carbon dioxide system studied in this contribution is the hydrogenation of 1-octene catalyzed by rhodium-triphenylphosphine to determine the effects of CO_2 pressure in a biphasic ionic liquid/CO_2 system. For reactions that were limited by mass transfer, the presence of CO_2 enhances the apparent reaction rate. However in well agitated systems and at constant moles of 1-octene, the pressure of CO_2 reduces the apparent reaction rate. Detailed phase equilibrium studies were conducted to determine volume expansion of the IL phase with CO_2 and the phase behavior and mixture critical points between the reactant, product and CO_2. The volume expansion decreases the concentration (molarity) of the reactant. In addition, the mixture critical points indicate that at higher pressures, the reactant can

partition away from the catalytic IL phase. Proper understanding of the phase equilibria is needed to engineer biphasic IL/CO_2 reaction systems for efficient processes.

This contribution will study another model reaction to illustrate the necessary thermodynamic, kinetic and mass transport properties needed for reaction engineering a biphasic ionic liquid/CO_2 system.

3.2.1 Background

The role of CO_2 and its effect on the reaction is often conflicting among various reports especially in terms of reaction rate/activity. One of the first examples of an IL/CO_2 biphasic system was olefin hydrogenation by Liu *et al.*.[55] They compared the results in a biphasic IL/CO_2 and IL/hexane system and found little difference in the reaction rate with pressurized CO_2 or hexane. Jessop, Eckert and co-workers performed asymmetric Ru-catalyzed hydrogenations in an ionic liquid/CO_2 biphasic system. Substrates were chosen whose enantio-selectivity (%ee) increased or decreased depending on high or low H_2 concentration. [56] They found a large increase in %ee with CO_2 pressure for substrates optimal under high H_2-concentration, which they attributed to an increase in H_2 solubility induced by CO_2. However, only a slight decrease in %ee was observed for the substrates optimal under dilute H_2-conditions. Leitner and coworkers [38] also observed an increase in iridium catalyzed hydrogenation of aromatic imines with the presence of CO_2 compared with just H_2 pressure. From high-pressure NMR studies, the solubility of H_2 in the IL (as indicated by the size of the H_2 peak) increases with increasing CO_2 pressure while maintaining constant H_2 loading.

3.2.2 Results and Discussion

The hydrogenation of 1-octene was chosen as another model reaction in the biphasic ionic liquid [HMIm][Tf_2N] and CO_2 system. Rhodium with triphenylphosphine ligands was chosen as a simple catalyst system. Focus was placed on the effect of mass transport and phase equilibria on the reaction rate.

3.2.2.1 Effect of Pressure on Reaction Rates

From the literature, the effect of pressure on reaction rates in biphasic IL/CO_2 reaction systems is somewhat inconsistent: some report that CO_2 pressure increases the

reaction rate; others say that it decreases the rate. Here, reactions were performed under well-mixed conditions and at various levels of pressure of CO_2 with 30 bar of hydrogen initially (>100% excess of H_2 loading over 1-octene) and Rh:TPP = 1:4 for three hours. As shown in Figure 3-11, the reaction rate seems to decrease with increasing CO_2 pressure. These results can be contrasted with the observed increase in reaction rate in the mass-transport controlled regime as discussed above. To study these phenomena the following studies on phase equilibria and thermodynamics are accomplished in the reaction condition.

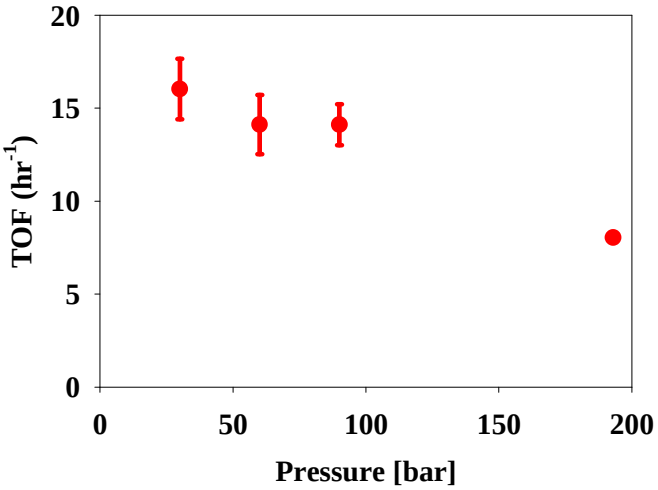

Figure 3-11 Reaction rate of the hydrogenation of 1-octene with total pressure by adding CO_2. Reaction conditions: 1-octene concentration = 44mM, P_{H2} = 30 bar, 70°C; 3 hours catalyzed by Rh-TPP (1:4)[31]

3.2.2.2 Phase Equilibria

3.2.2.2.2 Volume Expansion of the Ionic Liquid

As discussed above, CO_2 is highly soluble in ionic liquids and so it causes the total volume (and often molar volume) to be expanded. However, this expansion is often much smaller than the expansion in organic liquids at a similar solubility of CO_2. For example, CO_2 can expand the volume of methanol to 200% at 69.73 bar and 35°C, and 686.15% at 72.63 bar.[57] The volume expansion of the [HMIm][Tf_2N] with CO_2 and with a mixture of CO_2 and hydrogen have been measured at 70°C .(Ren-Scurto)[32] As seen in Figure 3-12, the IL phase expands by approximately 25% over the volume of the IL for a

pressure range of 120 bar. With an initial pressure of approximately 6 bar of H_2, the volume expansion is less with the pure CO_2.

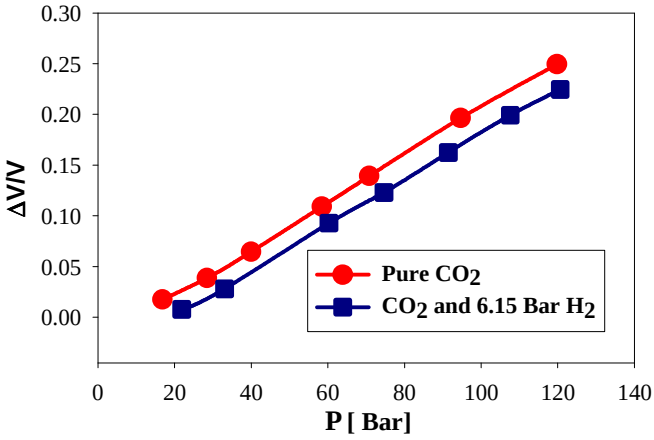

Figure 3-12 Volume expansion of [HMIm][Tf_2N] with CO_2 pressure with/without H_2 at 70°C; lines are smoothed data.[31]

3.2.2.2.3 Phase Behavior of the Reactant/Product

The phase behavior of the reactants and products with CO_2 (without the IL) also leads to a valuable insight into the reaction behavior. Organic liquids, such as 1-octene and octane, can become miscible with CO_2 at conditions (temperature, pressure, and composition) above the bubble point or at conditions beyond the mixture critical point. For liquid mixtures with two or more components, the mixture critical points can change with composition. Figure 3-13 illustrates the mixture critical pressure at 70°C as the proportion of 1-octene to octane is varied between pure 1-octene and pure octane (on a CO_2-free basis); above the line, a one phase mixture exists and below the line, 2-phase vapor-liquid equilibrium exists. This change in concentration can also be considered the conversion for the hydrogenation reaction.

As seen in the figure at pure 1-octene (0% conversion), pure octane (100% conversion), or intermediate concentrations, the mixture critical pressure stays almost constant due to similar physical and critical point properties of 1-octene and octane. The figure also demonstrates that adding H_2 to the CO_2 phase increases the mixture critical pressure compared with the pure CO_2. For instance, with an initial loading of 10 bar of

H_2, the mixture critical pressure increases by approximately 12 bar over the pure CO_2 conditions.

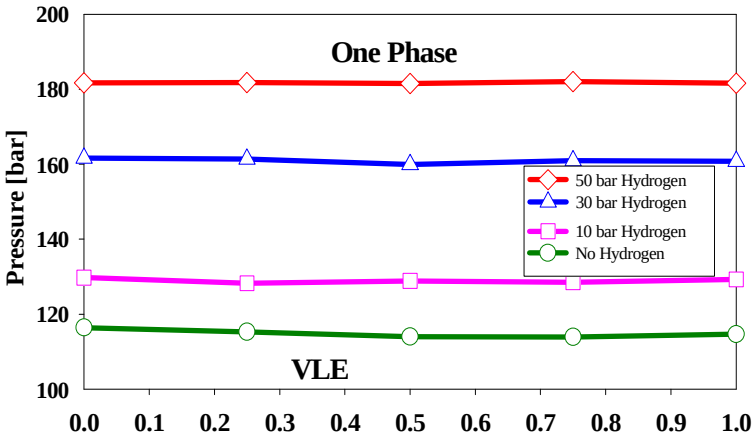

Figure 3-13 Phase behavior of 1-Octene and Octane and CO_2 as percent of initial amount of octane (CO_2-free basis); of can be read as phase behavior as a function of the conversion; line is smoothed data.[31]

3.2.2.2.4 Effects of Phase Equilibrium on the Catalytic Reaction Rate

The pressure of the mixture critical point, indicates a region where the solute/reactant, 1-octene, is normally completely soluble/miscible in the CO_2 phase. These data indicate that in the reaction mixture, the driving force for partitioning of the 1-octene from the catalytic IL-phase to the CO_2 phase increases as the CO_2 pressure increases. As 1-octene partitions away from the catalytic phase, the apparent reaction rate will decrease as the corresponding molarity of the reactant decreases. Thus, the more dramatic drop in reaction rate at the higher pressures can be ascribed to the decrease in solubility or concentration of the 1-octene reactant as seen in Figure 3-2**.** However, at lower pressures of CO_2, partitioning will not be the dominant factor.

The concentration of a reactant in the IL phase, at any pressure, is affected by the volume expansion. The data in Figure 3-5 indicate that the volumes of the reaction mixtures illustrated in Figure 3-2 will increase with the increasing pressure. While keeping mass or moles of the reactant in the initial IL constant, the addition of CO_2 will decrease the molarity of the reactant. For instance, if the concentration of 1-octene in the IL is 1M, then at 90 bar, the volume increases by 15% and the concentration reduces to

0.87 M. The actual reduction to the reaction rate will be determined by the order of the kinetic rate expression. Schrock and Osborn [58] and Grubbs et al.[59] have determined that Rh-catalyzed hydrogenation of olefins is 1st order in the olefin. Thus at similar catalyst and H_2 concentrations and constant moles of 1-octene, a CO_2 pressure that increases the volume by 15% will reduce the concentration and so the reaction rate by 13%.

Thus, the combination of volume expansion of the IL and the partitioning of the reactant will affect the reaction rate. With thorough characterization of the phase equilibrium, the actual concentrations of the reactants, including H_2, can be determined. The actual concentrations will allow intrinsic kinetic constants for a given rate mechanism to be determined. The effect of CO_2 concentration on the intrinsic kinetics is unknown.

3.2.2.3 Mass Transfer Effects

As discussed in section 3.1.2.2.2 and will be discussed in Chapter 4, the presence of CO_2 dramatically lowers the viscosity of the ionic liquid and increases the diffusivity. In order to study the effect of CO_2 on the mass transport phenomenon and the rate of the model hydrogenation reaction, interfacial mass-transfer limitations were established by eliminating agitation and reducing the interfacial area. Under these conditions with a constant molarity of 1-octene, as shown in Figure 3-14, the TOF increased by 25+% with pressure of gaseous CO_2 to 60 bar (5 bar H_2) at a constant concentration of 1-octene.[31] This rapid increase reaches a plateau afterwards, most probably due to transition to the kinetically-controlled regime. Rh-catalyzed hydrogenation of olefins is a relatively rapid reaction and the H_2 availability often becomes a limiting factor. Thus, the CO_2 pressure increased the apparent reaction rate most likely due to increased mass transport of H_2. Solinas *et al.*[38] observed similar finding for Ir-catalyzed imine hydrogenation in IL without stirring and with CO_2 pressure. While these results seem to indicate that increased mass transport properties improved the apparent reaction rate under mass-transport limited conditions, the possibility exists that CO_2 enhanced the solubility of H_2, which might also increase the reaction rate. This will be examined below. CO_2 pressure was found to enhance significantly the reaction rate as measured in turn-over frequency (TOF) of the hydrogenation reaction operated in a mass-transfer limited regime.

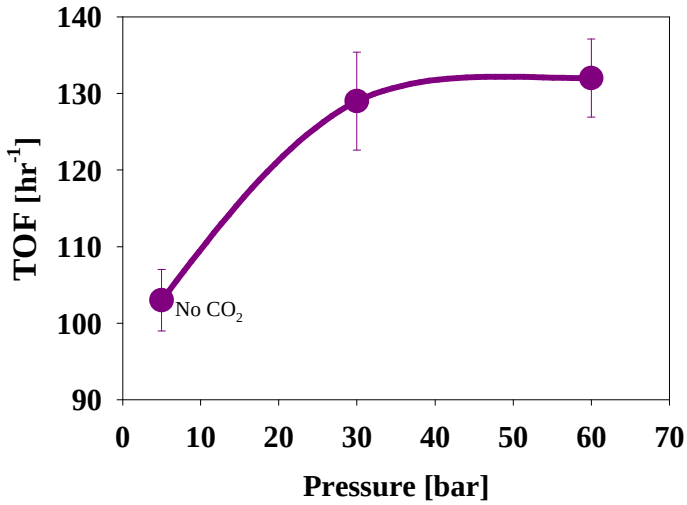

Figure 3-14 Reaction rate for the hydrogenation of 1-octene with Rh- TPP (1:25) in [HMIm][Tf_2N] with and without CO_2 without mechanical stirring, i.e. under initially mass-transfer limited conditions. Reaction conditions: 70°C, P_{H2}=5 Bar; Rh - TPP (1:25); 1-octene concentration = 156mM; 1 hour; line is smoothed data.[31]

In conclusion, CO_2 enhances the apparent reaction rate by increasing mass transfer between reactants inside the catalytic media. This may explain why some researchers observed an increase in the reaction rate with CO_2 pressure (see above).

3.3 Conclusion and subsequent studies

The hydroformylation and hydrogenation of 1-octene was used as model reactions to determine the effects of CO_2 pressure in biphasic ionic liquid/CO_2 systems. Rhodium with triphenylphosphine was chosen as a simple catalyst system. For reactions that were limited by mass transfer, the presence of CO_2 tended to increase the apparent reaction rate. However, in well agitated conditions and at constant loading of 1-octene, increased pressure of CO_2 decreased the apparent reaction rate. Thorough phase equilibrium studies were conducted (Ren and Scurto)[32] to determine the volume expansion of the IL phase with CO_2 and the phase behavior between the reactants/product and CO_2. Both volume expansion and the increased solvent power of CO_2 with pressure affect the concentration of the reactant which consequently affects the apparent kinetics. A biphasic IL/CO_2 system represents a highly tunable and flexible platform for conducting

homogeneously catalyzed reactions. Detailed studies on mass transfer phenomenon during the reaction condition can help to quantify the parameters and properly understand and engineer these reactions.

It has been learned from this chapter that transport properties of the catalytic platform (IL media) in reactions, which occur in a biphasic IL/CO_2 system, can be influenced by introducing CO_2. To increase the efficiency of these reactions, it is essential to use ionic liquids having lower viscosity to help reactants diffuse easier and have more chances to simply reach each others and react. Also, in some reactions managing the amount of viscosity of the solvent (ionic liquid) can help to tune the selectivity of desired products similar to efforts of Jessop, Eckert and co-workers to perform asymmetric Ru-catalyzed hydrogenations in an ionic liquid/CO_2 biphasic system.[56] Therefore, thorough quantitative studies and measurements are needed to be performed to have enough information related to the effect of structure of ionic liquids and compressed gases on the viscosity of reaction media. Our initial endeavours to achieve this knowledge are shown in Chapter 4. In the following chapter , firstly, the effect of the structure of pure imidazolium based ionic liquids at elevated pressures will be studied and then the effect of CO_2 pressure on the viscosity of three different imidazolium based ionic liquids will be quantified. Ultimately, the impact of adding different compressed gases on the viscosity and diffusivity of ionic liquids will be described by comparing the transport properties of mixture of R134a as well as CO_2 with [HMIm][Tf_2N].

Furthermore, to understand the phase behavior of the main reactant (1-octene) and product (nonanal) with [HMIm][Tf_2N] and know more about physical and thermodynamic properties of the pure compounds and their mixtures to obtain the mass transfer coefficient, consecutive studies will be accomplished and reported in Chapter 5.

Utilizing the abovementioned achievements and adding some more information taken from extra studies on mass transfer between [HMIm][Tf_2N] and 1-octene in a liquid-liquid extractor, mass transfer coefficient is determined in Chapter 6. So, all of these accomplishments are useful to develop a know-how package to increase the efficiency of reactions, manage the phase behaviour thermodynamic and physical properties of compounds specially ionic liquids and compressed gases, and model the best system to improve transport phenomena.

3.4 References

1. Cornils, B.; Herrmann, W. A., *Applied Homogeneous Catalysis with Organometallic Compounds*. Wiley-VCH: Weinheim, 1996.
2. Cornils, B.; Herrmann, W. A., *Aqueous Phase Organometallic Catalysis*. Wiley-VCH: Weinheim, 1998.
3. Anastas, P.; Warner, J. C., *Green Chemistry: Theory and Practice*. Oxford University Press: New York, 1998.
4. Anastas, P.; Zimmerman, J., Through the 12 Principles of Green Engineering. *Environ. Sci. Tech.* **2003,** 37, 5, 95A-101A.
5. Anon., Thermodynamics of Ionic Liquids, Ionic Liquid Mixtures, and the Development of Standardized Systems. *Chem. Int.* **2005,** 27, 5, 22-23.
6. Brasse, C. C.; Englert, U.; Salzer, A.; Waffenschmidt, H.; Wasserscheid, P., Ionic Phosphine Ligands with Cobaltocenium Backbone: Novel Ligands for the Highly Selective, Biphasic, Rhodium-Catalyzed Hydroformylation of 1-Octene in Ionic Liquids. *Organometallics* **2000,** 19, 19, 3818-3823.
7. Favre, F.; Olivier-Bourbigou, H.; Commereuc, D.; Saussine, L., Hydroformylation of 1-hexene with rhodium in non-aqueous ionic liquids: how to design the solvent and the ligand to the reaction. *Chem. Comm.* **2001**, 15, 1360-1361.
8. Mehnert, C. P.; Cook, R. A.; Dispenziere, N. C.; Afeworki, M., Supported Ionic Liquid Catalysis-A New Concept for Homogeneous Hydroformylation Catalysis. *J. Am. Chem. Soc.* **2002,** 124, 44, 12932-12933.
9. Haumann, M.; Riisager, A., Hydroformylation in Room Temperature Ionic Liquids (RTILs): Catalyst and Process Developments. *Chem. Rev.* **2008**.
10. Kong, F.; Jiang, J.; Jin, Z., Ammonium Salts with Polyether-Tail: New Ionic Liquids for Rhodium Catalyzed Two-Phase Hydroformylation of 1-Tetradecene. *Catal. Lett.* **2004,** 96, 1, 63-65.
11. Sellin, M. F.; Webb, P. B.; Cole Hamilton, D. J., Continuous flow homogeneous catalysis: hydroformylation of alkenes in supercritical fluid–ionic liquid biphasic mixtures. *Chem. Comm.* **2001**, 781-782.
12. Webb, P. B.; Kunene, T. E.; Cole-Hamilton, D. J., Continuous flow homogeneous hydroformylation of alkenes using supercritical fluids. *Green Chem.* **2005,** 7 373-379.
13. Scurto, A. M.; Leitner, W., Expanding the useful range of ionic liquids: melting point depression of organic salts with carbon dioxide for biphasic catalytic reactions. *Chem. Comm.* **2006**, 35, 3681-3683.
14. Ahosseini, A.; Ren, W.; Scurto, A. M., Understanding Biphasic Ionic Liquid/CO_2 Systems for Homogeneous Catalysis: Hydroformylation. *Ind. Eng. Chem. Res.***2009**, 95-101.
15. Bhanage, B. M.; Divekar, S. S.; Deshpande, R. M.; Chaudhari, R. V., Kinetics of hydroformylation of l-dodecene using homogeneous HRh (CO)(PPh_3)$_3$ catalyst. *J. Mol. Cat. A***1997,** 115, 2, 247-257.
16. Deshpande, R. M.; Bhanage, B. M.; Divekar, S. S.; Kanagasabapathy, S.; Chaudhari, R. V., Kinetics of Hydroformylation of Ethylene in a Homogeneous Medium: Comparison in Organic and Aqueous Systems. *Ind. Eng. Chem. Res.* **1998,** 37, 6, 2391-2396.

17. Deshpande, R. M.; Chaudhari, R. V., Kinetics of hydroformylation of 1-hexene using homogeneous HRh (CO)(PPh_3)$_3$ complex catalyst. *Ind. Eng. Chem. Res.* **1988,** 27, 11, 1996-2002.
18. Palo, D. R.; Erkey, C., Kinetics of the Homogeneous Catalytic Hydroformylation of 1-Octene in Supercritical Carbon Dioxide with $HRh(CO)[P(p\text{-}CF_3C_6H_4)_3]_3$. *Ind. Eng. Chem. Res.* **1999,** 38, 3786-3792.
19. Purwanto, P.; Delmas, H., Gas-Liquid-Liquid reaction engineering: hydroformylation of 1-octene using a water soluble rhodium complex catalyst. *Catal. Today* **1995,** 24, 135-140.
20. Chaudhari, R. V.; Seayad, A.; Jayasree, S., Kinetic Modeling of homogeneous catalytic processes. *Catal. Today* **2001,** 66, 371-380.
21. Ahosseini, A.; Scurto, A. M., Viscosity of Imidazolium-Based Ionic Liquids at Elevated Pressures: Cation and Anion Effects. *Int. J. Thermophys.* **2008,** 29, 1222-1243.
22. Liu, Z.; Wu, W.; Han, B.; Dong, Z.; Zhao, G.; Wang, J.; Jiang, T.; Yang, G., Study on the Phase Behaviors, Viscosities, and Thermodynamic Properties of CO_2/[C_4mim][PF_6]/Methanol System at Elevated Pressures. *Chem. Eur. J.* **2003,** 9, 16, 3897-3903.
23. Lu, J.; Liotta, C. L.; Eckert, C. A., Spectroscopically Probing Microscopic Solvent Properties of Room-Temperature Ionic Liquids with the Addition of Carbon Dioxide. *J. Phys. Chem. A* **2003,** 107, 19, 3995-4000.
24. Tomida, D.; Kumagai, A.; Qiao, K.; Yokoyama, C., Viscosity of [bmim][PF_6] and [bmim][BF_4] at High Pressure. *Int. J. Thermophys.* **2006,** 27, 1, 39-47.
25. Einstein, A., Über die von der molekularkinetischen Theorie der Wärme geforderte Bewegung von in ruhenden Flüssigkeiten suspendierten Teilchen. *Annalen der Physik* **1905,** 322, 8, 549-560.
26. Hou, Y.; Baltus, R. E., Experimental measurement of the solubility and diffusivity of CO2 in room-temperature ionic liquids using a transient thin-liquid-film method. *Ind. Eng. Chem. Res.* **2007,** 46, 24, 8166-8175.
27. Ferguson, L.; Scovazzo, P., Solubility, diffusivity, and permeability of gases in phosphonium-based room temperature ionic liquids: data and correlations. *Ind. Eng. Chem. Res* **2007,** 46, 4, 1369-1374.
28. Camper, D.; Becker, C.; Koval, C.; Noble, R., Diffusion and Solubility Measurements in Room Temperature Ionic Liquids. *Ind. Eng. Chem. Res.* **2006,** 45, 1, 445-450.
29. Morgan, D.; Ferguson, L.; Scovazzo, P., Diffusivities of gases in room-temperature ionic liquids: Data and correlations obtained using a lag-time technique. *Ind. Eng. Chem. Res* **2005,** 44, 13, 4815-4823.
30. Shiflett, M. B.; Yokozeki, A., Solubilities and Diffusivities of Carbon Dioxide in Ionic Liquids: [bmim][PF6] and [bmim][BF4]. *Ind. Eng. Chem. Res.* **2005,** 44, 12, 4453-4464.
31. Ahosseini, A.; Ren, W.; Scurto, A. M., Hydrogenation in biphasic ionic liquid-carbon dioxide systems. *ACS Symp. Ser. FIELD Full Journal Title:ACS Symposium Series* **2009,** 1006, Gas-Expanded Liquids and Near-Critical Media, 218-234.
32. Ren, W.; Sensenich, B.; Scurto, A. M., High-Pressure Phase Equilibria of Carbon Dioxide (CO2)+ n-Alkyl-Imidazolium Bis (trifluoromethylsulfonyl) amide Ionic Liquids. *J. Chem. Thermo.* **2009**.

33. Kumelan, J.; Kamps, Á.; Tuma, D.; Maurer, G., Solubility of CO in the ionic liquid [bmim][PF_6]. *Fluid Phase Equil.* **2005,** 228, 207-211.
34. Kumelan, J.; Perez-Salado Kamps, A.; Tuma, D.; Maurer, G., Solubility of H_2 in the ionic liquid[bmim][PF_6]. *J. Chem. Eng. Data* **2006,** 51, 1, 11-14.
35. Kumelan, J.; Pérez-Salado Kamps, Á.; Tuma, D.; Maurer, G., Solubility of CO_2 in the ionic liquid [hmim][Tf_2N]. *J. Chem. Thermo.* **2006,** 38, 11, 1396-1401.
36. Kumelan, J.; Pérez-Salado Kamps, Á.; Tuma, D.; Maurer, G., Solubility of the single gases H_2 and CO in the ionic liquid [bmim][CH_3SO_4]. *Fluid Phase Equil.* **2007,** 260, 1, 3-8.
37. Hert, D. G.; Anderson, J. L.; Aki, S. N. V. K.; Brennecke, J. F., Enhancement of oxygen and methane solubility in 1-hexyl-3-methylimidaxolium bis(trifluoromethylsulfonyl)imide using carbon dioxide. *Chem. Comm.* **2005**.
38. Solinas, M.; Pfaltz, A.; Cozzi, P. G.; Leitner, W., Enantioselective Hydrogenation of Imines in Ionic Liquid / Carbon Dioxide Media. *J. Am. Chem. Soc.* **2004,** 126, 16142-16147.
39. Solinas, M.; Wasserscheid, P.; Leitner, W.; Pfaltz, A.; Chemie, R.; Kamps, I.; Xia, I. J.; Maurer, I. G., Enantioselective Hydrogenation of Imines in Ionic Liquid/Carbon Dioxide media. *Chemie Ingenieur Technik* **2003,** 75, 8, 1153-1153.
40. Jin, H.; Subramaniam, B.; Ghosh, A.; Tunge, J., Intensification of catalytic olefin hydroformylation in CO_2-expanded media. *AIChE J.* **2003,** 52, 7, 2575-2591.
41. Lopez-Castillo, Z. K.; Aki, S. N. V. K.; Stadtherr, M. A.; Brennecke, J. F., Enhanced Solubility of Oxygen and Carbon Monoxide in CO_2-Expanded Liquids *Ind. Eng. Chem. Res.* **2006,** 45, 15.
42. Bezanehtak, K.; Dehghani, F.; Foster, N. R., Vapor-Liquid Equilibrium for the Carbon Dioxide + Hydrogen + Methanol Ternary System. *J. Chem. Eng. Data* **2004,** 49, 3, 430-434.
43. Scurto, A. M.; Aki, S.; Brennecke, J. F., CO_2 as a separation switch for ionic liquid/organic mixtures. *J. Am. Chem. Soc* **2002,** 124, 35, 10276-10277.
44. Scurto, A. M.; Aki, S.; Brennecke, J. F., Carbon dioxide induced separation of ionic liquids and water. *Chem. Comm.* **2003,** 2003, 5, 572-573.
45. Aki, S. N. V. K.; Scurto, A. M.; Brennecke, J. F., Ternary Phase Behavior of Ionic Liquid (IL)-Organic-CO_2 Systems. . *Ind. Eng. Chem. Res.* **2006,** 45 16, 5574-5585.
46. Mellein, B. R.; Brennecke, J. F., Characterization of the Ability of CO_2 To Act as an Antisolvent for Ionic Liquid / Organic Mixtures. *J. Phys. Chem. B* **2007,** 111, 18, 4837-4843.
47. Najdanovic-Visak, V.; Rebelo, L. P. N.; Nunes da Ponte, M., Liquid-liquid behaviour of ionic liquid-1-butanol-water and high pressure CO_2 - induced phase changes. *Green Chem.* **2005,** 7, 6, 443-450.
48. Zhang, Z.; Wu, W.; Gao, H.; Han, B.; Wang, B.; Huang, Y., Tri-phase behavior of ionic liquid - water - CO_2 system at elevated pressures. *PCCP* **2004,** 6 21, 5051-5055.
49. Zhang, Z.; Wu, W.; Wang, B.; Chen, J.; Shen, D.; Han, B., High-pressure phase behavior of CO_2/acetone/ionic liquid system. *J. Supercrit. Fluids* **2007,** 40, 1–6.
50. Blanchard, L. A.; Brennecke, J. F., Recovery of organic products from ionic liquids using supercritical carbon dioxide. *Ind. Eng. Chem. Res.* **2001,** 40, 1, 287-292.

51. Zhao, G.; Jiang, T., Electro-oxidation of Benzyl Alcohol in a Biphasic System Consisting of Supercritical CO_2 and Ionic Liquids. *J.Phys.Chem.B* **2004,** 108, 13052-13057.
52. Shimoyama, Y.; Sonoda, M.; Miyazaki, K.; Higashi, H.; Iwai, Y.; Arai, Y., Measurement of solubilities for rhodium complexes and ligands in supercritical carbon dioxide. *J. Supercrit. Fluids* **2008,** 44, 266-272.
53. Wagner, K.-D.; Dahmen, N.; Dinjus, E., Solubility of Triphenylphosphine, Tris(p-fluorophenyl)phosphine, Tris(pentafluorophenyl)phosphine, and Tris(p-trifluoromethylphenyl) phosphine in Liquid and Supercritical Carbon Dioxide. *J. Chem. Eng. Data* **2000,** 45, 672-677.
54. Fredlake, C. P.; Muldoon, M. J.; Aki, S. N. V. K.; Welton, T.; Brennecke, J. F., Solvent strength of ionic liquid/CO_2 mixtures. *Phys. Chem. Chem. Phys.* **2004,** 6, 3280 - 3285.
55. Liu, F.; Abrams, M. B.; Baker, R. T.; Tumas, W., Phase-separable catalysis using room temperature ionic liquids and supercritical carbon dioxide. *Chem. Comm.* **2001**, 433-434.
56. Jessop, P. G.; Stanley, R. R.; Brown, R. A.; Eckert, C. A.; Liotta, C. L.; Ngo, T. T.; Pollet, P., Neoteric solvents for asymmetric hydrogenation: supercritical fluids, ionic liquids, and expanded ionic liquids. *Green Chem.* **2003,** 5, 2, 123-128.
57. Bezanehtak, K.; Combes, G. B.; Dehghani, F.; Foster, N. R.; Tomasko, D. L., Vapor-Liquid Equilibrium for Binary Systems of Carbon Dioxide + Methanol, Hydrogen + Methanol, and Hydrogen + Carbon Dioxide at High Pressures. *J. Chem. Eng. Data* **2002,** 47, 2, 161-168.
58. Schrock, R. R.; Osborn, J. A., Catalytic hydrogenation using cationic rhodium complexes. I. Evolution of the catalytic system and the hydrogenation of olefins. *J. Am. Chem. Soc.* **1976,** 98, 8, 2134-2143.
59. Grubbs, R. H.; Kroll, L. C.; Sweet, E. M., The Preparation and Selectivity of a Polymer-Attached Rhodium (l) Olefin Hydrogenation Catalyst., *J. Macromol. Sci. Part A* **1973,** 7, 5, 1047-1063.

Chapter 4 Transport Properties

4 Transport Properties of Ionic Liquids and Mixtures with Compressed Gases at Ambient and High Pressure

The measurement of physicochemical properties of ionic liquids is necessary to understand and utilize these diverse media. As discussed in Chapter 3, transport properties, such as viscosity and diffusivity, are important for a number of processes involving reactions and separations. For instance, they determine the force and energy required to transfer and mix the ionic liquid with other substances and appear in many dimensionless groups used in mass and heat transfer correlations. Understanding structural effects on physicochemical properties is important for a rational approach for molecular design of ILs. Ionic liquids possess a wide range of viscosity. For instance, at 283.15 K (10°C) and ambient pressure, the viscosity of [EMIm][Tf_2N] is 63.6 mPa·s while for [OMIm][PF_6], it is 2439 mPa·s. This flexibility may be tailored to a particular application; for example, use as a solvent for reactions may require relatively low viscosity, while use as a lubricant or as a supported-membrane may require higher viscosity. For comparison, the viscosity of typical organic solvents at ambient conditions extends ranges from 0.2 to 10 mPa·s. [1]

Some compressed gases like CO_2 and 1,1,1,2-tetrafluoroethane (R134a) have high solubilities in ILs. These gases reduce viscosity and increase the diffusivity in the liquid phase of the biphasic system, and facilitate mass transfer between phases. To have the fundamental knowledge of momentum and mass transfer parameters, measuring viscosity and diffusion coefficient of pure ionic liquids and their mixture with solvents at ambient and high-pressure is necessary. The lack of enough data for the related parameters makes the following subjects very important. So, they will be discussed in detail in this chapter:

- Measuring and correlation of the viscosity of pure ILs and their mixtures with compressed gases at ambient and high-pressure.
- Diffusivity measurements of the IL and solvents at ambient and high pressures.

In these studies, imidazolium ionic liquids and their mixtures with CO_2 and R134a are used.

4.1 Viscosity of Imidazolium-Based Ionic Liquids at Elevated Pressures: Cation and Anion Effects

Room temperature ionic liquids (RTILs) are recently getting more and more attention because of their diverse chemistry and potential applications. These low-melting organic salts, which are comprised entirely of cations and anions, can be molecularly-engineered for specific physicochemical properties for use in a variety of fields. It has been estimated that approximately 10^{14} unique cation/anion combinations may exist [2-5] ; thus, precise tuning of properties is possible. For example, ionic liquids have been used as absorption media for gases[6, 7] and as an extractant in liquid separations. [8, 9] As ions, a number of electrochemical applications exist. [10-15] A large variety of reactions may be performed in ILs especially as support media for catalysis and biocatalysis. [16-21] ILs may be used for a variety of engineering applications including use as heat transfer fluids[22] and as hydraulic fluids. [23]

4.1.1 Introduction

The measurement of the physicochemical properties of ionic liquids such as viscosity, diffusivity, density, ionic conductivity, thermal behavior as well as, solubility and polarity can help to understand and use them in a diverse area. Applications that occur at high temperatures and/or pressures require reliable and accurate experimental data and mathematical models. A large number of models for correlating and predicting the viscosity of pure fluids and mixtures have appeared in the literature. Most of these methods are based on the principle of corresponding states, on the absolute rate theory of Eyring [24] and, more recently, on molecular dynamic calculations.[1] Abbott and coworkers [25-27] used a modified "hole theory" to predict the viscosities of ionic liquids at ambient conditions. The Vogel - Fulcher - Tammann (VFT) equation [28-30] and Litovitz [31] equation are empirical equations that have been used at ambient pressures for liquids in general with a temperature-dependent flow activation energy.

Crosthwaite *et al.* [32], measured the viscosity of a number imidazolium and pyridinium ionic liquids with a cone and plate rheometer at ambient pressures. Tokuda *et al.* [33] investigated the physicochemical properties of several ILs with a fixed 1-butyl-3-methylimidazolium ([BMIm]) cation, and different anions: $[(C_2F_5SO_2)_2N]$, $[(CF_3SO_2)_2N]$

(abbreviated [Tf_2N]), [CF_3SO_3], [PF_6], [CF_3CO_2], and [BF_4] at ambient pressures and various temperatures. [BMIm] with [PF_6] and [$(C_2F_5SO_2)_2N$] produced ILs with significantly higher viscosity that were attributed to strong coulombic forces among each ionic species in the ionic liquids. Watanabe and coworkers [34] also carried out similar experiments with different cation classes and a singular anion and determined that an increase in the alkyl chain length of the cation causes an increase in the viscosity. They also demonstrated that imidazolium cations have lower viscosity, higher diffusivity, higher density, and higher thermal stability compared to pyridinium, pyrrolidinium, and ammonium structures. [35]

The high-pressure viscosity of ionic liquids has only been measured for a few cation and anion combinations. Harris *et al.* [36-38] measured the viscosity of [BMIm] & [OMIm] [PF_6], and [OMIm][BF_4] with a falling-body viscometer to 353.15 K and approximately 200 MPa (2000 bar). They fitted the data with a modified Litovitz and Vogel-Fulcher-Tammann (VFT) equation to incorporate both temperature and pressure dependences. Kanakubo and co-workers [39] measured the diffusion coefficient and molar conductivity of [BMIm][PF_6] up to 200 MPa (2000 bar) and used the Stokes-Einstein equation to back calculate the viscosity. Tomida *et al.* [40, 41] measured the viscosity of similar systems: [BMIm][PF_6], [BMIm][BF_4], [OMIm][PF_6], and [HMIm][PF_6] to moderate pressures (<20 MPa) and different temperatures. They used the hybrid VFT-Tait equation to correlate the data. Recently, Kandil et al reported the viscosity of 1-hexyl-3-methylimidazolium bis(trifluorosulfonyl)imide, [HMIm][Tf_2N] at temperatures between (288 and 433) K and Pressures below 50 MPa. [42]

In this work, the viscosity for several different ionic liquids has been measured under high pressures (up to 126 MPa) and at three temperatures (25°C, 50°C, and 70°C). Both the cation and anion have been systematically changed to investigate the effect of structure on viscosity at elevated pressure. Figure 4-1 illustrates the cations and anions investigated. The Litovitz equation combined with the Tait equation [43, 44] were used to describe the viscosity of ionic liquids as a function of pressure and temperature.

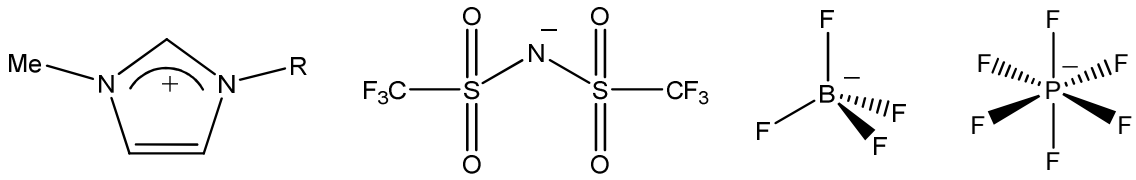

[R-MIm] $[Tf_2N]$ $[BF_4]$ $[PF_6]$

Figure 4-1 Structure of methyl imidazolium cations and anions investigated; for [R-MIm], R=ethyl- ([EMIm]), n-butyl- ([BMIm]), n-hexyl- ([HMIm]), n-octyl-(OMIm) and n-decyl- ([DMIm]).

4.1.2 Viscometer Justify

The accuracy of the viscometer was first verified using standard calibration solutions as obtained from the company. The viscosity of n-hexane was measured and compared with high-accuracy literature values [45-47] as shown in Figure 4-2. Despite the different experimental methods, e.g., falling-cylinder viscometer, vibrating-wire viscometer, and capillary-tube viscometer, the experimental results here yielded a very high consistency with literature data throughout the large pressure range. Interpolating our data at the pressures measured by each of the different data sets, the percent deviation at each point is plotted in Figure 4-3. The nominal reported experimental uncertainty for each of the literature studies is as follows: ±2% by Dymond et al. [47] using a capillary-tube method; ±3 % by Kiran and Sen [45] using a falling-cylinder method; and ±0.5 % by Oliveira and Wakeham [46] using a vibrating-wire viscometer.

As shown in Figure 4-3, our data are within the reported uncertainties of Dymond et al. and Kiran and Sen with percent average absolute relative deviation (%AARD) between our interpolated values and the literature values of 0.78 % and 1.1 %, respectively. The % AARD of 1.9 % with the data of Oliveira and Wakeham is outside their reported uncertainty.

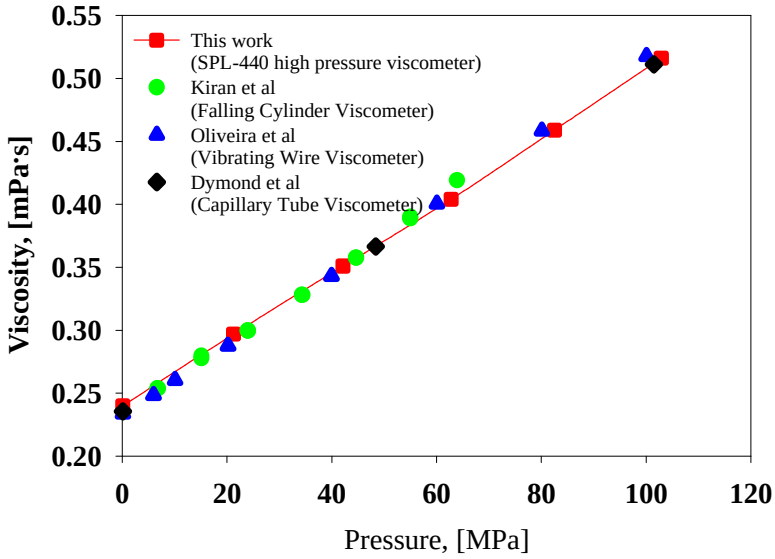

Figure 4-2 The effect of pressure on the viscosity of n-hexane at 323.15 K (literature: Kiran *et al.* [45], Oliveira *et al.* [46], Dymond *et al.* [47]).

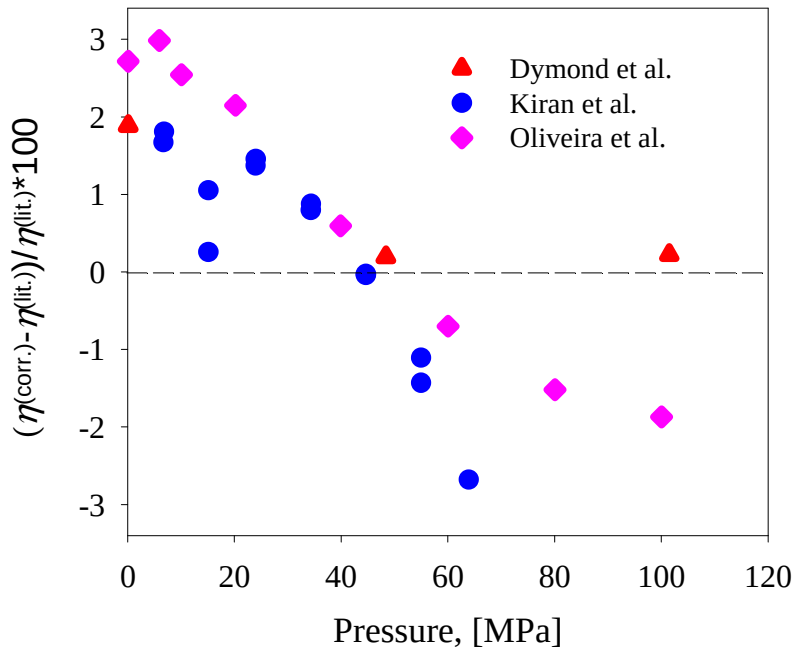

Figure 4-3 Deviation of measured viscosities of n-hexane at 323.15 K from the literature**.**

4.1.3 Data Modeling and Analysis

Various theoretical models and empirical expressions can be found in the literature that can be used to represent the viscosity of liquids as functions of pressure and temperature. The variation of viscosity with temperature can be derived in an approximate way from the rate theory approach of Eyring [24], in which the liquids are assumed to have a quasi-crystalline structure.[48] The lattice contains free volume sites that molecules can jump and occupy and make the liquid layer flow with respect to another. The liquid molecules need to pass over a potential energy barrier in order to flow. The height of the barrier, which is equivalent to the flow activation energy, is independent of the temperature, but is influenced by external forces acting on the liquid. The temperature dependence of viscosity based on the rate theory by the Arrhenius equation [45, 49, 50] is:

$$\ln \eta = \ln A + E / RT \qquad (4.1)$$

where A is a constant, E is the shear flow activation energy, and R is the gas constant.

However, few liquids demonstrate an Arrhenius viscosity behavior.[51] The flow activation energy of liquids is temperature-dependent and increases significantly with cooling. Glass forming [52] compounds, which can have an unorganized liquid-like structure below their melting point, often display non-Arrhenius behavior. In these liquids, the viscosity increases strongly with decreasing temperature. Based on these concepts, the Vogel - Fulcher - Tammann (VFT) equation [28-30] is often used, which uses an additional adjustable temperature parameter (T_0) to the exponential term;

$$\ln \eta = \ln A + B(T - C)^{-1} \qquad (4.2)$$

$$\eta = \eta' \exp(B/(T - T_0)) \qquad (4.3)$$

where η' is a pre-exponential factor and B and T_0 are specific adjustable parameters. This equation has been extensively used in the description of cooperative molecular motion in glass-forming and viscous liquids at different temperatures.[52] Most ionic liquids often form glass phases. [32, 34, 53] Angell [54] has proposed a classification for the fragility of liquids defined as a strength parameter, $D = B/T_0$, based on the VFT equation. According to this definition, strong liquids, where their viscosity approaches Arrhenius temperature dependence, have a large strength parameter (D>30).

Another empirical equation, which was derived in an approximate way from the rate theory of Eyring, was proposed by Fieggen [48]:

$$\ln\eta = B + A(T-C)^{-1} - D(T-T_1)^2 \qquad (4.4)$$

Fieggen applied this four-parameter equation for liquids such as water, ethanol, toluene, etc. over wide range of temperatures. Fieggen assumed that the thermal expansion is accompanied by an increase of the fraction of unoccupied sites and lattice volume. As in other non-Arrhenius type equations, the height of the potential-energy barrier will depend on temperature (T_1). Litovitz [31] has suggested another empirical equation which has been used at ambient pressures:

$$\eta = A\exp(B/RT^3) \qquad (4.5)$$

Harris *et al.* [36, 37] modified both VFT and Litovitz equations to incorporate the temperature and pressure dependence of the viscosity as follows for three pure imidazolium based ionic liquids:

$$\eta = \exp\{a + bp + (c + dp + ep^2)/T^3\}$$
$$\eta = \exp\{a'+b'+(c'+d'+e'\,p^2)/(T-T_0)\} \qquad (4.6a,b)$$

In these studies, Harris and co-workers regressed the viscosity of 1-butyl-3-methylimidazolioum hexafluorophosphate [37], 1-methyl-3-octylimidazolium hexafluorophosphate [36], and 1-methyl-3-octylimidazolium tetrafluoroborate [36] between (273.15 and 353.15) K and at pressures to 250 MPa, 176 MPa, and 224 MPa , respectively. They showed that the quality of the fits for both equations is very similar.

The Tait equation is well-known to represent the pressure-volume relationship of many liquids. [43, 44] The functional form is

$$\frac{V_0 - V}{PV_0} = \frac{A}{\pi + P} \qquad (4.7)$$

where V_0 and V represent the molar volume at ambient pressure and under pressure P; A and π are constants. Tammann modified the Tait equation [43] to:

$$\frac{(V_0 - V)}{V_0} = C\log\left(\frac{B+P}{B+0.1}\right) \qquad (4.8)$$

The modified equation has become widely accepted to represent high-pressure density data for liquids and liquid mixtures.

In a similar manner, the Tait equation has been used to correlate the pressure dependence of viscosity [44]:

$$\ln\left(\frac{\eta_p}{\eta_o}\right) = E\ln\left(\frac{D+P}{D+0.1}\right) \qquad (4.9)$$

where η_p and η_0 are the viscosities at a pressure P and at 0.1 MPa 1 bar, respectively. This equation contains only two fitted parameters and has yielded good correlation with experimental data as shown by Kashiwagi and Makita [44] for aromatic hydrocarbons and cyclohexane up to 110 MPa. Tomida *et al.* [40, 41] have used this equation to correlate the viscosity of [BMIm][PF_6], [BMIm][BF_4], [OMIm][PF_6], and [HMIm][PF_6], at moderate pressures (<20 MPa).

This investigation will utilize a hybrid Tait-Litovitz equation at elevated pressures (to 126 MPa) for the viscosity data for a series of room-temperature ionic liquids:

$$\eta_P = A\exp(B'/T^3)((D+P)/(D+0.1))^E \qquad (4.10)$$
$$B' = B/R$$

Data at ambient pressure are first correlated using the Litovitz equation, then the Tait parameters are fitted for the higher pressures. The aforementioned equation has the advantages of containing fewer fitting parameters (*A, B, D, E*) than other models and simplicity of data analysis. The values of independent parameters, *E* and *D*, have been determined as linear functions of temperature (Table 4-1).

Table 4-1 Tait-Litovitz equation parameters and AARD%[a].

	$\eta_0=Aexp(B'/(T^3))$		$D=a+bT$		$E=c+dT$		
IL	A (mPa·s)	B' $\times10^{-6}$ (K^3)	a (MPa)	b (MPa·K^{-1})	c	d (K^{-1})	AARD[a] (%)
[EMIm][Tf_2N]	0.8423	97.92	2947	-6.96	48.14	-0.1279	3.9
[HMIm][Tf_2N]	0.583	127	885.13	-1.111	22.03	-0.0508	2.2
[DMIm][Tf_2N]	0.6449	135.6	421.81	-0.1133	14.4	-0.03	2.4
[HMIm][BF_4]	0.6059	153.8	4966.88	-13.27	73.83	-0.2064	4.0
[HMIm][PF_6]	0.7208	172.1	2717.7	-5.066	82.11	-0.2136	3.1

[a] $\%AARD = \frac{100}{N}\sum_{i=1}^{N}\left|\frac{\eta_i^{pred}-\eta_i^{\exp}}{\eta_i^{\exp}}\right|$

4.1.4 Results and discussion

The viscosity of six methyl-imidazolium based ionic liquids (Figure 4-1), [HMIm][Tf_2N], [HMIm][PF_6], [BMIm][PF_6], [DMIm][Tf_2N], [EMIm][Tf_2N], and [HMIm][BF_4], has been measured to pressures of approximately 130 MPa. The results are tabulated in Table 4-3 to Table 4-7 for temperatures of 298.15 K, 323.15 K, and 343.15 K. Ambient pressure viscosity for two methods from this work and various literature sources are compiled in Table 4-2. The viscosity of five ionic liquids at 298.15 K was measured using both an ambient-pressure rheometer and the high-pressure viscometer; these data match within a few percent of each other. Both of these methods of measurement also correlate well with literature reports. Some of the scatter and deviations among these literature reports may be due to water content, which has been determined to significantly affect viscosity even at low concentrations. [55, 56]

Table 4-2 Viscosity (η [mPa·s]) of ionic liquids at ambient pressure measured by different methods

Reference:	**[EMIm][Tf_2N]**	**[HMIm][Tf_2N]**	**[DMIm][Tf_2N]**	**[HMIm][BF_4]**	**[HMIm][PF_6]**
T=298.15 K					
Huddlestone (2001) [53]					585(454[a])
Crosthwaithe (2005) [32]	32	68			
Tokuda (2006) [35]	32.6	69.7			
Sanmamed (2007) [78]				174.0	
Harris (2007) [38]					496.9
This work[b]	34.29±0.1	71.0±0.3	108.2±0.4	202.4±0.8	481.4±2.4
This work[c]	34.1±0.4	71.5±0.8	111.2±1.2	210.4±2.4	489.5±6
T=323.15 K					
Crosthwaithe (2005) [32]	15.0	26.0			
Tokuda (2005) [34]	14.7	24.8			
Tokuda (2006) [35]	15.5	25.8			
Sanmamed (2007) [78]				53.9	
Harris (2007) [38]					117.0
This work[b]	15.6±0.1	24.9±0.1	36.3±0.1	58.5±0.3	121.4±0.36
T=343.15 K					
Crosthwaithe (2005) [32]	9.0	15.0			
Tokuda (2005) [34]	9.4	13.7			
Tokuda (2006) [35]	9.5	14.1			
Harris (2007) [38]					49.7
This work[b]	9.55±0.03	14.1±0.2	18.20±0.05	27.0±0.1	48.1±0.3

[a] equilibrated with water; [b] oscillating - piston viscometer; [c] cone- and- plate viscometer

In addition, the first reported viscosity data for [DMIm][Tf_2N] are given here. Figure 4-4 depicts the measured viscosity of [HMIm][Tf_2N] with temperature at atmospheric

pressure with a comparison of literature data. [32, 34, 35] This plot illustrates the exponential decrease of viscosity with the temperature in a manner consistent with Litovitz behavior.

The data presented here has a good correlation with several literature data sources as shown in Figure 4-5. The literature reports seem to be approximately 5% different from each other; including roughly 4% difference from the same research group. Crosthwaite *et al.* [32] report errors at ±2%, while Tokuda *et al.* [34, 35] do not state an error range for their data. The viscosity of [BMIm][PF_6] has been measured at elevated pressures at 298.15 K and is illustrated in Figure 4-6 and Table 4-3. A nearly linear trend is observed until approximately 40 MPa, after which the viscosity begins to marginally increase at a faster rate with pressure. While little high pressure viscosity data for ionic liquids exists in the literature, those of Harris *et al.* [37] for this system are plotted and an excellent agreement (within 0.8% average absolute relative deviation (%AARD)) is obtained as shown in Figure 4-7.

Table 4-3 Measured viscosity (η) of [BMIm][PF_6] at 298.15 K with literature data.[37]

P [MPa]	η [mPa·s]	± SD[a]
0.1	270.9,(273[b])	1
3.4	289.7	2
6.9	305.7	2
12.1	329.2,(329[a])	2
17.2	353.7	1
24.7	396.3,(391[a])	2
25.7	398.2,(390[a])	4
41.4	473.8	1
50.6	543.4,(546[a])	5

[a] SD=Standard Deviation based on n= 20. [b] Data of Harris *et al.* [37]

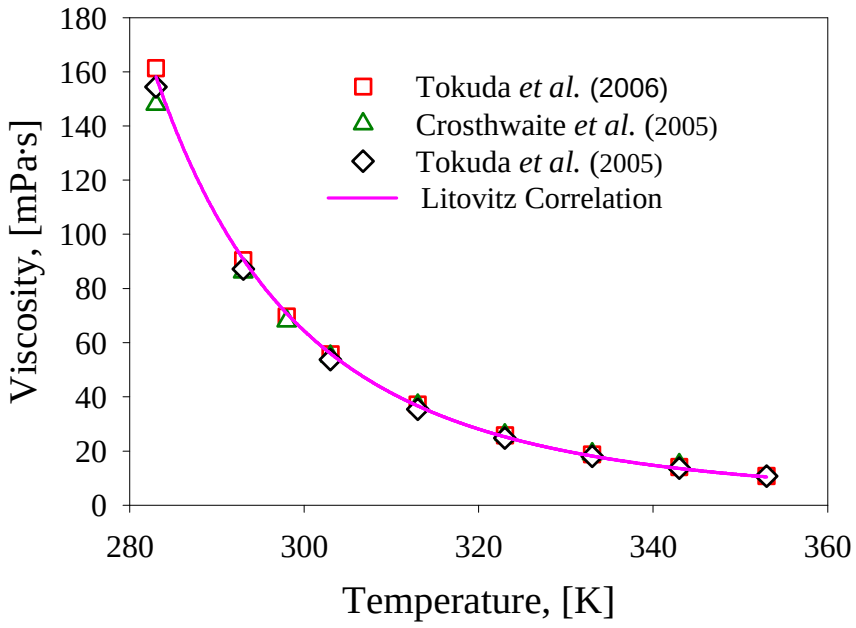

Figure 4-4 The effect of temperature on viscosity of [HMIm][Tf_2N] at atmospheric pressure with Tokuda *et al.* (2006) [35], Crosthwaite *et al.* [32], Tokuda *et al.* (2005). [34] The solid line is the Litovitz correlation of the data of this work.

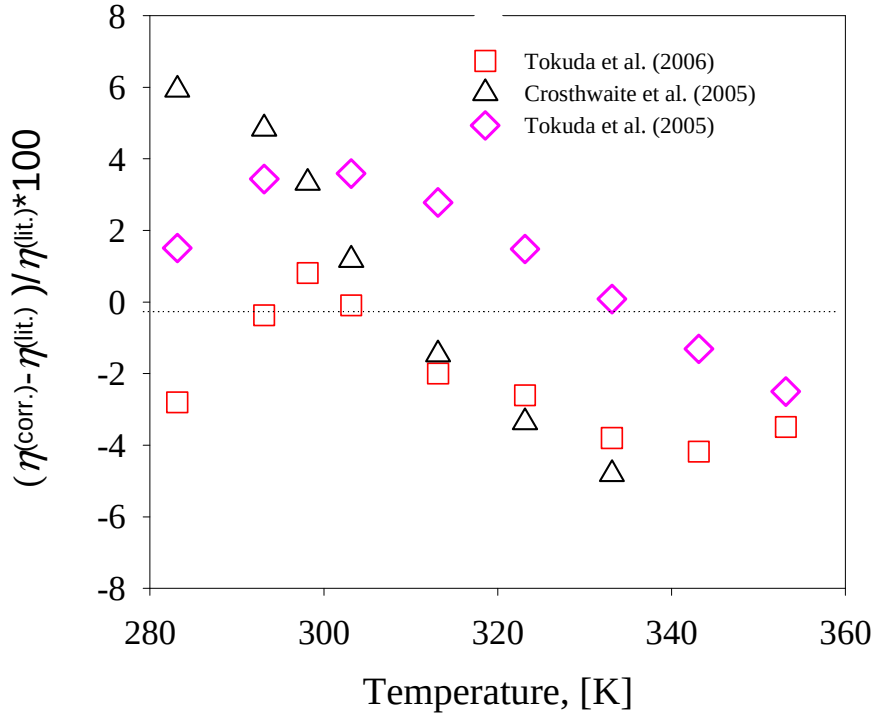

Figure 4-5 Deviation of measured viscosities of [HMIm][Tf_2N] at atmospheric pressure from the Litovitz correlation.

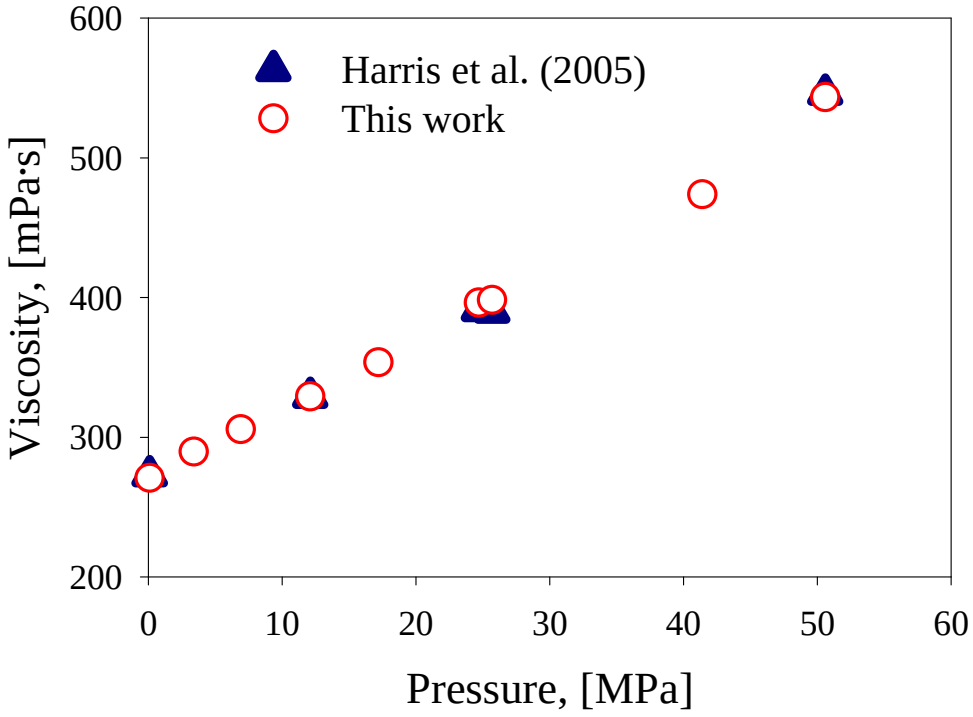

Figure 4-6 The effect of pressure on viscosity of [BMIm][PF_6] at 298.15 K compared with the literature data. [37]

Table 4-4 Measured Viscosity (η) of [EMIm][Tf_2N] as a function of pressure and temperature.

298.15 K			**323.15 K**			**343.15 K**		
P (MPa)	***η*** (mPa·s)	± SD	***P*** (MPa)	***η*** (mPa·s)	± SD	***P*** (MPa)	***η*** (mPa·s)	± SD
0.10	34.4	0.1	0.10	15.6	0.1	0.10	9.6	0.0
2.82	35.0	0.1	2.82	16.1	0.1	2.82	9.8	0.1
4.19	35.3	0.2	4.19	16.4	0.1	4.19	9.9	0.1
7.36	36.2	0.1	7.36	16.9	0.1	7.36	10.2	0.1
35.56	46.8	0.1	35.56	22.0	0.1	35.56	12.6	0.04
48.76	53.3	0.3	48.76	24.9	0.1	48.76	13.8	0.1
69.30	65.0	0.3	69.30	30.8	0.1	69.30	16.0	0.1
85.20	79.4	0.5	85.20	36.7	0.3	85.20	17.7	0.1
96.50	90.0	0.3	96.50	40.1	0.1	96.50	19.2	0.1
110.55	108.6	0.6	110.55	44.8	0.2	110.55	21.2	0.1
122.43	131.5	0.9	121.53	49.5	0.2	125.53	23.4	0.1

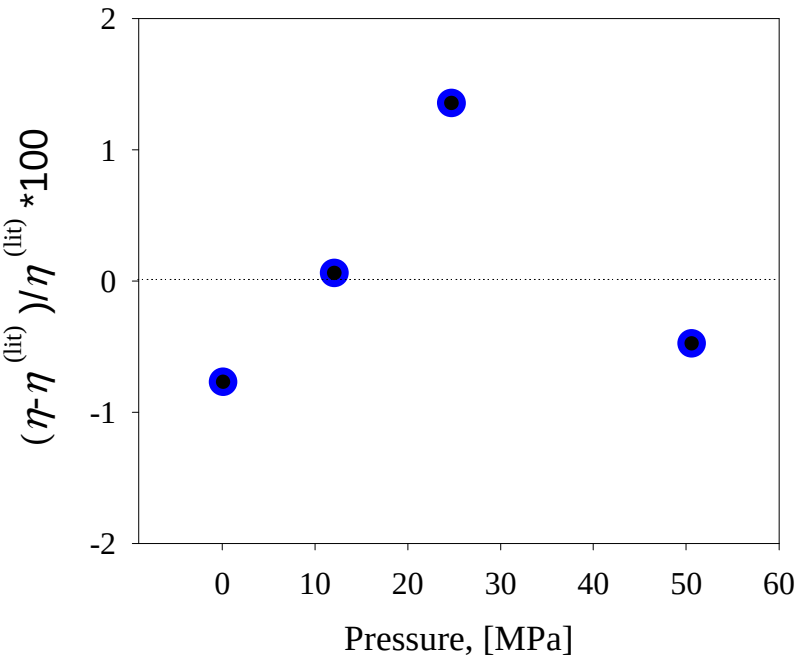

Figure 4-7 Deviation of interpolated viscosities of [BMIm][PF_6] at 298.15 K using the Tait-Litovitz equation compared with the literature data. [37]

Figure **4-8** and Figure **4-9** demonstrate the effect of high pressures at three different temperatures for the viscosity of [HMIm][Tf_2N] and [HMIm][PF_6]. These graphs illustrate that the viscosity at lower temperatures is more sensitive to pressures than at higher temperatures. For instance, for [HMIm][Tf_2N] the viscosity change from ambient pressure to 124 MPa, is approximately 288.5% at 298.15 K and 172.5% at 343.15 K. Thus, the viscosity is more linearly related to pressure at the high temperatures.

Figure **4-9** also demonstrates the good agreement of the data obtained from this viscosity of [HMIm][PF_6] measured by Harris *et al.*. [38]

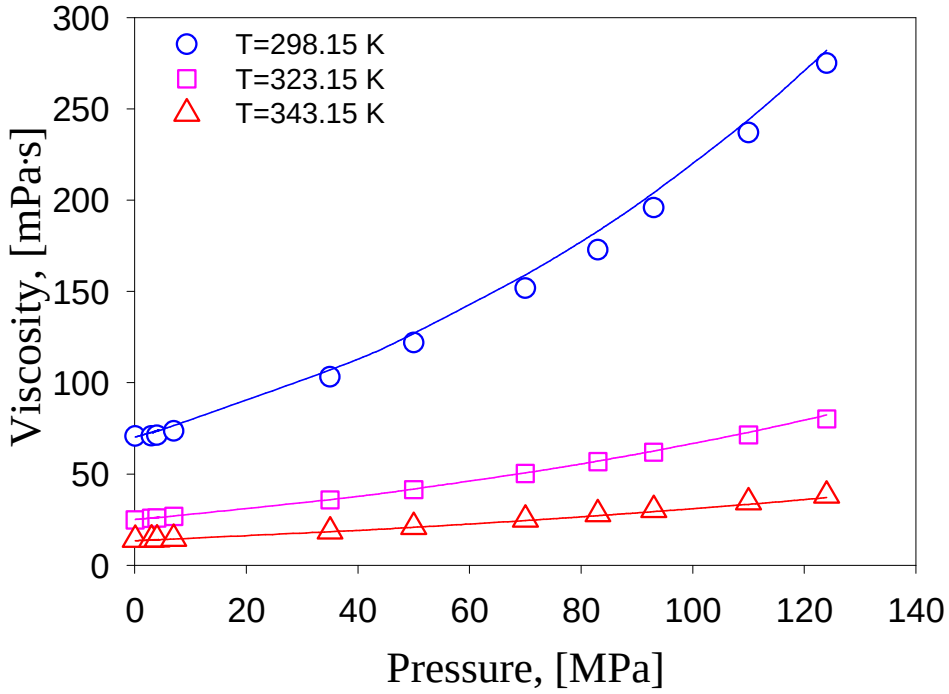

Figure 4-8 Viscosity of [HMIm][Tf_2N] at high pressures and different temperatures. All lines, herein, are correlations and predictions from the Tait-Litovitz correlation with parameters from Table 4-1

Table 4-5 Measured viscosity (η) of [HMIm][Tf_2N] as a function of pressure and temperature.

298.15 K			**323.15 K**			**343.15 K**		
P (MPa)	η (mPa·s)	± SD	***P*** (MPa)	η (mPa·s)	± SD	***P*** (MPa)	η (mPa·s)	± SD
0.10	70.96	0.28	0.10	24.9	0.1	0.10	14.07	0.17
2.99	71.04	0.28	2.99	25.81	0.13	2.99	14.12	0.17
4.00	71.38	0.21	4.00	25.98	0.13	4.00	14.22	0.16
7.00	73.71	0.52	7.00	26.87	0.05	7.00	14.6	0.15
35.00	103.4	0.21	35.00	35.96	0.07	35.00	18.62	0.15
50.00	122.2	0.24	50.00	41.57	0.29	50.00	21.1	0.11
70.00	152.2	0.61	70.00	50.43	0.3	70.00	25.17	0.23
83.00	173.2	1.21	83.00	56.96	0.34	83.00	28.12	0.17
93.00	196.3	0.98	93.00	62.11	0.03	93.00	30.42	0.15
110.00	237.6	2.14	110.00	71.6	0.29	110.00	34.65	0.17
124.00	275.7	1.38	124.00	80.46	0.16	124.00	38.34	0.23

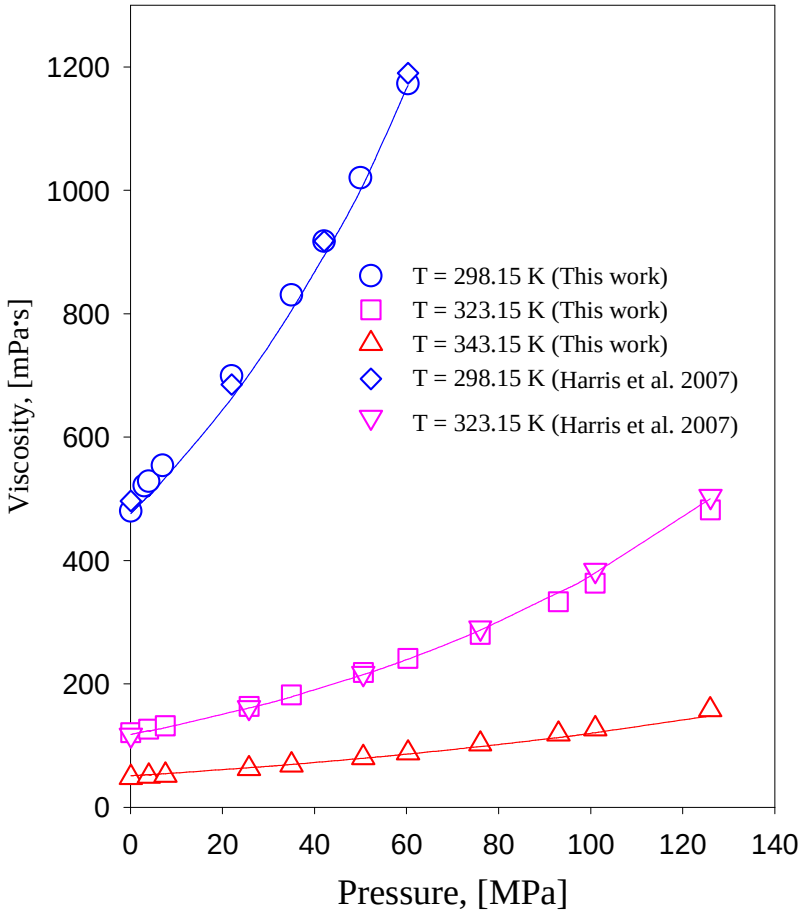

Figure 4-9 Viscosity of [HMIm][PF_6] at high pressures and different temperatures compared with Harris *et al.* [38] with correlations.

A series of experiments were performed to determine the effect of the anion on the high-pressure viscosity using a common cation, 1-hexyl-3-methyl-imidazolium [HMIm]. Three different anions were investigated: [Tf_2N] (Table 4-5), [BF_4] (Table 4-6), and [PF_6] (Table 4-7). Figure 4-10 illustrates the viscosity of the [HMIm] with the three different anions at 25°C. The viscosity of [HMIm][PF_6] is considerably higher than that of [HMIm][BF_4] and [HMIm][Tf_2N]. In addition, the rate of increase in viscosity with pressure is much greater than the other two ionic liquids.

Table 4-6 Measured viscosity (η) of [HMIm][BF_4] as a function of pressure and temperature.

298.15 K			**323.15 K**			**343.15 K**		
P (MPa)	η (mPa·s)	± SD	***P*** (MPa)	η (mPa·s)	± SD	***P*** (MPa)	η (mPa·s)	± SD
0.10	202	1	0.10	58.5	0.3	0.10	27.0	0.1
2.64	209	3	2.60	59.7	0.1	3.10	27.6	0.1
4.29	213	2	4.13	61.0	0.1	4.10	27.5	0.1
6.95	215	2	6.85	62.0	0.1	7.10	28.0	0.1
34.59	299	2	34.52	79.9	0.2	35.10	35.2	0.3
48.40	387	3	48.18	91.1	0.7	48.34	39.2	0.3
68.14	478	3	68.99	108.2	0.4	68.14	45.0	0.3
82.97	532	3	82.71	121.8	1.1	83.08	49.9	0.2
96.82	621	11	96.55	136.0	0.8	96.55	55.1	0.1
108.55	743	10	110.12	152.4	0.6	110.12	60.8	0.4
117.85	819	12	121.81	165.0	1.3	121.81	65.0	0.4

Table 4-7 Measured viscosity (η) of [HMIm][PF_6] as a function of pressure and temperature.

298.15 K			**323.15 K**			**343.15 K**		
P (MPa)	η (mPa·s)	± SD	***P*** (MPa)	η (mPa·s)	± SD	***P*** (MPa)	η (mPa·s)	± SD
0.10	481	2	0.10	121.4	0.4	0.10	48.1	0.3
2.99	523	5	4.00	127.1	0.5	4.00	50.3	0.3
4.00	530	3	7.60	132.4	0.7	7.60	52.0	0.3
7.00	556	4	25.80	164.0	0.7	25.80	62.6	0.2
22.00	701	6	35.00	182.6	0.4	35.00	68.6	0.3
35.00	833	7	50.60	218.9	1.5	50.60	80.5	0.2
42.10	920	8	60.30	241.7	0.7	60.30	88.1	0.4
50.00	1023	8	76.00	280.8	1.1	76.00	102.5	0.4
60.30	1176	5	93.00	334.2	0.3	93.00	118.7	0.6
			101.00	364.2	1.8	101.00	127.1	0.3
			126.00	483.1	1.9	126.00	157.8	0.6

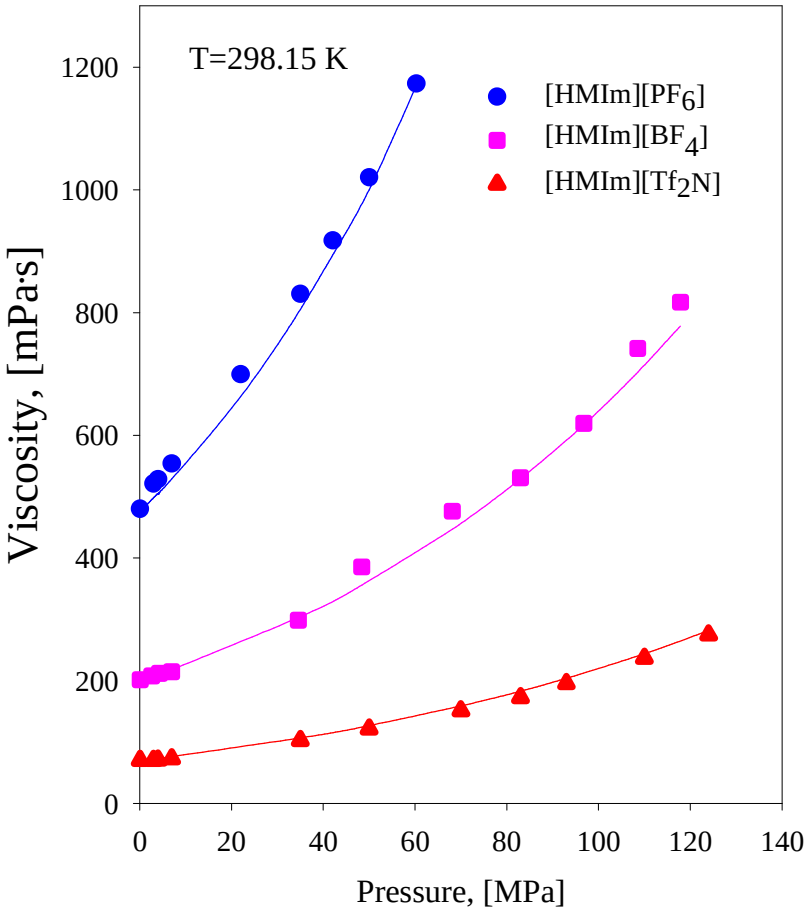

Figure 4-10 Viscosity of [HMIm] cations with different anions as a function of pressure at 298.15 K with correlations.

While there is not a complete set of physical properties data of these [HMIm] compounds, Table 4-8 lists some physical and thermal properties of a similar cation, BMIm, with [Tf_2N], [BF_4], and [PF_6]. The order of increasing viscosity for these three compounds at ambient conditions seems to scale with the melting point (T_m) or, more appropriately, the glass transition temperature (T_g). While this may correlate with the

difference in absolute viscosity, it does not predict the larger relative rate of increase with pressure of the [PF_6] anion. "Hole theory", applied to ILs by Abbott [25-27] , indicates that the viscosity of an ionic liquid is inversely related to the size of the molecule. However, with a similar cation, the anionic radius (R_-) increases from [BF_4] < [PF_6] < [Tf_2N] while the experimental viscosity increases in a mixed order of [Tf_2N] < [BF_4] < [PF_6]; see Table 4-8.

Table 4-8 Properties of [BMIm] ionic liquids.

Ionic Liquid	MW [33]	T_m [33]	T_g [33]	T_d [33]	R_- [25]	$\underline{V}$ [33]	η (298 K)
	(g/mol)	(K)			(Å)	(cm^3/mol)	(mPa·s)
[BMIm][Tf_2N]	419.4	270.15	186.15	696.15	3.62	292.4	50.9[38]
[BMIm][BF_4]	226	N/A	190.15	698.15	2.5	188.7	103.8[78]
[BMIm][PF_6]	284.2	283.15	196.15	706.15	2.78	208.3	273[37]

Thus, simple geometric factors such as the radius or hydrodynamic radius do not explain the viscosity behavior of all ionic liquids. Watanabe and coworkers [33] hypothesized that some of the differences observed in the transport properties of [BMIm] cation and these same anions may be due to different levels of "ionicity" (association/disassociation) that they elucidated from diffusion and ionic conductivity data. [BMIm][PF_6] is believed to have the highest level of dissociation, which may decrease the free volume. In addition, [BMIm][PF_6] is believed to form a greater number of higher order aggregates ([$BMIm]_2[PF_6$], [BMIm][$PF_6]_2$, [$BMIm]_2[PF_6]_3$, etc.) as determined by mass spectrometry. [33] These aggregates would have larger hydrodynamic radii and extended long-range molecular interactions increasing the barrier to motion. Rebelo and coworkers [57, 58] have determined the high pressure density and isothermal compressibility of these [BMIm] compounds and have found that the isothermal compressibility, κ_T, is relatively small (<0.53 GPa^{-1}) and decreases significantly with pressure. Thus, the density to 100 MPa will increase by less than ~5%. The [Tf_2N] compound has the highest κ_T, which may indicate a higher free volume and may explain the lowest viscosity despite the larger anion diameter. While the [PF_6] compound has a

lower κ_T , the slight increase in density with pressure may induce further aggregation/larger aggregates and viscosity augmentation similar to the results of Watanabe and coworkers. [33]

Figure 4-11, Table 4-5, Table 4-15**,** demonstrate the effect of the n-alkyl chain length on the viscosity of methyl-imidazolium cations for a fixed anionic species, [Tf_2N], at high pressures and different temperatures. As the graph illustrates, smaller alkyl chain lengths of the imidazolium cation, such as R=ethyl-, exhibit lower viscosity than the hexyl- or decyl- substituted methylimidazolium cation. In addition, the [DMIm] cation also exhibits a higher rate of change with pressure in the higher pressure regions of the data (>60 MPa).

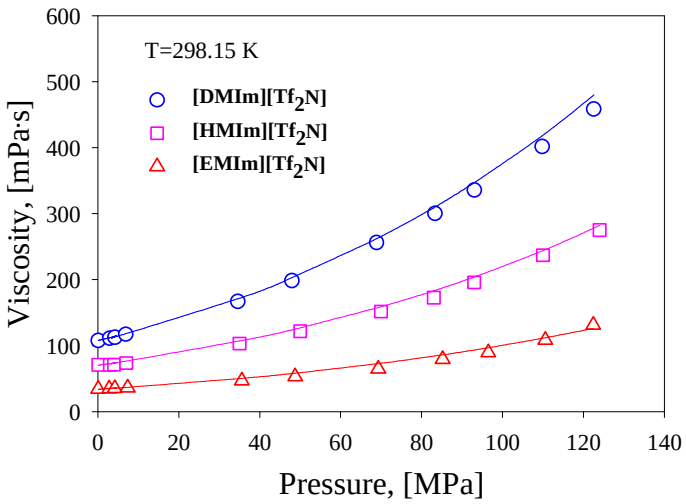

Figure 4-11 Pressure dependence of viscosity of [n-alkyl-MIm][Tf_2N] ionic liquids at 298.15 K with correlations.

The viscosity of the RTILs as function of temperature and pressure is correlated with the Litovitz and Tait equations as discussed above. Table 4-9 lists the regressed Litovitz and Tait equation parameters for each IL at each of the three different temperatures. The Tait parameters were then correlated to a linear equation and are listed in Table 4-1. The absolute average relative deviation (AARD%) of the correlated data indicate a good fit between the experimental data and those predicted by the equation. The AARD% of these ionic liquids is in the following order: [HMIm][Tf_2N]=2.2%, [DMIm][Tf_2N]=2.4%,

[HMIm][PF_6]=3.1%, [EMIm][Tf_2N]=3.9%, [HMIm][BF_4]=4%. Figure 4-12 shows graphically the deviations between the experimental and correlated viscosities using the Litovitz-Tait equation as a function of pressure and temperature for [HMIm][Tf_2N] and [HMIm][PF_6], which vary between a maximum of ±8%. While the deviations for several isotherms at increasing pressure appear systematic (e.g. at 70°C for [HMIm][PF_6] a nearly linearly decreasing trend), the majority of the errors for these and other ionic liquids are believed to have more random dependencies or bias (e.g. at 25°C for [HMIm][Tf_2N]).

Table 4-9 Tait-Litovitz Equation Parameters**.**

[EMIm][Tf_2N]			
T (K)	η_0 (mPa·s)	D (MPa)	E
298.15	33.89	871.9	10.0
323.15	15.33	697.9	6.8
343.15	9.50	558.7	4.3
[HMIm][Tf_2N]			
T (K)	η_0 (mPa·s)	D (MPa)	E
298.15	70.26	553.9	6.9
323.15	25.13	526.1	5.6
343.15	13.51	503.9	4.6
[DMIm][Tf_2N]			
T (K)	η_0 (mPa·s)	D (MPa)	E
298.15	107.52	388.0	5.5
323.15	35.86	385.2	4.7
343.15	18.49	382.9	4.1
[HMIm][BF_4]			
T (K)	η_0 (mPa·s)	D (MPa)	E
298.15	200.73	1010.4	12.3
323.15	57.78	678.7	7.1
343.15	27.26	413.3	3.0
[HMIm][PF_6]			
T (K)	η_0 (mPa·s)	D (MPa)	E
298.15	476.31	1207.3	18.4
323.15	118.22	1080.6	13.1
343.15	51.00	979.3	8.8

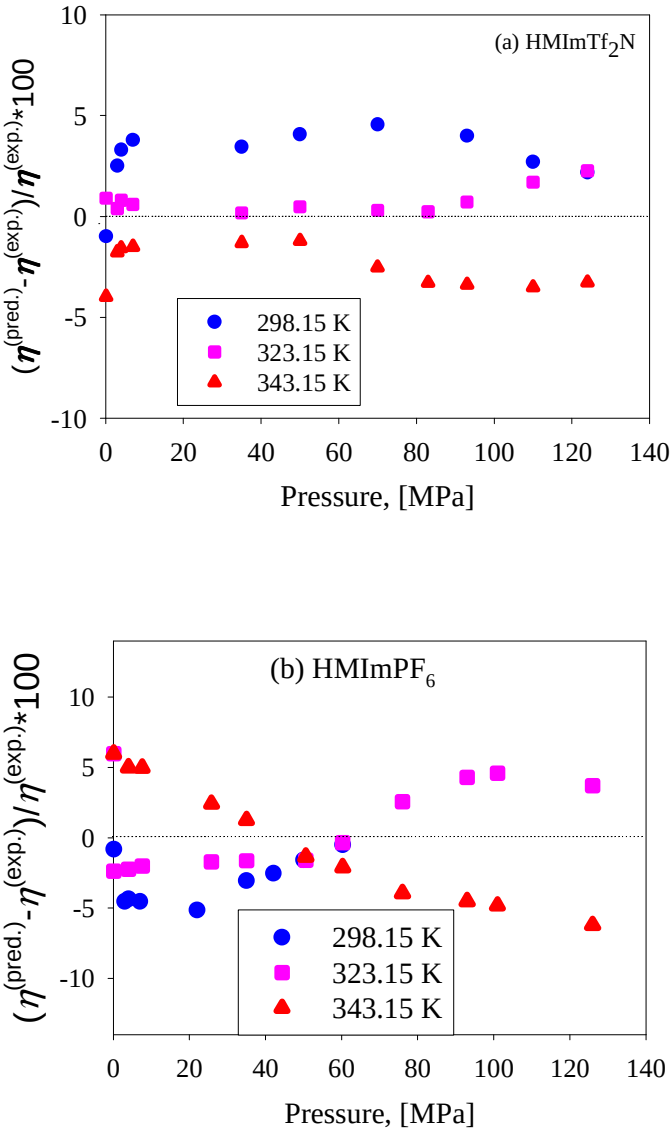

Figure 4-12 Deviations of measured viscosities from Tait-Litovitz equation as a function of pressure and temperature for (a) [HMIm][Tf_2N] and (b) [HMIm][PF_6].

4.1.5 Summary

The viscosity of a series of pure imidazolium based RTILs was measured to determine the effect of high pressures (up to 130 MPa) from 25°C to 70°C with changes

in the cation and anion. The data obtained have an uncertainty of less than 1% with this high-pressure viscometer and have been shown to have excellent agreement with the small number of literature reports of high-pressure viscosity of ILs. The data have been correlated with a hybrid Litovitz-Tait equation with average absolute relative deviation percentages (AARD%) from 2.2% for [HMIm][Tf_2N] to 4% for [HMIm][BF_4]. Data regression was performed with both SigmaPlot 2000-SPSS Inc. and CurveExpert (cvxpt32), which uses the Marquardt-Levenberg algorithm to determine Litovitz and Tait parameters using a sum-of-squares objective function.

4.2 Viscosity of Imidazolium Ionic Liquids with Compressed CO_2

The viscosity of imidazolium-based ionic liquids (ILs) saturated with gaseous, liquid and supercritical carbon dioxide (CO_2) was measured by a high-pressure viscometer at three different temperatures (25°C, 50°C, and 70°C). The high-pressure viscosity of 1-ethyl-3-methylimidazolium ([EMIm]), 1-*n*-hexyl-3-methylimidazolium ([HMIm]), and 1-*n*-decyl-3-methylimidazolium ([DMIm]) cations with a common anion, bis(trifluoromethylsulfonyl)amide ([Tf_2N]), saturated with CO_2 was measured up to maximum 287 bar. As CO_2 pressure is increased the viscosity of the IL mixture dramatically decreases. While, the ambient pressure viscosity of 1-alkyl-3-methyl-imidazolium [Tf_2N] ILs increases significantly with increasing chain length, the viscosity of all of the CO_2–saturated ILs becomes very similar at high CO_2 pressures.

From previous vapor-liquid equilibrium data, the viscosity with concentration was determined and found to be the primary factor to describe the fractional viscosity reduction. Several predictive and correlative methods were investigated for the mixture viscosity, given pure component properties, and included arithmetic mixing rules, the Irving (Predictive Arrhenius) model, Grunberg equation, etc. The modified Grunberg model with one adjustable parameter provided an adequate fit of the data.

4.2.1 Introduction

Coupling ionic liquids with compressed CO_2 systems has a number of applications for extractions [59], reactions [60-63], etc. We have recently quantified the beneficial effects of CO_2 on homogeneously catalyzed reactions in ILs [64, 65] (Chapter 3). The unique phase

behavior of IL with CO_2 makes it advantageous for biphasic systems. CO_2 is very soluble in the ionic liquid and in contrast, the ionic liquid is immeasurably insoluble in the pure CO_2 phase and does not become miscible (critical) even at elevated pressures. This is different from the behavior of CO_2 with most organic solvents, which become miscible (critical; one phase) at moderate pressures. Understanding and design of biphasic reactions and extractions in IL/CO_2 systems requires essential mass transport properties such as viscosities, of which little exist in literature. In addition, the mixture viscosity is needed for both heat and mass transfer.

As it is explained in the last section the viscosity of a series of pure imidazolium ionic liquids was measured at moderate pressures with different alkyl chain lengths of the cation and the effect of the anions. [66] While the choice of cation and anion affects the ambient condition viscosity, it also affects the behavior of the viscosity with pressure. Liu *et al.* [67] measured the viscosity of mixtures of 1-butyl-3-methylimidazolium hexafluorophosphate [BMIm][PF_6], methanol, and CO_2 using the falling ball viscometer. These studies demonstrated that the viscosity of the liquid mixtures decreases dramatically with increasing pressure. Laurenczy *et al.* [68] measured the viscosity of 1-butyl-3-methylimidazolium bis(trifluoromethylsulfonyl)amide [BMIm][Tf_2N] and [BMIm][PF_6] under subcritical CO_2 pressure with a falling-ball method. They also measured the solubility of CO_2 in these ionic liquids using a ^{13}C NMR method to correlate the viscosity with concentration. Tomida *et al.* [69, 70] measured the viscosity of CO_2 mixtures with 1-butyl-3-methyl-imidazolium tetrafluoroborate [BMIm][BF_4] and [BMIm][PF_6] by a rolling ball viscometer.

In this study, the viscosity of three n-alkyl-3-methyl-imidazolium bis(trifluoromethylsulfonyl)amide ionic liquids with compressed CO_2 was measured at temperatures of 25°C, 50°C, and 70°C and pressures to 287 bar by a newly constructed high-pressure viscometer system. The ILs are illustrated in Figure 4-13. The effect of the alkyl group of the cation on the viscosity of the IL/CO_2 mixture was investigated by varying from ethyl-, n-hexyl, to n-decyl-.

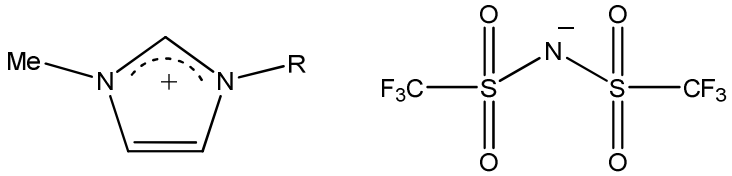

[R-MIm] [Tf_2N]

Figure 4-13 Structures of the n-alkyl-3-methyl-imidazolium bis(trifluoromethylsulfonyl)amides investigated here: [R-MIm], R=ethyl- ([EMIm]), n-hexyl- ([HMIm]), and n-decyl- ([DMIm])

4.2.2 Viscosity Correlation and Analysis

Various theoretical models and empirical expressions can be found in literature in order to represent the viscosity of liquid mixtures as a function of their pure component viscosity at the same temperature and pressure. Often, the ambient pressure viscosity of the liquid component is used without being adjusted for pressure. These models may be true predictions or have adjustable parameters to better fit the data. Different empirical correlations were investigated, and the most accurate 4 are used here. These equations, as listed below, are: the arithmetic mixing rule (Eqn. 4.11), Irving (Eqn 4.12.), Grunberg equation (Eqn. 4.13), and modified Grunberg equation (Eqn. 4.14).

$$\eta_{mix} = \eta_1 x_1 + \eta_2 x_2 \quad (4.11)$$

$$\ln(\eta_{mix}) = \omega_1 \ln(\eta_1) + \omega_2 \ln(\eta_2) \quad (4.12)$$

$$\eta_{mix} = \eta_1^{\omega_1} \eta_2^{\omega_2} \exp(\eta_1 \eta_2 \omega_1 \omega_2) \quad (4.13)$$

$$\eta_{mix} = \eta_1^{\omega_1} \eta_2^{\omega_2} \exp(G \omega_1 \omega_2) \quad (4.14)$$

The following equations are also tried:

$$\eta_{mix} = x_1 \eta_1 + x_2 \eta_2 + x_1 x_2 G \quad (4.15)$$

$$\eta_{mix} = \eta_1 x_1 + \eta_2 x_2 + (\eta_1 + \eta_2)/2 * (x_1 x_2)^{0.5} \quad (4.16)$$

$$\eta_{mix} = \eta_1 x_1 + \eta_2 x_2 + (\eta_1 \eta_2 x_1 x_2)^{0.5} \quad (4.17)$$

$$\eta_{mix} = \eta_1 x_1^2 + \eta_2 x_2^2 + k_{12} x_1 x_2 ((\eta_1 + \eta_2)/2 \quad (4.18)$$

K_{12}=3.6272

$$\eta_{mix} = \eta_1 x_1^2 + \eta_2 x_2^2 + k_{12} x_1 x_2 ((\eta_1 \eta_2)^{0.5} \quad (4.19)$$

k_{12}=34.7086

where η_{mix} is the viscosity of mixture as a function of temperature, pressure, and composition; η_i is the viscosity of the pure compound, *i*, as a function of temperature and pressure; x_i and ω_i are mole fraction and mass fraction concentrations respectively; and *G* is the Grunberg equation adjustable parameter. For the modified Grunberg equation (Eqn. 4.14), the adjustable parameter was fit using SigmaPlot 2000-SPSS Inc. The viscosity of the pure ionic liquids at the temperature and pressure of interest were interpolated from the data of Ahosseini and Scurto [66] (Chapter 4.1). The pure component CO_2 properties were determined by the ultra-accurate REFPROP v.8 database. [71]

4.2.3 Results and Discussion

The high-pressure viscosity of three ionic liquids, 1-ethyl-3-methylimidazolium ([EMIm]), 1-n-hexyl-3-methylimidazolium ([HMIm]), and 1-n-decyl-3-methylimidazolium ([DMIm]) cations with bis(trifluoromethylsulfonyl)amide ([Tf_2N]) anion (Figure 4-13) was measured with various pressure of CO_2 to a maximum of 287 bar at 25°C, 50°C, and 70°C. Table 4-10 lists the viscosity (η) of the ILs with pressure and composition of CO_2. The effect of pressure and temperature on the viscosity of CO_2-saturated [HMIm][Tf_2N] is shown in Figure 4-14.

The viscosity of the CO_2-free IL is plotted at 1 bar at each isotherm and changes considerably with temperature. The graph demonstrates that the viscosity decreases dramatically with CO_2 pressure to approximately 60 bar. At 25°C at 60 bar, the mixture viscosity is approximately 86% lower than the pure IL viscosity. After approximately 60 bar along each isotherm, the viscosity decrease becomes more moderate with increases in CO_2 pressure. As temperature increases, the decrease in viscosity becomes more moderate and more linear with increasing pressure. While the difference in the initial viscosity of the pure [HMIm][Tf_2N] at the three temperatures is large, the viscosity of the CO_2-saturated mixtures becomes less than 5 mPa·s at approximately 100 bar and beyond for all temperatures investigated.

Table 4-10 Viscosity (η) of [EMIm][Tf_2N], [HMIm][Tf_2N], and [DMIm][Tf_2N] with pressure and composition[a] of CO_2.

[EMIm][Tf_2N]											
25°C				50°C				70°C			
P [bar]	x_{CO2}	*η* [mPa·s]	± [b]	*P* [bar]	x_{CO2}	*η* [mPa·s]	±	*P* [bar]	x_{CO2}	*η* [mPa·s]	±
1	-	33.77	0.17	1	-	14.33	0.07	1	-	9.397	0.05
10.1	0.217	21.9	0.11	19.6	0.285	10.12	0.09	19.3	0.23	8.15	0.04
20.7	0.404	14.18	0.07	41.2	0.478	6.43	0.03	40.3	0.405	5.8	0.03
38.4	0.604	7.69	0.04	85.8	0.665	3.83	0.03	83.2	0.613	4	0.02
57.8	0.693	4.66	0.02	102.9	0.713	3.35	0.02	103.8	0.698	3.31	0.02
52.8	0.713	4.81	0.02	106.2	0.722	3.28	0.02	111.9	0.734	3.02	0.02
63.2	0.73	3.96	0.02	122.4	0.763	3.32	0.02	123.9	0.791	2.87	0.01
67.1	0.738	3.81	0.02	126.6	0.773	3.16	0.02	131.6	0.831	2.85	0.01
93.5	0.761	3.73	0.02	286	NA	2.72	0.01	282.4	NA	2.47	0.01
258.8	NA	3.71	0.02								
287.1	NA	3.52	0.02								
[HMIm][Tf_2N]											
1	-	71	0.36	1	0	24.9	0.12	1	-	14.1	0.07
7.8	0.159	51.15	0.26	10.5	0.169	21.27	0.11	10.5	0.066	12.45	0.06
11.4	0.237	42.79	0.21	29.7	0.482	14.98	0.07	31.6	0.268	10.27	0.05
17	0.343	26.95	0.13	48.9	0.553	10.6	0.05	48.7	0.398	9.83	0.05
23.4	0.445	20.42	0.1	74.4	0.67	6.09	0.03	69.5	0.521	7.69	0.04
43.7	0.661	15.97	0.08	94.3	0.736	4.19	0.02	98.3	0.644	5.03	0.03
69.8	0.783	5.88	0.03	97.4	0.745	3.85	0.02	112.4	0.69	3.79	0.02
96.7	0.84	4.77	0.02	112.8	0.775	3.39	0.02	125.2	0.725	3.58	0.02
110	0.867	4.5	0.02	123.6	0.775	3.24	0.02				
120.9	0.894	4.37	0.02								
[DMIm][Tf_2N]											
1	-	106.5	0.53	1	-	36.3	0.18	1	-	19.6	0.1
20.1	0.312	54.63	0.27	40.9	0.554	11.91	0.06	19.8	0.301	13.98	0.08
37.7	0.59	19.54	0.1	80.3	0.752	5.5	0.03	40.1	0.476	9.52	0.05
72.9	0.811	6.08	0.03	106.2	0.8	4.43	0.04	65.2	0.606	6.47	0.03
106	0.827	5.33	0.03	111.8	0.8	4.18	0.03	76.6	0.647	5.65	0.03
119.4	0.831	5.18	0.03	130.6	0.814	3.94	0.02	106.4	0.74	4.36	0.02
136.5	0.833	5.07	0.03	268.8	NA	3.87	0.03	117.4	0.762	3.93	0.02
247.2	NA	5.13	0.03					120.6	0.767	3.83	0.02
								125.5	0.776	3.7	0.02
								130.4	0.782	3.61	0.02
								248.1	NA	2.63	0.01

[a] compositions were interpolated from the vapor-liquid equilibrium data of Ren and Scurto[72] , except for some high pressure data points whose extrapolation is not confirmed (NA). [b] the standard deviation of 20 measurements.

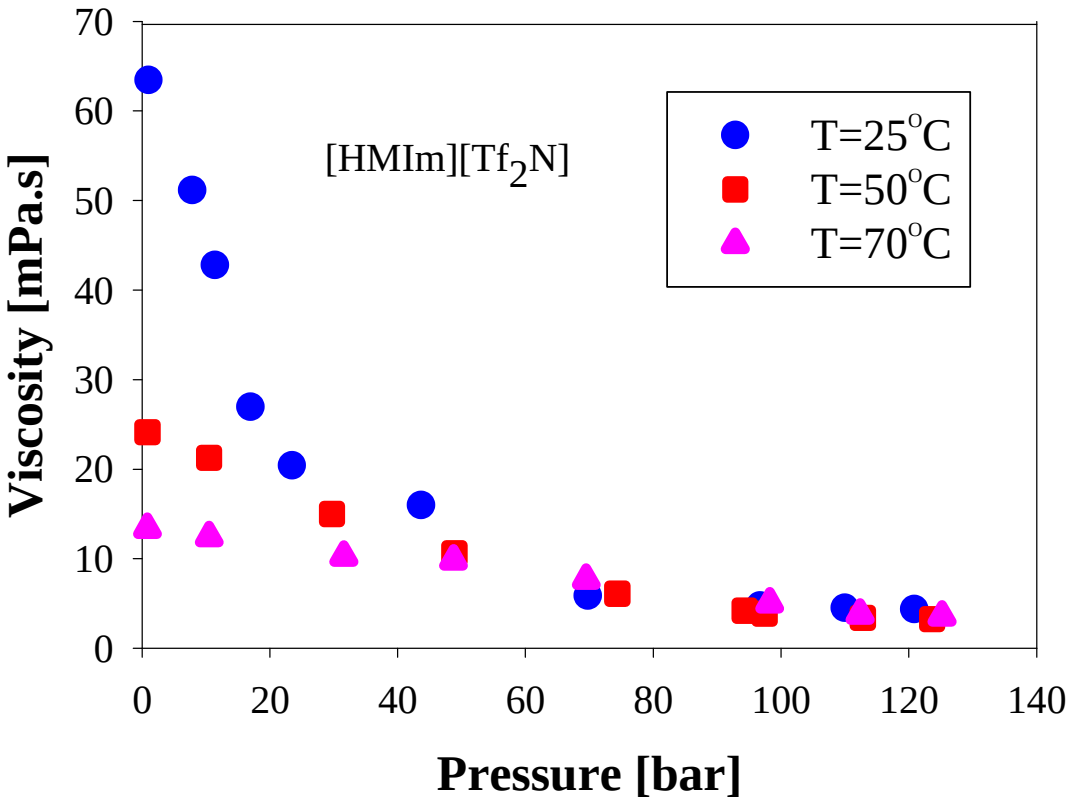

Figure 4-14 Viscosity of [HMim][Tf_2N] with CO_2 pressure at 25°C, 50°C, and 70°C .

In a recent study, Ren and Scurto have measured the high-pressure vapor-liquid phase equilibrium (VLE) of the CO_2 with these ionic liquids.[72] CO_2 is very soluble in these imidazolium [Tf_2N] ionic liquids. Figure 4-15 graphs simultaneously the viscosity and the solubility with CO_2 pressure at 25°C and illustrates a nearly inverse qualitative behavior as pressure is increased. It should be noted that the isotherm at 25°C is below the critical temperature of pure CO_2 and, thus, the vapor-liquid equilibrium becomes liquid-liquid equilibrium (LLE) at the vapor pressure of 64.3 bar and beyond. From the equilibrium data, the slope of the pressure versus mole fraction solubility curve slightly changes at this VLE-to-LLE transition. The viscosity data in Figure 4-14 seems to reflect this change in slope as well. The other isotherms are at supercritical temperatures for CO_2 and are continuous vapor-liquid equilibrium to high pressures. With the correlation between system CO_2 pressure, the viscosity of the three isotherms is presented in Figure 4-16 with respect to mole fraction solubility at saturation.

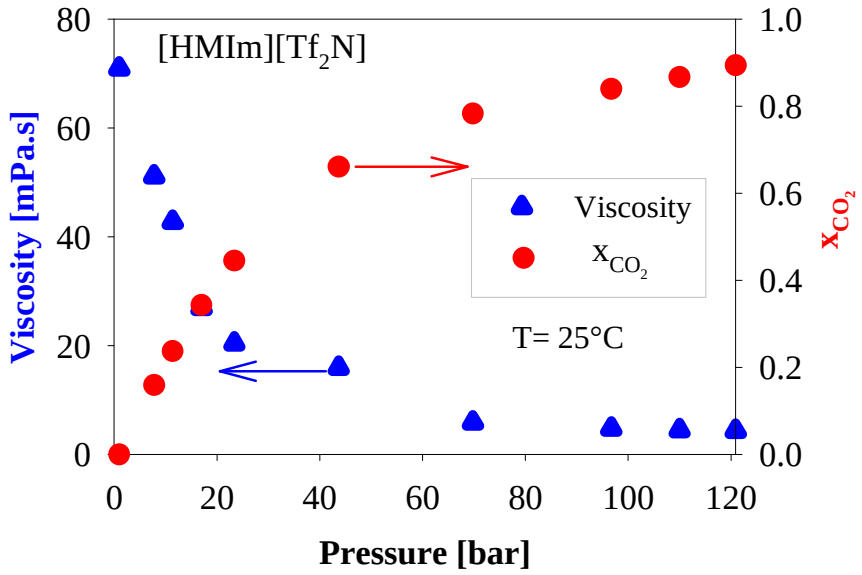

Figure 4-15 Viscosity of [HMIm][Tf_2N] and Solubility versus CO_2 pressure at 25°C. Solubility data from Ren and Scurto. [77]

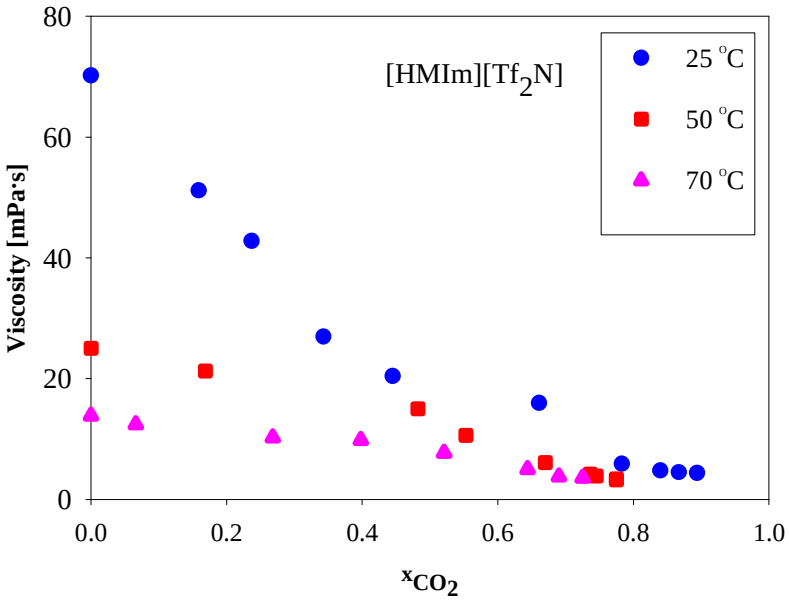

Figure 4-16 Viscosity of [HMIm][Tf_2N] with the mole fraction concentration of CO_2 at the saturation conditions.

To find out the effect of the alkyl-group on the imidazolium ring affects the CO_2-saturated viscosity, measurements were taken of a short chain alkyl group, ethyl- ([EMIm][Tf_2N]) and that of a long-chain, n-decyl- ([DMIm][Tf_2N]) at 25°C, 50°C, and 70°C to 287 bar. Figure 4-17 and Figure 4-18 show the effect of pressure of CO_2 and temperature on the viscosity of [EMIm][Tf_2N] and [DMIm][Tf_2N]. The qualitative behavior of each are quite similar to [HMIm][Tf_2N].

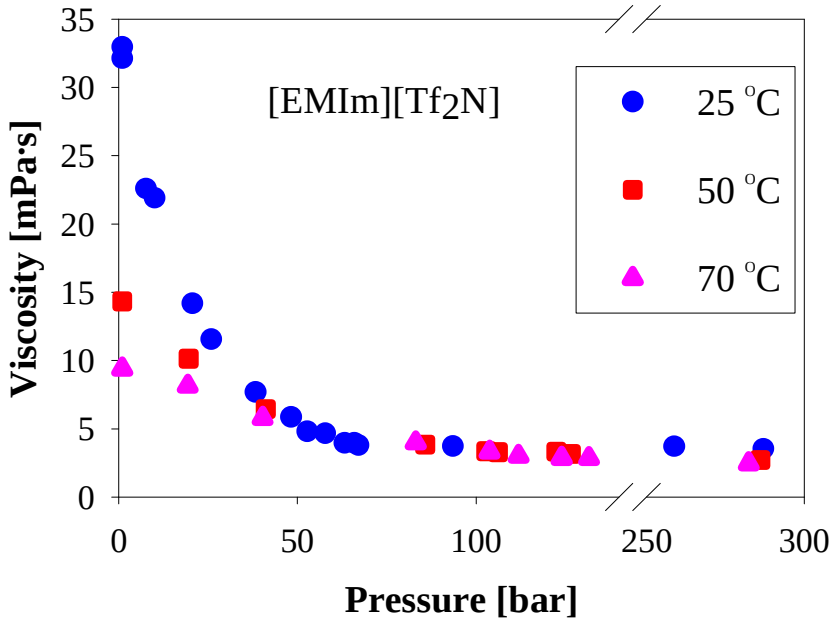

Figure 4-17 Viscosity of [EMIm][Tf_2N] with CO_2 pressure at 25°C, 50°C, and 70°C.

In Figure 4-19, the viscosity of all three types of ionic liquids is compared at the same temperature (25°C) and different CO_2 pressures. While the ambient pressure viscosity of pure [DMIm][Tf_2N] at 25°C is 106.5 mPa·s and of pure [EMIm][Tf_2N] is 33.8 mPa·s, their viscosity under similar CO_2 pressures becomes remarkably similar (5.33 mPa·s at 106 bar and 3.73 mPa·s at 93.5 bar, respectively). Interestingly, when the viscosities are normalized to their ambient pressure viscosity (η_0), the viscosities of the three ionic liquids at 25°C with CO_2 composition nearly collapse to the same line as shown in Figure 4-20.

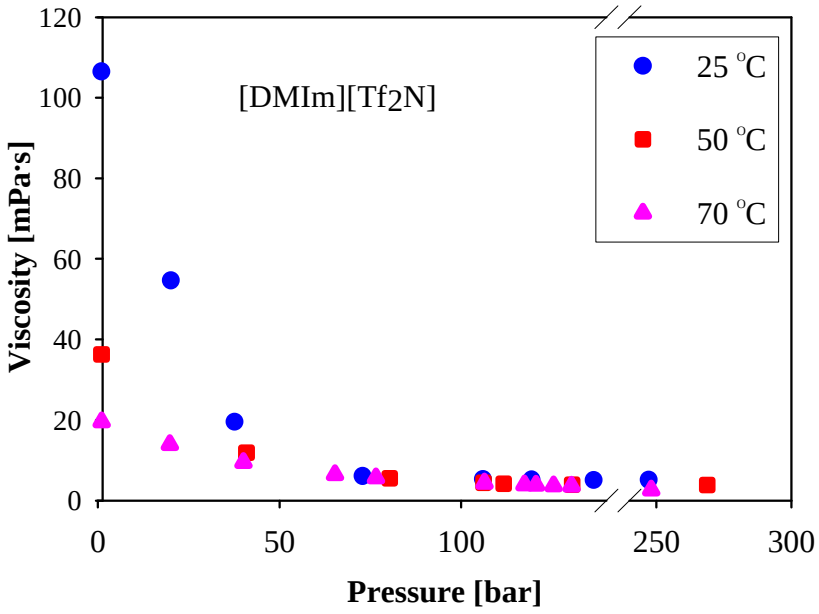

Figure 4-18 Viscosity of [DMIm][Tf_2N] with CO_2 pressure at 25°C, 50°C, and 70°C.

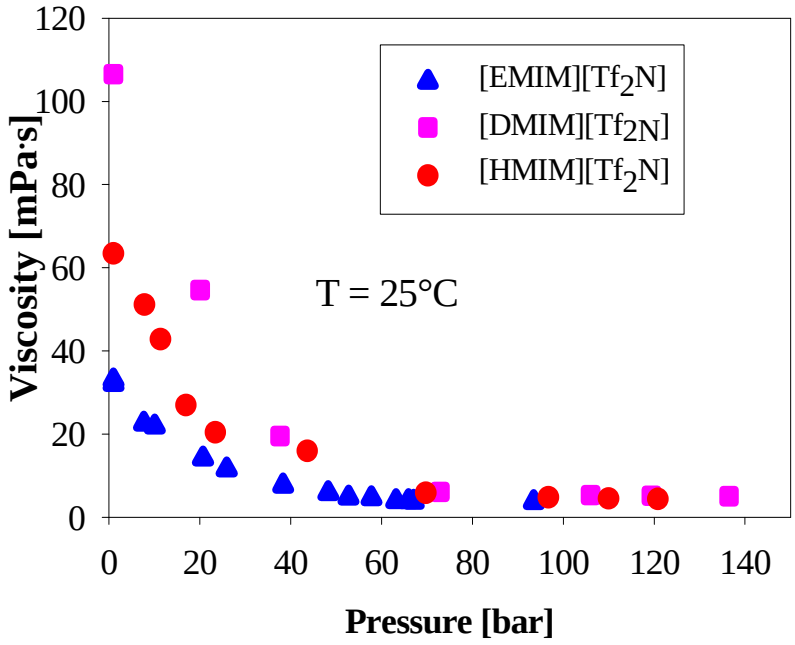

Figure 4-19 Viscosity of [EMIm][Tf_2N], [HMIm][Tf_2N], and [DMIm][Tf_2N] with CO_2 pressure at 25°C.

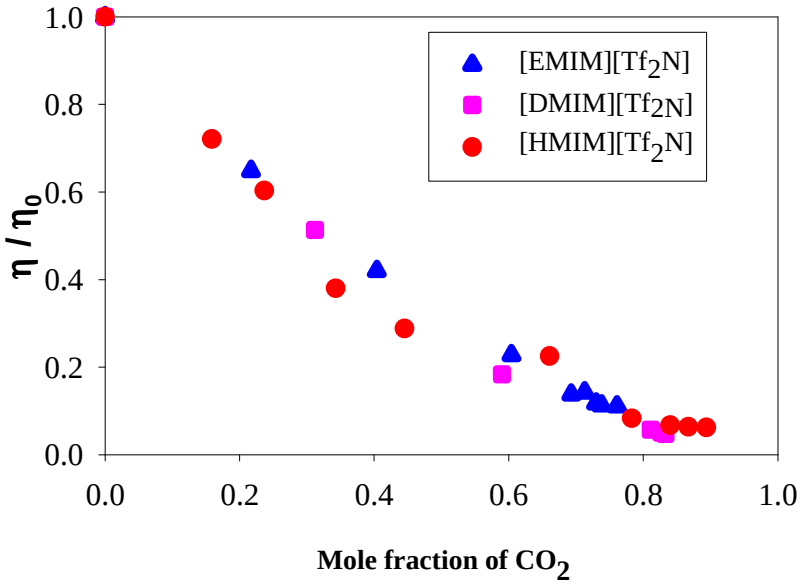

Figure 4-20 Viscosity of [EMIm][Tf_2N], [HMIm][Tf_2N], and [DMIm][Tf_2N] with CO_2 mole fraction at 25°C normalized to their ambient pressure viscosity.

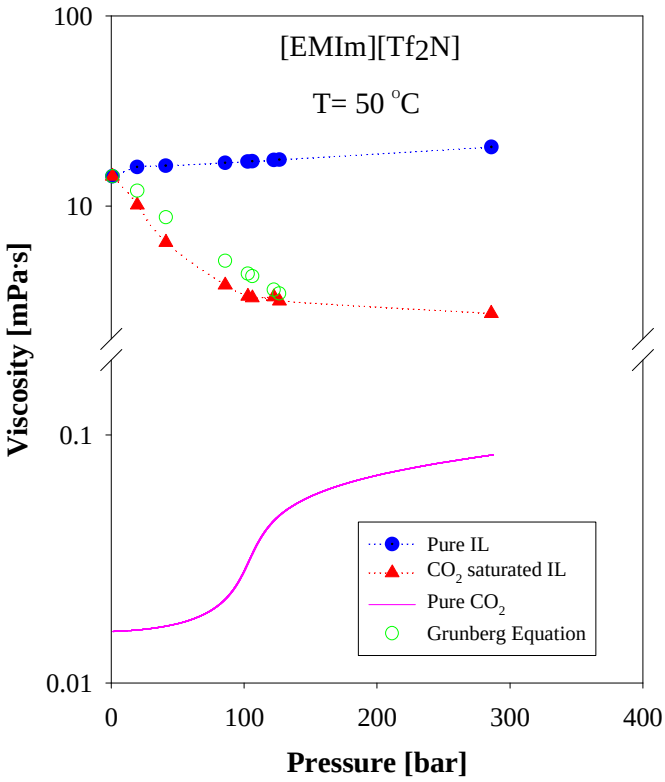

Figure 4-21 Viscosity Vs. pressure with pure IL and CO_2 at 50° C

While small differences are observed for the different alkyl-chain lengths especially in the intermediate concentration range, the mole fraction of CO_2 present in the IL is the dominant parameter for the viscosity reduction. Figure 4-21 illustrates the effect of pressure on viscosity of pure CO_2 and [HMIm][Tf_2N]. This figure also shows the effect of CO_2 pressure on viscosity of [HMIm][Tf_2N] compare to the correlation result using Grunberg equation. As it can be seen the viscosity of pure CO_2 and IL increases with the static pressure, while the pressure of CO_2 reduces the viscosity of the IL. The correlation results show a positive deviation from the experimental data.

As discussed above, biphasic IL/CO_2 systems have a number of advantages for extractions and reactions. Lower viscosity of the IL in the presence of CO_2 will allow more facile pumping and transport. Lower viscosity increases diffusivity and increases the mass transport for reactions and separations. We have observed increased apparent reaction rates of the rhodium-catalyzed hydrogenation of olefins in a IL/CO_2 reaction over that in the pure ionic liquid under mass-transport limited conditions. [65] Here, the IL phase is not stirred and the vapor-liquid surface area is limited, but the apparent rate increases with increasing CO_2 pressure due to improved mass transport properties. In addition, heat transfer would also improve in these biphasic IL/CO_2 systems. This would be a great advantage for highly exothermic reaction systems, in which thermal management is important.

The effect of pressure, temperature, and composition on the viscosity of the IL mixture can be described by various empirical relationships. In this work three common predictive equations (the arithmetic mixing rule, Irving Relation also called the Predictive Arrhenius Relation (Eqn. 4.12), and Grunberg equation (Eqn.4.13) and one correlative equation (Eqn.4.14) (modified Grunberg equation) are used to fit the data. These models use the composition in mole fraction or mass fraction and the pure component viscosities at the same temperature and pressure to predict the mixture viscosity. The pure component viscosity of the IL at various temperatures and pressures was measured previously to greater than 1300 bar. [66] In the pressure range of the experiments here (1-287 bar), the pure component IL viscosity does increase to some extent (<35%), and the actual viscosity at the temperature and pressure of interest was used for the correlations. To determine the viscosity of pure CO_2 at different conditions, the database program,

REFPROP, is used which is an acronym for REFerence fluid PROPerties. [71] This program, developed by the National Institute of Standards and Technology (NIST), provides tables and plots of the thermodynamic and transport properties of industrially important fluids and their mixtures. REFPROP is based on the most accurate pure fluid and mixture models currently available. It implements three models for the thermodynamic properties of pure fluids: equations of state explicit in Helmholtz energy, the modified Benedict-Webb-Rubin equation of state, and an extended corresponding states (ECS) model. Mixture calculations employ a model that applies mixing rules to the Helmholtz energy of the mixture components; it uses a departure function to account for the departure from ideal mixing. Viscosity is modeled with either fluid-specific correlations, an ECS method, or in some cases the friction theory method.

Table 4-11 illustrates the performance of each of these methods and demonstrates better performance for all for the models at the higher temperatures.

Table 4-11 Performance of the viscosity correlation methods for ionic liquids mixed with CO_2

Correlation	**AARD% [a]**									**All Data**
	[EMIm][Tf_2N]			**[HMIm][Tf_2N]**			**[DMIm][Tf_2N]**			***AARD%***
	25°C	**50°C**	**70°C**	**25°C**	**50°C**	**70°C**	**25°C**	**50°C**	**70°C**	
General Mixing Rule	42.8	24	15.9	39	26.6	8.7	55	36.6	14	29.2
Irving	43.9	23.2	18	29.5	21	8.1	43.3	23.7	6.8	24.2
Grunberg	30.5	17.7	21.1	34.5	14.9	6.5	150.3	11.7	6.4	32.6
Modified Grunberg	7.31	16.49	18.09	27.47	6.76	4.94	11.27	5.08	4.09	11.3
G [b]	5.10	0.74	0.01	0.61	2.22	0.99	3.57	1.56	0.28	

[a] $\%AARD = \frac{100}{N}\sum_{i=1}^{N}\left|\frac{\eta_i^{\exp} - \eta_i^{pred}}{\eta_i^{pred}}\right|$; [b] Grunberg adjustable parameter.

Despite its simplicity, the arithmetic mixing rule correlates the highest isotherm data surprisingly well. The Irving model is a slight improvement to the arithmetic mixing rule. The modified Grunberg model (Eqn. 4.14) perform the best, however even with this model the average absolute relative deviation (%AARD) was still about 11 % for all of the data. All of the models, except the modified Grunberg equation, had mostly a positive bias, i.e. higher predicted viscosity than experimental. Clearly better models would be needed for design and simulation work for these IL/CO_2 systems and should remain under investigation for the future studies.

4.2.4 Summary

The viscosity of the imidazolium ionic liquids, [EMIm][Tf_2N], [HMIm][Tf_2N], and [DMIm][Tf_2N], saturated with CO_2 was measured at 25°C, 50°C, and 70°C with pressures to 287 bar. Initially, an increase in CO_2 pressure dramatically decreases the viscosity, but the decrease becomes more marginal at the highest pressures. At higher temperatures, the initial viscosity is lower and the solubility of CO_2 decreases at a given pressure resulting in large but more moderate decreases in the IL viscosity. These trends are due to the high solubility and phase behavior of CO_2 in the ILs. The presence of CO_2 decreases the intermolecular forces between the cations and anions lowering the barrier of motion. The effect of the alkyl- chain length on the imidazolium cation with [Tf_2N] anion was investigated. While, the ambient viscosity increases in the order of ethyl- < n-hexyl < n-decyl, the fractional change in viscosity with CO_2 at the same concentrations of CO_2 is actually quite similar. Three predictive equations and one correlative method were used to correlate the mixture viscosity with composition. The best correlation was obtained from modified Grunberg model with one adjustable parameter with the average absolute relative deviation (%AARD) of approximately 11.3 % for all of the data. The results demonstrate that the value of the adjustable parameter (*G*) generally decreases with increasing temperature and reaches virtually zero for [EMIm][Tf_2N] at 70°C. This study indicates that the reduction of viscosity in the presence of CO_2 is favorable to enhance mass transfer in reactions and separations with biphasic IL/CO_2 systems.

4.3 Viscosity of 1-hexyl-3-methylimidazolium bis(trifluoromethylsulfonyl)amide with compressed 1,1,1,2-Tetrafluoroethane (R-134a)

The viscosity of the ionic liquid, 1-hexyl-3-methylimidazolium bis(trifluoromethylsulfonyl)amide ([HMIm][Tf_2N]), with compressed 1,1,1,2-tetrafluoroethane (R-134a) was measured with a high-pressure viscometer at three different temperatures (25°C, 50°C, 70°C). The high-pressure vapor-liquid equilibrium of the ionic liquids with R-134a was used to connect the viscosity and pressure to concentration.

4.3.1 Results and Discussion

The viscosity of [HMIm][Tf_2N] with R-134a has been measured to pressures of approximately 20 bar and three temperatures: 25°C, 50°C, and 70°C. Results are shown at Figure 4-22 , Figure 4-23, Table 4-12, and Table 4-13 and illustrate that at lower temperatures the viscosity changes considerably with the pressure. The viscosity at 70°C, which was measured to just below the multi-phase VLLE region, shows a linear trend with the pressure and with a slight slope.

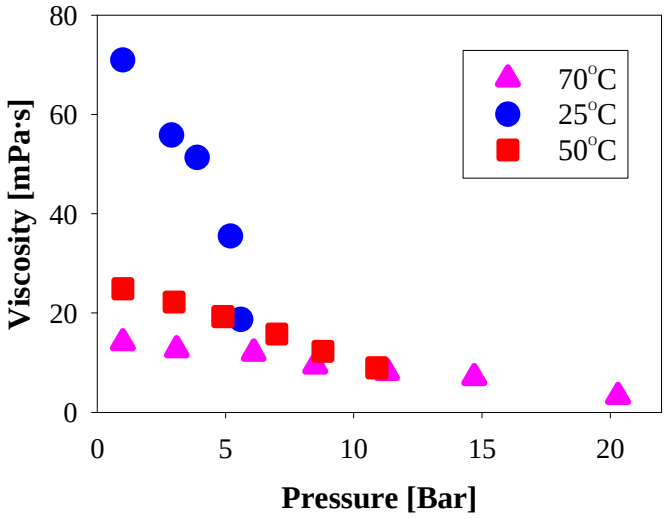

Figure 4-22 The viscosity of [HMIm][Tf_2N] with pressure of R-134a 25°C, 50°C and 70°C.

Table 4-12 Viscosity (η) of [HMIm][Tf_2N] with pressure and composition of R-134a.

25°C				50°C				70°C			
P [bar]	x_{R134a} [a]	*η [mPa·s]*	±	*P [bar]*	x_{R134a} [a]	*η [mPa·s]*	±	*P [bar]*	x_{R134a} [b]	*η [mPa·s]*	±
1[c]	0.000	70.96	0.71	1[c]	0.000	24.9	0.25	1[c]	0.000	14.07	0.14
2.9	0.387	55.83	0.50	3	0.223	22.2	0.22	3.1	0.148	12.62	0.13
3.9	0.511	51.31	0.46	4.9	0.349	19.29	0.19	6.1	0.276	11.97	0.12
5.2	0.672	35.48	0.32	7	0.473	15.76	0.16	8.5	0.364	9.33	0.09
5.6	0.725	18.69	0.19	8.8	0.575	12.29	0.12	11.3	0.459	8.09	0.08
				10.9	0.701	8.98	0.09	14.7	0.575	7.06	0.07
								20.3	0.813	3.24	0.03

[a] compositions were interpolated from the vapor-liquid equilibrium data of Ren and Scurto [73], [b] composition interpolated from VLE data presented here; [c] ambient pressure and R-134a-free conditions

Table 4-13 Viscosity (η) of [HMIm][Tf_2N]with pressure and composition of R_{134a}.

25℃								
P [bar]	**P** [MPa]	$\eta_{mix\text{-}exp}$ [mPa·s]	η_{ref} [mPa·s]	η_{IL}[mPa·s]	x_{IL}	$x_{R\text{-}134a}$	$\eta_{mix\text{-}corr}$ [mPa·s]	η^E [mPa·s]
1	0.1	70.96	0.1949	70.96	1.00	0.00	70.96	0.00
2.9	0.29	55.83	0.1949	70.98	0.61	0.39	43.57	12.26
3.9	0.39	51.31	0.1949	70.99	0.49	0.51	34.84	16.47
5.2	0.52	35.48	0.1949	71.01	0.33	0.67	23.39	12.09
5.6	0.56	18.69	0.1949	71.01	0.27	0.73	19.65	-0.96
50℃								
P [bar]	**P** [MPa]	$\eta_{mix\text{-}exp}$ [mPa·s]	η_{ref} [mPa·s]	η_{IL}[mPa·s]	x_{IL}	$x_{R\text{-}134a}$	$\eta_{mix\text{-}corr}$ [mPa·s]	η^E [mPa·s]
1	0.1	24.90	0.1418	24.90	1.00	0.00	24.90	0.00
3	0.3	22.20	0.1418	24.98	0.78	0.22	19.44	2.76
4.9	0.49	19.29	0.1418	25.03	0.65	0.35	16.35	2.94
7	0.7	15.76	0.1418	25.09	0.53	0.47	13.30	2.46
8.8	0.88	12.29	0.1418	25.14	0.42	0.58	10.76	1.53
10.9	1.09	8.98	0.1418	25.20	0.30	0.70	7.64	1.34
70℃								
P [bar]	**P** [MPa]	$\eta_{mix\text{-}exp}$ [mPa·s]	η_{ref} [mPa·s]	η_{IL}[mPa·s]	x_{IL}	$x_{R\text{-}134a}$	$\eta_{mix\text{-}corr}$ [mPa·s]	η^E [mPa·s]
1	0.1	14.07	0.1065	14.07	1.00	0.00	14.07	0.00
3.1	0.31	12.62	0.1065	14.08	0.85	0.15	12.00	0.62
6.1	0.61	11.97	0.1065	14.09	0.72	0.28	10.23	1.74
8.5	0.85	9.33	0.1065	14.10	0.64	0.36	9.01	0.32
11.3	1.13	8.09	0.1065	14.11	0.54	0.46	7.69	0.40
14.7	1.47	7.06	0.1065	14.12	0.42	0.58	6.06	1.00
20.3	2.03	3.24	0.1065	14.14	0.19	0.81	2.73	0.51

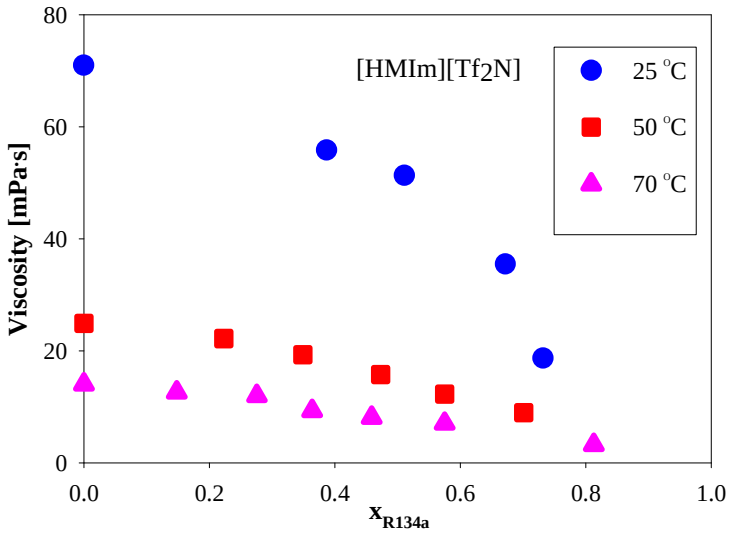

Figure 4-23 The viscosity of [HMIm][Tf_2N] with composition of R-134a 25°C, 50°C and 70°C

Figure 4-24 shows the significant effect of R-134a concentration on normalized viscosity (the viscosity at different pressures over the viscosity of pure IL) while the effect of temperature is not very considerable. The reason can be explained by the fact that the electrostatic interactions between cations and anions in IL molecules are affected by molecules of R134a and make the mobility of ions becomes faster. The effect of temperature can also be interpreted similarly. The excess viscosity that represents the deviation of viscosity of mixtures from the ideal behavior is also shown in Figure 4-25. They are calculated using the mixture viscosity, mole fraction of components and their pure viscosities:

$$\eta^{E} = \eta_{mix} - (\eta_1 x_1 + \eta_2 x_2) \qquad (4.20)$$

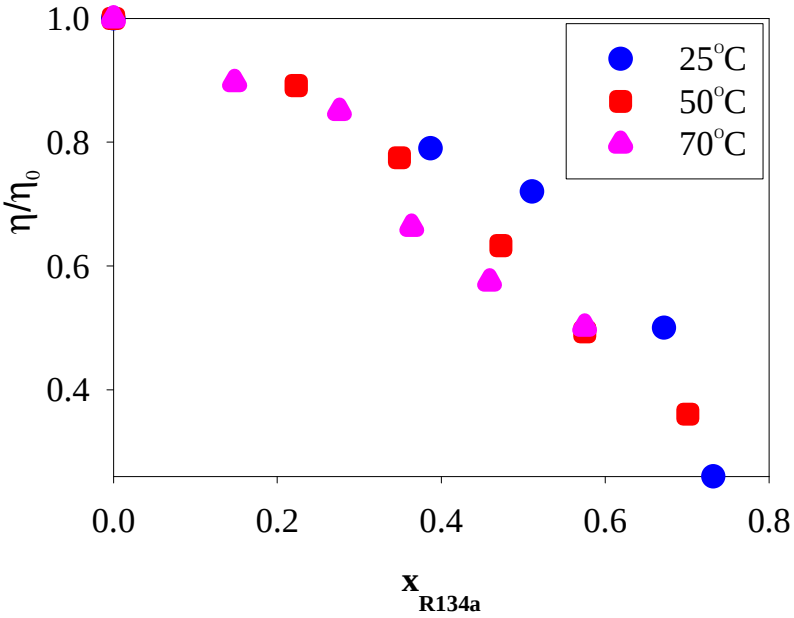

Figure 4-24 Normalized viscosity of the liquid phase with concentration of R-134a

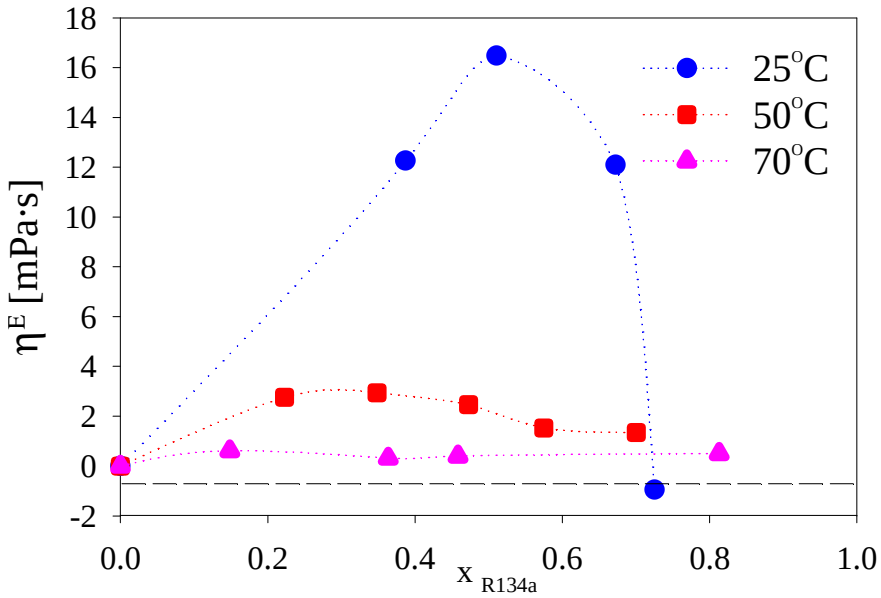

Figure 4-25 The variation of excess viscosity with the mole fraction of R134a in [HMIm][Tf_2N] at three different isotherms.

To determine the viscosity of pure R134a at different conditions the database program REFPROP is used. The positive values of excess viscosity represent the effect of presence of R134a in the free volume of ionic liquid structure. The less deviation at higher concentrations of R134a shows the lower stability of R134a molecules in cations and anions because of their weak interactions.

Excess viscosities at higher temperatures (50°C, 75 °C) are close to zero. Figure 4-26 and Table 4-14 also show the effect of CO_2 concentration on the excess viscosity at a similar condition. Negative deviation from ideal behavior can be explained by the impact of intermolecular forces and the polarity of molecules. In comparison with R134a, CO_2 is a nonpolar molecule without any hydrogen bonding effects and its presence between the free volume of cations and anions may make a mixture with lower stability than pure ionic liquid.

Table 4-14 Excess Viscosity (η) of [HMIm][Tf_2N] with pressure and composition of CO_2

x_{CO2}	η^E [mPa·s]	x_{CO2}	η^E [mPa·s]	x_{CO2}	η^E [mPa·s]
25°C		**50°C**		**70°C**	
0.000	0.00	0.000	0.00	0.000	0.00
0.159	-8.23	0.169	0.31	0.066	-0.58
0.237	-11.27	0.482	1.64	0.268	-0.12
0.343	-19.80	0.553	-1.15	0.398	1.15
0.445	-19.28	0.670	-2.81	0.521	0.66
0.783	-10.30	0.736	-3.09	0.644	-0.33
0.840	-7.53	0.745	-3.21	0.690	-0.94
0.867	-5.87	0.775	-2.95	0.725	-0.67
0.894	-3.99	0.775	-3.17		

Table 4-15 Measured viscosity (η) of [DMIm][Tf_2N] as a function of pressure and temperature.								
298.15 K			**323.15 K**			**343.15 K**		
P (MPa)	η (mPa·s)	± SD	***P*** (MPa)	η (mPa·s)	± SD	***P*** (MPa)	η (mPa·s)	± SD
0.10	108.2	0.4	0.10	36.2	0.1	0.10	18.15	0.05
2.95	111.5	0.2	2.95	37.5	0.3	2.95	18.55	0.06
4.27	112.8	0.8	4.27	38.2	0.2	4.27	18.75	0.04
6.90	117.6	1.1	6.90	39.2	0.1	6.90	19.30	0.14
34.60	167.5	0.5	34.60	53.6	0.3	34.60	25.76	0.18
47.96	199.0	1.8	47.96	61.8	0.4	47.96	29.15	0.20
68.87	257.0	2.3	68.87	76.0	0.6	68.87	35.72	0.11
83.29	301.1	1.8	83.29	85.9	0.1	83.29	40.47	0.12
93.03	336.7	1.0	93.03	94.3	0.2	93.03	44.56	0.18
109.80	402.7	2.8	109.80	110.8	0.3	109.80	51.26	0.15
122.57	459.8	4.6	122.57	122.6	0.4	122.57	56.74	0.28

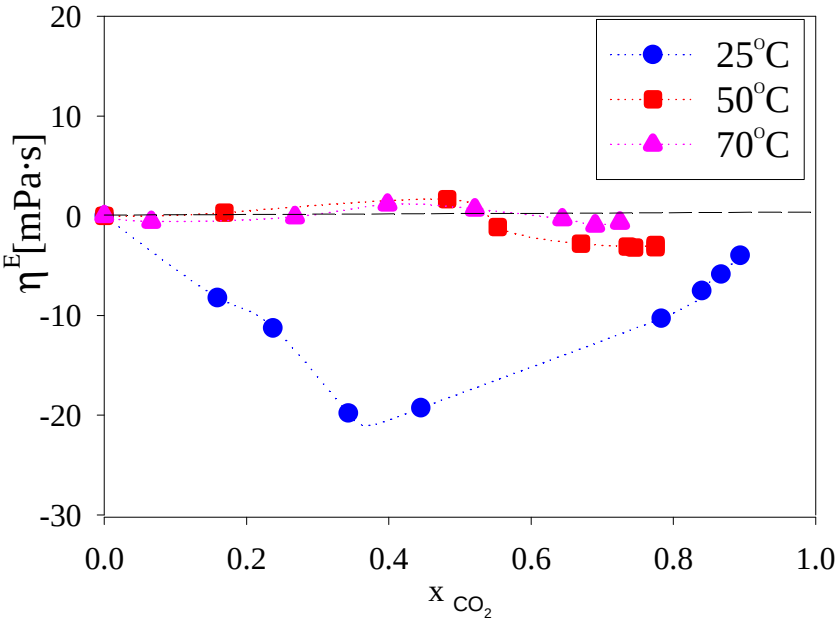

Figure 4-26 The variation of excess viscosity with the mole fraction of CO_2 in [HMIm][Tf_2N] at three different isotherms.

Correlated viscosity obtained from general mixing rule equation: $\eta_{mix} = \eta_1 x_1 + \eta_2 x_2$ AARD% for this equation at 25°C, 50°C, and 70°C are equal to 18.65, 11.77, and 8.25,

respectively. The results show that the standard deviation is decreasing with increasing temperature.

4.3.2 Summary

The viscosity of the ionic liquid, 1-hexyl-3-methylimidazolium bis(trifluoromethylsulfonyl)amide ([HMIm][Tf_2N]), with compressed 1,1,1,2-tetrafluoroethane (R-134a) was measured with a high-pressure viscometer at three different temperatures (25°C, 50°C, 70°C). Comparing the effect of pressure of different gases (R-134a and CO_2) on the viscosity of [HMIm][Tf_2N] showed interesting results. Adding the pressure of R-134a decreases the viscosity of IL considerably more than the CO_2 addition. The reason of this behavior can be clearly interpreted by probing the solubility of R-134a which is much higher than CO_2 solubility in [HMIm][Tf_2N]. [73] Also, the excess viscosity showed opposite trends with adding the concentration of two gases because of their unlike structures. Positive excess viscosity that illustrated the higher amount of mixture viscosity than its ideal behavior can express the incidence of R134a molecules among ionic liquid structure.

Compared to R134a, CO_2 is a nonpolar molecule without any hydrogen bonding effects and its presence between the free volume of cations and anions may make a mixture with lower stability than pure ionic liquid. At higher temperatures, the excess viscosities with both gases showed almost an ideal behavior because of poorer interactions between gas molecules and ions of the ionic liquid.

As it was illustrated in Chapter 3, to control the reaction conditions in proper mass transfer limited regim, transport properties should be elaborately managed. Thus, all of the obtained results can be extremely useful to direct reactions and/or separations of chemical processes to a desire region.

4.4 Diffusivity of Imidazolium Ionic Liquids with Compressed Gases (CO_2, R134a)

Diffusivity of gases like CO_2 and hydrofluorocarbons is measured and correlated by different groups.[74-76] Scovazzo et al.[74, 75] measured the CO_2 diffusivity in two different types of ionic liquids and showed that the CO_2 solubility and diffusivity are similar in the imidazolium-based RTILs and phosphonium-based RTILs. Diffusivity measurements are

done using a diffusion cell. The fundamental basic of working this cell is diffusing gas through a membrane and a chamber full of the sample of the ionic liquid. The flux through the membrane is measured by the pressure rise in the chamber. Shiflett et al.[76] also measured and correlated the diffusivity of hydrofluorocarbons in [BMIm][PF_6] and [BMIm][BF_4]. These experiments were performed using a gravimetric microbalance at various isothermal conditions (temperatures between 10°C and 75°C) and at pressures less than 2 MPa. In present study, the self-diffusivity of [HMIm][Tf_2N] with compressed CO_2 and 1,1,1,2-tetrafluoroethane (R-134a) is measured and reported.

4.4.1 Diffusivity in Liquid Mixtures of [HMIm][Tf_2N] and Compressed CO_2

Due to the high solubility and phase behavior of CO_2 in ILs, the presence of CO_2 decreases the intermolecular forces between the cations and anions and so reduces the barrier of motion. So, adding CO_2 enhances diffusivity and decreases viscosity. This effect is shown in Figure 4-27 and Figure 4-28, which illustrates adding 10 bar pressure of CO_2 increases diffusion coefficient almost 50%. The effect of CO_2 pressure on both viscosity and diffusivity of [HMIm][Tf_2N] at 25°C is shown in Figure 4-29.

If the diffusion coefficient and viscosity of the pure IL at ambient pressure as well as the viscosity of IL/CO_2 at a given temperature are known, then the diffusivity of the IL in mixtures with CO_2 can be predicted at other conditions with the equation that is derived from Stokes-Einstein equation.

Stokes – Einstein equation:

$$D = \frac{k_B T}{n \pi a \eta} \qquad (4.21)$$

where n is often 4 for smooth spherical objects (slip- boundary condition) and 6 for a rough one; a: is the hydrodynamic radius characteristic of the diffusing object; T, temperature; η, the viscosity; and k_B, Boltzmann constant.

The derived equation that is used:

$$D = \frac{D_0}{\eta / \eta_0} \qquad (4.22)$$

where the subscript 0 indicates the diffusivity and viscosity of the pure IL at ambient conditions.

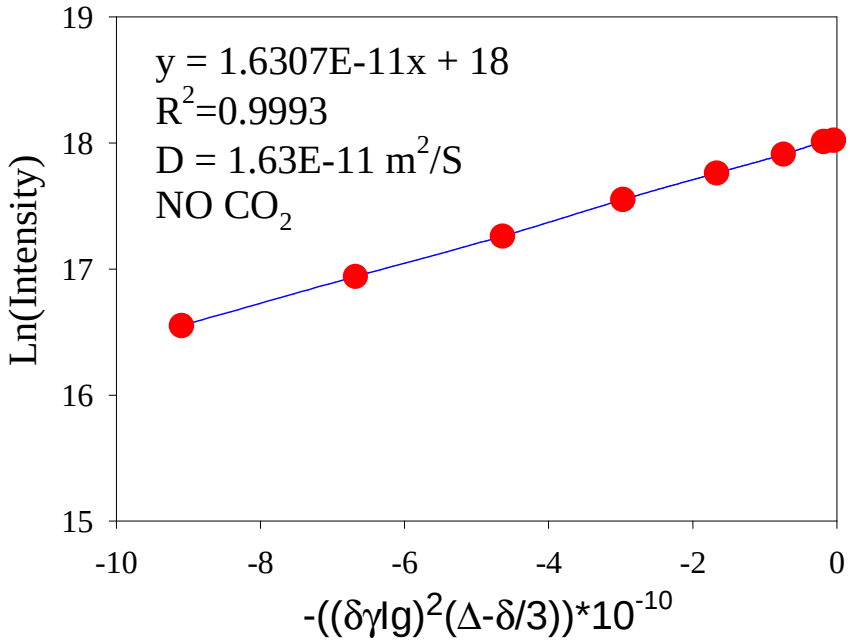

Figure 4-27 Self Diffusion Coefficient of pure [HMIm][Tf_2N] at 25°C

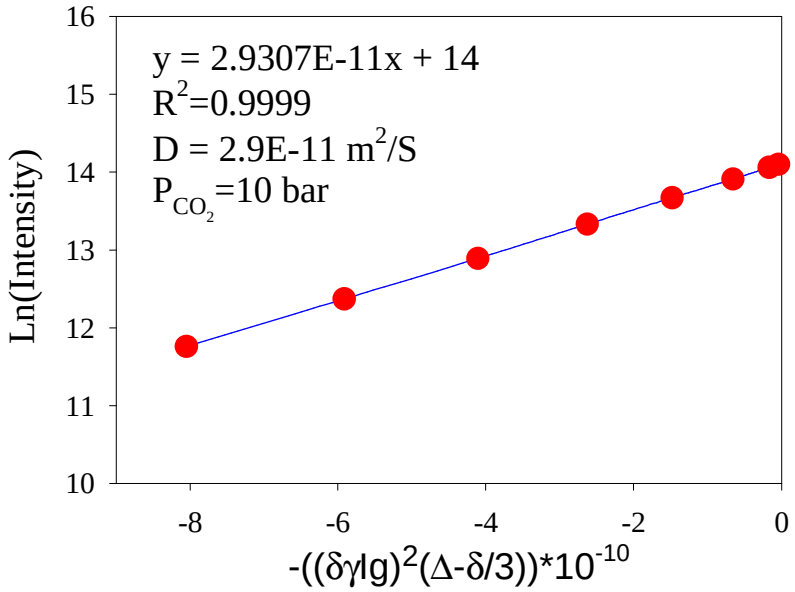

Figure 4-28 Self Diffusion Coefficient of [HMIm][Tf_2N] under CO_2 Pressure at 25°C

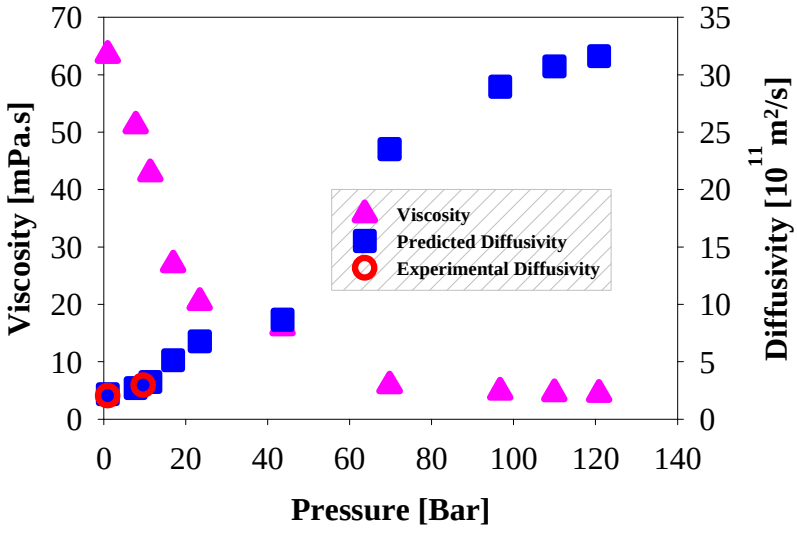

Figure 4-29 Viscosity and Diffusivity of [HMIm][Tf_2N] vs pressure of CO_2 at 25°C

4.4.2 Diffusivity in Liquid Mixtures of [HMIm][Tf_2N] and compressed Liquid R-134a

Because of the higher solubility of R-134a than CO_2 in [HMIm][Tf_2N] its effect on viscosity and diffusivity is much more considerable. The mutual diffusivity of [HMIm][Tf_2N]/R-134a at liquid-liquid condition (25°C and 6.5 bar) is measured and the result is shown in Figure 4-30 and Table 4-16 as can be seen from the graphs the diffusivity of R-134a in [HMIm][Tf_2N] increases faster than the cation of [HMIm][Tf_2N] in R-134a as the concentration of refrigerant increases. This effect is because of the smaller size of refrigerant.

As can be seen in Figure 4-31 and Table 4-16, the diffusion coefficient at 25°C increases about 42% with increasing pressure of R134a from ambient to 3 bar. This enhancement for 50°C and 70°C is around 25 % and 20%, respectively. Diffusion coefficient is also sensitive to the increasing of temperature at ambient pressure. Table 4-16 shows that diffusivity at 50 °C and 70°C is two and three fold bigger than the amount at 25°C. This effect can be explained by the temperature impact on the mobility, energy and movement of ions and R134a molecules. The effect of pressure of R134a on diffusivity can also be related to the presence of these molecules between cations and anions and weaken the electrostatic forces connecting them.

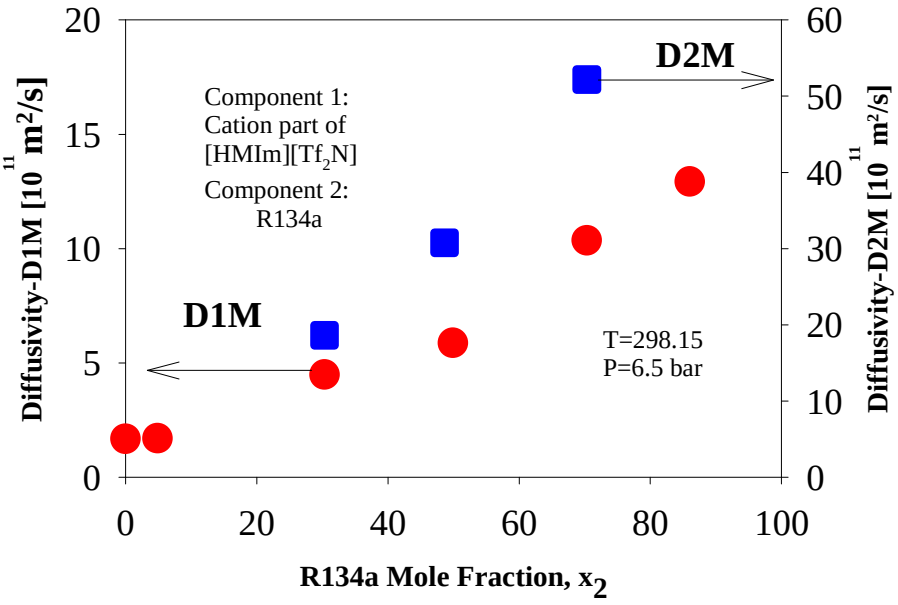

Figure 4-30 Diffusivity of cation of IL and R134a Vs Concentration of R134a
D1M: Diffusivity of [HMIm][Tf_2N] in the solution following the cation
D2M: Diffusivity of R134a in the solution
Diffusivities measured at P=6.5 bar using a high pressure NMR tube and PGSE method 400 MHz Ultrashield NMR

Table 4-16 Self-diffusivity of [HMIm][Tf_2N] cation (1) and R-134a (2) at various concentrations of compressed liquid R-134a at 25°C and 6.5 bar

x_2	$D_{12} \times 10^{-11}$ $[m^2/s]$	$D_{21} \times 10^{-11}$ $[m^2/s]$
0.00	1.67	
0.05	1.70	
0.30	4.49	18.62
0.50	5.87	30.76
0.70	10.35	52.19
0.86	12.93	
0.98	141.4	498.6
1.00		594.9

Table 4-17 Self-diffusivity of [HMIm][Tf_2N] saturated with R-134a.											
25°C				50°C				70°C			
P [bar]	D_{12exp} $\times 10^{11}$ [m^2/s]	D_{12corr} $\times 10^{11}$ [m^2/s]	Dev.[a]	*P* [bar]	D_{12exp} $\times 10^{11}$ [m^2/s]	D_{12corr} $\times 10^{11}$ [m^2/s]	Dev.[a]	*P* [bar]	D_{12exp} $\times 10^{11}$ [m^2/s]	D_{12corr} $\times 10^{11}$ [m^2/s]	Dev.[a]
0[b]	1.79	1.79	0.0	0[b]	*5.54*	5.54	0.0	0[b]	*10.66*	10.66	0.0
3.15	2.5	2.27	-9.2	3.14	6.86	6.28	-8.5	4.06	12.91	12.5	-3.2
4.19	2.55	2.63	3.1	4.12	6.97	6.82	-2.2	5.11	13.15	13.1	-0.4
5.01	2.54	3.13	23.2	5.15	6.85	7.49	9.3	6.08	13.41	13.8	2.9
[a] *Deviation*=(Dcorr-Dexp)/Dexp*100 ; [b] ambient pressure viscosity without gas.											

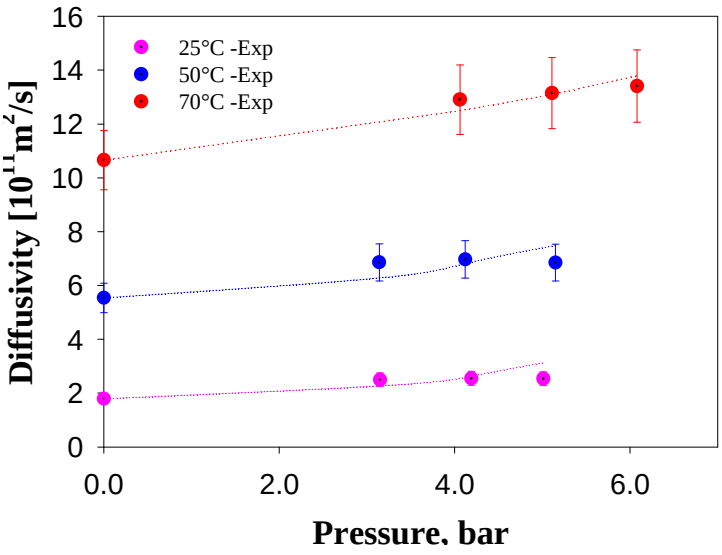

Figure 4-31 The effect of R134a pressure on diffusivity of ionic liquid at different temperatures. The solid lines represent the Stokes-Einstein correlation of data from the mixture viscosity data and the pure IL diffusivity. Dotted lines represent the correlated data

4.4.3 Summary

The diffusivity of [HMIm][Tf_2N] with CO_2 and with a refrigerant, 1,1,1,2-tetrafluoroethane (R-134a), was measured at 25°C, 50°C, and 70°C . The effect of adding CO_2 and R134a on diffusivity of ionic liquid was described and showed an increasing trend in diffusivity. The mutual diffusivity of [HMIm][Tf_2N]/R-134a at liquid-liquid condition (25°C and 6.5 bar) is also measured. The result illustrates that diffusivity of R-

134a in [HMIm][Tf_2N] increases faster than the cation of [HMIm][Tf_2N] in R-134a as the concentration of refrigerant increases.

4.5 References

1. Kelkar, M. S.; Maginn, E. J., Effect of Temperature and Water Content on the Shear Viscosity of the Ionic Liquid 1-Ethyl-3-methylimidazolium Bis (trifluoromethanesulfonyl) imide As Studied by Atomistic Simulations. *J. Phys. Chem. B* **2007,** 111, 18, 4867-4876.
2. Forsyth, S. A.; Pringle, J. M.; MacFarlane, D. R., Ionic Liquids-An Overview. *Aust. J. Chem.***2004,** 57, 2, 113-119.
3. Wilkes, J. S., Properties of ionic liquid solvents for catalysis. *J. Mol. Cat. A* **2004,** 214, 1, 11-17.
4. Ropel, L.; Belveze, L. S.; Aki, S.; Stadtherr, M. A.; Brennecke, J. F., Octanol-water partition coefficients of imidazolium-based ionic liquids. *Green Chem.* **2005,** 7, 83-90.
5. Ahosseini, A.; Ren, W.; Scurto, A., Homogeneous Catalysis in Biphasic Ionic Liquid/CO_2 Systems. *Chem. Today* **2007,** 25, 2, 40-42.
6. Blanchard, L. A.; Hancu, D.; Beckman, E. J.; Brennecke, J. F., Green processing using ionic liquids and CO_2. *Nature* **1999,** 399, 6731, 28-29.
7. Cadena, C.; Anthony, J. L.; Shah, J. K.; Morrow, T. I.; Brennecke, J. F.; Maginn, E. J., Why is CO_2 so soluble in imidazolium-based ionic liquids? *J. Am. Chem. Soc.* **2004,** 126, 16, 5300-5308.
8. Fadeev, A. G.; Meagher, M. M., Opportunities for ionic liquids in recovery of biofuels. *Chem. Commun.***2001**, 3, 295-296.
9. Visser, A. E.; Swatloski, R. P.; Reichert, W. M.; Griffin, S. T.; Rogers, R. D., Traditional Extractants in Nontraditional Solvents: Groups 1 and 2 Extraction by Crown Ethers in Room-Temperature Ionic Liquids. *Ind. Eng. Chem. Res* **2000,** 39, 10, 3596-3604.
10. Wilkes, J. S.; Levisky, J. A.; Wilson, R. A.; Hussey, C. L., Dialkylimidazolium chloroaluminate melts: a new class of room-temperature ionic liquids for electrochemistry, spectroscopy and synthesis. *Inorg. Chem.***1982,** 21, 3, 1263-1264.
11. Fuller, J.; Carlin, R. T.; Osteryoung, R. A., The Room-Temperature Ionic Liquid 1-Ethyl-3-Methylimidazolium Tetrafluoroborate-Electrochemical Couples and Physical-Properties. *J. Electrochem. Soc.* **1997,** 144, 11, 3881-3886.
12. Fuller, J.; Breda, A. C.; Carlin, R. T., Ionic liquid-polymer gel electrolytes from hydrophilic and hydrophobic ionic liquids. *J Electroanal Chem* **1998,** 459, 29-34.
13. Endres, F., Ionic Liquids: Solvents for the Electrodeposition of Metals and Semiconductors. *ChemPhysChem* **2002,** 3, 2, 144-154.
14. Lu, W.; Fadeev, A. G.; Qi, B.; Smela, E.; Mattes, B. R.; Ding, J.; Spinks, G. M.; Mazurkiewicz, J.; Zhou, D.; Wallace, G. G., Use of Ionic Liquids for p-Conjugated Polymer Electrochemical Devices. *Science* **2002,** 297, 5583, 983-987.
15. Quinn, B. M.; Ding, Z.; Moulton, R.; Bard, A. J., Novel electrochemical studies of ionic liquids. *Langmuir* **2002,** 18, 5, 1734-1742.
16. Chauvin, Y.; Mussmann, L.; Olivier, H., A Novel Class of Versatile Solvents for Two-Phase Catalysis: Hydrogenation, Isomerization, and Hydroformylation of Alkenes Catalyzed by Rhodium Complexes in Liquid 1, 3-Dialkylimidazoliurn Salts. *Angew. Chem. Int. Ed.***1995,** 34, 23-24, 2698-2700.
17. Kragl, U.; Eckstein, M.; Kaftzik, N., Enzyme catalysis in ionic liquids. *Curr. Opin. Biotechnol.* **2002,** 13, 6, 565-571.

18. Lozano, P.; De Diego, T.; Carrié, D.; Vaultier, M.; Iborra, J. L., Over-stabilization of Candida antarctica lipase B by ionic liquids in ester synthesis. *Biotech. Lett.* **2001,** 23, 18, 1529-1533.
19. Sheldon, R. A.; Lau, R. M.; Sorgedrager, M. J.; van Rantwijk, F.; Seddon, K. R., Biocatalysis in ionic liquids. *Green Chem.* **2002,** 4, 2, 147-151.
20. Welton, T., Room-temperature ionic liquids. Solvents for synthesis and catalysis. *Chem. Rev* **1999,** 99, 8, 2071-2083.
21. Zhao, D.; Wu, M.; Kou, Y.; Min, E., Ionic liquids: applications in catalysis. *Catal. Today* **2002,** 74, 157-189.
22. Valkenburg, M. E. V.; Vaughn, R. L.; Williams, M.; Wilkes, J. S., Thermochemistry of ionic liquid heat-transfer fluids. *Thermochim. Acta* **2005,** 425, 1-2, 181-188.
23. Koch, V. R.; Nanjundiah, C.; Carlin, R. T. Hydrophobic ionic liquids. U.S. Patent No.5,827,602, Oct.27,1998.
24. Glasstone, S.; Laidler, K. J.; Eyring, H., *The theory of rate processes*. McGraw-Hill New York: 1941.
25. Abbott, A. P., Application of hole theory to the viscosity of ionic and molecular liquids. *Chemphyschem* **2004,** 5, 8, 1242-1246.
26. Abbott, A. P., Model for the conductivity of ionic liquids based on an infinite dilution of holes. *ChemPhysChem* **2005,** 6, 12, 2503-2505.
27. Abbott, A. P.; Capper, G.; Gray, S., Design of Improved Deep Eutectic Solvents Using Hole Theory. *ChemPhysChem* **2006,** 7, 4, 803-806.
28. Vogel, H., Temperature dependence of viscosity of melts. *Phys. Z* **1921,** 22, 645–646.
29. Fulcher, G. S., Analysis of recent measurements of the viscosity of glasses. *Am. Ceram. Soc. Bull.* **1925,** 8, 339-355.
30. Tammann, G.; Hesse, W., Temperature dependence of viscosity of melted supercooled liquids. *Z. Anorg. Allg. Chem* **1926,** 156, 245–247.
31. Litovitz, T. A., Temperature Dependence of the Viscosity of Associated Liquids. *J. Chem. Phys.***1952,** 20, 1088-1089.
32. Crosthwaite, J. M.; Muldoon, M. J.; Dixon, J. K.; Anderson, J. L.; Brennecke, J. F., Phase transition and decomposition temperatures, heat capacities and viscosities of pyridinium ionic liquids. *J. Chem. Thermodyn.* **2005,** 37, 6, 559–568.
33. Tokuda, H.; Hayamizu, K.; Ishii, K.; Susan, M.; Watanabe, M., Physicochemical properties and structures of room temperature ionic liquids. 1. Variation of anionic species. *J. Phys. Chem. B* **2004,** 108, 42, 16593-16600.
34. Tokuda, H.; Hayamizu, K.; Ishii, K.; Susan, M.; Watanabe, M., Physicochemical properties and structures of room temperature ionic liquids. 2. Variation of alkyl chain length in imidazolium cation. *J. Phys. Chem. B* **2005,** 109, 13, 6103-6110.
35. Tokuda, H.; Ishii, K.; Susan, M.; Tsuzuki, S.; Hayamizu, K.; Watanabe, M., Physicochemical Properties and Structures of Room-Temperature Ionic Liquids. 3. Variation of Cationic Structures. *J. Phys. Chem. B, Condensed matter, materials, surfaces, interfaces, & biophysical chemistry* **2006,** 110, 6, 2833-2839.
36. Harris, K. R.; Kanakubo, M.; Woolf, L. A., Temperature and Pressure Dependence of the Viscosity of the Ionic Liquids 1-Methyl-3-octylimidazolium

Hexafluorophosphate and 1-Methyl-3-octylimidazolium Tetrafluoroborate. *J. Chem. Eng. Data* **2006,** 51, 3, 1161-1167.
37. Harris, K. R.; Woolf, L. A.; Kanakubo, M., Temperature and Pressure Dependence of the Viscosity of the Ionic Liquid 1-Butyl-3-methylimidazolium Hexafluorophosphate. *J. Chem. Eng. Data* **2005,** 50, 5, 1777-1782.
38. Harris, K. R.; Kanakubo, M.; Woolf, L. A., Temperature and Pressure Dependence of the Viscosity of the Ionic Liquids 1-Hexyl-3-methylimidazolium Hexafluorophosphate and 1-Butyl-3-methylimidazolium Bis (trifluoromethylsulfonyl) imide. *J. Chem. Eng. Data* **2007,** 52, 3, 1080-1085.
39. Kanakubo, M.; Harris, K. R.; Tsuchihashi, N.; Ibuki, K.; Uenos, M., Effect of pressure on transport properties of the ionic liquid 1-butyl-3-methylimidazolium hexafluorophosphate. *J. Phys. Chem. B* **2007,** 111, 8, 2062-2069.
40. Tomida, D.; Kumagai, A.; Kenmochi, S.; Qiao, K.; Yokoyama, C., Viscosity of 1-Hexyl-3-methylimidazolium Hexafluorophosphate and 1-Octyl-3-methylimidazolium Hexafluorophosphate at High Pressure. *J. Chem. Eng. Data* **2007,** 52, 577-579.
41. Tomida, D.; Kumagai, A.; Qiao, K.; Yokoyama, C., Viscosity of [bmim][PF_6] and [bmim][BF_4] at High Pressure. *Int. J. Thermophys.* **2006,** 27, 1, 39-47.
42. Kandil, M. E.; Marsh, K. N.; Goodwin, A. R. H., Measurement of the viscosity, density, and electrical conductivity of 1-hexyl-3-methylimidazolium bis (trifluorosulfonyl) imide at temperatures between (288 and 433) K and pressures below 50 MPa. *J. Chem. Eng. Data* **2007,** 52, 6, 2382-2387.
43. Dymond, J. H.; Malhotra, R., The Tait equation: 100 years on. *Int. J. Thermophys.* **1988,** 9, 6, 941-951.
44. Kashiwagi, H.; Makita, T., Viscosity of Twelve Hydrocarbon Liquids in the Temperature Range 298-348 K at Pressures up to 110 MPa. *Int. J. Thermophys.* **1982,** 3, 4, 289-305.
45. Kiran, E.; Sen, Y. L., High-pressure viscosity and density of n-alkanes. *Int. J. Thermophys.* **1992,** 13, 3, 411-442.
46. Oliveira, C.; Wakeham, W. A., The viscosity of five liquid hydrocarbons at pressures up to 250 MPa. *Int. J. Thermophys.* **1992,** 13, 5, 773-790.
47. Dymond, J. H.; Young, K. J.; Isdale, J. D., Transport properties of nonelectrolyte liquid mixtures—II. Viscosity coefficients for the n-hexane+ n-hexadecane system at temperatures from 25 to 100°C at pressures up to the freezing pressure or 500 MPa. *Int. J. Thermophys.* **1980,** 1, 4, 345-373.
48. Fieggen, W., On the dependence of viscosity on temperature for liquids. *Recueil des Travaux Chimiques des Pays-Bas* **1970,** 89, 6, 625-635.
49. Xiong, Y.; Kiran, E., Miscibility, density, and viscosity of polystyrene in n-hexane at high pressures. *Polymer* **1997,** 38, 20, 5185-5193.
50. Ray, H. S.; Pal, S., Simple method for theoretical estimation of viscosity of oxide melts using optical basicity. *Ironmaking & Steelmaking* **2004,** 31, 2, 125-130.
51. Dyre, J. C.; Christensen, T.; Olsen, N. B., Elastic models for the non-Arrhenius viscosity of glass-forming liquids. *J. Non-Cryst. Solids* **2006,** 352, 42-49, 4635-4642.
52. Mano, J. F.; Pereira, E., Data Analysis with the Vogel-Fulcher-Tammann-Hesse Equation. *J. Phys. Chem. A* **2004,** 108, 49, 10824-10833.
53. Huddleston, J. G.; Visser, A. E.; Reichert, W. M.; Willauer, H. D.; Broker, G. A.; Rogers, R. D., Characterization and comparison of hydrophilic and hydrophobic room

temperature ionic liquids incorporating the imidazolium cation. *Green Chem.* **2001,** 3, 156-164.
54. Angell, C., Perspectives on the glass transition. *J. Phys. Chem. A, Solids* **1988,** 49, 8, 863-871.
55. Seddon, K. R.; Stark, A.; Torres, M. J., Influence of chloride, water, and organic solvents on the physical properties of ionic liquids. *Pure Appl. Chem.* **2000,** 72, 12, 2275-2287.
56. Widegren, J. A.; Laesecke, A.; Magee, J. W., The effect of dissolved water on the viscosities of hydrophobic room-temperature ionic liquids. *Chem. Comm.* **2005,** 2005, 12, 1610-1612.
57. Gomes de Azevedo, R.; Esperança, J.; Szydlowski, J.; Visak, Z. P.; Pires, P. F.; Guedes, H. J. R.; Rebelo, L. P. N., Thermophysical and thermodynamic properties of ionic liquids over an extended pressure range:[bmim][NTf_2] and [hmim][NTf_2]. *J. Chem. Thermodyn.* **2005,** 37, 9, 888-899.
58. de Azevedo, R. G.; Esperança, J.; Najdanovic-Visak, V.; Visak, Z. P.; Guedes, H. J. R.; da Ponte, M. N.; Rebelo, L. P. N., Thermophysical and Thermodynamic Properties of 1-Butyl-3-methylimidazolium Tetrafluoroborate and 1-Butyl-3-methylimidazolium Hexafluorophosphate over an Extended Pressure Range. *J. Chem. Eng. Data* **2005,** 50, 3, 997-1008.
59. Zhao, H.; Xia, S.; Ma, P., Use of ionic liquids as 'green' solvents for extractions. . *J. Chem. Technol. Biotechnol.***2005,** 80, 10, 1089-1096.
60. Jessop, P. G.; Stanley, R.; Brown, R. A.; Eckert, C. A.; Liotta, C. L.; Ngo, T. T.; Pollet, P., Neoteric solvents for asymmetric hydrogenation: supercritical fluids, ionic liquids, and expanded ionic liquids. *Green Chem.* **2003,** 5, 123-128.
61. Liu, F.; Abrams, M. B.; Baker, R. T.; Tumas, W., Phase-separable catalysis using room temperature ionic liquids and supercritical carbon dioxide. *Chem. Comm.* **2001**, 433-434.
62. Webb, P. B.; Kunene, T. E.; Cole-Hamilton, D. J., Continuous flow homogeneous hydroformylation of alkenes using supercritical fluids. *Green Chem.* **2005,** 7 373-379.
63. Zhao, G.; Jiang, T., Electro-oxidation of Benzyl Alcohol in a Biphasic System Consisting of Supercritical CO_2 and Ionic Liquids. *J.Phys.Chem.B* **2004,** 108, 13052-13057.
64. Ahosseini, A.; Ren, W.; Scurto, A. M., Understanding Biphasic Ionic Liquid/CO_2 Systems for Homogeneous Catalysis: Hydroformylation. *Ind. Eng. Chem. Res.* **2009**, 95-101.
65. Ahosseini, A.; Ren, W.; Scurto, A. M., Hydrogenation in biphasic ionic liquid-carbon dioxide systems. *ACS Symp. Ser. FIELD Full Journal Title:ACS Symposium Series* **2009,** 1006, Gas-Expanded Liquids and Near-Critical Media, 218-234.
66. Ahosseini, A.; Scurto, A. M., Viscosity of Imidazolium-Based Ionic Liquids at Elevated Pressures: Cation and Anion Effects. *Int. J. Thermophys.* **2008,** 29, 4, 1222-1243.
67. Liu, Z.; Wu, W.; Han, B.; Dong, Z.; Zhao, G.; Wang, J.; Jiang, T.; Yang, G., Study on the Phase Behaviors, Viscosities, and Thermodynamic Properties of CO_2/[C_4mim][PF_6]/Methanol System at Elevated Pressures. *Chem. Eur. J.* **2003,** 9, 16, 3897-3903.

68. Laurenczy, G.; Dyson, P. J., Determination of the Viscosity of the Ionic Liquids [bmim][PF_6]. *J. Chem. Sci.* **2008**, 681-684.
69. Tomida, D.; Kumagai, A.; Qiao, K.; Yokoyama, C., Viscosity of 1-Butyl-3-methylimidazolium Hexafluorophosphate+ CO_2 Mixture. *J. Chem. Eng. Data* **2007,** 52, 5, 1638-1640.
70. Tomida, D.; Kumagai, A.; Qiao, K.; Yokoyama, C., Viscosity of 1-butyl-3-methylimidazolium tetrafluoroborate+ CO_2 mixture. *High Temp. High Press.* **2008,** 37, 1, 81.
71. Lemmon, E. W., M. L. Huber, et al. (2007). NIST Reference Fluid Thermodynamic and Transport Properties - REFPROP. Version 8.0. Gaithersburg, Maryland.
72. Ren, W.; Scurto, A. M., High-Pressure Phase Equilibria of Imidazolium Ionic Liquids and CO_2 Mixtures. **2009**, *Submitted.*
73. Ren, W.; Scurto, A. M., Phase equilibria of imidazolium ionic liquids and the refrigerant gas, 1, 1, 1, 2-tetrafluoroethane (R-134a). *Fluid Phase Equil.* **2009,** 286, 1, 1-7.
74. Ferguson, L.; Scovazzo, P., Solubility, diffusivity, and permeability of gases in phosphonium-based room temperature ionic liquids: data and correlations. *Ind. Eng. Chem. Res* **2007,** 46, 4, 1369-1374.
75. Morgan, D.; Ferguson, L.; Scovazzo, P., Diffusivities of gases in room-temperature ionic liquids: Data and correlations obtained using a lag-time technique. *Ind. Eng. Chem. Res* **2005,** 44, 13, 4815-4823.
76. Shiflett, M. B.; Yokozeki, A., Solubility and diffusivity of hydrofluorocarbons in room-temperature ionic liquids. *AIChE J.* **2006,** 52, 3, 1205-1219.
77. Ren, W.; Sensenich, B.; Scurto, A. M., High-Pressure Phase Equilibria of Carbon Dioxide (CO2)+ n-Alkyl-Imidazolium Bis (trifluoromethylsulfonyl) amide Ionic Liquids. *J. Chem. Thermo.***2009**.
78. Sanmamed, Y. A.; González-Salgado, D.; Troncoso, J.; Cerdeiriña, C. A.; Romaní, L., Viscosity-induced errors in the density determination of room temperature ionic liquids using vibrating tube densitometry star, open. *Fluid Phase Equil.* **2007,** 252, 1-2, 96-102.

Chapter 5 Understanding Thermodynamics, Interfacial, and Transport Properties in Biphasic [HMIm][Tf_2N] and 1-octene

5 Understanding thermodynamics, interfacial, and transport properties in biphasic 1-Hexyl-3-Methyl-Imidazolium Bis(Trifluoromethylsulfonyl)amide and 1-octene

Working with ionic liquids has some main issues such as high viscosity, low solubility, special phase behavior, etc. that may be solved by using multiphase systems involving organic liquids and compressed gases. For instance, as it is described in Chapter 3, the mixture of solvents and reactants (ionic liquid, CO_2, and 1-octene) in some catalytic reactions (hydrogenation, hydroformylation) showed exceptional properties and phase behavior that affected the results of mass transfer and kinetics of reaction. In these reaction results, the significant impact of mass and momentum transport properties especially in mass transfer-limited region has been shown. But, nevertheless, there is no enough data in literature for these systems. Thus, fundamental studies on interfacial mass and momentum transfer for biphasic ionic liquid systems are necessary for any process intensification and implementation.

In this chapter, the thermodynamics and interfacial phenomena for a biphasic system of a common ionic liquid and an organic liquid has been studied. To probe properties of ionic liquid – organic compounds the system of 1-octene (component (1)) 1-hexyl-3-methylimidazolium bis(trifluoromethylsulfonyl)amide ([HMIm][Tf_2N]) (component (2)) is chosen because of the following reasons: (Figure 5-1)

- [HMIm][Tf_2N] is a common ionic liquid and was selected by the coordinators of the IUPAC Project 2002-005-1-100 entitled “Thermodynamics of ionic liquids, ionic liquid mixtures, and the development of standardized systems” to be used as a model, and standard ionic liquid.[1]

- [HMIm][Tf_2N] is used as a solvent in this work in hydrogenation and hydroformylation reaction of 1- octane and so the result of these studies can be helpful in better understanding of kinetics of reaction.

- The solubility of [HMIm][Tf_2N] in 1-octene is very small (see below); so, low cross contamination is observed and the mass transfer will occur just in one direction. This behavior is very helpful to simplify the mass transfer study in the biphasic system.

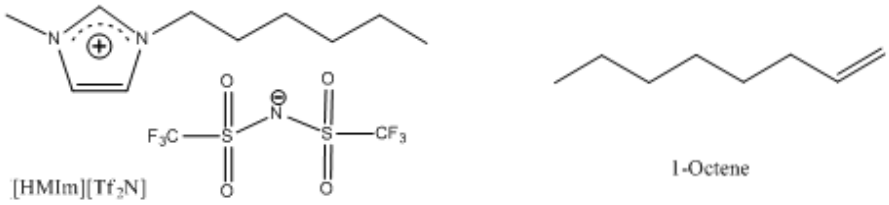

Figure 5-1 Structure of 1-n-hexyl-3-methylimidazolium bis(trifluoromethylsulfonyl)amide ([HMIm][Tf_2N]) and 1-octene.

In the first part, thermodynamic properties such as phase equilibrium, density, interfacial tension, and surface tension parameters are studied and in the second subsection transport properties like viscosity and mutual diffusivity are measured. These studies will be followed in Chapter 6 by mass transfer studies in liquid-liquid contact columns. To predict the concentration rate at each point, mass (Fickian) and momentum (Navier-Stocks) equations need to be solved simultaneously. Therefore, a fundamental modeling of Weatherley and Petera [2] is used with a robust, efficient, and realistic finite element method to solve these equations.

The main objective of studies in the present chapter is to provide the thorough information of the phase behavior as well as thermodynamic and transport properties for biphasic [HMIm][Tf_2N] / 1-octene system for supporting further modeling and correlations. Focus is placed on quantifying the effect of 1-octene concentration on these various properties.

5.1 Phase Equilibrium, Volumetric, and Interfacial Properties

Biphasic systems involving ionic liquids (ILs) form the basis of many applications in

extractions and reactions. In this section, the liquid-liquid phase equilibrium, molar volume, excess molar volume, density, and interfacial and surface tensions are measured for saturated and sub-saturated mixtures of [HMIm][Tf_2N] and 1-octene at four different temperatures, 10°, 25°, 50°, and 75°C. Before talking about the thermodynamic and transport properties of the system in this study, it must be remembered that the impurities can have a significant impact on the properties of ionic liquids. So, purification and storage of ionic liquids are very important to obtain consistent and accurate data. The main contaminants for [HMIm][Tf_2N], which are bromide and water, can crucially alter the properties and change the results of measurements. The influence of water, chloride and organic solvents on viscosity and density of ionic liquids has particularly been discussed by other research groups. [3]

5.1.1 Liquid – liquid equilibrium

The phase behavior of ionic liquids with other compounds is considerably important in properties of mixtures and will affect their applications in different areas, such as reaction, extraction, and material processing. For instance, dissolving compressed gases like CO_2 and refrigerants can decrease the viscosity of ionic liquids so that the ones which are good candidates to be used as lubricants and hydraulic liquids can be then utilized as low viscosity solvents and media for reactions and separations.[4-6] Also, for using ionic liquids in extraction (liquid-liquid)[7], leaching (cellulous dissolution)[8], and adsorption – desorption (column in GC)[7] techniques, the amount of solute that is dissolved in the ionic liquid phase can specify the ability and limitation of these applications.

In this work, measuring solubility of components is needed for fundamental studies of interfacial phenomena. Therefore, the mutual solubility of 1-octene and [HMIm][Tf_2N] is measured. Detailed procedures for sampling and measurement are found in section 2. The NRTL (Non-Random Two-Liquid) activity coefficient model [9] was utilized to correlate the experimental data.

The equations are given as:

$$\ln \gamma_1 = x_2^2 \left[\tau_{21} \left(\frac{G_{21}}{x_1 + x_2 G_{21}} \right)^2 + \frac{\tau_{12} G_{12}}{(x_2 + x_1 G_{12})^2} \right] \qquad (5.1)$$

$$\ln \gamma_2 = x_1^2 \left[\tau_{12} \left(\frac{G_{12}}{x_2 + x_1 G_{12}} \right)^2 + \frac{\tau_{21} G_{21}}{(x_1 + x_2 G_{21})^2} \right] \qquad (5.2)$$

$$G_{12} = \exp(-\alpha_{12}\tau_{21})$$
$$G_{21} = \exp(-\alpha_{12}\tau_{12}) \qquad (5.3,5.4)$$

where α_{12} is related to non-randomness in the mixture and is set equal to 0.2. The binary interaction parameters, τ_{12} and τ_{21}, were fitted to the data at each temperature using CHEMCAD software version 6.1.2, and using the binary interaction parameters (BIP) regression algorithm (Complex method) and the objective function:

$$\min \sum_{p=1}^{2} \sum_{i=1}^{NP} \left(x_i^{p,calc} - x_i^{p,\exp} \right)^2 \qquad (5.5)$$

5.1.1.1 Results and discussion

The mutual solubility of 1-octene and [HMIm][Tf_2N] was measured at 10°C, 25°C, 50°C, and 75°C and the values are listed in Table 5-1.

As shown in Figure 5-2, appreciable quantities of the 1-octene are soluble in the ionic liquids phase. For instance at 25°C, the solubility is approximately 20% mole. However, the solubility of [HMIm][Tf_2N] in 1-octene was very low (<0.0001 mole fraction). Even at 75°C, the solubility of the ionic liquid in the 1-octene phase is only about 4.5 mole%.

Table 5-1 The experimental liquid-liquid equilibrium of 1-octene (1) and [HMIm][Tf_2N] (2).

T [°C]	x^{II}_1	x^{I}_1
10	0.16 ± 0.01	0.9999±0.0001
25	0.19 ± 0.01	0.9999±0.0004
50	0.23 ± 0.02	0.9986±0.0009
75	0.28 ± 0.02	0.9552±0.0008

[I] indicates the 1-octene-rich phase; [II] is the [HMIm][Tf_2N]-rich phase

This produces a highly asymmetric liquid-liquid region. This general phase behavior has interesting ramifications for mass transfer in a biphasic system. When 1-octene and [HMIm][Tf_2N] are contacted, mass transfer will only be in virtually one direction especially at lower temperatures, i.e. 1-octene dissolution in [HMIm][Tf_2N]. The NRTL model was used to correlate the data. The model accurately correlates the 1-octene mutual solubility data at the temperatures investigated, albeit with slight undercorrelation of the 1-octene solubility in each phase. The model performance and binary interaction parameters are listed in Table 5-2.

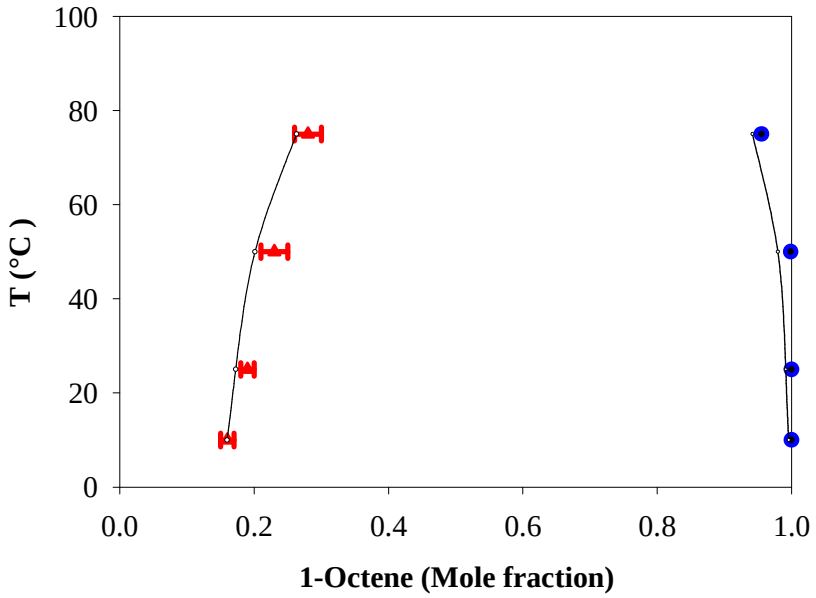

Figure 5-2 Liquid-liquid equilibrium of 1-octene (1) + [HMIm][Tf_2N] (2). The line is the correlation by the NRTL model.

There are a few studies in literature for n-alkene solubility in ionic liquids.[10-12] Stark *et al.*[13] determined the relative solubility of 1-octene in several imidazolium ionic liquids and showed that the solubility increases with the cation of 1-butyl-3-methylimidazolium ([BMIm]) in the order of: [BF_4]<[PF_6]<[OTf]<[Tf_2N] where [OTf] is the trifluoromethylsulfonate anion. However, they do not report the quantitative solubility. They also showed that for a given anion, longer alkyl chains yield a higher solubility of 1-octene. Other reports indicate that the smaller 1-hexene is slightly more soluble in ionic liquids than 1-octene.[10, 12, 14, 15] For instance, the solubility of 1-hexene in [BMIm][PF_6] at 30°C is approximately 12% mole.[16] Most imidazolium ILs have much larger solubility

for olefins compared with alkanes as the solubility of n-hexane in [BMIm][PF_6] at 41.3°C is 5.8% mole.[15] However, the solubility of most imidazolium ionic liquids in the alkene or alkane phase is very low; usually much less than 1% mole at ambient conditions.[17] This large difference in alkene/alkane solubility and low solubility of the IL is being exploited for olefin extraction.[18, 19]

Table 5-2 Regressed NRTL parameters and performance for solution of mixtures of 1-octene (1) + [HMIm][Tf_2N] (2).

	***T* [°C]**			
	10	**25**	**50**	**75**
τ_{12}	4.8985	3.8672	3.7535	3.1465
τ_{21}	0.3532	0.3354	0.3095	0.291
Dev.[a] (x^I_1)	-0.0053	-0.0174	-0.0288	-0.0168
Dev.[a] (x^{II}_1)	-0.0043	-0.0074	-0.019	-0.0135
%AARD[b] (x^I_1)	7.75			
%AARD[b] (x^{II}_1)	1.12			

[a] deviation =($x_1^{P,pred}$ - $x_1^{P,exp}$);

[b] $$\%AARD = \frac{100}{N}\sum_{i=1}^{N}\left[\left|\frac{x_1^{I,pred}(T_i)-x_1^{I,exp}(T_i)}{x_1^{P,exp}(T_i)}\right|+\left|\frac{x_1^{II,pred}(T_i)-x_1^{II,exp}(T_i)}{x_1^{P,exp}(T_i)}\right|\right]$$

5.1.1.1.2 Excess enthalpy

The excess enthalpy, $\underline{H}^{EX}$, can be computed from the NRTL activity coefficient/G^{EX} model from the regressed parameters.

$$\underline{H}^{EX} = \underline{G}^{EX} - T\left(\frac{\partial \underline{G}^{EX}}{\partial T}\right)_{P,x} \qquad (5.6)$$

From this relationship, the excess enthalpy is positive throughout the composition range and indicates that mixing is endothermic.[20-23] The model predicts that the excess enthalpy increases with temperature at a given composition. Nebig et al.[20] measured the excess

enthalpy for this [HMIm][Tf_2N]/1-octene system at 140°C and found that the excess enthalpy is positive at this much elevated temperature.

5.1.2 Density

While the density of many different pure ionic liquids has been extensively studied, fewer studies exist for mixtures. In this work, the density of mixtures of [HMIm][Tf_2N] and 1-octene to their saturation point was measured at 10°C, 25°C, 50°C, and 75°C and listed in Table 5-3. The density of the IL decreases with increasing concentration of 1-octene as seen in Figure 5-3.

Table 5-3 The density of solution of mixtures of 1-octene (1) and [HMIm][Tf_2N] (2).

	Density (ρ) [g/cm^3]			
x_1	10°C	25°C	50°C	75°C
0	1.3854 ± 0.0004	1.3707±0.0006	1.348 ±0.002	1.324 ±0.002
0.05	1.3721 ±0.0008	1.358±0.006	1.336 ±0.002	1.313 ±0.005
0.10	1.356 ±0.005	1.342±0.002	1.319 ±0.006	1.30 ±0.01
0.139	1.34 ±0.01	1.328±0.007	1.306 ±0.006	1.282 ±0.006
0.154	1.34 ±0.01	1.326±0.003	1.303 ±0.002	1.279 ±0.011
0.16[a]	1.340 ±0.009			
0.19[a]		1.3204±0.0001		
0.23[a]			1.300 ±0.002	
0.28[a]				1.267 ±0.012
1.0	0.7235 ±0.0006	0.7112 ±0.0006	0.69 ±0.01	0.668 ±0.012

[a] Reflects the saturation value at each isotherm

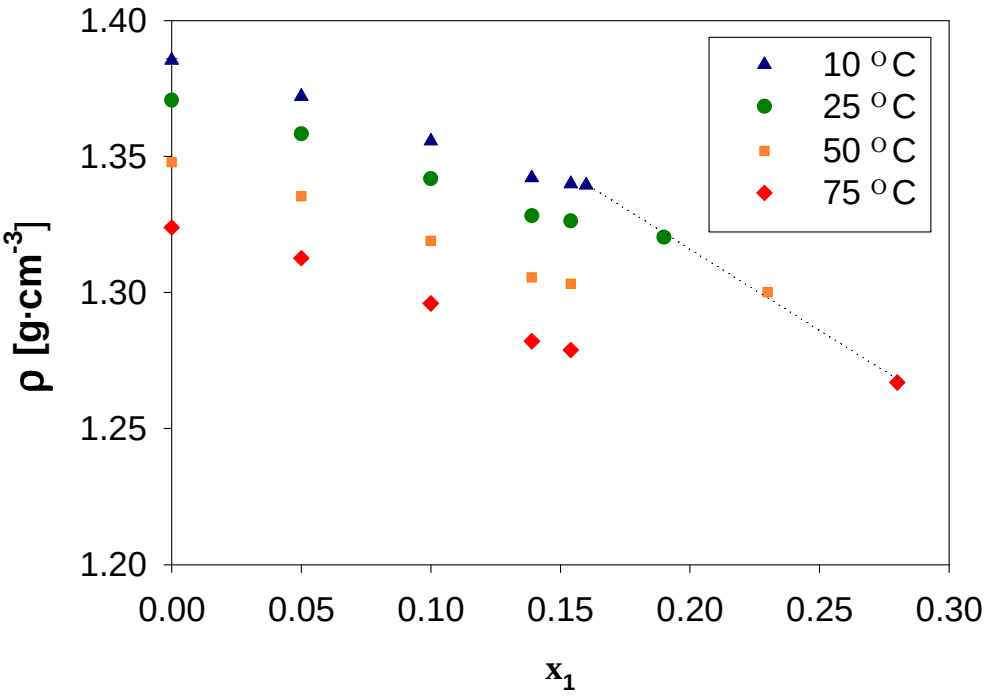

Figure 5-3 The density of 1-octene (1) + [HMIm][Tf_2N] (2). Dashed line indicates saturation limit.

The change is not a strictly linear decrease. At 75°C, the density difference between pure [HMIm][Tf_2N] and a mixture of [HMIm][Tf_2N] with 28% mole 1-octene (saturation) is only approximately -4.3%. The temperature-dependence of density at each composition is linearly dependent between 10°C and 75°C and shown in Figure 5-4.

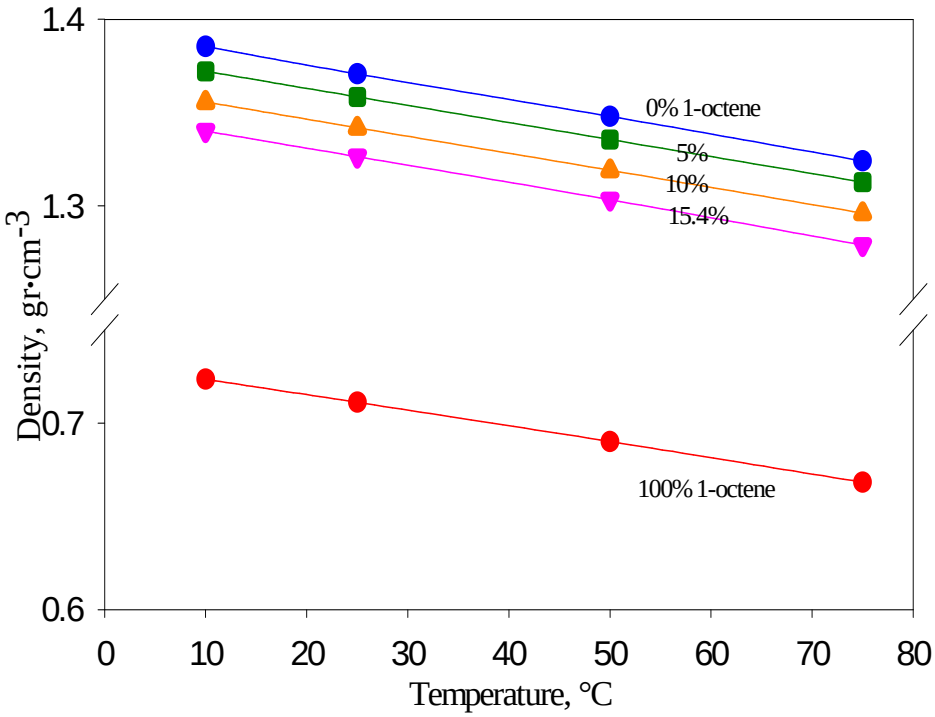

Figure 5-4 Density of the 1-octene (1) + [HMIm][Tf_2N] (2) with temperature and composition of 1-octene. Line is of smoothed data.

5.1.3 Excess Molar Volume

From the density data and the composition of the mixture, the excess molar volume ($\underline{V}^{EX}$) or volume of mixing ($\Delta\underline{V}^{mixing}$) can be computed from:

$$\underline{V}^{EX} = \Delta\underline{V}^{mixing} = \underline{V}_m - x_1\underline{V}_1 - x_2\underline{V}_2 = \frac{x_1MW_1 + x_2MW_2}{\rho_m} - \frac{x_1MW_1}{\rho_1} - \frac{x_2MW_2}{\rho_2} \quad (5.7)$$

where $\underline{V}_i$ and ρ_i are the molar volumes and densities, respectively of pure 1-octene (*1*), pure [HMIm][Tf_2N] (*2*), and their mixture (*m*), respectively; MW_i and x_i are their molecular masses and mole fractions of component *i*, respectively. A full error analysis was performed to determine the inherent errors in the excess molar volume at each point; the maximum uncertainty for excess molar volume is about 0.2 cm^3/mole. (Table 5-4**)**

Table 5-4 Excess molar volume of mixtures of 1-octene (1) + [HMIm][Tf_2N] (2) at 4 temperatures.				
T=10 °C				
x_1	$\underline{V_m}$ [$cm^3 mole^{-1}$]	±	$\underline{V^{EX}}$ [$cm^3 mole^{-1}$]	±
0	322.93	0.02	0	
0.05±0.0001	313.85	0.14	-0.69	0.14
0.1±0.0001	305.29	0.13	-0.85	0.14
0.139±0.0001	298.62	0.13	-0.98	0.14
0.154±0.0001	295.35	0.13	-1.73	0.14
0.16*±0.01	293.97	0.13	-2.11	0.14
1	155.08	0.02	0	
T=25 °C				
0	326.40	0.03	0	
0.05±0.0001	317.03	0.14	-0.94	0.15
0.1±0.0001	308.44	0.14	-1.10	0.19
0.139±0.0001	301.75	0.14	-1.22	0.19
0.154±0.0001	298.41	0.14	-2.03	0.19
0.19*±0.01	290.61	0.03	-3.76	0.13
1	157.77	0.03	0	
T=50 °C				
0	331.92	0.03	0	
0.05±0.0001	322.45	0.15	-1.01	0.20
0.1±0.0001	313.78	0.14	-1.21	0.14
0.139±0.0001	307.00	0.14	-1.38	0.14
0.154±0.0001	303.69	0.14	-2.15	0.14
0.23*±0.02	284.82	0.13	-8.15	0.14
1	162.58	0.15	0	
T=75 °C				
0	337.92	0.15	0	
0.05±0.0001	328.06	0.15	-1.35	0.21
0.1±0.0001	319.35	0.15	-1.57	0.20
0.139±0.0001	312.61	0.15	-1.68	0.20
0.154±0.0001	309.47	0.15	-2.27	0.20
0.28*±0.02	279.05	0.13	-11.26	0.20
1	167.89	0.15	0	
* saturated value.				

Excess molar volume of the solution indicates the deviation from ideal solution behavior at the same temperature and pressure. As can be seen in Figure 5-5, the excess

molar volume for the mixture of ionic liquids and 1-octene is slightly negative for all isotherms below approximately 15% mole of octene. Above this concentration, the excess molar volume becomes more negative until the saturation composition is reached. The excess molar volume slightly increases (more negative) with temperature, $\left(\partial \underline{V}^{EX} / \partial T\right)_{P,x} < 0$, thus, these contraction effects become a bit more pronounced with temperature. These trends may indicate that as small amounts of 1-octene are added, the intermolecular forces are dominated by IL-IL interactions and that the 1-octene may simply occupy the spaces between the ions or by weak dispersion interactions between the 1-hexyl- group of the cation and 1-octene. However, as the mixture becomes more concentrated in the 1-octene, the compounds may begin to have stronger interactions possibly between the unsaturated regions of the cation and 1-octene, which results in a volume contraction.

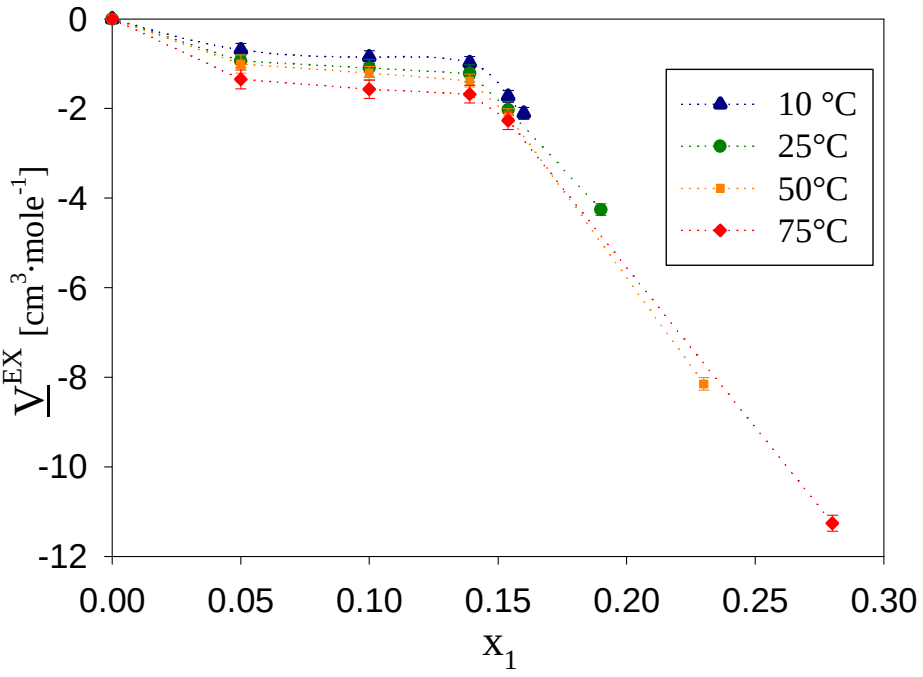

Figure 5-5 Excess molar volume of 1-octene (1) + [HMIm][Tf_2N] (2). The last point of the isotherm is the value at saturation. Smoothed line for visual aid.

Wang *et al.*[24, 25] also observed similar negative trends for the mixtures of [BMIm][PF_6] and organic compounds, such as acetonitrile, dichloromethane, 2-butanone,

and dimethylformamide. Heintz *et al*[26] explained that the negative values of the molar excess volume between 4-methyl-*N*-butylpyridinium tetrafluoroborate ([4MBP][BF_4]) upon mixing with methanol molecules are most likely stabilized by ion-dipole interactions in the mixture. However, positive excess molar volumes have been reported for [BMIm][BF_4] + H_2O and [EMIm][BF_4]+ H_2O mixtures by Seddon *et al.*[3]

In a recent experimental thermodynamic and molecular dynamics simulation study of CO_2 + imidazolium-based ionic liquids by Cadena *et al.*[27], it was suggested that the anions and cations of the ionic liquids form a strong network with the interstices available in the fluid. Therefore, it is possible that the relatively small organic molecules fit into the interstices upon mixing. In addition, it was found from molecular dynamics simulations [28] that the non-hydrogen bonding polar solutes, such as the organic compounds investigated in this work, interact much more strongly with the cations of the ionic liquids by ion–dipole interactions. The filling effect of organic compounds in the network of ionic liquids, and the ion–dipole interactions between organic compound and the imidazolium ring of the ionic liquids, all contribute to the negative values of the molar excess volumes. Lopes *et al.* [29] investigated the effect of different cations and anions on the excess molar volume of ionic liquid mixtures and revealed that the value of excess molar volume, which is positive, increases as the difference between the sizes of the two cations or anions becomes larger.

5.1.4 Surface tension

There are several studies in the literature concerning surface tension of pure ionic liquids. Huddleson *et al.* [30] measured surface tension for several ILs and demonstrated that these values are higher than for organic solvents, such as hexane and toluene, but not as high as water at the same temperature. Law *et al.* [31] also measured the surface tension of some *N*-alkylimidazolium ILs and showed the decreasing trend of these values with temperature. Dzyuba *et al.*[32] studied the structural effect on surface tension for some ILs and found that increasing the length of 1-alkyl chain on imidazolium cations decreases the surface tension. Here, we have measured the surface tension of mixtures of [HMIm][Tf_2N] and 1-octene to their saturation point at 10°C, 25°C, 50°C, and 75°C and the data are listed in Table 5-5.

Table 5-5 Surface tension (σ) [mN/m] of 1-octene (1)+ [HMIm][Tf_2N] (2) and their mixtures.								
x_1	10 °C		25 °C		50 °C		75 °C	
0	31.2	±0.1	30.8	±0.2	28.9	±0.4	27.6	±0.2
0.05±0.0001	30.9	±0.1	30.3	±0.1	28.8	±0.6	27.4	±0.3
0.1±0.0001	29.8	±0.1	29.4	±0.0	28.7	±0.5	27.2	±0.6
0.15±0.0001	27.8	±0.1	27.4	±0.1	26.6	±0.2	26.3	±0.6
0.16[a]±0.01	27.7	±0.1						
0.19 [a]±0.01			27.0	±0.1				
0.23 [a]±0.02					25.5	±0.4		
0.28 [a]±0.02							25.3	±0.4
1	22.5	±0.1	21.2	±0.1	18.5	±0.1	15.7	±0.1
[a] Reflects the saturation value at each isotherm								

As can be seen from the result in Figure 5-6, the surface tension decreases as the 1-octene concentration increases; the pure component surface tension of 1-octene is much lower than the IL. However, this effect diminishes percentage wise at the higher temperatures. Kimura *et al.* [33] measured the surface tension of 1-octene (23.4 mN/m at 20 °C), which was close to the value that Jasper *et al.* [34] reported (21.8 mN/m) compared with our data at 25°C of 21.2mN/m. Domanska and Marciniak[35] measured the surface tension of pure [HMIm][Tf_2N] at 25°C with a value of 31.2 mN/m, which compares with the value measured in the current work of 30.8 mN/m. Coutinho and coworkers[36] measured the surface tension at 50°C with a value of 30.6 mN/m, compared with 28.9 mN/m from this study.

5.1.5 Interfacial tension

The interfacial tension of mixtures of saturated mixtures of [HMIm][Tf_2N] and 1-octene were measured at 10°C, 25°C, 50°C, and 75°C and listed in Table 5-6. The results illustrate that the interfacial tension decreases with temperature to a small extent at 10°C and 25°C, and more significantly at the higher temperatures.

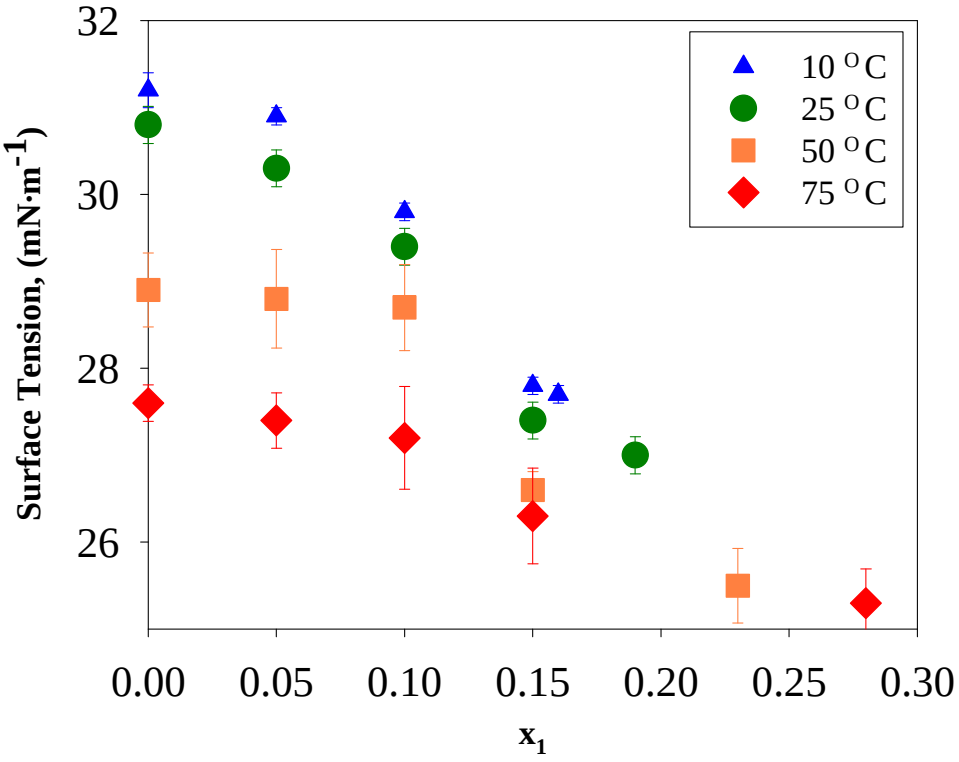

Figure 5-6 Surface tension of [HMIm][Tf_2N] (1) and 1-octene (2) and their mixtures.

Matsuda *et al.* [37] investigated the system of [HMIm][PF_6] saturated with n-hexane and n-decane and reported interfacial tensions at 25°C of 8.36 and 9.76 mN/m, respectively. These amounts are lower than the interfacial tensions reported for [HMIm][Tf_2N]/1-octene system in current study.

Table 5-6 Interfacial Tensions and model interaction parameters for 1-octene (1) + [HMIm][Tf_2N] (2) at different temperatures

T [°C]	σ_{IT} [mN/m]	ϕ
10	13.3 ± 1.3	0.76
25	13.0±1.3	0.76
50	9.7±1.3	0.82
75	4.4±1.3	0.93

The interfacial tension between two liquids has been often related to their air-liquid surface tension. An expression has been proposed by van Oss[38] and recently applied to ionic liquid-alkane systems:

$$\sigma_{IT}^{IL-Oct} = \sigma^{IL} + \sigma^{Oct} - 2\phi\sqrt{\sigma^{IL} * \sigma^{Oct}} \qquad (5.8)$$

where ϕ is the interaction parameter which, from other systems in the literature, is near zero for non polar mixtures, less than one for nonpolar/polar systems, and greater than one for polar/polar systems.[37] The regressed parameter ϕ for 1-octene-[HMIm][Tf_2N] system at the four different temperatures is shown in Table 5-6. The parameter is just less than unity with a slight temperature dependence in accordance with a non-polar/polar mixture. Figure 5-7 compares the surface tension of pure 1-octene and [HMIm][Tf_2N] with the interfacial tension of saturated mixtures at different temperatures. As can be seen in this figure the surface tension of 1-octene is less than ionic liquid and the interfacial tension between two saturated compounds is less than the surface tensions of pure components.

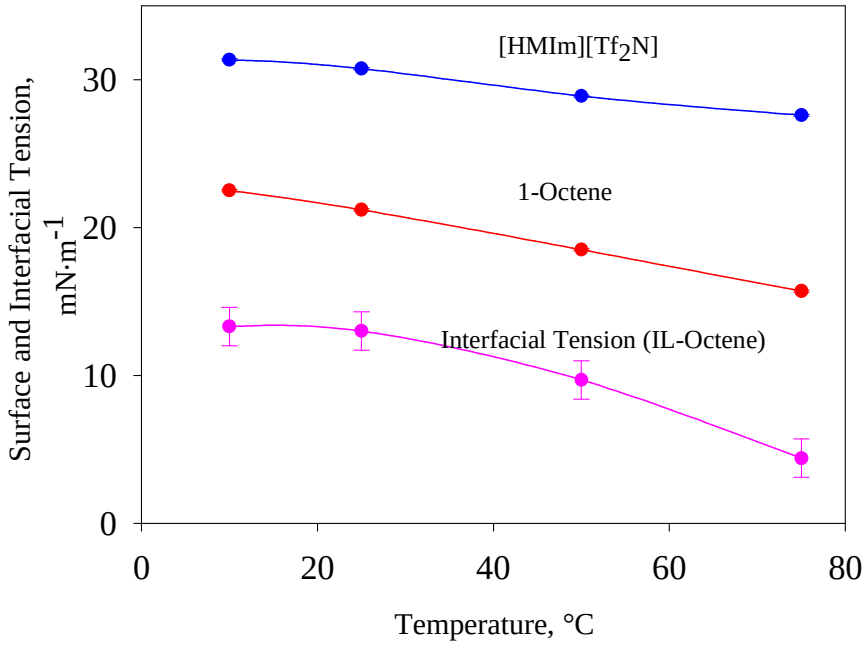

Figure 5-7 Interfacial tension of the saturated 1-octene (1) + [HMIm][Tf_2N] (2) system with temperature compared to the pure component surface tensions.

5.2 Transport properties

Viscosity and diffusivity of [HMIm][Tf_2N] with 1-octene is determined in different isotherms (10, 25, 50, and 75°C). The improvement of mass transfer parameters by adding 1-octene is discussed quantitatively. The values of excess viscosity showed a negative trend that matches with the negative amounts of excess molar volume.

5.2.1 Viscosity

To compare the results of viscosity measurements with the literature, Table 5-7 and Table 5-8 show the viscosity of octane, octene, and [HMIm][Tf_2N] measured with different methods. As these results show, the amounts of viscosity for octene and octane at low temperatures (10°C) are very different and have a relative deviation of almost 60%. This difference decreases as temperature increases (6% at 25°C) and reaches 1-2 % at higher temperatures (50°C-75°C).

Table 5-7 Viscosity of octane from literature comparing experimental data for 1-octene

Viscosity (mPa.s)				
Compound	10°C	25°C	50°C	75°C
Octane[45]	0.6146	0.516	0.3875	0.3072
1-octene (this work)	0.99	0.54	0.39	0.3

Table 5-8 Viscosity([mPa.s]) of [HMIm][Tf_2N] at ambient pressure measured by different methods	
T=25 °C	
Crosthwaithe-2005 [46]	68
Tokuda-2006 [44]	69.7
This work [47]	70.0
T=50 °C	
Crosthwaithe-2005 [46]	26
Tokuda-2005 [48]	24.8
Tokuda-2006 [44]	25.8
This work [47]	25.8
T=70 °C	
Crosthwaithe-2005 [46]	15
Tokuda-2005 [48]	13.7
Tokuda-2006 [44]	14.1
This work [47]	14.1

5.2.2 Diffusivity

Self-diffusion, which is different from spin diffusion or rotational diffusion is defined as the random translational movement of molecules motivated by internal energy. [39]Translational diffusion is the most important form of transport in reactions that causes collision and interactions between reactants before they can react. A Bruker 400 MHz ^1H NMR was used to measure the translational diffusion with a pulsed-field gradient (PFG) method. The software used to analyze the data was Topspin version 1.3. The procedure was described in detail in Chapter 2 and Appendix A. To evaluate the accuracy of this method the results for diffusivity (m^2/s) of [HMIm][Tf_2N], octane and octene at ambient pressure measured and compared with different methods (Table 5-9). The results show a good consistency for the amounts of IL compared with the literature.

Table 5-9 Diffusivity (m^2/s) of [HMIm][Tf_2N], octane and octene at ambient pressure measured by different methods.		
Diffusivity (m^2/s)		
Temperature	25°C	50°C
[HMIm][Tf_2N] Cation (This work)	1.67E-11	5.54E-11
[HMIm][Tf_2N] Cation [44]	1.75E-11	5.05E-11
Octane [49]	283	321
1-octene (This work)	228.3	344.2

5.2.3 Results and discussion

The experimental results of dynamic viscosity for pure 1-octene and [HMIm][Tf_2N] and their mixtures at different temperatures are presented in Table 5-11. The results, which are graphically shown in Figure 5-8 and Figure 5-9, illustrated that the viscosity of IL decreases with adding 1-octene concentration and temperature. The reason can be explained by the fact that the electrostatic interactions between cations and anions in IL molecules are affected by neutral molecules of 1-octene and make the mobility of ions become faster. The effect of temperature can also be interpreted similarly. The viscosity of different solutions in Figure 5-9 shows a decreasing trend with the temperature and levels off at higher temperatures (>50°C).

Table 5-10 Viscosity and excess viscosity (mPa·s) for pure 1-octene (1) + [HMIm][Tf_2N] (2) and their mixtures at different temperatures			
T=10°C			
x_1	η (mPa·s)	η^{EX} (mPa·s)	$(\ln \eta)^{EX}$
0	135.6 ± 1.5	0	0
0.05	126.8 ± 1.4	-2.13	0.168
0.1	105.7± 1.2	-16.5	0.222
0.15	92.7± 1.0	-22.8	0.326
0.16	90.9 ± 1.0	-23.2	0.353
1	0.99 ± 0.1	0	0
T=25°C			
x_1	η (mPa·s)	η^{EX} (mPa·s)	$(\ln \eta)^{EX}$
0	70.1 ± 0.8	0	0
0.05	66.6 ± 0.7	0.019	0.183
0.1	56.2 ± 0.8	-6.86	0.247
0.15	51.2 ± 0.6	-8.44	0.386
0.19	48.0 ± 0.6	-8.92	0.507
1	0.54 ± 0.07	0	0
T=50°C			
x_1	η (mPa·s)	η^{EX} (mPa·s)	$(\ln \eta)^{EX}$
0	25.8 ± 0.3	0	0
0.05	24.4 ± 0.3	-0.19	0.135
0.1	21.6 ± 0.3	-1.72	0.205
0.15	20.5 ± 0.3	-1.56	0.346
0.23	18.7 ± 0.3	-1.33	0.562
1	0.39 ± 0.06	0	0
T=75°C			
x_1	η (mPa·s)	η^{EX} (mPa·s)	$(\ln \eta)^{EX}$
0	14.1 ± 0.2	0	0
0.05	13.0 ± 0.2	-0.41	0.115
0.1	11.6 ± 0.2	-1.12	0.197
0.15	11.4 ± 0.2	-0.63	0.375
0.28	10.7 ± 0.2	0.47	0.821
1	0.3 ± 0.06	0	0

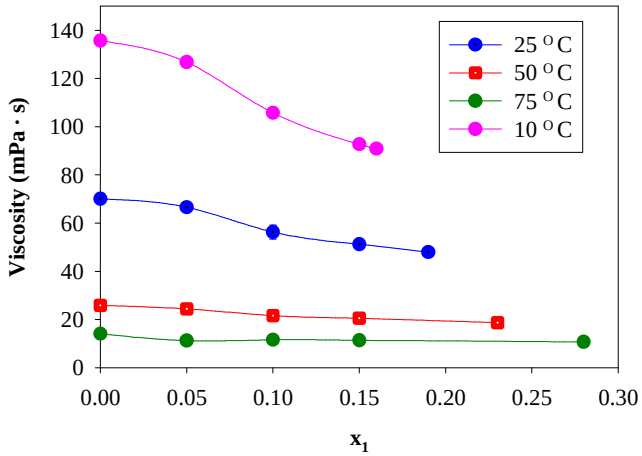

Figure 5-8 The effect of adding 1-octene to the viscosity of [HMIm][Tf_2N] at different isotherms

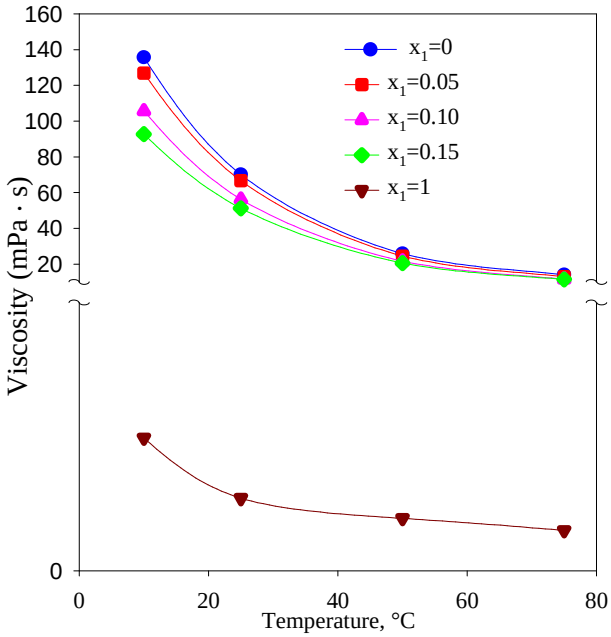

Figure 5-9 The effect of temperature on viscosity of [HMIm][Tf_2N] (2) at different concentrations of 1-octene(1)

The excess viscosity and logarithm excess viscosity that represent the deviation of viscosity of mixtures from the ideal behavior is also shown in Table 5-10, Figure 5-10,

and Figure 5-11. They are calculated using the mixture viscosity, mole fraction of components and their pure viscosities:

$$\eta^{E} = \eta_{mix} - (\eta_1 x_1 + \eta_2 x_2) \qquad (5.9)$$

$$(\ln\eta)^{E} = \ln\eta_{mix} - (x_1 \ln\eta_1 + x_2 \ln\eta_2) \qquad (5.10)$$

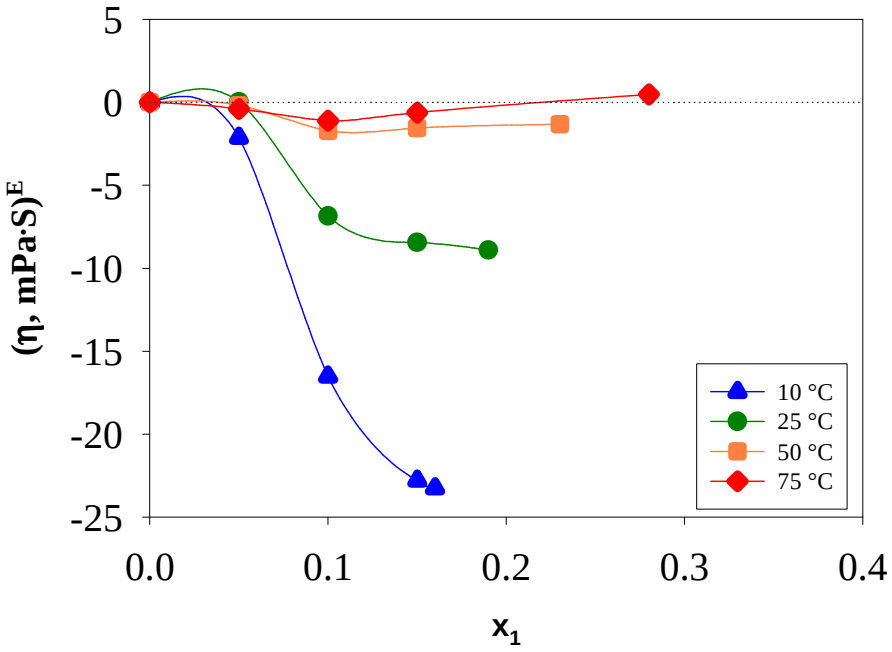

Figure 5-10 The effect of 1-octene (1) concentration on excess viscosity (mPa·s) of its mixture with [HMIm][Tf_2N] (2) at different isotherms. Lines are smoothed data.

The negative values of excess viscosity (Figure 5-10) matches with the negative amounts of excess molar volume reported in our previous paper. [42] (Section 5.1.3) The negative trend for both of these properties represents the effect of presence of octene in the free volume of ionic liquid structure. The more deviation at higher concentrations of 1-octene and lower temperatures shows the lower stability of 1-octene molecules in cations and anions because of their strong interactions. Excess viscosities at higher temperatures (50°C, 75 °C) are close to the ideal behavior.

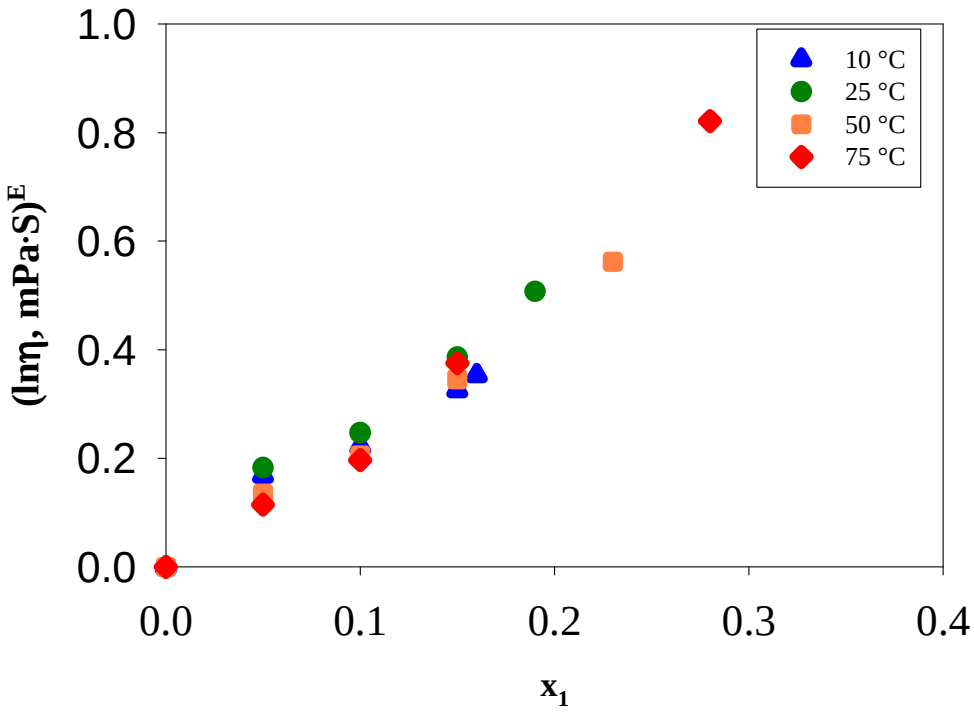

Figure 5-11 Excess logarithm viscosities $(\ln \eta)^E$

The reason is possibly because of the enough free volume available between ions at high temperatures for 1-octene.

Mutual self diffusivities of 1-octene and cation of [HMIm][Tf_2N] at two temperatures are shown in Table 5-11, Figure 5-12, and Figure 5-13. [43] Diffusivity of cation of IL at 25°C and 50°C (for pure IL is $1.67*10^{-11}$ m^2/s at 25 °C and $5.54*10^{-11}$ m^2/s at 50 °C) is increased about 40-45% by adding 1-octene up to the saturation condition. The diffusivity of pure 1-octene at 25°C is $228.3*10^{-11}$ m^2/s and $344.2*10^{-11}$ m^2/s.

Table 5-11 The diffusivity for pure 1-octene (1) + cation of [HMIm][Tf_2N] (2) and their mixtures at different temperatures			
T=25°C			
x_1	**D_{21} *10^{11}(m^2/s)**	x_1	**D_{12}*10^{11}(m^2/s)**
0	1.67	0	1.7
0.01	1.81	0.05	6.5
0.05	1.96	0.1	7.4
0.1	2.13	0.15	9.0
0.15	2.33	0.19	9.1
0.19	2.44	1	228.3
1	228.3		
T=50°C			
x_1	**D_{21} *10^{11}(m^2/s)**	x_1	**D_{12} *10^{11}(m^2/s)**
0	5.54	0	5.5
0.01	5.67	0.05	26.3
0.05	6.50	0.1	29.3
0.1	7.30	0.15	31.3
0.15	7.67	0.23	30.8
0.23	7.73	1	344.2
1	344.17		

Also, diffusivity of 1-octene molecules into [HMIm][Tf_2N] is enhanced 40% at 25°C for concentrations from 5% to 19%. However, at the same condition and 50°C adding 1-octene can enhance the diffusivity just 17%. Increasing self diffusivity with the concentration of 1-octene and temperature is because of their effects on strong electrostatic forces and interactions between cations and anions in IL molecules. [44]

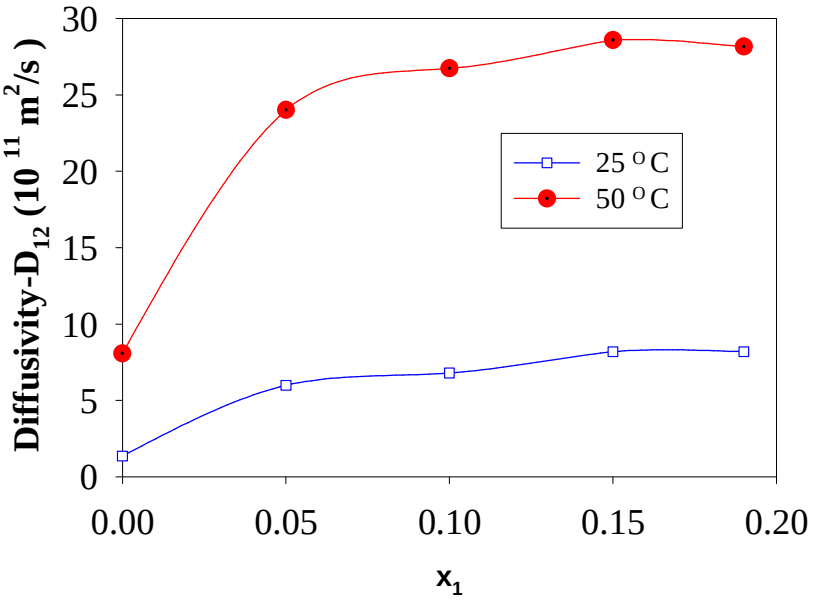

Figure 5-12 Diffusivity of 1-octene (1) at different concentrations in [HMIm][Tf_2N] (2) at two isotherms. Lines are smoothed data.

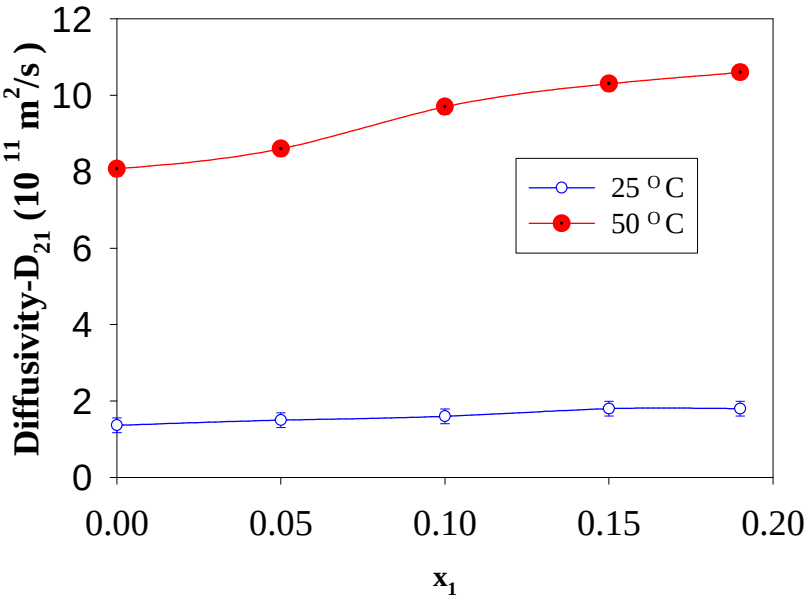

Figure 5-13 The effect of concentration of 1-octene (1) on diffusivity of cation of [HMIm][Tf_2N] (2) at two different temperatures. Lines are smoothed data.

5.3 Summary

Ionic liquids have a number of applications in multiphase reactions, extractions, and material processing. However, for an accurate understanding of the mass transfer, the phase equilibrium and thermodynamic properties must be understood, especially the effect of concentration. This investigation measured thermodynamic and interfacial properties for the system of 1-hexyl-3-methylimidazolium bis(trifluoromethylsulfonyl)amide ([HMIm][Tf_2N]) and 1-octene, focusing on both the pure components and mixtures. Liquid-liquid equilibrium data indicated that the ionic liquid exhibits minimal solubility in the 1-octene phase, whereas 1-octene has moderate solubility in the IL phase. Thus, mass transfer when the two components are mixed would occur in virtually one direction. The NRTL model satisfactorily correlated the LLE data with just a slight under-prediction of the 1-octene fraction in each phase. The density of the ionic liquid decreases about -6.3% when the concentration of 1-octene increases from 0% to 15%. Increasing temperature from 10°C to 75°C makes the density of IL decrease -4.4%. So, increasing just a small amount of 1-octene can considerably decrease the density of IL.

The excess molar volume for the mixture of ionic liquids and 1-octene is slightly negative for all isotherms. Air-liquid surface tensions of mixtures of the IL/1-octene have been measured along with saturated interfacial tensions of the two phases.

Transport properties of ([HMIm][Tf_2N]) with 1-octene are also determined in different isotherms (10, 25, 50, and 75°C). The result showed that the viscosity of IL decreases with adding 1-octene concentration and temperature. The reason for this trend can probably be inferred from the electrostatic interactions between cations and anions in IL molecules and molecules of 1-octene. The negative values of excess viscosity and the negative amounts of excess molar volume represented the effect of presence of octene in the free volume of ionic liquid structure.

The achievements and results of this chapter now provide us with the useful information to study interfacial liquid-liquid mass transfer through a contact column. So, the physical and thermodynamic properties, which are necessary to find dimensionless groups and the overall mass transfer coefficient, are available for further studies of the next chapter.

5.4 References

1. Anon., Thermodynamics of Ionic Liquids, Ionic Liquid Mixtures, and the Development of Standardized Systems. *Chem. Int.* **2005,** 27, 5, 22-23.
2. Petera, J.; Weatherley, L. R., Modelling of mass transfer from falling droplets. *Chem. Eng. Sci.* **2001,** 56, 16, 4929-4947.
3. Seddon, K. R.; Stark, A.; Torres, M. J., Influence of chloride, water, and organic solvents on the physical properties of ionic liquids. *Pure Appl. Chem.* **2000,** 72, 12, 2275-2287.
4. Seddon, K. R., Ionic liquids for clean technology. *J. Chem. Technol. Biotechnol.* **1997,** 68, 4.
5. Welton, T., Room-temperature ionic liquids. Solvents for synthesis and catalysis. *Chem. Rev.* **1999,** 99, 8, 2071-2083.
6. Wasserscheid, P.; Keim, W., Ionic liquids - New "solutions" for transition metal catalysis. *Angew. Chem. Int. Ed.* **2000,** 39, 21, 3773-3789.
7. Pandey, S., Analytical applications of room-temperature ionic liquids: A review of recent efforts. *Anal. Chim. Acta* **2006,** 556, 1, 38-45.
8. Murugesan, S.; Linhardt, R. J., Ionic Liquids in Carbohydrate Chemistry–Current Trends and Future Directions. *Curr. Org. Synth.* **2005,** 2, 4, 437-451.
9. Prausnitz, J. M.; Lichtenthaler, R. N.; de Azevedo, E. G., *Molecular thermodynamics of fluid-phase equilibria*. Prentice Hall PTR: **1986**.
10. Favre, F.; Olivier-Bourbigou, H.; Commereuc, D.; Saussine, L., Hydroformylation of 1-hexene with rhodium in non-aqueous ionic liquids: how to design the solvent and the ligand to the reaction. *Chem. Comm.* **2001**, 15, 1360-1361.
11. Wasserscheid, P.; Hilgers, C.; Gordon, C. M.; Muldoon, M. J.; Dunkin, I. R., Ionic liquids: polar, but weakly coordinating solvents for the first biphasic oligomerisation of ethene to higher α-olefins with cationic Ni complexes. *Chem. Comm.* **2001**, 13, 1186-1187.
12. Brasse, C. C.; Englert, U.; Salzer, A.; Waffenschmidt, H.; Wasserscheid, P., Ionic Phosphine Ligands with Cobaltocenium Backbone: Novel Ligands for the Highly Selective, Biphasic, Rhodium-Catalyzed Hydroformylation of 1-Octene in Ionic Liquids. *Organometallics.* **2000,** 19, 19, 3818-3823.
13. Stark, A.; Ajam, M.; Green, M.; Raubenheimer, H. G.; Ranwell, A.; Ondruschka, B., Metathesis of 1-Octene in Ionic Liquids and Other Solvents: Effects of Substrate Solubility, Solvent Polarity and Impurities. *Adv. Synth. Catal.* **2006,** 348, 14.
14. Lei, Z.; Arlt, W.; Wasserscheid, P., Separation of 1-hexene and n-hexane with ionic liquids. *Fluid Phase Equil.* **2006,** 241, 1-2, 290-299.
15. Domanska, U.; Marciniak, A., Solubility of 1-Alkyl-3-methylimidazolium Hexafluorophosphate in Hydrocarbons. *J. Chem. Eng. Data* **2003,** 48, 3, 451-456.
16. Jiqin, Z.; Jian, C.; Chengyue, L.; Weiyang, F., Study on the separation of 1-hexene and trans-3-hexene using ionic liquids. *Fluid Phase Equil.* **2006,** 247, 1-2, 102-106.
17. Meindersma, G. W.; Podt, A. J. G.; de Haan, A. B., Ternary liquid–liquid equilibria for mixtures of toluene+ n-heptane+ an ionic liquid. *Fluid Phase Equil.* **2006,** 247, 1-2, 158-168.
18. Munson, C. L.; Boudreau, L. C.; Driver, M. S.; Schinski, W. L., Separation of olefins from paraffins using ionic liquid solutions. In US Patents- 6 339 182 **2002**.

19. Munson, C. L.; Boudreau, L. C.; Driver, M. S.; Schinski, W. L., Separation of olefins from paraffins using ionic liquid solutions. In US Patents- 6 623 659: **2003**.
20. Nebig, S.; Bölts, R.; Gmehling, J., Measurement of vapor–liquid equilibria (VLE) and excess enthalpies (H^E) of binary systems with 1-alkyl-3-methylimidazolium bis (trifluoromethylsulfonyl) imide and prediction of these properties and using modified UNIFAC (Dortmund). *Fluid Phase Equil.* **2007,** 258, 2, 168-178.
21. Liebert, V.; Nebig, S.; Gmehling, J., Experimental and predicted phase equilibria and excess properties for systems with ionic liquids. *Fluid Phase Equil.* **2008,** 268, 1-2, 14-20.
22. Nebig, S.; Liebert, V.; Gmehling, J., Measurement and prediction of activity coefficients at infinite dilution, vapor–liquid equilibria (VLE) and excess enthalpies (H^E) of binary systems with 1, 1-dialkyl-pyrrolidinium bis (trifluoromethylsulfonyl) imide using mod. UNIFAC (Dortmund). *Fluid Phase Equil.* **2009,** 277, 1, 61-67.
23. Abbas, R.; Gmehling, J., Vapour–liquid equilibria, azeotropic data, excess enthalpies, activity coefficients at infinite dilution and solid–liquid equilibria for binary alcohol–ketone systems. *Fluid Phase Equil.* **2008,** 267, 2, 119-126.
24. Wang, B.; Kang, Y. R.; Yang, L. M.; Suo, J. S., Epoxidation of a, ß-unsaturated carbonyl compounds in ionic liquid/water biphasic system under mild conditions. *J. Mol. Cat. A* **2003,** 203, 1-2, 29-36.
25. Wang, J.; Zhu, A.; Zhao, Y.; Zhuo, K., Excess molar volumes and excess logarithm viscosities for binary mixtures of the ionic liquid 1-butyl-3-methylimidazolium hexaflurophosphate with some organic compounds. *J. Solution Chem.* **2005,** 34, 5, 585-596.
26. Heintz, A.; Klasen, D.; Lehmann, J. K., Excess molar volumes and viscosities of binary mixtures of methanol and the ionic liquid 4-methyl-N-butylpyridinium tetrafluoroborate at 25, 40, and 50 ^oC. *J. Solution Chem.* **2002,** 31, 6, 467-476.
27. Cadena, C.; Anthony, J. L.; Shah, J. K.; Morrow, T. I.; Brennecke, J. F.; Maginn, E. J., Why is CO_2 so soluble in imidazolium-based ionic liquids? *J. Am. Chem. Soc.* **2004,** 126, 16, 5300-5308.
28. Hanke, C. G.; Atamas, N. A.; Lynden-Bell, R. M., Solvation of small molecules in imidazolium ionic liquids: a simulation study. *Green Chem.* **2002,** 4, 2, 107-111.
29. Lopes, J. N. C.; Cordeiro, T. C.; Esperanca, J.; Guedes, H. J. R.; Huq, S.; Rebelo, L. P. N.; Seddons, K. R., Deviations from ideality in mixtures of two ionic liquids containing a common ion. *J. Phys. Chem. B* **2005,** 109, 8, 3519-3525.
30. Huddleston, J. G.; Visser, A. E.; Reichert, W. M.; Willauer, H. D.; Broker, G. A.; Rogers, R. D., Characterization and comparison of hydrophilic and hydrophobic room temperature ionic liquids incorporating the imidazolium cation. *Green Chem.* **2001,** 3, 156-164.
31. Law, G.; Watson, P. R., Surface tension measurements of N-alkylimidazolium ionic liquids. *Langmuir* **2001,** 17, 20, 6138-6141.
32. Dzyuba, S. V.; Bartsch, R. A., Influence of structural variations in 1-alkyl (aralkyl)-3-methylimidazolium hexafluorophosphates and bis (trifluoromethylsulfonyl) imides on physical properties of the ionic liquids. *ChemPhysChem* **2002,** 3, 2, 160-166.
33. Kimura, T.; Fujita, M.; Ando, T., Sonochemical and photochemical reactions of bromotrichloromethane in the presence and absence of 1-alkene. *Ultrason. Sonochem.* **1999,** 6, 1-2, 93-96.

34. Jasper, J. J., The surface tension of pure liquid compounds. *J. Phys. Chem. Ref. Data* **1972,** 1, 4, 841–1009.
35. Domanska, U.; Marciniak, A., Activity coefficients at infinite dilution measurements for organic solutes and water in the ionic liquid triethylsulphonium bis (trifluoromethylsulfonyl) imide. *J. Chem. Thermodyn.* **2008**.
36. Carvalho, P. J.; Freire, M. G.; Marrucho, I. M.; Queimada, A. J.; Coutinho, J. A. P., Surface Tensions for the 1-Alkyl-3-methylimidazolium Bis (trifluoromethylsulfonyl) imide Ionic Liquids. *J. Chem. Eng. Data* **2008,** 53, 6, 1346-1350.
37. Matsuda, T.; Mishima, Y.; Azizian, S.; Matsubara, H.; Takiue, T.; Aratono, M., Interfacial tension and wetting behavior of air/oil/ionic liquid systems. *Colloid Polym. Sci.* **2007,** 285, 14, 1601-1605.
38. VanOss, C. J., Interface Forces in Aqueous Media. In Marcel Dekker, New York: **1994**.
39. Price, W., Pulse-Field Gradient Nuclear Magnetic Resonance as a Tool for Studying Translational Diffusion: Part 1. *Basic Theory, Conepts Magn. Reson* **1997,** 9, 299-336.
40. Ahosseini, A.; Ren, W.; Weatherley, L.; Scurto*, A., Viscosity and Self-Diffusivity of the Ionic Liquid, 1-hexyl-3-methylimidazolium bis(trifluoromethylsulfonyl)amide with Compressed 1,1,1,2-Tetrafluoroethane (R-134a). **2009**, In preparation.
41. Schleicher, J. C., Kinetics and Solvent Effects in the Synthesis of Ionic Liquids. **2007**.
42. Ahosseini, A.; Sensenich, B.; Weatherley, L.; Scurto, A., Phase Equilibrium, Volumetric, and Interfacial Properties of the Ionic Liquid, 1-Hexyl-3-Methyl-Imidazolium Bis(Trifluoromethylsulfonyl)amide and 1-Octene. *J. Chem. Eng. Data* **Accepted**.
43. Ahosseini, A.; Ortega, E.; Sensenich, B.; Scurto, A. M., Viscosity of n-alkyl-3-methyl-imidazolium bis (trifluoromethylsulfonyl) amide ionic liquids saturated with compressed CO_2. *Fluid Phase Equil.* **2009,** 286, 1, 62-68.
44. Tokuda, H.; Ishii, K.; Susan, M.; Tsuzuki, S.; Hayamizu, K.; Watanabe, M., Physicochemical Properties and Structures of Room-Temperature Ionic Liquids. 3. Variation of Cationic Structures. *J. of phys. chem. B, Condensed matter, materials, surfaces, interfaces, & biophysical chemistry* **2006,** 110, 6, 2833-2839.
45. Harris, K. R.; Malhotra, R.; Woolf, L. A., Temperature and density dependence of the viscosity of octane and toluene. *J. Chem. Eng. Data* **1997,** 42, 6, 1254-1260.
46. Crosthwaite, J. M.; Muldoon, M. J.; Dixon, J. K.; Anderson, J. L.; Brennecke, J. F., Phase transition and decomposition temperatures, heat capacities and viscosities of pyridinium ionic liquids. *J. Chem. Thermodyn.* **2005,** 37, 6, 559–568.
47. Ahosseini, A.; Scurto, A. M., Viscosity of Imidazolium-Based Ionic Liquids at Elevated Pressures: Cation and Anion Effects. *Int. J. Thermophys.* **2008,** 29, 4, 1222-1243.
48. Tokuda, H.; Hayamizu, K.; Ishii, K.; Susan, M.; Watanabe, M., Physicochemical properties and structures of room temperature ionic liquids. 2. Variation of alkyl chain length in imidazolium cation. *J. Phys. Chem. B* **2005,** 109, 13, 6103-6110.

49. Harris, K. R.; Alexander, J. J.; Goscinska, T.; Malhotra, R.; Woolf, L. A.; Dymond, J. H., Temperature and density dependence of the selfdiffusion coefficients of liquid n-octane and toluene. *Mol. Phys.* **1993,** 78, 1, 235-248.

Chapter 6 Interfacial mass transfer studies in biphasic ([HMIm][Tf_2N)-(1-octene) system

6 Interfacial mass transfer studies in a biphasic (ionic liquid)-(1-octene) system

In this chapter the mass transfer phenomenon from a continuous phase (1-octene) (component 1) to a droplet of IL ([HMIm][Tf_2N]) (component (2)) are studied by measuring concentration over time under a variety of geometries and hydrodynamic conditions.(Figure 6-1)

The procedure for experiments and analysis and descriptions of equipment are explained in detail in Chapter 2.

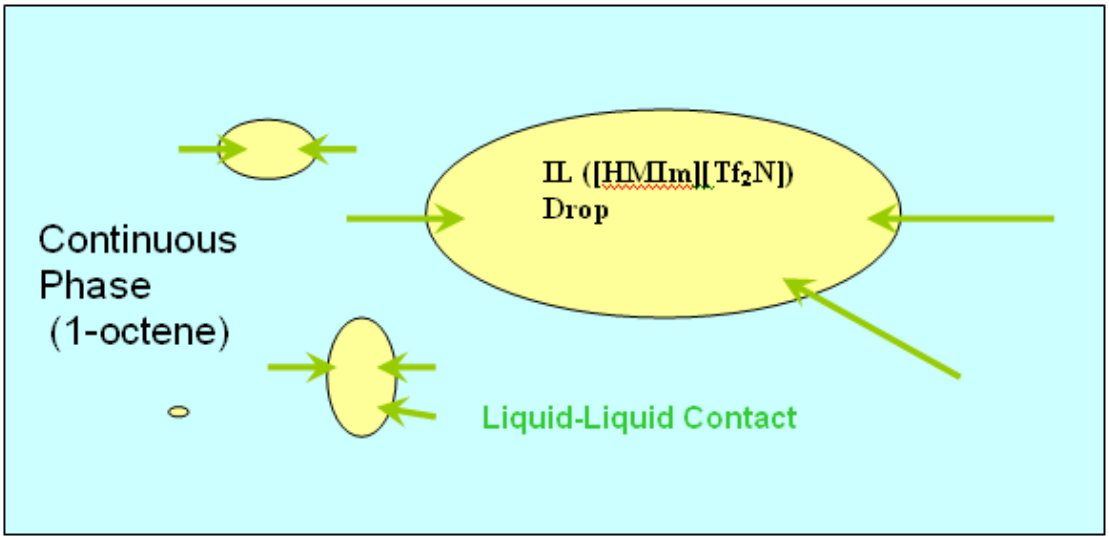

Figure 6-1 Liquid - liquid mass transfer between droplets and the continuous phase

6.1 Introduction

Varieties of applications of ionic liquids (ILs) are often based upon biphasic liquid-liquid systems which are being developed for extraction [1-3], absorption -desorption in spectroscopy [4], and chemical reactions [5-7]. However, there is a lack of information for systems involving ionic liquids in interfacial mass transfer area. So, in this work, liquid-liquid biphasic systems with ionic liquids have been studied, and as it is mentioned above, a system of [HMIm][Tf_2N] droplets interacting with the continuous 1-octene phase is selected for this study.

For fundamental studies in interfacial mass transfer, the phase equilibrium and thermodynamic properties must be deeply understood. These properties are often concentration dependent. Thus, momentum and mass transfer equations must be solved simultaneously for predicting the concentration versus time and the location.

Fluid mechanics (Navier-Stockes, (1)) and mass transfer (Fickian, (2)) equations are shown as follows: [8]

$$\rho_p\left(\frac{\partial \mathbf{u}_p}{\partial t}+\mathbf{u}_p\cdot\nabla\mathbf{u}_p\right)=\nabla\cdot\boldsymbol{\Gamma}_p \qquad \nabla\cdot\mathbf{u}_p=0$$
$$\boldsymbol{\Gamma}_p=-P_p\mathbf{I}+2\eta_P\mathbf{D}_p \qquad \mathbf{D}_p=0.5\left(\nabla\mathbf{u}_p+\left(\nabla\mathbf{u}_p\right)^{\mathrm{T}}\right) \tag{6.1}$$

$$\left(\boldsymbol{\Gamma}_{p2}-\boldsymbol{\Gamma}_{p1}\right)\cdot\mathbf{n}=2H\sigma\mathbf{n}$$

$$\frac{\partial C_{a,p}}{\partial t}+\mathbf{u}_p\cdot\nabla C_{a,p}\mathbf{u}_p=\nabla\cdot\left(\frac{D_{a,p}}{1-\omega_{a,p}}\nabla C_{a,p}\right) \tag{6.2}$$

where $\rho \equiv$ density; $u \equiv$ Velocity vector; $\Gamma \equiv$ stress tensor; $P \equiv$ pressure; $\eta \equiv$ viscosity; $H \equiv$ Curvature; $\sigma \equiv$ interfacial tension; Subscript *"p"* represents each phase; $C \equiv$ Concentration; $\omega \equiv$ weight fraction; $u \equiv$ Velocity; and $D \equiv$ Diffusivity.

The model of Petera and Weatherley [8] has been found applicable to solve these equations and predict the concentration change of falling spherical segregated droplets using a robust, efficient, and realistic finite element method.

In Chapter 5, the liquid-liquid equilibrium envelope at the ambient pressure was developed for the 1-octene/[HMIm][Tf_2N] system. The results showed that mass transfer will only happen in virtually one direction especially at lower temperatures. Experiments yielded the equilibrium concentrations at four isotherms. Also, thermodynamic and transport properties of [HMIm][Tf_2N] at different concentrations of 1-octene in several isotherms have been measured. In the current chapter, all of these results have been used to study mass transfer phenomenon between segregated droplets of IL ([HMIm][Tf_2N]) and 1-octene continuous phase through a liquid-liquid contact column. In order to obtain

a general relationship between dimensionless groups and determine the overall mass transfer coefficient, quantifying the diameter and velocity of droplets as well as the concentration of 1-octene in dispersed phase (IL) throughout the column is required.

In the following sections, thorough studies are discussed on the liquid-liquid contact column and a high speed optical system is introduced to find diameter and velocity of droplets falling into the column.

6.2 Interfacial mass transfer studies

6.2.1 Modeling

As it has been determined in Chapter 5, the [HMIm][Tf_2N] solubility in 1-octene specially at room temperature is negligible. Thus, the mass transfer occurs only in one direction. Based upon this result and supported from the experimental data for thermodynamic and transport properties of two phases (Chapter 5), a model has been developed by Professor Jerzy Petera from the Technical University of Łódź, Poland. In this model a finite element method is used to solve momentum and mass transfer equations simultaneously to find the concentration change with time at each point of the mass transfer region. The result of this model is shown in Figure 6-2. This figure demonstrates the progress of diffused 1-octene (continuous red zone) into the droplet (the blue sphere) after 3s, 8s, 11s, and 14s of fall. The pattern of concentration (green and light blue regions on the droplet) shows the effect of time and the falling length on the mass transfer rate. As can be seen, the diffusion of 1-octene into the ionic liquid droplet increases with the falling time. White meshes, which are determined by the finite element method, show the flow pattern around and inside of the droplet.

6.2.2 Experiments

6.2.2.1 Liquid-Liquid contact column

To support the above model it is necessary to have enough data. More data can provide a better model that is able to interpret transport phenomena for falling droplets of ionic liquids into a column filled with 1-octene. For instance, knowing the effect of temperature, pressure, droplet size, and falling height on mass transfer phenomena can help to have an improved model.

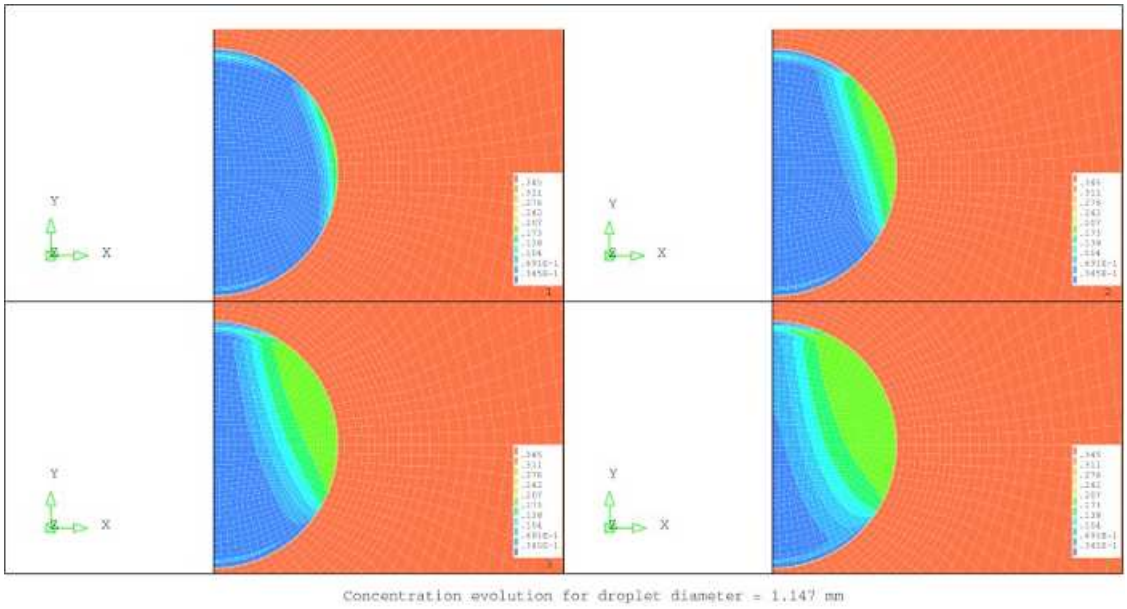

Figure 6-2 The 1-octene concentration evolution inside the falling ionic liquid drop. The consecutive pictures correspond to 3s, 8s, 11s and 14s of the flight time. *Modeling* courtesy of Prof. Jerzy Petera

As it has been described in Chapter 2, the mass transfer phenomenon from a continuous phase to a disperse media can be followed in a simple column (Figure 6-3). In these experiments, [HMIm][Tf_2N] droplets are falling discretely through 1-octene continuous phase in a long column and creating the streamlines for flow around and within the droplets as can be seen in Figure 6-3. 1-octene moves upward relative to each falling ionic liquid and circulating happens inside of the droplets because of interfacial tension between phases and their relative velocities. These movements and circulations help 1- octene molecules to transfer inside the ionic liquid droplets. The ionic liquid is collected from the bottom of column after passing through a layer of water to quench the mass transfer. In each batch, 3 mL of ionic liquid are collected and separated from water by decanting. The concentration of 1-octene in droplets at the end of column (C_f) is measured by an NMR method.

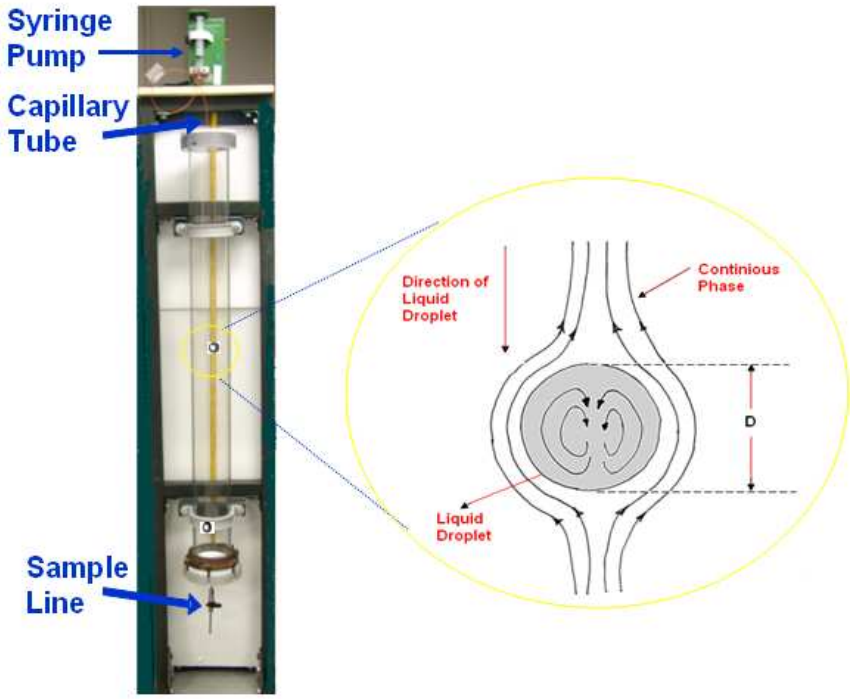

Figure 6-3 The liquid-liquid contact column and interfacial flow patterns

As it has been shown before, the mole ratio (intensity ratio) obtained from NMR spectroscopy represents the moles of 1-octene per one mole of IL; so, it should be translated to the mole fraction and molarity of 1-octene in the solution. The mole fraction of 1-octene in the ionic liquid sample (x_1) can be obtained directly from the NMR measurements.

x_1= (Mole ratio)/(1+Mole ratio) (6.3)

Mole ratio = Mole 1-octene/ Mole IL (6.4)

The concentration (molarity) of 1-octene in ionic liquid droplets at the end of column (C_{1f}) is determined by using the density of mixture $\rho_{(m)}$ and the mole fraction of 1-octene (x_1) as demonstrated in Table 6-1. The amount of density of mixture (ρ_{mix}) at each concentration was measured earlier and derived from Chapter 5.

Fitting the data for the concentration of 1-octene (C_1) against mole fractions ($x_{1)}$ gives the following equation:

$$C_{1f} = 3.4249 * x_1 - 0.0072 \quad (6.5)$$

Table 6-1 Concentration of 1-octene (mole/L) at the end of mass transfer process inside the column. T=25°C, MW_2([HMIm][Tf_2N])= 447.4 MW_1(1-Octene)= 112.2		
x_1	$\rho_{(m)}$	$C_{1f}=1000*\rho_m*x_1/(x_1*MW_1+x_2*MW_2)$
0	1.371	0
0.01	1.369	0.031
0.05	1.36	0.158
0.1	1.344	0.325
0.15	1.326	0.501
0.19	1.323	0.644
1	0.711	6.338

Now the column efficiency, which is equal to the outlet concentration of drops over equilibrated concentration (C_f / C_{eq}) can be determined. However, since the size and shape of droplets can affect the outlet concentration and so the efficiency of the column, these parameters have been determined in the following sections.

6.2.2.2 The high speed optical system

To discover the droplet shape, size and velocity during the formation and falling into the continuous phase having a very apparent and clear imagine is needed. Because of the large difference between the density of ionic liquid droplets and the Newtonian continuous 1-octene phase, the falling rate of drops is very fast. Also, the drops are transparent and have no color contrasts with the continuous phase. So, using just ordinary cameras cannot help to distinguish the phase differences that have no color disparity. Also, using any dye is not suggested to make droplets colored because of the probable interferes on the mass transfer studies. Thus, a special technique is needed as well as a fast camera to take an obvious picture of transparent falling drops. This technique is able to visualize the falling of ionic liquid droplets in a transparent medium with a great precision. As shown in Figure 6-4, the basic set up for this optical system contains a telecentric lens connected to a FireWire CCD color camera (Edmund optics – AVT PIKE F-100B MONO 2/3IN) and a light source. The light source goes through the testing container (L*W*H=10*10*15 cm) and the lens transfers the light beam parallel to the

camera. This camera is able to take up to 60 images per second with the resolution of 1000 * 1000 pixels. (See Chapter 2 for detail instructions)

This high speed optical system is used to prepare desired images. Besides, the ImageJ program developed at the National Institutes of Health is used to process and measure the area and diameter of drops.

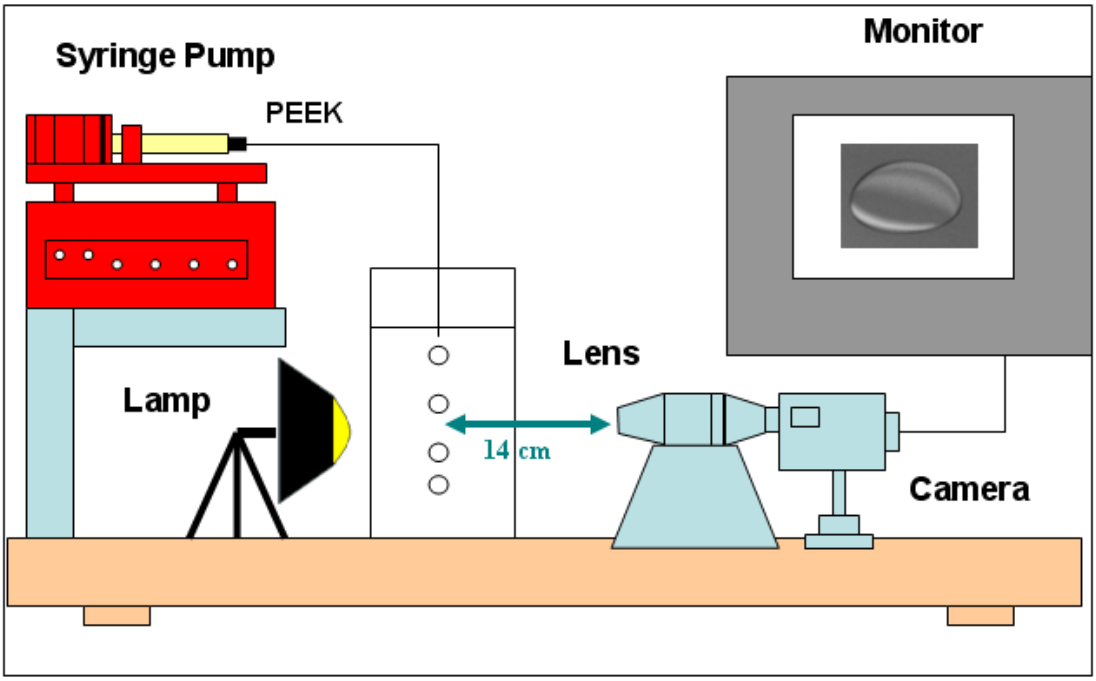

Figure 6-4 The high speed optical system

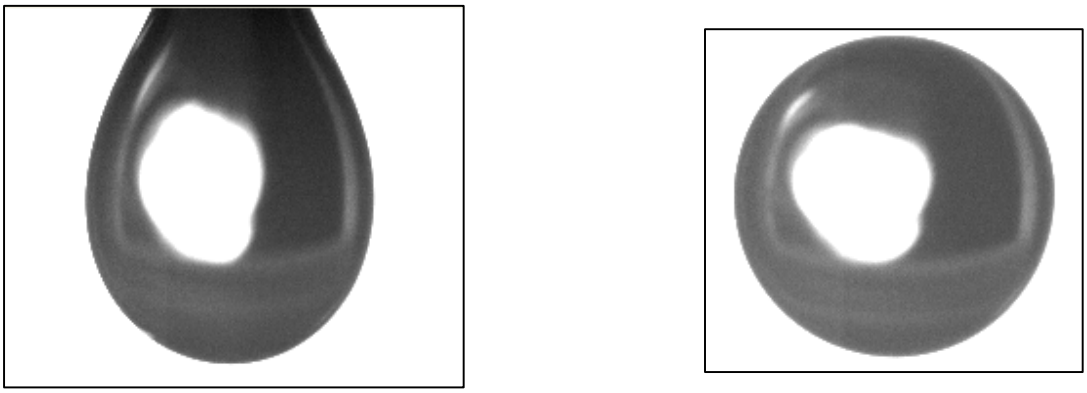

Figure 6-5 The picture of an ionic liquid droplet in air
a) Leaving the tube in the air
b) Falling into the air

Pictures obtained from the high speed camera showed that the shape of ionic liquid droplets inside the 1-octene phase is not spherical, as it looks to the naked eye, but oval (Figure 6-4). However, the pictures of the droplets falling into the air have a spherical shape (Figure 6-5 a,b). So, the shape of droplets is related to the interfacial tension and interactions between two phases.

The other important point in these studies is monitoring the formation of droplets during leaving the tube that may affect the droplet shape, size, and mass transfer results.

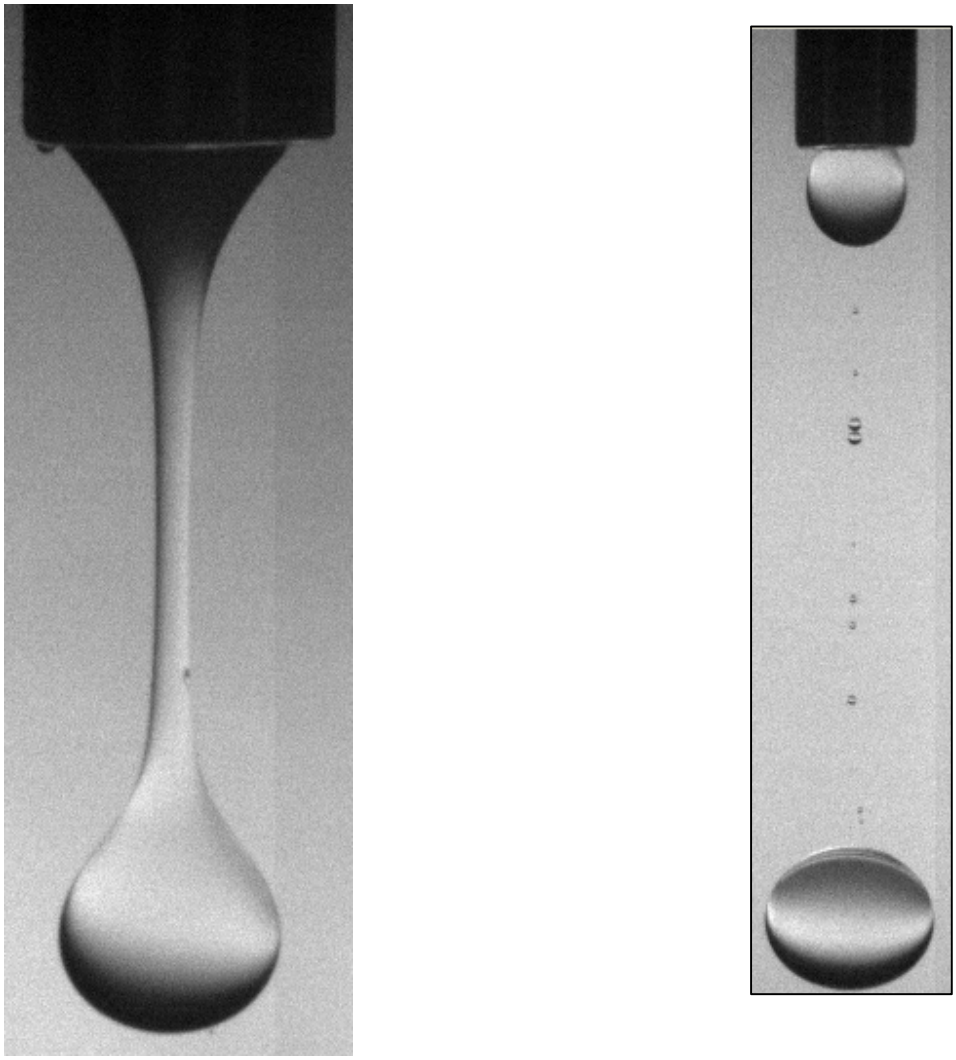

Figure 6-6 a: A droplet of ionic liquid falling into the 1-octene phase, b: Satellite droplets

Figure 6-6 a and b show the formation of tiny droplets of ionic liquid behind a big drop falling into the 1-octene phase. In this study, the effect of these small satellites, which have different shapes and sizes, in mass transfer has been ignored.

Figure 6-7 a and b demonstrate the formation of droplets through a stainless steel and a PEEK tube. As can be seen, the ionic liquid droplet spreads out on the outside diameter of the PEEK tube during leaving it. The reason possibly is due to the adhesive forces between the tube and the ionic liquid droplet. This effect has not been seen using stainless steel tubes because of the low cohesiveness between the droplet and tube. So, in order to study the effect of diameter of droplets on mass transfer efficiency, the different outlet diameters for PEEK tubes should be selected to create various sizes of drops.

6.2.2.3 Study the size alteration of droplets through the column

To find the overall mass transfer coefficient and to model the interfacial mass and momentum transfer, the shape and size of droplets through the falling into the column should be determined. Since in the current condition, *in situ* monitoring of the droplets by using the high speed optical system is not applicable, it is suggested to use a testing container. However, firstly, it should be confirmed that the changing of the droplet size through the column is not considerable.

As it is illustrated before, the droplets of ionic liquids interact with 1-octene during falling into the column. Because the mass transfer occurs just in one direction from 1-octene to the droplet of ionic liquids, the concentration of 1-octene increases in ionic liquid phase that can affect the size of droplets. In order to determine the maximum changing of the droplet size falling through the column, the mass of 1-octene transferred from the continuous phase to the droplet of IL should be calculated. So, it can be written as follows:

Mass of 1-octene transferred = (mass of droplet) out – (mass of droplet) in

$$V_i \rho_{IL} = (V_f \rho_f) * (1 - x_{1f} * MW_{oct} / MW_m) \qquad (6.6)$$

$$V_i / V_f = (\rho_f / \rho_{IL}) * (1 - x_{1f} * MW_{oct} / MW_m) \qquad (6.7)$$

Where ρ_f is the density of mixture at the end of column, ρ_{IL} is the density of droplet entering the column that is equal to the density of pure ionic liquid. Vi and V_f are

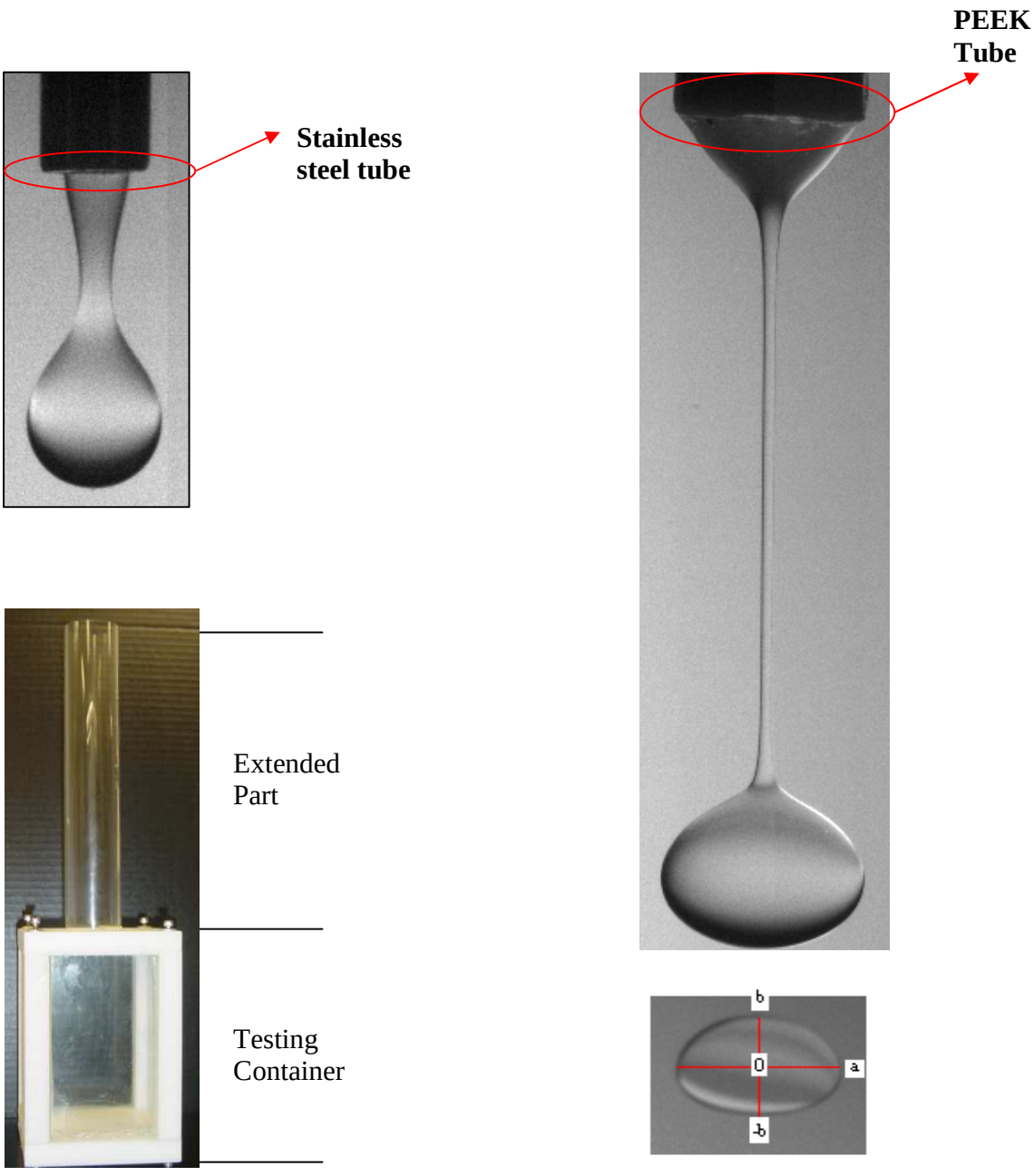

Figure 6-7 Falling droplets from a) a stainless steel tube b) a PEEK tube
Figure 6-8 Testing container
Figure 6-9 Elliptic shape of a droplet in the 1-octene phase

volumes of the inlet and outlet droplet, MW_{Oct} and MW_f are molecular weight of pure 1-octene and the droplet collecting from the end of column, and x_{1f} is the mole fraction of 1-octene in the ionic liquid droplet when the mass transfer terminated. The results showed in Table 6-2 illustrate the small changing of the diameter of droplets through the column (d_f/d_i) is negligible. So, the droplets can be monitored through a testing container. (Figure 6-8)

Table 6-2 Increasing the diameter of drops through the column (h=2.3 m)

D_{tube} (mm)	x_{1f}	C_f (mole/L)	ρ_f ($gr \cdot cm^{-3}$)	ρ_{IL} ($gr \cdot cm^{-3}$)	V_f/V_i	d_f/d_i
IDss =1.8	0.0598	0.1977	1.3565	1.3711	1.0269	1.0089
OD_{PEEK} =1.59	0.0619	0.2049	1.3558	1.3711	1.028	1.0093
IDss = 0.6	0.0879	0.294	1.3464	1.3711	1.0429	1.0141

6.2.2.4 Measuring velocity and diameter of droplets

To obtain the terminal velocity and diameter of droplets using the camera, the scale ratio (the size of the picture comparing to the real dimension) should be determined. On the way to find this scale, a calibration target has been used as explained in detailed in Chapter 2. To use the target, it is very important to hang it perpendicularly and at the same position with falling droplets into the container. If the bottom of the container is considered to be at xy surface, then z will be at the same direction with the height of the container, and then the target plate should stand exactly in the yz position. Any deviation from this plane can affect the measurement and ruin the result. Since it is very difficult to keep the target precisely at this surface, we should hang it free so that at least the vertical dimension can be consistent.

By knowing the length of the squares in the target, the scale ratio can be determined, and with this number, the distance that the droplet falls between two consecutive frames can be calculated. This length times the frame rate (60 sec^{-1}) will provide the velocity of the droplet. (Figure 6-10)

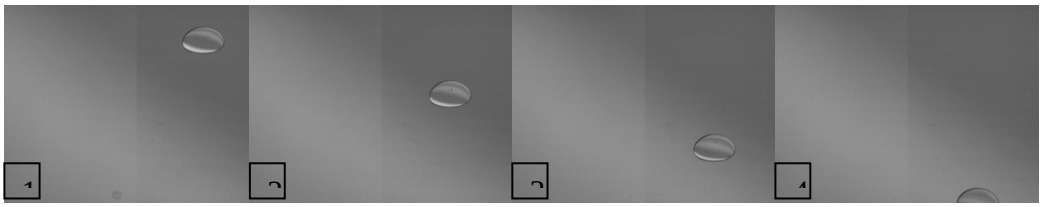

Figure 6-10 Consecutive frames for measuring the velocity of drops

To measure the diameter of droplets (the biggest diameter of the elliptical shape, 2a in (Figure 6-9) the ImageJ software is used and calibrated. For this calibration the amount of outside diameter of the stainless steel injector, which situates horizontally and its size is available accurately, is used. Table 6-3 shows the results of measured diameter and velocity of droplets produced by different tubes.

Table 6-3 Diameter and velocity of droplets

D_{tube} (mm)	Ellipsoid droplet diameters (Major axis horizontal) (D_E)mm	Avg.(v)m/s camera	Avg.(v)m/s timer
ID_{ss} =1.8	2.09 ± 0.04	----------	0.153 [a] ± 0.03
OD_{PEEK} =1.59	1.84 ± 0.04	0.143 ± 0.007	0.144 ± 0.003
ID_{ss} = 0.6	1.32 ± 0.04	0.112 ± 0.011	0.115 ± 0.003

[a] Because of the high speed of droplets in this case, using the camera could not help. This amount is measured from the length of moving droplets through the column (2.3 m) divided by the falling time.

6.2.2.5 Equivalent diameter

As it is mentioned before, the picture of the droplet shows that it is elliptical. To model this system, calculating the volume of the droplet is needed as well as the equivalent diameter of the droplet with an equal spherical volume. The volume of the object can be created by rotating the plane of “boa” around “a” or “b”. 2a and 2b are the biggest and smallest diameters as are shown in Figure 6-11. 2c is the width of the

ellipsoid droplet. In this study, 2c is assumed to be equal to 2b because of the selected rotation axis (a). (Figure 6-11)

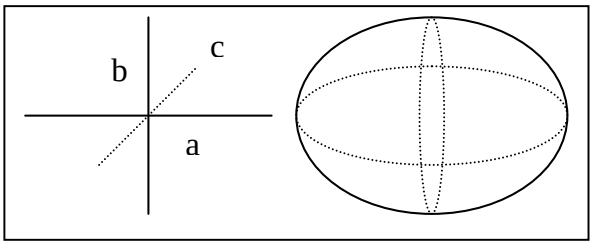

Figure 6-11 Ellipsoid dimensions

$$V = 2\int_0^a \pi f^2(x) \qquad (6.8)$$

$$\frac{y^2}{b^2} + \frac{x^2}{a^2} = 1 \qquad (6.9)$$

$$V = 2\int_0^a \pi b^2 (1 - \frac{x^2}{a^2})dx = 2\left[\pi b^2 x - \frac{\pi b^2 x^3}{3a^2}\right]_0^a \qquad (6.10)$$

$$V_E = 2(\pi b^2 a - \frac{\pi b^2 a^3}{3a^2}) = \frac{4}{3}\pi b^2 a \qquad (6.11)$$

V_E is the volume of the ellipsoid droplet.

The equivalent diameter of the droplet with an equal spherical volume can be determined as follows:

$$V_S = \frac{4}{3}\pi R^3 \qquad (6.12)$$

$$V_S = V_E \qquad (6.13)$$

$$R = (b^2 a)^{\frac{1}{3}} \qquad (6.14)$$

V_S or Veq is the equivalent volume of droplets with a spherical volume. The results for the widest diameter (D_E=2a) and the equivalent diameter (D_s = d_{eq}) are presented in Table 6-4. The flow rate of injecting drops is constant and equal to 15 mL/s.

Table 6-4 The diameters of droplets formed from different tubes				
D_{tube} (mm)	a(mm)	b=c(mm)	$D_E(mm)^a=2a$	$D_s=d_{eq}(mm)^b$
ID_{ss} =1.8	1.045	0.657	2.09	1.53
OD_{PEEK} =1.59	0.92	0.606	1.84	1.39
ID_{ss} = 0.6	0.66	0.488	1.32	1.08
a- The ellipsoid droplet diameter (major axis horizontal) b- The equivalent diameter of the droplet with an equal volume sphere.				

To make sure that the elliptical shape of droplets remains similar through a longer path, the container length is extended as it is shown in Figure 6-8. The result proved a steadiness in the shape of droplets without any oscillation. (Figure 6-10)

6.2.2.6 The column efficiency

Now, with the knowledge of the size of the droplet, final concentration, and saturated concentration at 25°C, the efficiency of the liquid-liquid contact column can be determind. Table 6-5 demonstrates all of the above parameters as well as the velocity of droplets. The effect of the size of droplets on the column efficiency is also shown in (Figure 6-12). The graph shows that the efficiency decreases from 0.195 to 0.123 when the diameter of the droplet increases about 58%.

Table 6-5 Velocity and column efficiency for different droplet sizes		
T (298 K) , P (1 bar), Flow Rate (15mL/hr), h (2.31m)		
ID,OD (SS tube)	1.8, 2.41	mm
D_E	2.09	mm
$D_S=d_{eq}$	1.53	mm
V	0.153	m/s
C_0	0	mole/L
x_f	0.025 ± 0.003	----------
x_{eq}	0.19	----------
C_f	0.08 ± 0.01	mole/L
C_{eq}	0.644	mole/L
Eff.	0.123 ± 0.015	----------
ID,OD (PEEK tube)	1, 1.59	mm
D_E	1.84	mm
$D_S=d_{eq}$	1.39	mm
V	0.143	m/s
C_0	0	mole/L
x_f	0.031 ± 0.0001	----------
x_{eq}	0.19	----------
C_f	0.099 ± 0.001	mole/L
C_{eq}	0.644	mole/L
Eff.	0.154 ± 0.001	----------
ID,OD (SS tube)	0.6, 0.91	mm
D_E	1.32	mm
$D_S=d_{eq}$	1.08	mm
V	0.112	m/s
C_0	0	mole/L
x_f	0.037 ± 0.003	----------
x_{eq}	0.19	----------
C_f	0.12 ± 0.01	mole/L
C_{eq}	0.644	mole/L
Eff.	0.19 ± 0.02	----------

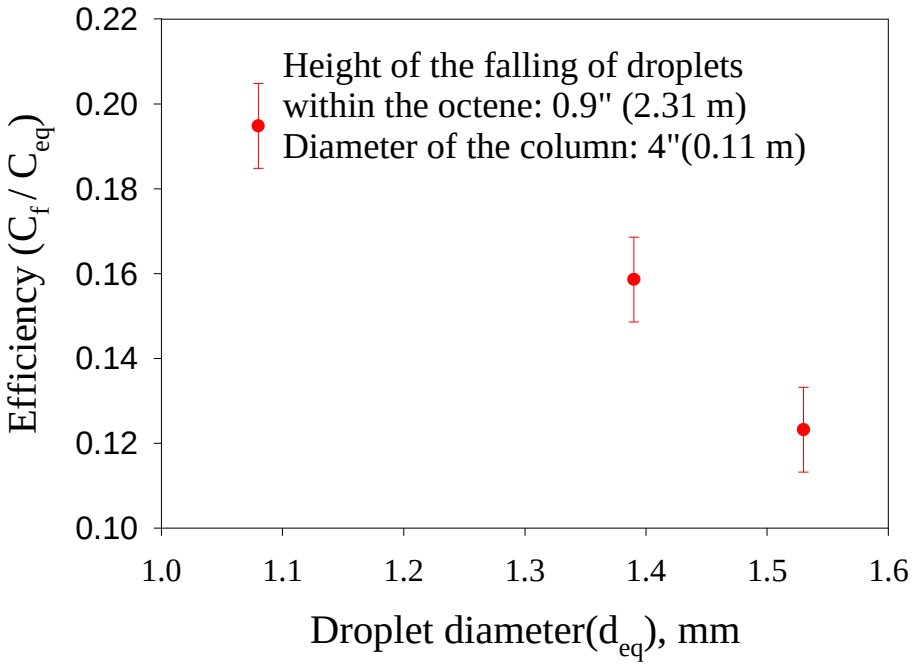

Figure 6-12 The effect of the diameter of the droplet on column efficiency at 25 °C.

6.2.2.6.1 Diffusion through a stagnant droplet

From Table 6-5 and Figure 6-12, the biggest droplet size (d_{eq}=1.53 mm) reaches the efficiency equal to 0.123 after 15 seconds falling into the column containing 1-octene. To compare this result with the unsteady state diffusion of 1-octene into a stagnant droplet with the same size (d_{eq}=1.53 mm), the efficiency can be found from the following equations: [17]

$$\frac{C_f}{C_{sat}} = 1 + \frac{2R}{\pi r}\sum_{n=1}^{\infty}\frac{(-1)^n}{n}\sin(\frac{n\pi r}{R})\exp(-Dn^2\pi^2 t/R^2)$$

$$\frac{C_f}{C_{sat}} = 1 + 2\sum_{n=1}^{\infty}(-1)^n \exp(-Dn^2\pi^2 t/R^2) \qquad (6\text{-}14, 15)$$

Where R is equal to D_{eq}/2, r is the distance from the center of the droplet, and D is the diffusivity of 1-octene in IL droplet at 25° C. The second equation is used to determine the efficiency at the center. The results, which obtained from the above equations considering series with n=200, are shown in Figure 6-13. As can be seen from graphs, the

efficiency at the surface is equal to one and means that the concentration at the surface is equal to the saturated concentration. The efficiency decreases inside of the droplet and approaches to the minimum amount at the center (r/R=0).

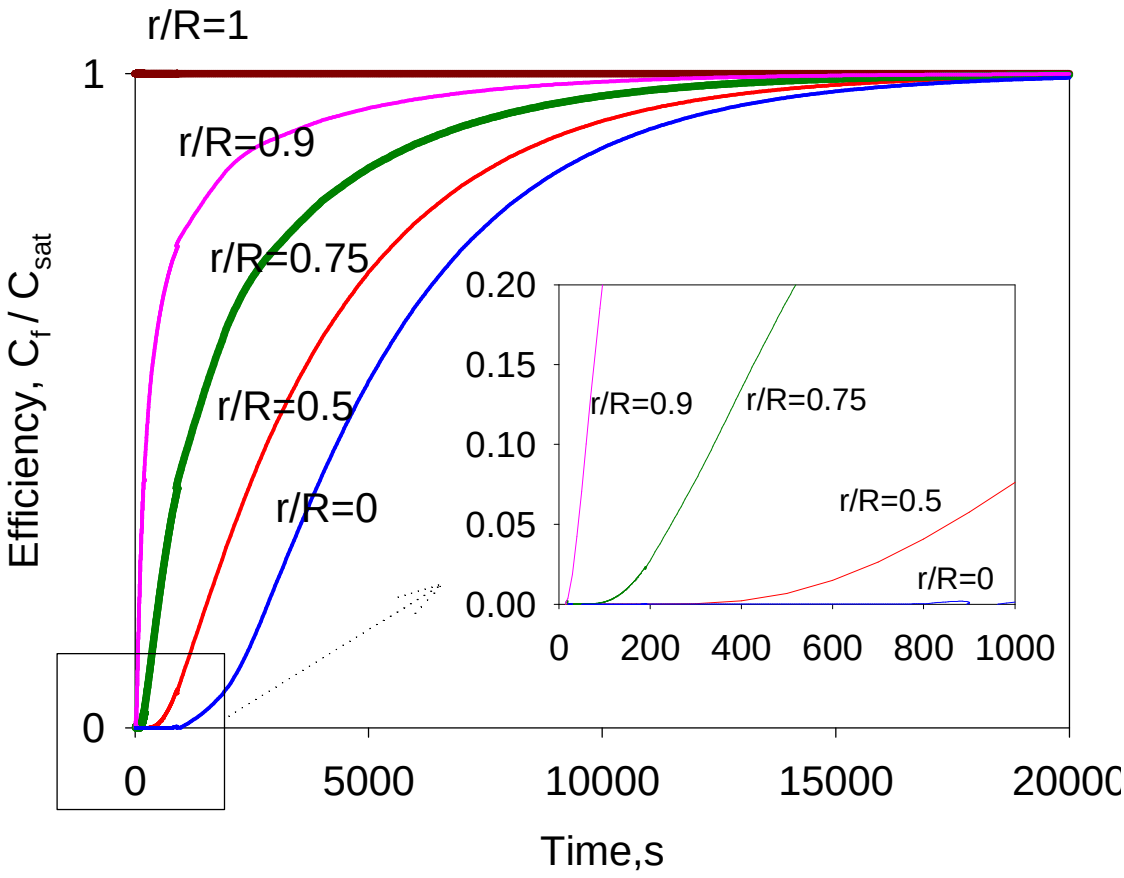

Figure 6-13 The efficiency gradient for a stagnant IL droplet (Deq = 1.53 mm) in 1-octene with time at 25°C

To evaluate the efficiency obtained from modeling at the static condition with experimental results after 15 seconds, the average efficiency inside of the droplet has to be determined. For a spherical droplet, the average concentration can be written as follows:

$$\bar{C} = \frac{1}{4\pi R^3/3} \int_0^R 4\pi r^2 C(r) dr$$

$$\frac{\bar{C}}{C_{sat}} = \frac{3}{R^3} \int_0^R \frac{r^2 C(r) dr}{C_{sat}} = \int_0^R f(r) dr$$

Where R is the radius of the droplet and C(r) is the concentration of a thin element assumed within the droplet with the thickness of dr and radius of r.

To determine the average efficiency ($\frac{\bar{C}}{C_{sat}}$), the area under the curve of $f(r)=\frac{3}{R^3}(\frac{r^2C(r)dr}{C_{sat}})$ versus r has been calculated numerically using Trapezoidal rule after 15 seconds. This amount (0.069), which represents the average efficiency in the droplet achieved just from diffusion in a static condition, is about 56% of the efficiency obtained from the column (0.123). As it has been shown before (streamlines in Figures 6-2 and 6-3), due to convection between two phases at the surface of the falling droplet and the circulation inside of the droplet, the mass transfer of 1-octene is expected to happen faster than diffusing into the stagnant droplet, which is in agreement with the obtained results from the abovementioned experiments and modeling. So, by increasing the contact time or the length of the column the column efficiency can be enhanced.

6.2.3 Correlation

6.2.3.1 Background

In general, mass transfer coefficients for different flow fields can often be empirically related to dimensionless groups. These empirical models are different depending upon the inertia effects (creeping, laminar, transient, or turbulent flow), viscose resistance, manner of droplet motion (oscillating or behaving as rigid spheres), and internal circulations. For instance, the empirical correlation of Garner and Tayeban [9] for circulating droplets is:

$$Sh_C = 0.6(\mathrm{Re})^{1/2}(Sc)_C^{1/2} \qquad (6.16)$$

$$Sh_C = \frac{k_m d_d}{D_c}, \mathrm{Re} = \frac{\rho_c v_d d_d}{\mu_c}, Sc_C = \frac{\mu_c}{\rho_c D_c}$$

where the Sherwood number (*Sh*) is convective mass transfer vs. diffusional mass transfer; Schmidt (*Sc*) is momentum transfer vs. diffusional mass transfer; and Reynolds (*Re*) is inertial vs. momentum transfer. Also, d_d and v_d represent droplet diameter and

velocity through the column. ρ_c, η_c, and Dc are density, viscosity, and diffusion coefficient of the continuous phase, and k_m is the overall coefficient of mass transfer. In this model, during each time that the drop oscillated, the circulation occurred inside of the drop, and it was mixed completely.

Other groups Garner - Grafton [10] and Garner – Suckling [11] obtained another equation by measuring the rate of dissolution of organic spheres:

$$Sh_C = 2 + 0.95(\mathrm{Re})^{\alpha}(Sc)_C^{\beta} \qquad (6.17)$$

The correlation of Ranz and Marshall [12] for the low laminar region, when Re is between 2 and 200, provided the following equation for mass transfer from drops of pure liquids:

$$Sh_C = 2 + 0.6(\mathrm{Re})^{1/2}(Sc)_C^{1/3} \qquad (6.18)$$

For low mass transfer rates and slightly soluble components the following equation is offered: [13]

$$Sh_C = K(\mathrm{Re})(Sc)_C^{1/3} \qquad (6.19)$$

Steiner has also derived an equation for rigid droplets: [14]

$$Sh_C = 2.43 + 0.775(\mathrm{Re})^{1/2}(Sc)_C^{1/3} + 0.0103(\mathrm{Re})(Sc)_C^{1/3} \qquad (6.20)$$

Lochiel [15] has developed another equation for the effect of surfactants on the surface of droplets. Adsorption of these surface active agents can reduce circulation inside drops and affect the mass transfer rate.

$$Sh_C = \frac{2}{\sqrt{\pi}}(\alpha)^{1/2}(\mathrm{Re})^{1/2}(Sc)_C^{1/2}$$

$$\alpha = 1 - \frac{2 + 3\frac{\mu_d}{\mu_c} + m}{1 + [\frac{\rho_d \mu_d}{\rho_c \mu_c}]^{0.5}} * \frac{1.45}{\mathrm{Re}^{0.5}} \qquad (6.21)$$

“m represents the level of contamination”.

6.2.4 Correlated and experimental mass transfer coefficient

As it is abovementioned, the overall mass transfer coefficient (Km) can empirically be related to dimensionless groups. Also, by writing a mass balance through the column (the entire mass transport area), K_m can be determined experimentally from the concentration change and the velocity of droplets as follows: [16]

$$\frac{dc_i}{dt} = -\frac{6K_m}{d}(c_i - c_{eq}) \qquad (6.22)$$

$$\frac{6K_m}{d}t = \ln(\frac{(c_{eq} - c_1)}{(c_{eq} - c_2)}) \qquad (6.23)$$

$$K_m = \frac{d}{6t}(\ln\frac{(c_{eq} - c_1)}{(c_{eq} - c_2)}) \qquad (6.24)$$

where c_i is the average concentration of octene in the IL droplet vs time, c_{eq} is the saturated concentration, t is the residence time, c_1 and c_2 are inlet and outlet concentrations, and d is diameter of the droplet.

To derive the above equation, the following assumptions were considered:

1- The drop is spherical

2- 6/d is the ratio of area to volume ($\frac{S}{V} = \frac{4\pi R^2}{4/3\,\pi R^3} = \frac{3}{R} = \frac{6}{d}$)

For an ellipsoid droplet, it is shown that the volume is equal to:

$$V = \frac{4}{3}\pi abc \qquad (6.25)$$

The surface area of a general ellipsoid is not similar to the surface area of a sphere. The following expression, which is not an elementary function, can be written for the surface area of an ellipsoid droplet:

$$S \approx 4\pi(\frac{a^p b^p + a^p c^p + b^p c^p}{3})^{1/p} \qquad (6.26)$$

for the Knud Thomson formula, the error will be 1.061% if:

$p = 1.6075$

So, the surface area over volume can be written as follows:

$$S/V = \frac{3}{abc}\left(\frac{a^p b^p + a^p c^p + b^p c^p}{3}\right)^{1/p} \qquad (6.27)$$

Considering b=c then:

$$S/V = \frac{3}{ab^2}\left(\frac{2a^p b^p + b^{2p}}{3}\right)^{1/p} \qquad (6.28)$$

Table shows the ratio of area over volume obtained from the above equation and from $6/d_{eq}$. Since the results are very close (AARD% lower than 3%), so from now on droplet will be considered a sphere with an equivalent diameter (d_{eq}). (Table 6-6)

Table 6-6 The volume and surface area of droplets formed from different tubes

D_{tube} (mm)	a(mm)	b=c(mm)	d_{eq}(mm)	V(mm^3)	S(mm^2)	S/V (mm^{-1})	6/deq (mm^{-1})
ID_{ss} =1.8	1.045	0.657	1.53	1.89	7.65	4.0	3.9
OD_{PEEK} =1.59	0.92	0.606	1.39	1.41	6.27	4.4	4.3
ID_{ss} = 0.6	0.66	0.488	1.08	0.66	3.71	5.6	5.6

Table 6-7 Continuous and dispersed phase properties for mass transfer coefficient and Sherwood number

The length of column(m)	D_{tube} (mm)	Dc(m^2/s)	ρ_c(kg/m^3)	v_d(m/s)	η_c(kg/m.s)	Falling time(s)
2.31	ID_{ss} =1.8	2.28E-09	711.2	0.154	0.00054	15.1
2.31	OD_{PEEK} =1.59	2.28E-09	711.2	0.144	0.00054	16.2
2.31	ID_{ss} = 0.6	2.28E-09	711.2	0.112	0.00054	20.6

Table 6-7 and Table 6-8 present the amount of parameters that are needed to obtain the observed Sherwood number .

Table 6-8 Mass transfer coefficient and Sherwood number

d_{eq} (m)	C_{eq} (mol/lit)	C_1 (mol/lit)	C_2 (mol/lit)	$K_{m,\,obs.}$ (m/s)= $\frac{V}{St}(\ln\frac{(c_{eq}-c_1)}{(c_{eq}-c_2)})$	Sh(obs.) = $K_{m,\,obs}\, d_{eq}/D_c$
1.53E-03	0.644	0	0.08	2.24E-06	1.50
1.39E-03	0.644	0	0.10	2.41E-06	1.47
1.08E-03	0.644	0	0.12	1.80E-06	0.85

Since,

$$Sh_{(obs.)} = K_{m,\,obs.}\, d_{eq} / Dc = \kappa (Re)^{\alpha} (Sc)^{\beta} \qquad (6.29)$$

So, using the obtained results and performing data regression with SigmaPlot 2000-SPSS Inc., the following correlation is developed for this system:

$$Sh_{(Corr.)} = 0.004 * (Re)^{0.7} (Sc)^{0.3} \qquad (6.30)$$

Table 6-9 Observed and correlated mass transfer coefficient

(D_E) (m)	D_{eq} (m)	$K_{m\,(obs.)}$ $(m\cdot s^{-1}\cdot 10^6)$	Re	Sc	$K_{m\,(corr.)}$ $(m\cdot s^{-1}\cdot 10^6)$	$((K_{m\,(obs.)} - K_{m\,(corr.)})/ K_{m\,(corr.)})*100$
0.00209	0.00153	2.24	423	333	2.34	- 5.0
0.00184	0.00139	2.41	348	333	2.23	6.5
0.00132	0.00108	1.80	196	333	1.88	- 8.1

Table 6-8 illustrates the increasing Sherwood number and Re number by diameter of droplets. In Figure 6-14, the experimental results for mass transfer coefficient compares with the correlated values. As can be inferred from Table 6-9, the experimental and correlated numbers match each other with a reasonable consistency.

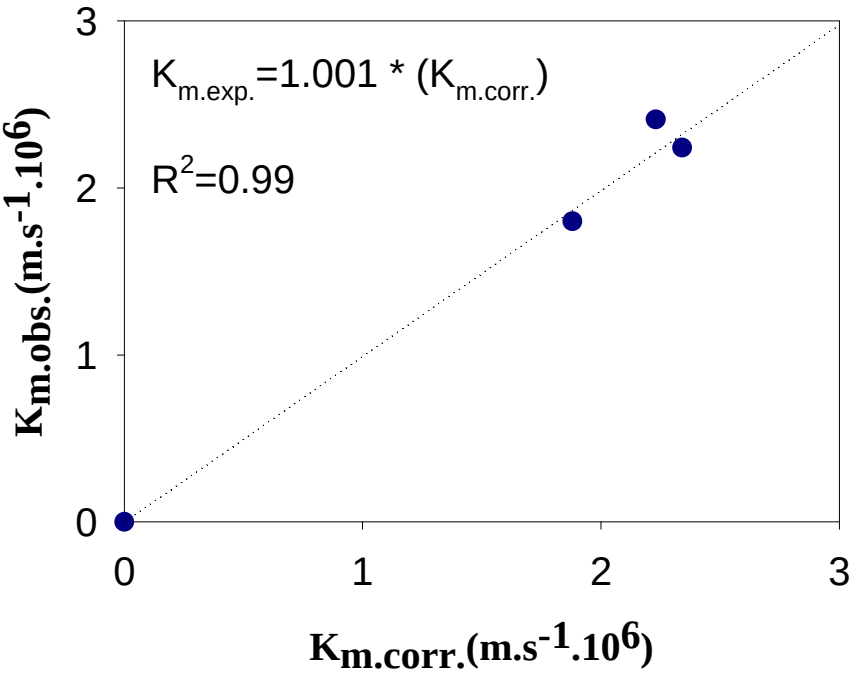

Figure 6-14 Observed and correlated mass transfer coefficient

6.3 Summary

For an accurate study of the mass transfer, the phase equilibrium and thermodynamic properties must be understood, especially the effect of concentration. In this investigation, thermodynamic and interfacial properties for the system of [HMIm][Tf_2N]) and 1-octene are measured in Chapter 5 and the results indicated just one direction mass transfer. In this chapter, phase behavior, thermodynamics, and transport properties of a biphasic ionic liquid–olefin system, which obtained from the last section, have been employed for interfacial mass transfer studies. Abovementioned information was crucial to support the modeling and correlation of this biphasic system.

To find the concentration rate of 1-octene in the dispersed ionic liquid phase at each point, the model of Petera and Weatherley has been developed using an efficient finite element method. In this model, the droplet is considered to be spherical. Simultaneously, liquid-liquid contact experiments have been carried out in a column to determine the overall mass transfer coefficient between a segregated ionic liquid droplet and the 1-octene continuous phase.

In order to explore the real shape, size, and velocity of droplets inside of the continuous phase, a high speed optical system was set up. The result showed that the droplets are not spherical but oval. Thus, the equivalent diameter and volume of the droplet are calculated and then used in correlations and determinations.

The most important achievement of this chapter is developing an empirical correlation for the biphasic [HMIm][Tf_2N]) / 1-octene system to connect dimensionless groups to each other at 25°C. To compare the outcome of experiments with the modeling results, further simulations with the real geometry of the droplets are required.

6.4 References

1. Zhao, H.; Xia, S.; Ma, P., Use of ionic liquids as 'green' solvents for extractions. . *J. Chem. Technol. Biotechnol.* **2005,** 80, 10, 1089-1096.
2. Roettger, D.; Nierlich, F.; Krissmann, J.; Wasserscheid, P.; Keim, W., Method for separation of substances by extraction or by washing them with ionic liquids. In US Patent 7,304,200: 2007.
3. Smith, R. S.; Herrera, P. S.; Reynolds, J. S.; Krzywicki, A., Use of ionic liquids to separate diolefins. In US Patent App. 10/308,307: 2002.
4. Pandey, S., Analytical applications of room-temperature ionic liquids: A review of recent efforts. *Anal. Chim. Acta* **2006,** 556, 1, 38-45.
5. Ahosseini, A.; Ren, W.; Scurto, A. M., Hydrogenation in Biphasic Ionic Liquid/CO_2 Systems. In *Green Chemistry and Engineering with Gas Expanded Liquids and Near-Critical Media*, Hutchenson, K. W.; Scurto, A. M.; Subramaniam, B., Eds. ACS Symposium Series: Washington, D.C., **2008**.
6. Ahosseini, A.; Ren, W.; Scurto, A. M., Understanding Biphasic Ionic Liquid/CO_2 Systems for Homogeneous Catalysis: Hydroformylation. *Ind. Eng. Chem. Res.* **2009**, 95-101.
7. Ahosseini, A.; Ren, W.; Scurto, A. M., Homogeneous Catalysis in Biphasic Ionic Liquids/CO_2 Systems. *Chem. Today* **2007,** 25, 2, 40-42.
8. Petera, J.; Weatherley, L. R., Modelling of mass transfer from falling droplets. *Chem. Eng. Sci*. **2001,** 56, 16, 4929-4947.
9. Garner, F. H.; Tayeban, M., Continuous phase mass transfer coefficients in oscilating drops. *Anal. Real. Soc. Espan. Fis. Quim.(Madrid)* **1960,** 56, 479.
10. Garner, F. H.; Grafton, R. W., Mass transfer in fluid flow from a solid sphere. *Proceedings of the Royal Society of London. Series A, Mathematical and Physical Sciences* **1954**, 64-82.
11. Garner, F. H., RD Suckling *AIChE J.* **1958,** 4, 114.
12. Ranz, W. E.; Marshall, W. R., Evaporation from drops, Chem. *Engng Prog* **1952,** 48, 141-173.
13. Bird, R. B.; Stewart, W. E.; Lightfoot, E. N., *Transport Phenomena, Wiley, New York*. 1960.
14. Steiner, L., Mass-transfer rates from single drops and drop swarms. *Chem. Eng. Sci.* **1986,** 41, 8, 1979-86.
15. Lochiel, A. C., The influence of surfactants on mass transfer around spheres. *Can. J. Chem. Eng.* **1965,** 43, 40-44.
16. Handlos, A. E.; Baron, T., Mass and heat transfer from drops in liquid-liquid extraction. *AIChE J.* **1957,** 3, 1.
17. Crank, J. The mathematics of diffusion. Brunel University Uxbridge, second edition

Chapter 7 Conclusions and recommendations

7 Conclusions and recommendations

7.1 Conclusions

In this research the hydroformylation and hydrogenation of 1-octene were selected as model homogeneous catalytic reactions to study kinetics, momentum & mass transfer, and phase behavior to efficiently manage the reaction in biphasic ionic liquid/CO_2 systems. Rhodium with triphenylphosphine was chosen as a simple catalyst system and reactions conducted in 1-hexyl-3-methylimidazolium bis(trifluoromethylsulfonyl)amide ([HMIm][Tf_2N]) as a common ionic liquid medium.

There are several conflicting conclusions in literature about the effect of CO_2 on the rate of homogeneous reactions, some declared CO_2 increases the reaction rate and several reported the decreasing trend of reaction efficiency by adding CO_2 pressure. The real impact of CO_2 on reactions of this study was investigated in different situations. In well agitated conditions and at constant loading of 1-octene, increased pressure of CO_2 reduced the rate of reaction because of the volume expansion of the solvent. Phase equilibrium studies determined the volume expansion of the IL phase with CO_2 and the phase behavior between the reactants/product and CO_2. Both volume expansion and the better solvent power of CO_2 with pressure decreased the concentration of the reactant. The lower concentration (molarity) of reactants in the expanded solvent is responsible for reducing the rate. The equations reported in literature for these reactions imply a first-order reaction rate with 1-octene concentration which supports the obtained results.

On the other condition, for those reactions limited by mass transfer, the presence of CO_2 helps to increase the apparent reaction rate. The reason for this effect has been explained by measuring transport properties of ionic liquids under CO_2 pressure. It has been learned from this study that transport properties of the catalytic platform (IL medium) in homogeneously catalyzed reactions can be influenced by introducing CO_2. Detailed studies on mass transfer phenomenon during the reaction condition helped us to quantify the parameters and properly understand and engineer these reactions. For instance, in Rh-catalyzed hydrogenation of olefins that is a relatively rapid reaction, the

H_2 availability often becomes a limiting factor. Thus, the CO_2 pressure increases the apparent reaction rate most likely because of enhancing mass transport of H_2. To increase the efficiency of these kinds of reactions it is essential to use ionic liquids having lower viscosity to help reactants diffuse easier and have more chances to simply reach each others and react. Also, in some reactions managing the amount of viscosity of the main solvent (ionic liquid) can help to tune the selectivity of desire products. Therefore, detailed quantitative studies and measurements are performed to have enough information related to the effect of structure of ionic liquids and compressed gases on the viscosity of reaction media.

Our initial endeavours to achieve the effect of the structure of some pure imidazolium-based ionic liquids at elevated pressures are shown in this work. The results showed that smaller alkyl chain lengths of the imidazolium cation, such as R=ethyl-, exhibit lower viscosity than the hexyl- or decyl- substituted methylimidazolium cation. In addition, the [DMIm] cation also exhibits a higher rate of change with pressure in the higher pressure regions of the data (>60 MPa). The viscosity of [HMIm][PF_6] is considerably higher than that of [HMIm][BF_4] and [HMIm][Tf_2N]. In addition, the rate of increase in viscosity with pressure is much greater than the other two ionic liquids. Detailed discussion was introduced in Chapter 4 about the possible reasons of the above behaviors. However, in summary, the size of hydrodynamic radii and molecular interactions such as columbic and hydrogen bonding may influence the barrier to motion and so the viscosity.

The impact of adding different compressed gases on the viscosity and diffusivity of ionic liquids has been described by comparing the transport properties of mixtures of R134a as well as CO_2 with [HMIm][Tf_2N]. The result showed that adding the pressure of R-134a decreases the viscosity of IL considerably more than the CO_2 addition. The reason for this behavior has been interpreted by their unlike structures. In comparison with R-134a, CO_2 is a nonpolar molecule without any hydrogen bonding effects and so with a lower potential to stay between the free volume of cations and anions of ionic liquid molecules. This may explain the different solubility of R-134a and CO_2 in [HMIm][Tf_2N] and also their different influences on viscosity of pure ionic liquids.

The phase behavior of the main reactant (1-octene) with the ionic liquid solvent ([HMIm][Tf_2N]) is another important issue to determine mass transfer effects in both hydroformylation and hydrogenation reactions. Measuring mutual solubilities indicated the minimal solubility of IL in the 1-octene phase and moderate solubility of 1-octene in the IL phase. Thus, mass transfer when the two components are mixed would occur in virtually one direction. The NRTL model satisfactorily correlated the LLE data with just a slight under prediction of the 1-octene mole fraction in each phase. These studies were followed by measuring thermodynamic and interfacial properties for the system focusing on both pure components and mixtures that can ultimately help to learn more about mass transfer phenomenon happening in reactions, especially hydroformylation and hydrogenation reactions of 1-octene, and olefin extractions.

The density of the ionic liquid mixture decreases with increasing the concentration of 1-octene and temperature. The excess molar volume for the mixture of ionic liquids and 1-octene is slightly negative for all isotherms. Air-liquid surface tensions of pure and mixtures of the IL/1-octene have been measured to their saturation points. The results showed that the surface tension of pure IL is much higher than 1-octene and decreases for their mixture as the 1-octene concentration increases. However, this effect becomes smaller at the higher temperatures. The interfacial tension of mixtures of saturated [HMIm][Tf_2N] and 1-octene that were measured at different isotherms illustrated a decreasing trend with temperature. The diminishing slope was smaller at lower temperatures and more significant at the higher temperatures.

Transport properties of ([HMIm][Tf_2N]) with 1-octene were also determined in different isotherms. The result showed that the viscosity of IL decreases with adding 1-octene concentration and temperature. The reason for this trend can probably be inferred from the electrostatic interactions between cations and anions in IL molecules and molecules of 1-octene. The negative values of excess viscosity and the negative amounts of excess molar volume represented the effect of octene in the free volume of ionic liquid structure.

All of the abovementioned achievements and results provided us with the required information to study mass transfer phenomenon between segregated droplets of IL ([HMIm][Tf_2N]) and 1-octene continuous phase through a liquid-liquid contact column.

These studies showed that the mass transfer can be enhanced by convection between two phases comparing with the diffusion through a static droplet.

In order to obtain a general relationship between dimensionless groups and determine the overall mass transfer coefficient, the diameter and velocity of droplets were quantified using a high speed optical system. Furthermore, thorough studies have been accomplished to measure and analyze the concentration of 1-octene in dispersed phase (IL) throughout the column and finally overall mass transfer coefficient has been determined for different droplet sizes.

7.2 Recommendations

For further studies, the following activities are suggested:

- The achievements of this research can be utilized to manage catalytic homogeneous reactions in a more convenient platform. By choosing different media the reaction region can be controlled on mass transfer or kinetics region. For instance, hydroformylation and hydrogenation reactions can be examined in a lower viscose ionic liquid and a compressed gas with a higher solubility to enhance mass transfer and get an efficient reaction.
- Thorough feasibility assessments of the hydroformylation and hydrogenation reactions of 1-octene in IL/CO_2 media at optimum conditions are obtained from this study to distinguish if they are economically viable and environmentally benign for any process intensification.
- Design consecutive experiments and required apparatus to study mass transfer, phase behavior and interfacial phenomena between 1-octene and ionic liquid droplets under compressed CO_2 pressures. A high pressure contact column is needed to be designed for these experiments. High pressure measurements of density, interfacial tension, and surface tension of IL/1-octene under compressed CO_2 should be equipped and arranged for further modeling and correlations.
- Determination and modeling of the mass transfer behavior of swarming droplets of the ionic liquid in 1-octene with and without compressed CO_2 to approach the real multi-phase reaction situation. Developed models can also predict the mass transfer and phase behavior for the advanced process design.

Appendices

Appendix A - Diffusion coefficient measurement with the NMR spectroscopy

To measure diffusion coefficient, the following procedure, which is a modified version of the previous report [1] , is used by means of the NMR spectroscopy. A Bruker 400 MHz ^{1}H NMR was used to measure the translational diffusion with a pulsed-field gradient (PFG) method. The software used to analyze the data was Topspin version 1.3. In this method an automatic optimization technique is developed to find an accurate 90 degree pulse (which is perpendicular to the magnetic field, z axis) for non-deuterated solvent shimming. This modification helps to have more precise results at the considerably shorter time.

Detail procedure is described stepwise as follows:

1. Make a sample of a known system with a given diffusion rate.
2. Place the sample in a clean NMR tube. When placing the sample in the NMR tube only fill the NMR tube to a height of 3 cm with the sample. The heating element for the NMR is restricted to only the bottom 3.5 cm of the NMR tube. Any excess sample in the NMR tube could result in a temperature gradient in the NMR tube resulting in convection as well as molecular diffusion.
3. Log into the NMR machine and open a shell. Type **topspin** then press enter. After the software is loaded type **edte**. A box will come up with the temperature and flow rate of the NMR. Change the temperature and turn the temperature controller on. Change the flowrate to 535 L/min. Close the box. Let the NMR warm up for 20-30 minutes before running the sample.
4. **NOTE 1: To run high temperature diffusion experiments make sure not to exceed the boiling point and/or a pressure of 4 bar within the NMR tube when the temperature of the sample reaches the desired set point. NOTE 2: Never exceed a temperature of 50^{o}C for the NMR setting without a special spinner**

5. Place the NMR tube in a spinner then place the NMR tube in the NMR gauge. Make sure the bottom of the gauge is set to 2 and place the NMR tube in the gauge.

6. On the control panel press the on/off button to flow the air. Place the NMR tube in the carossel. Press the on/off button again and the air flow will decrease, thus loading the NMR tube into the equipment.

7. In the topspin software close the software. In a shell type the following: **cd_/opt/topspin/data/(your user name here)/nmr** then press enter. Next type **ls** then press enter. Type **cp_–r_1difftemp_/opt/topspin/data/(your username)/nmr/(file name here)** press enter**.** This will make a copy of the 1difftemp file and names it what ever you type for the (File Name Here). If you do not have the 1difftemp file you cannot proceed past this part. Type **shmrm** press enter then type **topspin** press enter.

8. After topspin loads look for your file, which you named in the namethefile. When you open this file you will notice there are 9 files. The first file is a typical proton run and the 2-9 are the actual diffusion files which will be used. Open the first file and type **rpar,** choose **PROTON, getprosol** press enter, **rsh** choose **AAQNP** press read. If you are using a deutarated solvent lock the solvent as you would normally and go to step 9. If you do not have a deutarated solvent on the control panel press the sweep button so the light is off on the control panel. Type **gradshim** and press enter. Let the gradshim run through three iterations(1d, midz=16, midz4=18, highz=18). After it is done close the gradshim box and the spectrum it generated with the straight vertical line with a little zigzag in it.
9. Type **rga** press enter. When it is done type **zg** then press enter. There will only be one scan which is taken. When zg has finished type **ef** press enter, **apk** press enter. Find one of the peaks which belongs to the diffusing specie of interest. Zoom in around that particular peak and place the cursor at the highest point on the peak. Center it using the special button in the tool bars and then type **o1p**

press enter. Type in the box the number next to the ppm you see at the top left of the spectrum screen then press enter. This will center the spectrum around this particular peak. Next click on the tab that says *Aqupars* and change the PULPROG from zg30 to zg. Click on the Spectrum tab. To find an accurate 90 degree pulse (which is perpendicular to the magnetic field, z axis) set number of scans (NS=1), and dummy scans DS=0. Type dpl1 (to save parameters F1P/F2P). Set parameter as p1, optimum as zero, start at 30 and end at 40 variable mode as linear and increment as 1.Start optimization and overwrite the previous one. If it doesn't show up use /8. The number will be displayed after a while.p1 will be this number divided by 4. **NOTE: At this point you have to stay with this peak. If you change peaks you have to redo all the p1 calculations to get the proper 90 degree flip angle, so make sure it is the diffusing species peak before doing all of this. By dividing by four you get the true 90 degree flip needed for the diffusion experiments.**

10. Type **rg** press enter write down this number. Type **o1p** and write the value down. Take the number found for the 90 degree pulse i.e. the p1 value divided by 4 and write this number down.
11. Open up file number 3. Type **rg** and type the value you wrote here. Type **o1p** and place the value you wrote down here. Type **p1** and type the value determined for the 90 degree pulse here (it should be around ~8 to ~9). Do this for files 3-10.
12. Open file 3 and type **p30** press enter. Change the value to 500. Do the same for file 4. While you are in file 4 type **gpz6** press enter. Change this value to 70. This initial change in file 4 will look at the maximum value that the pulse gradient will go through. **Note: gpz6 is the gradient strength it is different for each diffusion experiment number. (File 3 gpz6=5, File 4 gpz6=10, File 5 gpz6=20, File 6 gpz6=30……..)The maximum value for gpz6 is 70. gpz6 should not be greater than 70 to prevent damage to the coil. Typically the gradient strength is linearly proportional to the Amps through the coil. i.e. gpz6=100 is equivalent to 10A, gpz6=5 is equivalent to 5A. See Bruker's manual for more details.**

13. Open file 3 and type **multizg** press enter a dialog box will come up press 2 enter. This will run through file 3 and 4. When the message multizg complete press okay and open file 3. Type **ef** press enter, **apk** press enter, **abs** press enter, then type **multiefp** press enter. When the dialog box pops up type 3 enter then type 2 enter. Multiefp analyzes both files 3 and 4 the same. While in file 3 zoom in on the peak that everything has been based on. Find the maximum intensity and write the number down. Do the same for file 4. Divide the Intensity from file 3 by the intensity of 4. If the ratio is 10 ± 0.5 you can move on to next step. If however it is not 10 ± 0.5 you have to change the value for p30 for both 3 and 4 and try running the multizg command again. Make sure the value for p30 in files 3 and 4 are the same before running the multizg command again**. NOTE: If the ratio is less than 10 increase the value for p30 for both files 3 and 4. If the value is greater than 10 decrease the value for p30 in both files 3 and 4. Keep iterating p30 until the ratio is 10 ± 0.5. It is very important to get this ratio as close as possible to 10.**

14. Once an appropriate p30 value is obtained open file 4 and change the gpz6 setting back to 10. Next change all p30 values from files 3-10 to the determined p30 value. **Check to make sure all files 3-10 have the same rg, p1, p30, o1p, and d20 value.** Then, open up file 3 and type **multizg** press enter. This time type 8. This will run through all the diffusion files. Once it is completed open file 3 and type **ef** press enter, **apk** press enter, **abs** press enter, then type **multiefp**. When the dialog box opens up type 3 press enter then 8 press enter. Find the peak of interest and write down the maximum intensity. Do this for files 3-10.
15. Type **edte** press enter. Turn the temperature controller off and set the flow rate back to 200L/min. Make sure you leave 10 minutes for the NMR to cool down before leaving the NMR room.
16. Plot in the excel sheet given. The slope gives the g^2 value. Take the square root and you will have the g value for later determining the diffusion rate. This procedure has to be done for every temperature. At current a g value has only been calculated for 25^oC.

17. After all calibrations are done the same procedure is followed, however, instead of looking for the g value you will be looking for the Diffusion Coefficient.

References

1. Schleicher, J. Kinetics and Solvent Effects in the Synthesis of Ionic Liquids. MS Thesis, University of Kansas, Lawrence, 2007.

Appendix B - CHEMCAD Results

The following results are taken by predicting mutual solubilities of 1-octene and [HMIm][Tf_2N] using CHEMCAD 6.1.2. The correlated data were compared with the experimental results and the deviation are determined and reported for each isotherm as follows:

Hint: $T_{ij}=\tau_{ij}$

```
------------------------------------------------------------------------
------------------------------------------------------------------------
------------------------------------------------------------------------

CHEMCAD 6.1.2
Page 1

Job Name: ionic liquid_octene-1   Date: 08/19/2009 Time: 16:05:53

COMPONENTS
          ID #     Name              Formula
   1        83     1-Octene          C8H16
   2      8001     HMIMTF2N

User/Pool Components Data Source
   2      8001     HMIMTF2N          in User Components

THERMODYNAMICS

 K-value model     :  NRTL
                      No correction for vapor fugacity
 Enthalpy model    :  SRK
 Liquid density    :  Library

 Std vapor rate reference temperature is 0 C.
 Atmospheric pressure is  101324.9793 Pa.

NRTL Parameters: Tij = Aij + Bij/T + Cij * Ln(T) + Dij * T (T Deg K)

  I   J      Bij      Bji   Alpha   Aij    Aji    Cij    Cji    Dij    Dji
  1   2       -        -      -     0.00   0.00   0.00   0.00   0.00   0.00*
```

```
------------------------------------------------------------------------
CHEMCAD 6.1.2
Page 1

Job Name: ionic liquid_octene-1   Date: 08/19/2009  Time: 16:14:10
```

Regression has converged in 15 iterations.

System: 1-Octene / HMIMTF2N

T Deg C	Experimental Data X11	X12	Deviation D_X11	D_X12
10.00	0.9999	0.1600	-0.0053	-0.0043

Mean Deviation	0.0053	0.0043
Max. Deviation	0.0053	0.0043

Regressed Parameters:

B12 =	1.3870e+003
B21 =	1.0003e+002
Alpha =	2.0000e-001

CHEMCAD 6.1.2
Page 1

Job Name: ionic liquid_octene-1 Date: 08/19/2009 Time: 16:19:07

Regression has converged in 45 iterations.

System: 1-Octene / HMIMTF2N

T Deg C	Experimental Data X11	X12	Deviation D_X11	D_X12
25.00	0.9999	0.1900	-0.0174	-0.0074

Mean Deviation	0.0174	0.0074
Max. Deviation	0.0174	0.0074

Regressed Parameters:

B12 =	1.1530e+003
B21 =	1.0016e+002
Alpha =	2.0000e-001

CHEMCAD 6.1.2
Page 1

Job Name: ionic liquid_octene-1 Date: 08/19/2009 Time: 16:21:06

Regression has converged in 49 iterations.

System: 1-Octene / HMIMTF2N

T Deg C	Experimental Data X11	X12	Deviation D_X11	D_X12
50.00	0.9986	0.2300	-0.0288	-0.0190

Mean Deviation	0.0288	0.0190
Max. Deviation	0.0288	0.0190

```
Regressed Parameters:
   B12 =   1.1119e+003
   B21 =   1.0014e+002
 Alpha =   2.0000e-001
```

```
CHEMCAD 6.1.2
Page 1

Job Name: ionic liquid_octene-1   Date: 08/19/2009  Time: 16:22:38

Regression has converged in 62 iterations.

System: 1-Octene / HMIMTF2N

    Experimental Data       Deviation
T Deg C    X11     X12    D_X11   D_X12
   75.00  0.9552  0.2800 -0.0168 -0.0135

    Mean Deviation        0.0168  0.0135
    Max. Deviation        0.0168  0.0135

Regressed Parameters:
   B12 =   1.0168e+003
   B21 =   1.0140e+002
 Alpha =   2.0000e-001
```

Appendix C - Error analysis for the molar excess volume of 1-octene and [HMIm][Tf_2N] solution

C.1 Definitions

Experimental data and results from measurements help us to obtain a physical and realistic sense of an event. Thus, it is so significant to describe and analyze data accurately to have a reasonable conclusion at the end. To follow this, it is very important to know the point that all measurements are subject to uncertainties which are expected to be minimized. To report the results of experiments, measuring condition should be defined with all circumstances. However, even if all specific conditions are defined precisely, the result would still have an error. Thus, the best way is to report results with a convenient analysis and an uncertainty. Obviously, all accepted data in literature or handbooks cannot be considered as right data because they have just achieved by others and may have some errors. There are two most important types of errors. Systematic errors and random errors. Systematic errors are caused by the precision during reading or measuring the variables. In systematic errors often something wrong logically happens that should be eliminated before reporting the result. For instance, when the calibration of the apparatus is not accurate, systematic errors will be observed. In a different way, random errors oscillate around the mean value (positively or negatively) are unavoidable and just should be reported with uncertainties [1, 2].

So, a safe way to make sure the data are reported in a right manner is repeating experiments to find the systematic and random errors and analyze their main reasons and origins.

One of the most important parameters to determine the distribution of experimental results from the mean values (uncertainty) is the standard deviation that can be explained by the following equation:

$$\sigma = \sqrt{\frac{\sum_i (x_i - \bar{x})^2}{N}}$$

Which $\bar{x}$ is defined as Mean value (Average):

$$\bar{x} = \frac{\sum_{i}^{N} x_i}{N}$$

Mostly experiments uncertainties come from several steps and their combination will affect the final result. For instance, measuring density is the function of two sub-measurements, mass and volume. For any function of "f" related to independent parameters a, b, …, n; the error can be written as follows:

$$f = f(a,b,\ldots,n)$$

$$df = \left(\frac{\partial f}{\partial a}\right)da + \left(\frac{\partial f}{\partial b}\right)db + \cdots + \left(\frac{\partial f}{\partial n}\right)dn$$

Assumes no "cross" derivatives/coupling.

$$d^2 f = \left(\frac{\partial f}{\partial a}\right)^2 d^2 a + \left(\frac{\partial f}{\partial b}\right)^2 d^2 b + \cdots + \left(\frac{\partial f}{\partial n}\right)^2 d^2 n$$

For small errors of measurements d^2f goes to $(\Delta f)^2$, d^2a goes to $(\Delta a)^2$, etc.

The square root of $(\Delta f)^2$ is taken as the inherent uncertainty in the readings.

Replacing Δ with δ for the error of measured quantities (uncertainties), the following equation can be written:

$$(\delta_f)^2 = \left(\frac{\partial f}{\partial a}\right)^2 (\delta_a)^2 + \left(\frac{\partial f}{\partial b}\right)^2 (\delta_b)^2 + \cdots + \left(\frac{\partial f}{\partial n}\right)^2 (\delta_n)^2$$

As a good example, an error analysis that is done in this work for the molar excess volume can be explained in detail.

C.2.Calculation and error analysis for the molar excess volume of 1-octene and [HMIm][Tf_2N] solution

For a liquid mixture, the molar excess volume V^{EX} is the molar volume of solution that is in excess of molar volume of an ideal solution at the same conditions of temperature, pressure, and composition. [3]

$V^{EX} = V_m - x_1V_1 - x_2V_2$

$\underline{V}_1$ and $\underline{V}_2$ are molar volumes of [HMIm][Tf_2N] (component 1) and 1-octene (component 2)

$V^{EX} = (MW_m/\rho_m) - x_1 (MW_1/\rho_1) - x_2 (MW_2/\rho_2)$

$MWm = x_1MW_1 + x_2MW_2$

Excess molar volume (V^{EX}) in a binary solution is a function of density of mixture (ρ_m) and of each component (ρ_1, ρ_2) and their mole fractions (x_1, x_2). Molecular weight of mixture (MWm) also can be written as a linear function of molecular weight of each component (MW_1, MW_2) and their relative mole fractions. Finally, to show the mass of each compound, m_1 and m_2 are used.

To measure the density, a densitometer is used as explained in Chapter 2. The uncertainty of measuring the density of a pure compound by this instrument is ±0.0006 gr·cm^{-3}. However, the uncertainty of measuring two different injections of the same solution is ±0.007 grcm^{-3} and of two samples made in different time is ±0.014 grcm^{-3}.

The solution is prepared by mixing desire amounts of 1-octene and IL using an analytical balance with an uncertainty of ±0.0002 gr. Figure C-1 shows the graph of excess molar volume of solution [HMIm][Tf_2N] at different temperatures vs. the mole fraction of solute (1-octene).

To find uncertainties for each point the following procedure is pursued and results are reported in Tables C-1 to C-4 and summarized in Table C-5. The result of error analysis shows that the original uncertainty (δV^{EX}) is sensitive to the density of mixture ($(\partial V^{EX}/\partial \rho_m)^2(\delta\rho_m)^2$) and the solvent (ionic liquid) ($(\partial V^{EX}/\partial \rho_1)^2(\delta\rho_1)^2$), much more than the density of 1-octene and mole fractions because of the higher molecular weight and mole fraction of the ionic liquid. From the above analysis the calculated mean value of uncertainty for all of temperatures and concentrations is 0.19±0.02 that has been demonstrated for each point in Figure C-1 by error bars.

C.3 Error Analysis Procedure

In the following equations [HMIm][Tf_2N] and 1-octene are considered as components (1) and (2) respectively:

$V^{EX} = f (\rho_1,\rho_2,\rho_m,x_1,x_2)$

$V^{EX} = (MW_m/\rho_m)-x_1(MW_1/\rho_1)-x_2(MW_2/\rho_2)$

$MWm=x_1MW_1+x_2MW_2$

$x_1=(m_1/MW_1)/(m_1/MW_1+m_2/MW_2)$

$x_2 =1- x_1$

$(\delta V^{EX})^2 = (\partial V^{EX}/\partial\rho_1)^2(\delta\rho_1)^2+(\partial V^{EX}/\partial\rho_2)^2(\delta\rho_2)^2 + (\partial V^{EX}/\partial\rho_m)^2(\delta\rho_m)^2 +$

$(\partial V^{EX}/\partial x_1)^2(\delta x_1)^2 + (\partial V^{EX}/\partial x_2)^2(\delta x_2)^2$

$(\delta x_1)^2 = (\partial x_1/\partial m_1)^2(\delta m_1)^2 + (\partial x_1/\partial m_2)^2(\delta m_2)^2$

$(\delta x_2)^2 = (\partial x_2/\partial m_1)^2(\delta m_1)^2 + (\partial x_2/\partial m_2)^2(\delta m_2)^2$

$x_2=(m_2/MW_2)/(m_1/MW_1+m_2/MW_2)$

$(\partial V^{EX}/\partial\rho_1)=x_1MW_1/\rho_1^2$

$(\partial V^{EX}/\partial\rho_2)=x_2MW_2/\rho_2^2$

$(\partial V^{EX}/\partial\rho_m)= -MWm/\rho_m^2$

$(\partial V^{EX}/\partial x_1)=MW_1(1/\rho_m -1/\rho_1)+MW_2(1/\rho_2-1/\rho_m)$

$(\partial V^{EX}/\partial x_2)=-MW_1(1/\rho_m -1/\rho_1)-MW_2(1/\rho_2-1/\rho_m)$

$(\partial x_1/\partial m_1)=(m_2/MW_2)/(MW_1)(m_1/MW_1+m_2/MW_2)^2$

$(\partial x_1/\partial m_2)=-(m_1/MW_2)/(MW_1)(m_1/MW_1+m_2/MW_2)^2$

$(\partial x_2/\partial m_1)= -(m_2/MW_2)/(MW_1)(m_1/MW_1+m_2/MW_2)^2$

$(\partial x_2/\partial m_2)=(m_1/MW_1)/(MW_2)(m_1/MW_1+m_2/MW_2)^2$

$(\delta\rho_1)$,$(\delta\rho_2)$ from experiments: 0.0006 (gr/cm^3)

(δm_1) from balance: 0.0002 gr

(δm_2) from balance: 0.0002 gr

$MW_{1\text{-Octene}}$ = 112.2

$MW_{[HMIm][Tf2N]}$ = 447.4

Table C-1 Error Analysis Results at T=10°C								
x_2= 1-x_1	IL(gr)	1-OCTENE (gr)	IL(mole)	Wt%	1-OCTENE (mole)	MOLE%	ρ_m(avg)	$\delta\rho_m$ (STDEV)
0							1.38544	0.0001
0.05	6.00	0.08	0.013	1.32	0.001	5.04574	1.37212	0.0006
0.1	6.00	0.17	0.013	2.72	0.001	10.03992	1.35568	0.0006
0.139	6.00	0.24	0.013	3.89	0.002	13.90404	1.3422	0.0006
0.154	6.00	0.28	0.013	4.38	0.002	15.44339	1.34003	0.0006
0.16	7.00	0.33	0.016	4.56	0.003	16.00899	1.3395	0.0006
1							0.7235	
V^{EX}	$\partial V^{EX}/\partial\rho_1$	$(\partial V^{EX}/\partial\rho_2)$	MWm	$\partial V^{EX}/\partial\rho_m$	$(\partial V^{EX}/\partial x_1)$	$(\partial V^{EX}/\partial x_2)$	$(\partial x_1/\partial m_1)$	$(\partial x_1/\partial m_2)$
0			447.40					
-0.69	221.43	10.72	430.64	-228.73	76.44	-76.44	0.01	-0.60
-0.85	209.78	21.43	413.88	-225.20	79.41	-79.41	0.02	-0.54
-0.98	200.69	29.79	400.81	-222.49	81.89	-81.89	0.02	-0.49
-1.73	197.19	33.01	395.78	-220.41	82.29	-82.29	0.02	-0.47
-2.11	195.79	34.30	393.77	-219.46	82.39	-82.39	0.02	-0.40
0			112.2					
$(\delta x_1)^2$	$\partial x_2/\partial m_1$	$(\partial x_2/\partial m_2)$	$(\delta x_2)^2$	$(\partial V^{EX}/\partial\rho_1)^2 (\delta\rho_1)^2$	$(\partial V^{EX}/\partial\rho_2)^2 (\delta\rho_2)^2$	$(\partial V^{EX}/\partial\rho m)^2 (\delta\rho m)^2$	$(\partial V^{EX}/\partial x_1)^2 (\delta x_1)^2$	$(\partial V^{EX}/\partial x_2)^2 (\delta x_2)^2$
1E-08	-0.0080	0.5989	0.0000	0.0177	0.0000	0.0188	0.0001	0.0001
1E-08	-0.0150	0.5376	0.0000	0.0158	0.0002	0.0183	0.0001	0.0001
1E-08	-0.0199	0.4926	0.0000	0.0145	0.0003	0.0178	0.0001	0.0001
9E-09	-0.0218	0.4749	0.0000	0.0140	0.0004	0.0175	0.0001	0.0001
6E-09	-0.0248	0.4019	0.0000	0.0138	0.0004	0.0173	0.0000	0.0000

Table C-1 Cont. (T=10°C)							
x_2=1-x_1	0	0.05	0.1	0.139	0.154	0.16	1
$(\delta V^{EX})^2$	0	0.0367	0.0344	0.0328	0.0320	0.0317	0
(δV^{EX})	0	0.19	0.19	0.18	0.18	0.18	0

Table C-2 Error Analysis Results at T=25°C								
x_2= 1-x_1	IL(gr)	1-OCTENE(gr)	IL(mole)	Wt%	1-OCTENE(mole)	MOLE%	ρ_m(avg)	$\delta\rho_m$(STDEV)
0							1.37069	0.0006
0.05	6.00	0.08	0.013418	1.32	0.000713	5.045739	1.35836	0.0006
0.1	6.00	0.17	0.013416	2.72	0.001497	10.03992	1.34183	0.0006
0.139	6.00	0.24	0.013411	3.89	0.002166	13.90404	1.32828	0.0006
0.154	6.00	0.28	0.01342	4.38	0.002451	15.44339	1.32631	0.0006
0.19	7.00	0.41	0.015646	5.54	0.003661	18.96097	1.32038	0.0001
1							0.71117	
V^{EX}	$(\partial V^{EX}/\partial\rho_1)$	$(\partial V^{EX}/\partial\rho_2)$	MWm	$(\partial V^{EX}/\partial\rho_m)$	$(\partial V^{EX}/\partial x_1)$	$(\partial V^{EX}/\partial x_2)$	$(\partial x_1/\partial m_1)$	$(\partial x_1/\partial m_2)$
0.00			447.40					
-0.94	226.23	11.09	430.64	-233.39	78.13	-78.13	0.01	-0.60
-1.10	214.32	22.18	413.88	-229.87	81.17	-81.17	0.02	-0.54
-1.22	205.03	30.84	400.81	-227.17	83.72	-83.72	0.02	-0.49
-2.03	201.46	34.16	395.78	-224.99	84.09	-84.09	0.02	-0.41
-4.26	192.89	42.15	383.71	-220.09	85.23	-85.23	0.02	-0.57
0.00			112.2					
$(\delta x_1)^2$	$(\partial x_2/\partial m_1)$	$(\partial x_2/\partial m_2)$	$(\delta x_2)^2$	$(\partial V^{EX}/\partial\rho_1)^2 (\delta\rho_1)^2$	$(\partial V^{EX}/\partial\rho_2)^2 (\delta\rho_2)^2$	$(\partial V^{EX}/\partial\rho m)^2 (\delta\rho m)^2$	$(\partial V^{EX}/\partial x_1)^2 (\delta x_1)^2$	$(\partial V^{EX}/\partial x_2)^2 (\delta x_2)^2$
1E-08	-0.0080	0.5989	0.0000	0.0184	0.0000	0.0196	0.0001	0.0001
1E-08	-0.0150	0.5376	0.0000	0.0165	0.0002	0.0190	0.0001	0.0001
1E-08	-0.0200	0.4926	0.0000	0.0151	0.0003	0.0186	0.0001	0.0001
7E-09	-0.0217	0.4100	0.0000	0.0146	0.0004	0.0182	0.0000	0.0000
1E-08	-0.0220	0.5696	0.0000	0.0134	0.0006	0.0007	0.0001	0.0001

Table C-2 Cont. (T=25°C)							
x_2=1-x_1	0	0.05	0.1	0.139	0.154	0.19	1
$(\delta V^{EX})^2$	0	0.0388	0.0363	0.0344	0.0334	0.0148	0
(δV^{EX})	0	0.20	0.19	0.19	0.18	0.12	0

Table C-3 Error Analysis Results at T=50°C								
x_2= 1-x_1	IL(gr)	1-OCTENE (gr)	IL (mole)	Wt%	1-OCTENE (mole)	MOLE%	ρ_m (avg)	$\delta\rho_m$ (STDEV)
0							1.34792	0.0001
0.05	6.00	0.08	0.013418	1.32	0.000713	5.045739	1.33554	0.0006
0.1	6.00	0.17	0.013416	2.72	0.001497	10.03992	1.31902	0.0006
0.139	6.00	0.24	0.013411	3.89	0.002166	13.90404	1.30556	0.0006
0.154	6.00	0.28	0.01342	4.38	0.002451	15.44339	1.30324	0.0006
0.23	7.00	0.52	0.015646	6.95	0.004659	22.94344	1.30013	0.0006
1							0.69013	
V^{EX}	$(\partial V^{EX}/\partial\rho_1)$	$(\partial V^{EX}/\partial\rho_2)$	MWm	$\partial V^{EX}/\partial\rho_m$	$(\partial V^{EX}/\partial x_1)$	$(\partial V^{EX}/\partial x_2)$	$(\partial x_1/\partial m_1)$	$(\partial x_1/\partial m_2)$
0.00			447.40					
-1.01	233.93	11.78	430.64	-241.44	79.34	-79.34	0.01	-0.60
-1.21	221.62	23.56	413.88	-237.89	81.64	-81.64	0.02	-0.54
-1.38	212.02	32.75	400.81	-235.15	84.79	-84.79	0.02	-0.49
-2.15	208.32	36.28	395.78	-233.03	87.41	-87.41	0.02	-0.47
-7.02	189.61	54.18	370.30	-219.07	87.86	-87.86	0.03	-0.34
0.00			112.2					
$(\delta x_1)^2$	$(\partial x_2/\partial m_1)$	$(\partial x_2/\partial m_2)$	$(\delta x_2)^2$	$(\partial V^{EX}/\partial\rho_1)^2$ $(\delta\rho_1)^2$	$(\partial V^{EX}/\partial\rho_2)^2$ $(\delta\rho_2)^2$	$(\partial V^{EX}/\partial\rho m)^2$ $(\delta\rho m)^2$	$(\partial V^{EX}/\partial x_1)^2$ $(\delta x_1)^2$	$(\partial V^{EX}/\partial x_2)^2$ $(\delta x_2)^2$
1E-08	-0.0080	0.5989	0.0000	0.0197	0.0000	0.0210	0.0001	0.0001
1E-08	-0.0150	0.5376	0.0000	0.0177	0.0002	0.0204	0.0001	0.0001
1E-08	-0.0200	0.4926	0.0000	0.0162	0.0004	0.0199	0.0001	0.0001
9E-09	-0.0217	0.4749	0.0000	0.0156	0.0005	0.0195	0.0001	0.0001
5E-09	-0.0253	0.3382	0.0000	0.0129	0.0011	0.0173	0.0000	0.0000

Table C-3 Cont. (T=50°C)							
$x_2=1-x_1$	0	0.05	0.1	0.139	0.154	0.23	1
$(\delta V^{EX})^2$	0	0.0409	0.0384	0.0366	0.0358	0.0313	0
(δV^{EX})	0	0.20	0.20	0.19	0.19	0.18	0

Table C-4 Error Analysis Results at T=75°C								
x_2= $1-x_1$	IL(gr)	1-OCTENE (gr)	IL (mole)	Wt%	1-OCTENE (mole)	MOLE%	ρ_m (avg)	$\delta\rho_m$ (STDEV)
0							1.32398	0.0006
0.05	6.00	0.08	0.013418	1.32	0.000713	5.045739	1.31267	0.0006
0.1	6.00	0.17	0.013416	2.72	0.001497	10.03992	1.296	0.0006
0.139	6.00	0.24	0.013411	3.89	0.002166	13.90404	1.28213	0.0006
0.154	6.00	0.28	0.01342	4.38	0.002451	15.44339	1.2789	0.0006
0.28	7.00	0.68	0.015646	8.86	0.006062	27.92443	1.235	0.0006
1							0.71117	
V^{EX}	$(\partial V^{EX}/\partial\rho_1)$	$(\partial V^{EX}/\partial\rho_2)$	MWm	$(\partial V^{EX}/\partial\rho_m)$	$(\partial V^{EX}/\partial x_1)$	$(\partial V^{EX}/\partial x_2)$	$(\partial x_1/\partial m_1)$	$(\partial x_1/\partial m_2)$
0.00			447.40					
-1.35	242.47	12.53	430.64	-249.92	85.14	-85.14	0.01	-0.60
-1.57	229.71	25.07	413.88	-246.41	88.43	-88.43	0.02	-0.54
-1.68	219.75	34.84	400.81	-243.82	91.22	-91.22	0.02	-0.49
-2.27	215.93	38.60	395.78	-241.98	91.88	-91.88	0.02	-0.47
-10.83	183.77	70.19	353.54	-231.80	101.20	-101.20	0.03	-0.30
0.00			112.2					
$(\delta x_1)^2$	$(\partial x_2/\partial m_1)$	$(\partial x_2/\partial m_2)$	$(\delta x_2)^2$	$(\partial V^{EX}/\partial\rho_1)^2 (\delta\rho_1)^2$	$(\partial V^{EX}/\partial\rho_2)^2 (\delta\rho_2)^2$	$(\partial V^{EX}/\partial\rho m)^2 (\delta\rho m)^2$	$(\partial V^{EX}/\partial x_1)^2 (\delta x_1)^2$	$(\partial V^{EX}/\partial x_2)^2 (\delta x_2)^2$
1E-08	-0.0080	0.5989	0.0000	0.0212	0.0001	0.0225	0.0001	0.0001
1E-08	-0.0150	0.5376	0.0000	0.0190	0.0002	0.0219	0.0001	0.0001
1E-08	-0.0200	0.4926	0.0000	0.0174	0.0004	0.0214	0.0001	0.0001
9E-09	-0.0217	0.4749	0.0000	0.0168	0.0005	0.0211	0.0001	0.0001
4E-09	-0.0288	0.2959	0.0000	0.0122	0.0018	0.0193	0.0000	0.0000

Table C-4 Cont. T=75°C							
$x_2=1-x_1$	0	0.05	0.1	0.139	0.154	0.28	1
$(\delta V^{EX})^2$	0	0.0439	0.0413	0.0394	0.0386	0.0333	0
(δV^{EX})	0	0.21	0.20	0.20	0.20	0.18	0

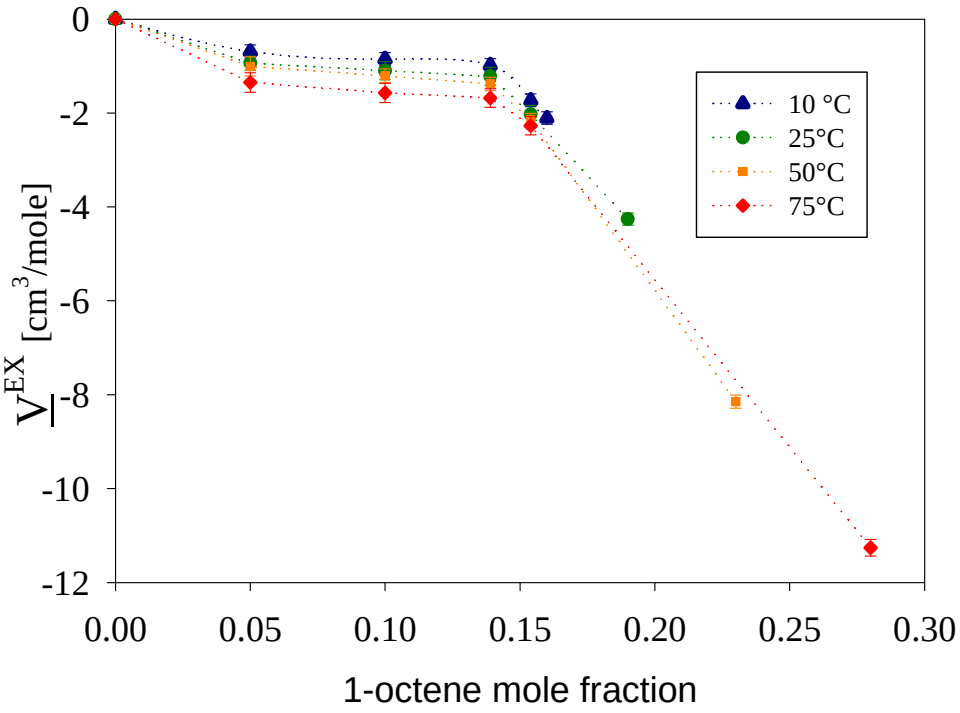

Figure C-1 Excess molar volume of [HMIm][Tf_2N] with 1-octene. The last point of the isotherm is the value at saturation. Dotted line for visual aid.

Table C-5 Excess molar volume and uncertainty at different isotherms and concentrations

T=10°C

x_2	ρ	MW	ρ_m	$\underline{Vm}$	$\underline{V}^{EX}= \underline{Vm}-x_1\underline{V_1}-x_2\underline{V_2}$	(δV^{EX})
0	1.38544	447.4	0.0031	322.93	0.00	0.00
0.05	1.37212	430.6	0.0032	313.85	-0.69	0.19
0.1	1.35568	413.9	0.0033	305.29	-0.85	0.19
0.139	1.3422	400.8	0.0033	298.62	-0.98	0.18
0.154	1.34003	395.8	0.0034	295.35	-1.73	0.18
0.16	1.3395	393.8	0.0034	293.97	-2.11	0.18
1	0.7235	112.2	0.0064	155.08	0.00	0.00

T=25°C

x_2	ρ	MW	ρ_m	$\underline{Vm}$	$\underline{V}^{EX}= \underline{Vm}-x_1\underline{V_1}-x_2\underline{V_2}$	(δV^{EX})
0	1.37069	447.4	0.0031	326.4	0.00	0.00
0.05	1.35836	430.6	0.0032	317.03	-0.94	0.20
0.1	1.34183	413.9	0.0032	308.44	-1.10	0.19
0.139	1.32828	400.8	0.0033	301.75	-1.22	0.19
0.154	1.32631	395.8	0.0034	298.41	-2.03	0.18
0.19	1.32267	383.7	0.0034	290.1	-4.26	0.12
1	0.71117	112.2	0.0063	157.77	0.00	0.00

T=50°C

x_2	ρ	MW	ρ_m	$\underline{Vm}$	$\underline{V}^{EX}= \underline{Vm}-x_1\underline{V_1}-x_2\underline{V_2}$	(δV^{EX})
0	1.34792	447.4	0.0030	331.92	0.00	0.00
0.05	1.33554	430.6	0.0031	322.45	-1.01	0.20
0.1	1.31902	413.9	0.0032	313.78	-1.21	0.20
0.139	1.30556	400.8	0.0033	307	-1.38	0.19
0.154	1.30324	395.8	0.0033	303.69	-2.15	0.19
0.23	1.295	370.3	0.0035	285.95	-7.02	0.18
1	0.69013	112.2	0.0062	162.58	0.00	0.00

T=75°C

x_2	ρ	MW	ρ_m	$\underline{Vm}$	$\underline{V}^{EX}= \underline{Vm}-x_1\underline{V_1}-x_2\underline{V_2}$	(δV^{EX})
0	1.32398	447.4	0.0030	337.92	0.00	0.00
0.05	1.31267	430.6	0.0030	328.06	-1.35	0.21
0.1	1.296	413.9	0.0031	319.35	-1.57	0.20
0.139	1.28213	400.8	0.0032	312.61	-1.68	0.20
0.154	1.2789	395.8	0.0032	309.47	-2.27	0.20
0.28	1.265	353.5	0.0036	279.48	-10.83	0.18
1	0.6683	112.2	0.0060	167.89	0.00	0.00

References

1. Bork, P. V.; Grote, H.; Notz, D.; Regler, M., Data Analysis Techniques in High Energy Physics Experiments. *Cambridge University Press*, **1993**.
2. Taylor, J. R., An Introduction to Error Analysis: The Study of Uncertainties if Physical Measurements. *University Science Books* **1982**.
3. Prausnitz, J. M.; Lichtenthaler, R. N.; de Azevedo, E. G., *Molecular thermodynamics of fluid-phase equilibria*. Prentice Hall PTR: **1986**.

Appendix D - Liquid-Liquid Extraction Column Schematic

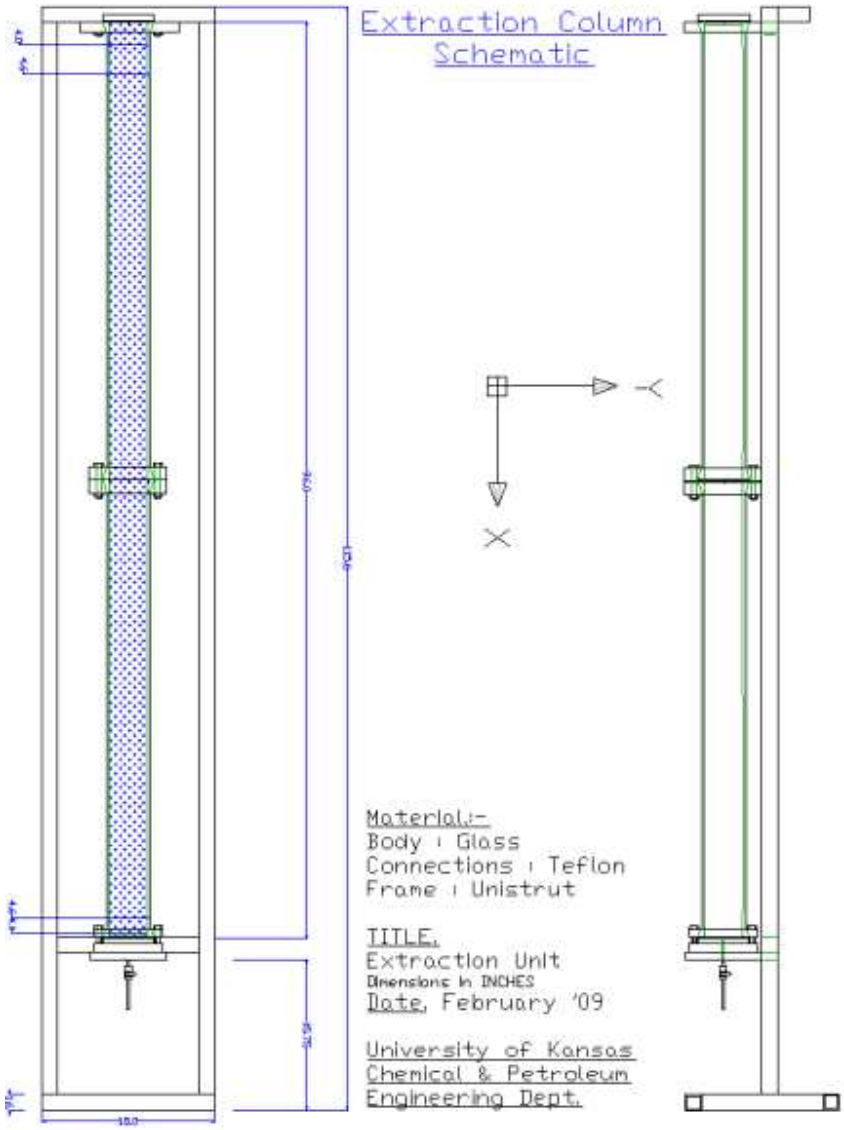

Top Part

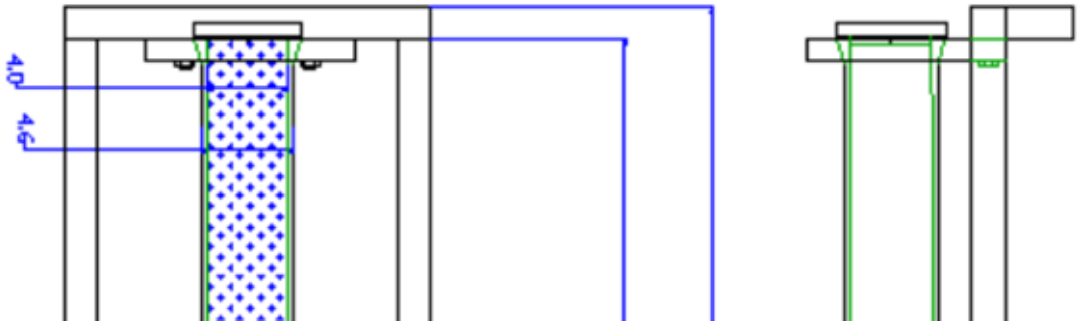

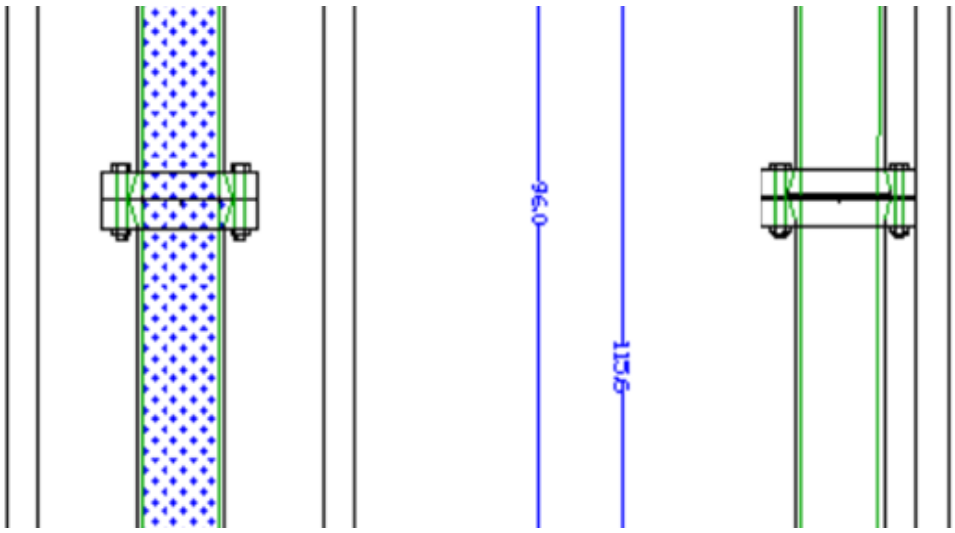

Middle Part

Bottom Part